1988

Stage effects on stalling and recovery of a high-speed 10-stage axial-flow compressor

William Ward Copenhaver
Iowa State University

INFORMATION TO USERS

The most advanced technology has been used to photograph and reproduce this manuscript from the microfilm master. UMI films the text directly from the original or copy submitted. Thus, some thesis and dissertation copies are in typewriter face, while others may be from any type of computer printer.

The quality of this reproduction is dependent upon the quality of the copy submitted. Broken or indistinct print, colored or poor quality illustrations and photographs, print bleedthrough, substandard margins, and improper alignment can adversely affect reproduction.

In the unlikely event that the author did not send UMI a complete manuscript and there are missing pages, these will be noted. Also, if unauthorized copyright material had to be removed, a note will indicate the deletion.

Oversize materials (e.g., maps, drawings, charts) are reproduced by sectioning the original, beginning at the upper left-hand corner and continuing from left to right in equal sections with small overlaps. Each original is also photographed in one exposure and is included in reduced form at the back of the book. These are also available as one exposure on a standard 35mm slide or as a 17" x 23" black and white photographic print for an additional charge.

Photographs included in the original manuscript have been reproduced xerographically in this copy. Higher quality 6" x 9" black and white photographic prints are available for any photographs or illustrations appearing in this copy for an additional charge. Contact UMI directly to order.

U·M·I

University Microfilms International
A Bell & Howell Information Company
300 North Zeeb Road, Ann Arbor, MI 48106-1346 USA
313/761-4700 800/521-0600

Order Number 8909139

Stage effects on stalling and recovery of a high-speed 10-stage axial-flow compressor

Copenhaver, William Ward, Ph.D.

Iowa State University, 1988

U·M·I
300 N. Zeeb Rd.
Ann Arbor, MI 48106

Stage effects on stalling and recovery of a high-speed 10-stage axial-flow compressor

by

William Ward Copenhaver

A Dissertation Submitted to the
Graduate Faculty in Partial Fulfillment of the
Requirements for the Degree of
DOCTOR OF PHILOSOPHY

Major: Mechanical Engineering

Approved:

Signature was redacted for privacy.

In Charge of Major Work

Signature was redacted for privacy.

For the Major Department

Signature was redacted for privacy.

For the Graduate College

Members of the Committee:

Signature was redacted for privacy.

Iowa State University
Ames, Iowa

1988

TABLE OF CONTENTS

		Page
	DEDICATION	xx
	SYMBOLS AND NOTATION	xxi
	ABSTRACT	xxv
I.	INTRODUCTION	1
II.	LITERATURE REVIEW	16
	A. Surge/Rotating-stall Boundary Speeds	18
	B. In-stall Performance Characteristics	20
	C. "Zonal" Compressor Performance	25
	D. Recovery Hysteresis	31
	E. Active Controls	33
	F. Summary	34
III.	TEST FACILITY	36
	A. Facility Computer Control System	38
	B. Facility Power Conditioning and Drive Systems	40
	C. Facility Flow Conditioning and Measurement Hardware	42
	D. Facility Data Acquisition System	47
IV.	TEST COMPRESSOR	50
	A. Compressor Hardware	52
	1. Inlet	52
	2. Compression section	54
	3. Discharge	57

B. Compressor Instrumentation 61

1. Inlet instrumentation 61

2. Compressor system instrumentation 67

3. Discharge instrumentation 75

V. DATA ACQUISITION CONFIGURATION 79

A. High-Response Pressure Measurements 80

B. Time-Averaged Pressure and Temperature Measurements and Close-Coupled Pressure Measurements 95

VI. TEST PROCEDURES AND DATA ACQUISITION 113

A. Steady and Quasi-steady Procedures 114

1. Data acquisition procedures 114

2. Test variables 115

B. Time-resolved Performance 121

1. Data acquisition procedures 121

2. Test variables 122

VII. DATA ANALYSIS AND RESULTS 124

A. Multistage Model Description 125

1. Governing equations 127

2. Stage characteristics 130

3. Solution methods and model validation 131

a. Three-stage low-speed case 132

b. Nine-stage high-speed compressor case 134

B. Steady Unstalled and Quasi-steady In-stall Perfromance 135

1. Compressor speed effects 137

2. Variable geometry effects 192

C. Time-resolved Compressor Stall and In-stall Performance 207

1. Compresssor stall cell details 208

2. Dynamic stalling comparisions 245

VIII. SUMMARY AND CONCLUSIONS 258

IX. RECOMMENDATIONS FOR FUTURE RESEARCH 266

X. REFERENCES 269

XI. ACKNOWLEDGMENTS 275

XII. APPENDIX A: DETAILED INSTRUMENTATION LOCATIONS 277

XIII. APPENDIX B: DETAILED CHARACTERISTICS 49.8% DESIGN SPEED 292

XIV. APPENDIX C: DETAILED CHARACTERISTICS 59.7% DESIGN SPEED 304

XV. APPENDIX D: DETAILED CHARACTERISTICS 67.7% DESIGN SPEED 316

XVI. APPENDIX E: DETAILED CHARACTERISTICS 74.5% DESIGN SPEED 328

XVII. APPENDIX F: DETAILED CHARACTERISTICS 78.5% DESIGN SPEED 340

XVIII. APPENDIX G: DETAILED CHARACTERISTICS 74.5% DESIGN SPEED +7VV 352

XIX. APPENDIX H: HIGH-RESPONSE FORWARD AND AFT FACING PROBE SIGNALS 364

LIST OF FIGURES

		Page
Figure 1.1	Compressor map	4
Figure 1.2	Compressor operating region	6
Figure 1.3	Compressor stall margin	7
Figure 1.4	Compressor surge/rotating stall boundary	9
Figure 1.5	Compressor surge characteristic	10
Figure 1.6	Compressor in-stall characteristic	11
Figure 2.1	Detail of Day's stall cell blockage estimation method	32
Figure 3.1	Compressor research facility	37
Figure 3.2	Control computer configuration	39
Figure 3.3	CRF power conditioning equipment	41
Figure 3.4	CRF drive configuration	43
Figure 3.5	10-stage test compressor installation	44
Figure 3.6	CRF flow conditioning screens	46
Figure 3.7	CRF data acquisition system	48
Figure 4.1	CRF 10-stage test compressor	51
Figure 4.2	Test compressor inlet section	53
Figure 4.3	Test compressor compression section	55
Figure 4.4	Test compressor interstage instrumentation axial locations	58
Figure 4.5	Test compressor discharge section	59
Figure 4.6	Test compressor inlet instrumentation axial locations	62
Figure 4.7	Forward and aft facing pressure probe	66

Figure 4.8	Test compressor discharge instrumentation axial locations	76
Figure 5.1	High-response instrumentation axial and circumferential locations	83
Figure 5.2	Test compressor inner and outer case configuration	84
Figure 5.3	High-response pressure transducer measurement configuration	88
Figure 5.4	High-response data acquisition system schematic	89
Figure 5.5	Close-coupled data acquisition system schematic	99
Figure 5.6	Close-coupled instrumentation axial and circumferential locations	101
Figure 5.7	Pressure attenuation characteristics of close-coupled measurements	104
Figure 5.8	Phase shift characteristics of close-coupled measurements	105
Figure 7.1	CRF test compressor overall pressure characteristics	138
Figure 7.2	Speed effects on multistage compressor in-stall hysteresis	142
Figure 7.3	Performance comparison of multistage compressors	144
Figure 7.4	CRF test compressor overall temperature characteristics	145
Figure 7.5	Test compressor first stage pressure characteristics	148
Figure 7.6	Rotating stall cell effect on first stage characteristic	150
Figure 7.7	Test compressor second stage pressure characteristics	154

Figure 7.8	Test compressor third stage pressure characteristics	156
Figure 7.9	Test compressor fourth stage pressure characteristics	158
Figure 7.10	Test compressor fifth stage pressure characteristics	162
Figure 7.11	Test compressor sixth stage pressure characteristics	163
Figure 7.12	Test compressor seventh stage pressure characteristics	164
Figure 7.13	Test compressor eighth stage pressure characteristics	167
Figure 7.14	Test compressor ninth stage pressure characteristics	168
Figure 7.15	Test compressor tenth stage pressure characteristics	169
Figure 7.16	Test compressor pressure with throttle closing	173
Figure 7.17	Test compressor temperature with throttle closing	174
Figure 7.18	Test compressor pressure rise in-stall	175
Figure 7.19	Test compressor first stage temperature characteristics	178
Figure 7.20	Test compressor second stage temperature characteristics	179
Figure 7.21	Test compressor third stage temperature characteristics	180
Figure 7.22	Test compressor fourth stage temperature characteristics	181
Figure 7.23	Test compressor fifth stage temperature characteristics	182
Figure 7.24	Test compressor sixth stage temperature characteristics	183

Figure 7.25 Test compressor seventh stage temperature characteristics 184

Figure 7.26 Test compressor eighth stage temperature characteristics 185

Figure 7.27 Test compressor ninth stage temperature characteristics 186

Figure 7.28 Test compressor tenth stage temperature characteristics 187

Figure 7.29 Axial total pressure and temperature profiles (in-stall) 188

Figure 7.30 Axial total pressure and temperature profiles (unstalled) 191

Figure 7.31 Test compressor overall pressure characteristics (variable vane effects) 193

Figure 7.32 Test compressor first stage pressure characteristics (variable vane effects) 196

Figure 7.33 Test compressor second stage pressure characteristics (variable vane effects) 197

Figure 7.34 Test compressor third stage pressure characteristics (variable vane effects) 198

Figure 7.35 Test compressor fourth stage pressure characteristics (variable vane effects) 200

Figure 7.36 Test compressor fifth stage pressure characteristics (variable vane effects) 201

Figure 7.37 Test compressor sixth stage pressure characteristics (variable vane effects) 202

Figure 7.38 Test compressor seventh stage pressure characteristics (variable vane effects) 203

Figure 7.39 Test compressor eighth stage pressure characteristics (variable vane effects) 204

Figure 7.40 Test compressor ninth stage pressure characteristics (variable vane effects) 205

Figure 7.41	Test compressor tenth stage pressure characteristics (variable vane effects)	206
Figure 7.42	High-response and close-coupled data acquisition system response during test compressor stalling	210
Figure 7.43	Test compressor time-resolved near annulus hub total pressure at 78.5% speed in-stall, exit throttle area 10 sq. in. (64.5 sq. cm)	212
Figure 7.44	Test compressor 78.5% speed overall performance (exit throttle area details)	213
Figure 7.45	Test compressor time-resolved outside annulus static pressure at 78.5% speed in-stall, exit throttle area 10 sq. in. (64.5 sq. cm)	216
Figure 7.46	Test compressor time-resolved tip region total and static pressure at 78.5% speed in-stall, exit throttle area 10 sq. in. (64.5 sq. cm)	217
Figure 7.47	Test compressor time-resolved tip region total and static pressure at 78.5% speed in-stall, exit throttle area 20 sq. in. (129.0 sq. cm)	219
Figure 7.48	Test compressor 59.7% speed overall performance (exit throttle area details)	221
Figure 7.49	Test compressor high-response exit pressures 59.7% speed, exit throttle area 15.2 sq. in. (98.0 sq. cm)	222
Figure 7.50	Sensitivity of rotor ten inlet relative Mach number to calculation parameters	224
Figure 7.51	Test compressor high-response exit pressures 78.5% speed, exit throttle area 15.0 sq. in. (98.0 sq.cm)	226
Figure 7.52	Test compressor exit throttle effects on rotating stall cell blockage level	227
Figure 7.53	Test compressor rotating-stall cell speed variations	229

Figure 7.54	Tenth stage blade geometry	234
Figure 7.55	Test compressor exit throttle and speed effects on relative Mach numbers in the tenth stage rotor	236
Figure 7.56	Test compressor tenth stage pressure characteristic (exit throttle area details)	239
Figure 7.57	Test compressor 78.5% speed seventh stage double valved pressure characteristic	244
Figure 7.58	Multistage model control volume definition	247
Figure 7.59	Exit total pressure during compressor stalling comparison	248
Figure 7.60	Entrance to ninth stage total pressure during compressor stalling comparison	251
Figure 7.61	Entrance to seventh stage total pressure during compressor stalling comparison	253
Figure 7.62	Entrance to fifth stage total pressure during compressor stalling comparison	254
Figure 7.63	Entrance to third stage total pressure during compressor stalling comparison	255
Figure 12.1	Test compressor detailed instrumentation locations (inlet flow conditioning screen)	278
Figure 12.2	Test compressor detailed instrumentation locations (bellmouth throat and compressor inlet)	279
Figure 12.3	Test compressor detailed instrumentation locations (inlet to stage 1)	280
Figure 12.4	Test compressor detailed instrumentation locations (inlet to stage 2)	281
Figure 12.5	Test compressor detailed instrumentation locations (inlet to stage 3)	282

Figure 12.6 Test compressor detailed instrumentation locations (inlet to stage 4) 283

Figure 12.7 Test compressor detailed instrumentation locations (inlet to stage 5) 284

Figure 12.8 Test compressor detailed instrumentation locations (inlet to stage 6) 284

Figure 12.9 Test compressor detailed instrumentation locations (inlet to stage 7) 286

Figure 12.10 Test compressor detailed instrumentation locations (inlet to stage 8) 287

Figure 12.11 Test compressor detailed instrumentation locations (inlet to stage 9) 288

Figure 12.12 Test compressor detailed instrumentation locations (inlet to stage 10) 289

Figure 12.13 Test compressor detailed instrumentation locations (exit to stage 10) 290

Figure 12.14 Test compressor detailed instrumentation locations (discharge) 291

Figure 13.1 Test compressor overall characteristics 49.8% design corrected speed 293

Figure 13.2 Test compressor first stage characteristics 49.8% design corrected speed 294

Figure 13.3 Test compressor second stage characteristics 49.8% design corrected speed 295

Figure 13.4 Test compressor third stage characteristics 49.8% design corrected speed 296

Figure 13.5 Test compressor fourth stage characteristics 49.8% design corrected speed 297

Figure 13.6 Test compressor fifth stage characteristics 49.8% design corrected speed 298

Figure 13.7 Test compressor sixth stage characteristics 49.8% design corrected speed 299

Figure 13.8 Test compressor seventh stage characteristics 49.8% design corrected speed 300

Figure 13.9 Test compressor eighth stage characteristics 49.8% design corrected speed 301

Figure 13.10 Test compressor ninth stage characteristics 49.8% design corrected speed 302

Figure 13.11 Test compressor tenth stage characteristics 49.8% design corrected speed 303

Figure 14.1 Test compressor overall characteristics 59.7% design corrected speed 305

Figure 14.2 Test compressor first stage characteristics 57.7% design corrected speed 306

Figure 14.3 Test compressor second stage characteristics 59.7% design corrected speed 307

Figure 14.4 Test compressor third stage characteristics 59.7% design corrected speed 308

Figure 14.5 Test compressor fourth stage characteristics 59.7% design corrected speed 309

Figure 14.6 Test compressor fifth stage characteristics 59.7% design corrected speed 310

Figure 14.7 Test compressor sixth stage characteristics 59.7% design corrected speed 311

Figure 14.8 Test compressor seventh stage characteristics 59.7% design corrected speed 312

Figure 14.9 Test compressor eighth stage characteristics 59.7% design corrected speed 313

Figure 14.10 Test compressor ninth stage characteristics 59.7% design corrected speed 314

Figure 14.11 Test compressor tenth stage characteristics 59.7% design corrected speed 315

Figure 15.1 Test compressor overall characteristics 67.7% design corrected speed 317

Figure 15.2 Test compressor first stage characteristics 67.7% design corrected speed 318

Figure 15.3 Test compressor second stage characteristics 67.7% design corrected speed 319

Figure 15.4 Test compressor third stage characteristics 67.7% design corrected speed 320

Figure 15.5 Test compressor fourth stage characteristics 67.7% design corrected speed 321

Figure 15.6 Test compressor fifth stage characteristics 67.7% design corrected speed 322

Figure 15.7 Test compressor sixth stage characteristics 67.7% design corrected speed 323

Figure 15.8 Test compressor seventh stage characteristics 67.7% design corrected speed 324

Figure 15.9 Test compressor eighth stage characteristics 67.7% design corrected speed 325

Figure 15.10 Test compressor ninth stage characteristics 67.7% design corrected speed 326

Figure 15.11 Test compressor tenth stage characteristics 67.7% design corrected speed 327

Figure 16.1 Test compressor overall characteristics 74.5% design corrected speed 329

Figure 16.2 Test compressor first stage characteristics 74.5% design corrected speed 330

Figure 16.3 Test compressor second stage characteristics 74.5% design corrected speed 331

Figure 16.4 Test compressor third stage characteristics 74.5% design corrected speed 332

Figure 16.5 Test compressor fourth stage characteristics 74.5% design corrected speed 333

Figure 16.6 Test compressor fifth stage characteristics 74.5% design corrected speed 334

Figure 16.7 Test compressor sixth stage characteristics 74.5% design corrected speed 335

Figure 16.8 Test compressor seventh stage characteristics 74.5% design corrected speed 336

Figure 16.9 Test compressor eighth stage characteristics 74.5% design corrected speed 337

Figure 16.10 Test compressor ninth stage characteristics 74.5% design corrected speed 338

Figure 16.11 Test compressor tenth stage characteristics 74.5% design corrected speed 339

Figure 17.1 Test compressor overall characteristics 78.5% design corrected speed 341

Figure 17.2 Test compressor first stage characteristics 78.5% design corrected speed 342

Figure 17.3 Test compressor second stage characteristics 78.5% design corrected speed 343

Figure 17.4 Test compressor third stage characteristics 78.5% design corrected speed 344

Figure 17.5 Test compressor fourth stage characteristics 78.5% design corrected speed 345

Figure 17.6 Test compressor fifth stage characteristics 78.5% design corrected speed 346

Figure 17.7 Test compressor sixth stage characteristics 78.5% design corrected speed 347

Figure 17.8 Test compressor seventh stage characteristics 78.5% design corrected speed 348

Figure 17.9 Test compressor eighth stage characteristics 78.5% design corrected speed 349

Figure 17.10 Test compressor ninth stage characteristics 78.5% design corrected speed 350

Figure 17.11 Test compressor tenth stage characteristics 78.5% design corrected speed 351

Figure 18.1 Test compressor overall characteristics 74.5% design corrected speed (+7 VV) 353

Figure 18.2 Test compressor first stage characteristics 74.5% design corrected speed (+7 VV) 354

Figure 18.3 Test compressor second stage characteristics 74.5% design corrected speed (+7 VV) 355

Figure 18.4 Test compressor third stage characteristics 74.5% design corrected speed (+7 VV) 356

Figure 18.5 Test compressor fourth stage characteristics 74.5% design corrected speed (+7 VV) 357

Figure 18.6 Test compressor fifth stage characteristics 74.5% design corrected speed (+7 VV) 358

Figure 18.7 Test compressor sixth stage characteristics 74.5% design corrected speed (+7 VV) 359

Figure 18.8 Test compressor seventh stage characteristics 74.5% design corrected speed (+7 VV) 360

Figure 18.9 Test compressor eighth stage characteristics 74.5% design corrected speed (+7 VV) 361

Figure 18.10 Test compressor ninth stage characteristics 74.5% design corrected speed (+7 VV) 362

Figure 18.11 Test compressor tenth stage characteristics 74.5% design corrected speed (+7 VV) 363

Figure 19.1 High-response compressor exit forward and aft facing pressure probe signals with stall cell blockage extent detailed, 59.7% design corrected speed, exit throttle area 3.1 sq. in. (20.0 sq. cm) 365

Figure 19.2 High-response compressor exit forward and aft facing pressure probe signals with stall cell blockage extent detailed, 59.7% design corrected speed, exit throttle area 5.0 sq. in. (32.2 sq. cm) 366

Figure 19.3 High-response compressor exit forward and aft facing pressure probe signals with stall cell blockage extent detailed, 59.7% design corrected speed, exit throttle area 8.8 sq. in. (56.8 sq. cm) 367

Figure 19.4 High-response compressor exit forward and aft facing pressure probe signals with stall cell blockage extent detailed, 59.7% design corrected speed, exit throttle area 20.0 sq. in. (129.0 sq. cm) 368

Figure 19.5 High-response compressor exit forward and aft facing pressure probe signals with stall cell blockage extent detailed, 59.7% design corrected speed, exit throttle area 22.5 sq. in. (145.2 sq. cm) 369

Figure 19.6 High-response compressor exit forward and aft facing pressure probe signals with stall cell blockage extent detailed, 78.5% design corrected speed, exit throttle area 10.0 sq. in. (64.5 sq. cm) 370

Figure 19.7 High-response compressor exit forward and aft facing pressure probe signals with stall cell blockage extent detailed, 78.5% design corrected speed, exit throttle area 19.9 sq. in. (128.4 sq. cm) 371

Figure 19.8 High-response compressor exit forward and aft facing pressure probe signals with stall cell blockage extent detailed, 78.5% design corrected speed, exit throttle area 24.9 sq. in. (160.6 sq. cm) 372

Figure 19.9 High-response compressor exit forward and aft facing pressure probe signals with stall cell blockage extent detailed, 78.5% design corrected speed, exit throttle area 27.4 sq. in. (176.8 sq. cm) 373

Figure 19.10 High-response compressor exit forward and aft facing pressure probe signals with stall cell blockage extent detailed, 78.5% design corrected speed, exit throttle area 29.2 sq. in. (188.4 sq. cm) 374

LIST OF TABLES

		Page
Table 4.1	Inlet instrumentation	63
Table 4.2	Compressor instrumentation	68
Table 4.3	Compressor discharge instrumentation	77
Table 5.1	High-response measurements	82
Table 5.2	Close-coupled measurements	100
Table 7.1	Tenth stage velocity properties	235

DEDICATION

This dissertation is dedicated to my family,

my wife Elizabeth,

my parents,

Mr. Raymond G. Copenhaver

and

Mrs. Merial B. Copenhaver,

my wife's parents,

Mr. Alva Blankenship (deceased Aug. 1986)

and

Mrs. Lorene Blankenship,

who all firmly supported the philosophy that education should be regarded as one of the most important goals in life.

SYMBOLS AND NOTATION

A	Flow area
AC	Alternating current
A/D	Analog to digital
B	Blockage percent
B_m	Measurement bias error
CC	Close-coupled
CEA	Centers of equal area
CRF	Compressor research facility
C_p	Specific heat of air at constant pressure
C_x	Axial velocity
DC	Direct current
DAC	Data acquisition computer
DCS	Design corrected compressor speed
e	Specific internal energy
F	Force
FCC	Facility control computer
FM	Frequency modulated
FX	Axial force distribution
F_B	Blade force
g_c	Gravitational constant
h	Specific enthalpy
H_f	Hysteresis factor

HR	High-response
HPDAS	High perfromance data acquisition system
ID	Inside diameter
IGV	Inlet guide vane
IRIG	International recording
LE	Leading edge
M	Mach number
MOC	Method of characteristics
MS	Midspan
M_R	Mach number, relative to rotor revolution of the fluid entering rotor
N	Rotor speed
OD	Outside diameter
P	Pressure
PLC	Programmable logic controller
PR	Pressure ratio
Q	Heat transfer
R	Gas constant
R1	Rotor one
R2	Rotor two
R3	Rotor three
R4	Rotor four
R5	Rotor five
R6	Rotor six

R7	Rotor seven
R8	Rotor eight
R9	Rotor nine
R10	Rotor ten
S_m	Measurement precision error
SW	Shaft work
t	Time
t_{95}	Student T distribution
T	Temperature
Ta	Time-averaged
TA	Throttle area at exit to compressor
TAC	Test article control computer
TDC	Top dead center
T_{ref}	Standard day reference temperature
u	Velocity magnitude
U	Rotor speed at midspan of rotor blade
U_m	Measurement uncertainty
UTR	Universal temperature reference
VV	Variable vane
V_R	Velocity relative to rotor revolution
W	Mass flow rate
W_B	Mass flow rate of bleed air

γ	Ratio of specific heats of air
θ	Ratio of total temperature and T_{ref}
ϕ	Flow coefficient (page 130)
ϕ_{IIP}	Flow coefficient at initial install point
ϕ_{NRP}	Flow coefficient at near recovery point
ρ	Density
ψ^P	Pressure coefficient (page 130)
ψ^T	Temperature coefficient (page 130)
τ	Time constant (page 131)

Subscripts

x	Axial component
S	Static
T	Total
SS	Steady state

ABSTRACT

Results of a high-speed 10-stage axial-flow compressor test involving overall compressor and individual stage performance while stalling and operating in quasi-steady rotating stall are described. Test procedures and data acquisition methods used to obtain the dynamic stalling and quasi-steady in-stall data are explained. Unstalled and in-stall time-averaged data obtained from the compressor operating at five different shaft speeds and one off-schedule variable vane condition are presented. The effects of compressor speed and variable geometry on overall compressor in-stall pressure rise and hysteresis extent are illustrated through the use of quasi-steady stage temperature rise and pressure rise characteristics. The results indicate that individual stage performance during overall compressor rotating stall operation varies considerably throughout the length of the compressor. Time-resolved in-stall data acquired at two different shaft speeds are presented in support of the notion that stage operation varies significantly from entrance to exit of the compressor. Both time-averaged and time-resolved individual stage results suggest that stage matching is important, not only for unstalled performance but also for in-stall performance and recoverability from stall.

The measured high-speed 10-stage test compressor individual stage pressure and temperature characteristics were input into a stage-by-stage dynamic compressor performance model. The analytical model had been previously validated for the prediction of low-speed compressor stalling and in-stall performance. Dynamic pressures measured during stalling of the high-speed 10-stage test compressor are compared with analytical model results. The comparison of the model results and the measured pressures provided the additional validation necessary to demonstrate the model's ability to predict high-speed multistage compressor stalling and in-stall performance.

I. INTRODUCTION

The gas turbine engine is used in two primary capacities. The first is a stationary application as a shaft power generating device. The relatively large amount of shaft power generated for the size of machine involved is a major advantage of the gas turbine engine. Gas turbine engines designed for generation of ground-based shaft power have minimal restrictions on weight and under ordinary conditions operate at near design conditions. A second important use of the gas turbine engine is for propulsion in a variety of air, land and sea vehicle configurations. Vehicle and in particular aircraft gas turbine engines are designed with reduced weight as a major requirement. Additionally, the off-design performance of an aircraft engine is an important consideration because of maneuverability demands. Modern high performance aircraft require operating conditions for the gas turbine engine that are far from design.

Three primary components of a gas turbine engine are the compressor, combustor, and turbine. The compressor provides part of the pressure rise of working fluid necessary for the amount of expansion through the turbine required by the application. Enough additional energy

must be added to the working fluid through combustion of fuel in the combustor to overcome losses in the compressor and turbine, as well as produce output power. The overall performance of the gas turbine engine is limited by component efficiencies and, in the case of aircraft engines, off-design performance must be sustained at reasonable power levels. The compressor is the critical component in determining the design and off-design performance of a gas turbine engine. Break down of the compressor flow field during off-design operation can results in losses that are large enough to prevent sustained operation of the gas turbine engine. A compressor designed for superior off-design performance will expand the operating range of a gas turbine engine, making that engine more suitable for use in high performance aircraft.

Modern axial-flow compressor stages are capable of generating exit total pressures as large as twice the inlet level. The use of multiple stages in series in an axial-flow compressor allows for increased overall pressure rise. This multiple staging is necessary to achieve the pressure levels required for high performance gas turbine engines. Therefore, the off-design performance of multistage, axial-flow compressors, rather than only single-stage compressors, is very important to

the success of high performance gas turbine engine designs.

Modern single-spool, multistage, axial-flow compressors are capable of generating a pressure rise as large as 28 to 1 with 10 stages as reported by Hosny et al. [1]. In generating this pressure rise the compressor must also provide the required mass flow to produce the thrust required by the application involved. Overall compressor performance is often displayed graphically on a "compressor map" as shown in Figure 1.1. Pressure rise, efficiency and mass flow rate are conveniently related for different shaft speeds with a map like this. The actual mass flow through the compressor is corrected for inlet pressure and temperature conditions so performance comparisons can be made between compressors operating with different inlet conditions. A more complete description of the corrections made is provided in Ref. [2]. In addition to pressure rise and mass flow, compressor efficiency is also critical to rating performance. Efficiency levels can be shown, along with the compressor pressure ratio, as a function of operating point (see Figure 1.1). For a given compressor speed, the operating point is prescribed by the intersection of the throttle line and the compressor speed line.

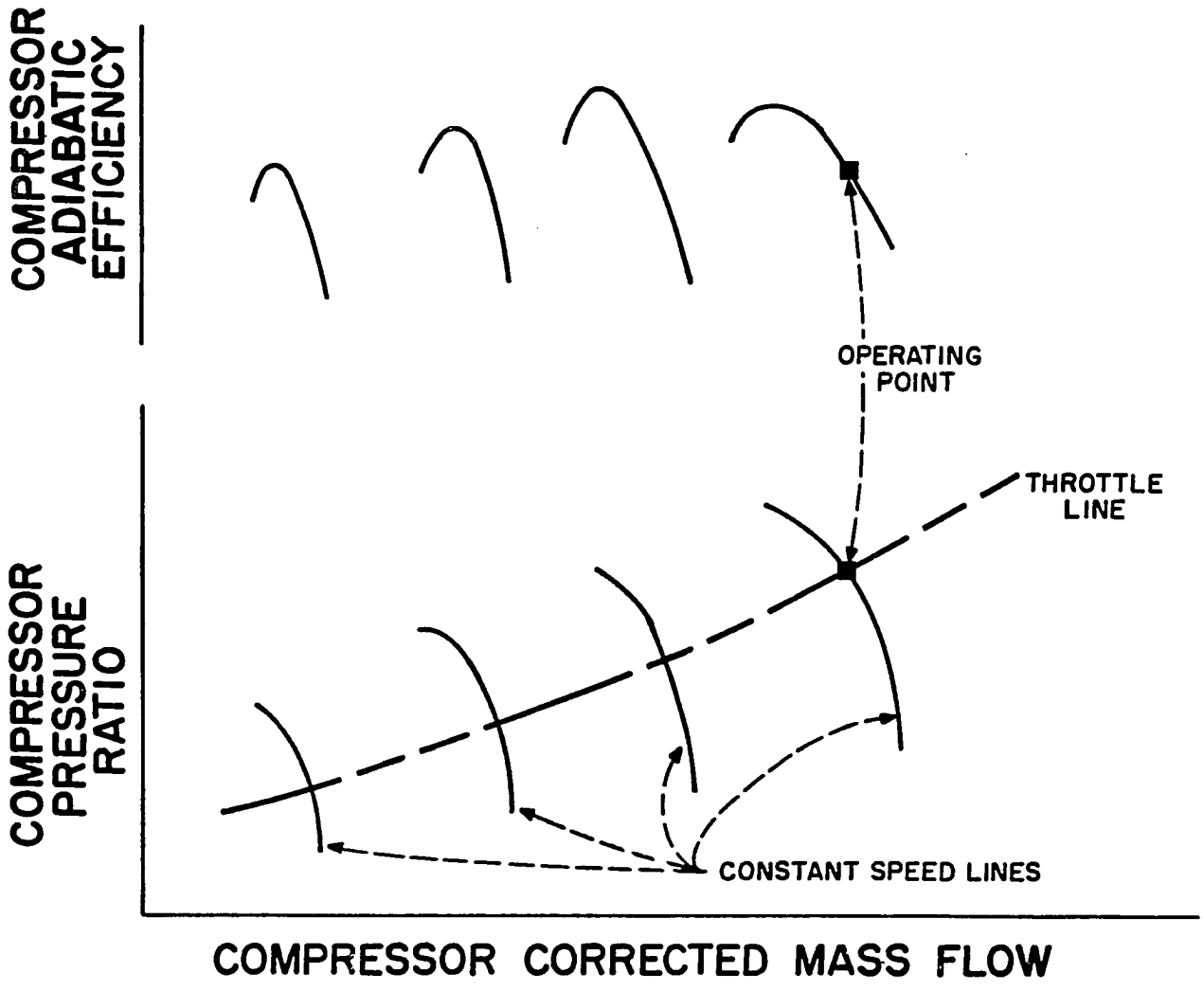

Figure 1.1 Compressor map

The compressor is designed to operate at a particular speed and throttle setting for which compressor, combustor and turbine component matching is achieved. Operation at any other operating point is considered as off-design operation. Maximum off-design operation in a compressor is limited by blade passage choking, on the high flow end, and blade and endwall stalling, on the low flow end, as illustrated in Figure 1.2. One important variable related to range of operation is stall margin. Stall margin is a measure of how much compressor back pressure can be increased at a constant flow or flow rate reduced at a constant speed from the design operating point before the compressor stalls as shown in Figure 1.3. The greater the stall margin the less likely the compressor will stall in engine operation. Even with large stall margins, however, compressors can be forced to stall by inlet distortions that occur with current aircraft mission demands. When a compressor stalls, engine performance is reduced below the level that can sustain flight. Because compressor stalling does occur and because aircraft have been consequently lost, the performance of a compressor while operating in stall and its ability to recover from stall are extremely important. Recoverability is a measure of

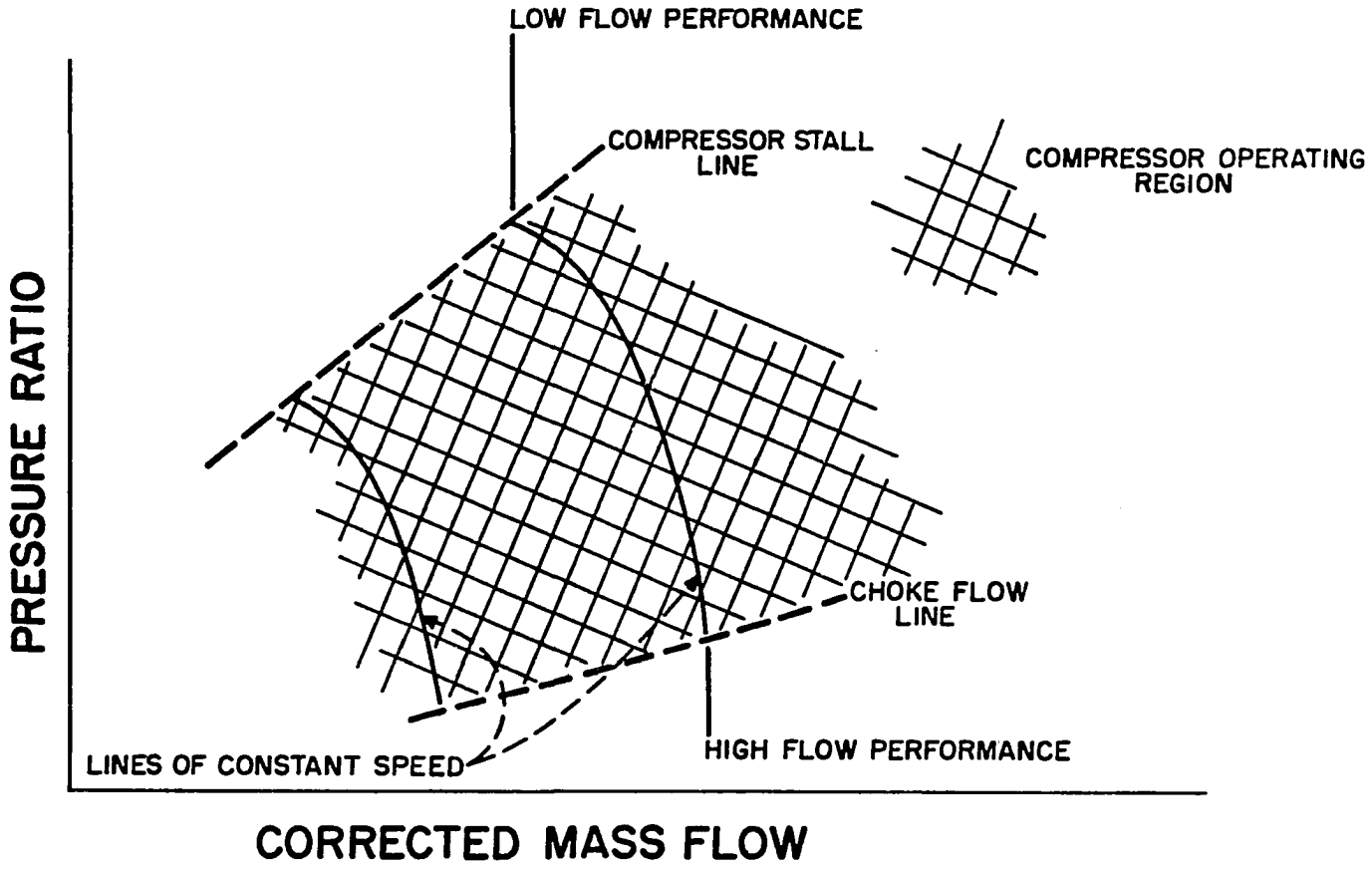

Figure 1.2 Compressor operating region

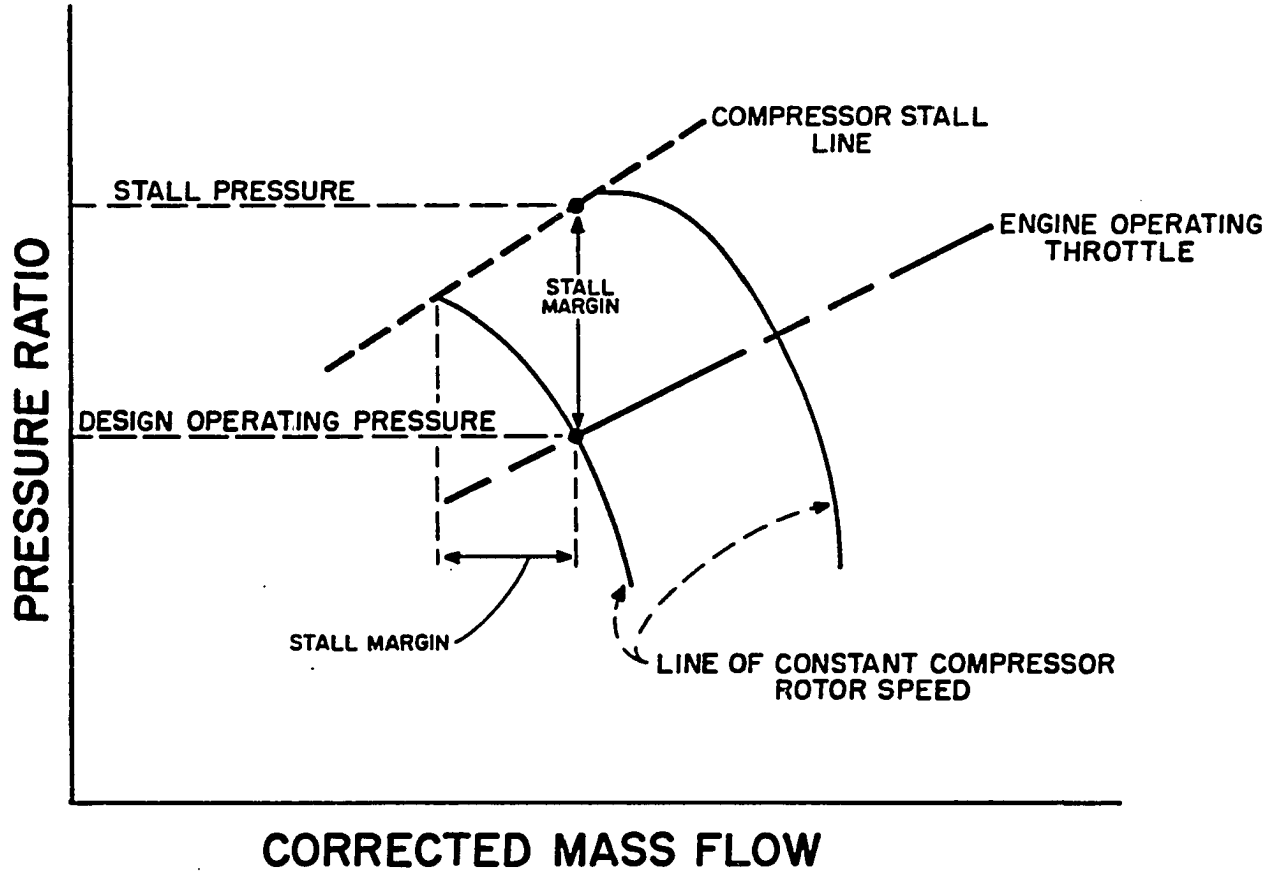

Figure 1.3 Compressor stall margin

how easily the compressor can recover from stall to a condition that will allow adequate operation of the engine.

When a compressor stalls, two types of flow instabilities, surge or rotating stall, can result. Surge is more likely to occur at higher speeds while rotating stall occurs at lower speeds as illustrated in Figure 1.4. If the instability is cyclic in nature (surge), the overall compressor operates on or near its unstalled characteristic during part of the surge cycle as shown in Figure 1.5. The unstalled characteristic is defined as the line of unstalled operating points. If the perturbation that caused the instability is removed prior to any part of the cycle, then the compressor will return to its normal operating condition. Surge is an instability which occurs at high operating speeds in multistage compressors. Surge in compressors is a condition from which recovery is easy and therefore is more desired, from the standpoint of recovery, than rotating stall which is discussed next.

If the instability resulting from a compressor stall is rotating stall (stalled region of flow rotating around the annular flowpath) then at no time is the overall compressor operating on its usual unstalled characteristic, as demonstrated in Figure 1.6.

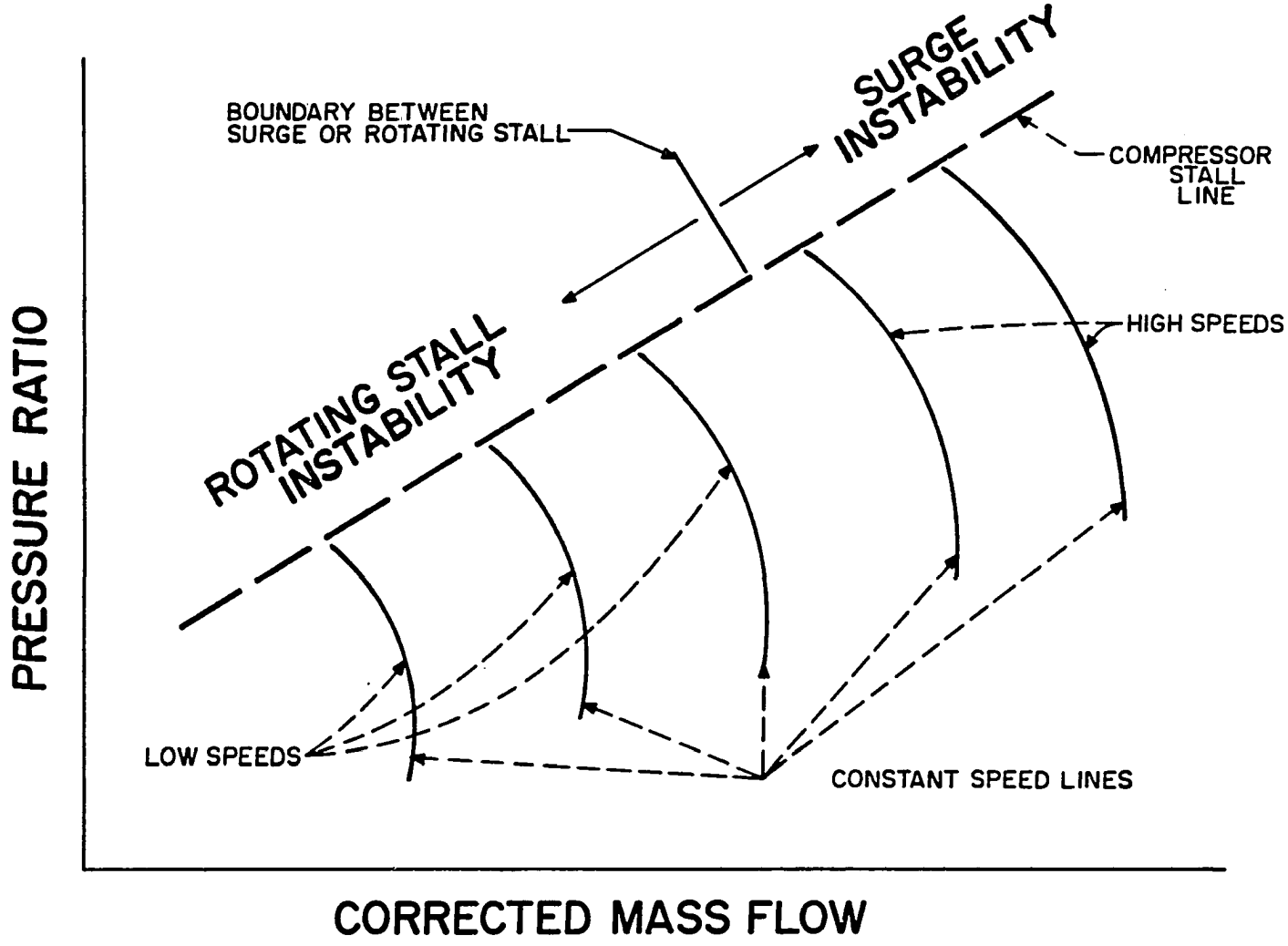

Figure 1.4 Compressor surge/rotating stall boundary

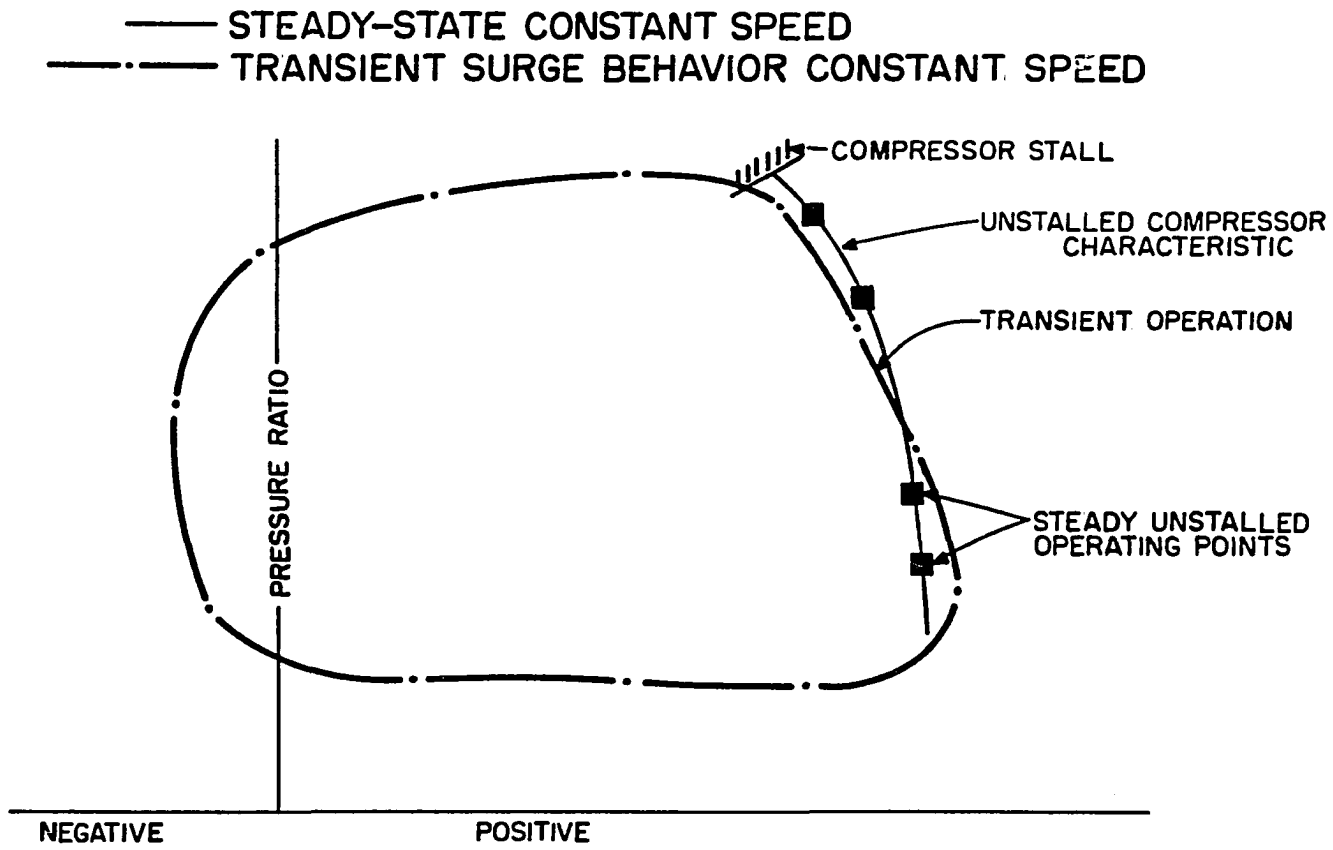

Figure 1.5 Compressor surge characteristic

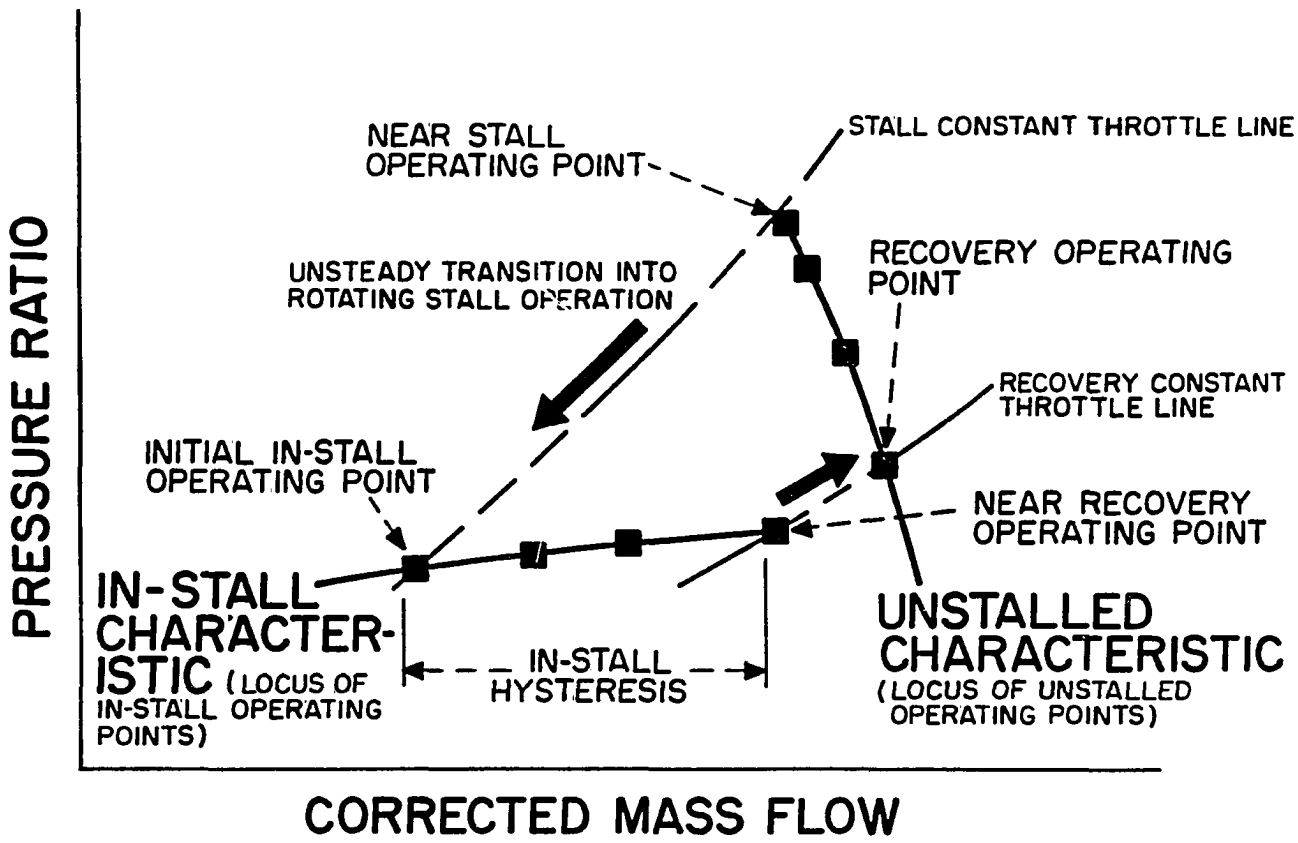

Figure 1.6 Compressor in-stall characteristic

Instead, a hysteresis loop including stalled operating points is formed (see Figure 1.6). This line of stalled operating points is defined as the in-stall characteristic. When the perturbation that caused rotating stall to occur is removed, the compressor must recover along its in-stall performance characteristic. Recovery can be improved in engine applications if the extent of the in-stall hysteresis (see Figure 1.6) is kept small by design. Minimizing the extent of the in-stall hysteresis is prerequisite to improving compressor rotating stall recoverability.

Investigations of compressor recoverability from stall have primarily focused on the performance of low speed, low pressure ratio compressors. These investigations have provided some important fundamental concepts about in-stall compressor performance and recovery. Generally, two kinds of analysis have prevailed. One approach treats the compressor or compressor stages as lumped control volumes with stage or overall compressor pressure forces and shaft work considered known from experimentally determined unstalled and in-stall compressor characteristics. To account for the dynamics of the stall event, which requires several rotor revolutions to reach quasi-steady operation, time lags are imposed on these characteristics. Changes are

made to compressor exit boundary conditions, such as pressure and temperature levels, and dynamic responses are predicted. The other strategy is directed toward understanding details of the flow field within the compressor at off-design, and based on this understanding, predicting the performance of the compressor when a perturbation is imposed. Due to the complexity of the second approach, which requires three-dimensional, nonlinear theory, the lumped control volume approach is considered more likely to affect near term compressor designs.

The lumped volume approach requires that the dynamic performance of the compression system be defined as a global phenomenon with each local component of the system being individually modeled. The system local components consist of large plenum volumes and ducts upstream and downstream of the compressor, the multistage compressor and the compressor discharge throttle. The multistage compressor component can be modeled as either a single volume with compressor rotor shaft work and pressure forces input or as a series of smaller volumes for each stage with the stage shaft work and pressure forces input. The discharge throttle component is model as a step drop in total pressure. The dynamics of the ducts, volumes and discharge throttles are well understood. Little is

presently known, however about the dynamics of stalling compressor stages. Several computer code models of low-speed axial-flow compressors have been developed based on these lumped control volume concepts and a small amount of low-speed compressor stall data (see Refs. [3], [4], [5], [6]). These models predict performance of low-speed, low-pressure-ratio test compressors during stalling, operating in-stall and recovering from stall. In general for low-speed, low-pressure-ratio compressors they predict this performance well. They do not address the effects of compressibility and off-design stage matching present in high-speed multistage compressors, effects that must be considered if modern multistage, high-speed, high-pressure-ratio, axial-flow compressor in-stall performance is to be predicted. Models have been developed by Koff et al. [7] and Davis and O'Brien [8] to address the aspects of off-design stage matching and compressibility present in high-speed multistage compressors. These models have not yet been fully exercised because only a very limited amount of experimental data from high pressure ratio multistage compressors exists presently.

This dissertation documents some of the results of an experiment which involved in-stall operation of a

10-stage, high-speed, high-pressure-ratio axial-flow compressor. The experiment was designed to investigate the component performance of an axial-flow compressor while stalling and operating in rotating stall. No attempt was made to simulate complete engine system responses to compressor stalling which would apply more directly to gas turbine engine recoverability. It is envisioned that the analysis of results from this component test will provide important information and additional insight necessary to continue development and improvement of models that predict high-speed, multistage, axial-flow compressor stall performance and recoverability within an gas turbine engine system.

II. LITERATURE REVIEW

To meaningfully review the status of past compressor rotating stall and surge research, several notions about stall and surge must be addressed. These notions about the performance of compressors in stall or surge have been largely developed from single-stage and low-speed multistage compressor research. More recently these notions have been examined carefully and modified using information obtained from high-speed multistage compressor stall and surge research. Existing important stall/surge theories described in the open literature, are reviewed. The relationship of these theories to the 10-stage compressor test results presented in this dissertation are discussed.

Current compressor design procedures must consider compressor recoverability from stall. The need for this requirement surfaced in the mid-1970s when recovery problems with a production augmented turbofan engine occurred. Early production models of the engine were susceptible to stagnation [9], defined as a condition characterized by the engine no longer responding to throttle commands while the compressor operated in rotating-stall. Stagnation occurred when compressor operation changed from a surge like condition into

rotating-stall after autoignition of raw fuel in the augmentor tube. Once into rotating-stall, the engine would require shutdown and restarting to clear the instability. Research efforts aimed at investigation of multistage compressor recoverability and development of designs with improved recoverability increased appreciably after this problem was recognized.

Therefore, much experimental and theoretical effort has been expended on determining what parameters are important to compressor recoverability and on incorporating these parameters into modeling codes. Topics that are important when considering compressor recoverability are:

Surge/rotating-stall boundary speed
In-stall performance characteristics
"Zonal" compressor performance
Recovery hysteresis extent
Active control

Research on each of these subjects will be summarized in this literature review.

A. Surge/Rotating-stall Boundary Speed

Surge is a more recoverable condition than rotating stall, as defined in Section I. Therefore, it is important to understand what compressor parameters will influence whether the compressor will surge or operate in rotating-stall after initial stalling. The surge/rotating stall boundary was defined earlier in Section I (See Figure 1.4). To determine parameters affecting the surge/rotating stall boundary, Greitzer [3],[4] developed a non-linear, one-dimensional model of a compression system with the compressor and its ducting replaced by an actuator disk, across which a pressure rise occurred, and fluid in a constant area pipe. The discharge throttle was modeled as an actuator disk, across which a pressure drop occurred, and fluid in a constant area duct. Compressor pressure rise as a function of mass flow was provided by experimental data. To account for lag between the onset of compressor instability and the establishment of fully developed rotating stall, a first order transient response model for the pressure rise across the compressor (modeled as an actuator disk) was adopted.

The model indicated that the major determining factor for instability type, surge or rotating stall, was the

ratio of the proportions of two forces, pressure forces and inertial forces. Measurements of overall transient compressor performance were obtained for a low-speed three-stage compressor with a variable volume discharge plenum attached. From tests it was determined that this ratio, termed "B", would predict surge when greater than 0.8 and rotating stall when less than 0.8.

This "B" parameter could be used to predict the nature of the instability, either surge or rotating stall, in low-speed compressors. However, the "B" parameter was not sufficient for high-speed compressors according to Moore and Greitzer [6,10,11]. Their analysis indicated that in addition to the "B" parameter (previously defined as critical to low speed prediction), compressor length-to-diameter ratio can affect whether a high-speed compression system response to an instability is surge or rotating stall. The length-to-diameter ratio is important in multistage compressor designs because of inherent increased overall compressor length. Compressors having lower length-to-radius ratios appeared to be more likely to surge.

Small and Lewis [12] used the "B" parameter to determine an exit volume, other than nominal that would result in stalling of their high-speed three-stage compressors at speeds near 100 percent of design. They

discovered however, that surge/rotating stall boundary speed was only shifted by a few percent from the boundary speed associated with the nominal volume. This indicated that more sophisticated models are required to predict the surge/rotating stall boundary speed of high-speed multistage compressors.

Davis and O'Brien [8] reported recently that inlet resistance to flow in a multistage compressor had an effect on the surge/rotating stall boundary. Their one-dimensional compressible multistage control volume model indicated that increased inlet resistance resulted in increased surge/rotating stall boundary speed.

B. In-stall Performance Characteristics

Research to date has shown that it is difficult to design a multistage compressor that will surge rather than stall over all operating speeds. Therefore, consideration must be given to improving rotating stall recovery characteristics of multistage compressors. Prediction of in-stall performance of a multistage compressor is critical for determining the parameters that effect recovery from stall.

Low-speed compressor test results reported by Day et al. [13] and Rostafinski [14] indicated that the

determination of in-stall performance of multistage compressors can be based on the hypothesis that a stage in rotating stall generates a constant nondimensional total-to-static pressure rise (defined as exit static pressure - inlet total pressure/ρu^2) independent of geometry. This nondimensional pressure rise is set by the stall cell blockage percent. At shutoff, the nondimensional pressure rise is assumed to be 0.11 for all compressor stages.

Small and Lewis [12] concluded from their high-speed three-stage compressor test data that contrary to Day et al.'s [13] conclusion based on low-speed compressor tests, stall headrise was not a constant per stage, but varied with compressor speed. This conclusion of Small and Lewis is supported by the results from the 10-stage test described in this dissertation. Therefore the concept of a constant headrise per stage is not generally valid for high-speed multistage compressors.

The importance of stage pressure rise and temperature rise characteristics is apparent when reviewing control volume models developed to predict compressor stall performance. Models developed by Davis and O'Brien [8], and by Greitzer [3] require experimentally determined, reverse flow, in-stall and unstalled characteristics for

inputs of pressure forces and shaft work into the control volume. These characteristics have been determined in low-speed compressor tests by Greitzer [4], and Koff and Greitzer [15]. Koff and Greitzer [15] determined an axisymmetric compressor characteristic from surge test data for a two-dimensional reversed flow model. They defined a method for determining compressor axisymmetric characteristics based on blade geometry.

In an effort to determine reverse flow compressor characteristics, Gamache and Greitzer [16] reported results obtained from a multistage low-speed compressor operating in the reverse flow regime. These results indicated a discontinuity between rotating stall operation at small negative flow coefficients, and annulus stall flow for larger negative flow levels. Stage flow field characteristics for annulus stalled reverse flows were also considered.

Small and Lewis [12] concluded that steady state, stalled performance modeling efforts require quasi-steady, in-stall operation characteristics since these conditions are needed to quantify the equilibrium point that drives the dynamic event. Contrary to this, Moore [5] concluded that based on a time scale evaluation of stall cell formation and mass flow change time, information obtained from a steady-state compressor test with the compressor

operating in rotating stall may not be representative of performance during rapid post stall transients.

Overall high-speed compressor in-stall characteristics were determined by Small and Lewis [12] for a 3-stage compressor, and by Hosny and Steenken [17] in a 10-stage compressor. Small and Lewis [12] reported nearly horizontal in-stall pressure rise characteristics. Hosny and Steenken [17] indicated that the overall in-stall characteristics were flat at lower speeds and increased in slope at higher speeds.

The goal in the prediction of compressor stalled performance and recovery is to use stage geometry to predict characteristics necessary as input to the lumped volume models. Differences between isolated stage performance and "stacked" stage performance were defined in early research by Huppert and Benser [18]. They pointed out that in single-stage compressor tests, the recovery hysteresis of the stage characteristic was often overlooked. They also suggested that discontinuities and double valued characteristics must be considered in predicting multistage characteristics.

Urasek et al. [19] tested an isolated first stage of a five-stage high-speed compressor to determine part-speed performance for unstalled and in-stall operation. Urasek reported from unpublished data that during part speed

operation of the five-stage compressor the first stage remained in or near stall. In-stall performance of the stage had not been predicted during design, and therefore stage matching at part speeds was difficult. These tests indicated the need to deal with matching of stages in a multistage compressor with one or more stages operating in rotating stall. The isolated rotor operating in stall produced increases in total temperature and decreases in total pressure as the mass flow was reduced to deep stall levels. It was noted during tests of the five-stage compressor that the stall line of the first stage at design speed shifted to somewhat lower flow in the multistage environment.

Recent research by Giannissis et al. [20] indicated, based on results from tests on a mismatched three-stage compressor, that interaction between stages is high when operating in rotating stall.

The relatively large amount of research in determining in-stall and reverse flow compressor characteristics indicates that the prediction of these characteristics, based on compressor design, is extremely important to the improvement of prediction models.

C. "Zonal" Compressor Performance

When a compressor is driven into rotating stall operation, portions of the annulus are blocked by the stalling of a packet of blades. Since only a portion of the annulus is blocked by the stall cell, there exist different circumferential zones of operation. Each zone has variations in temperature, pressure and flow from other zones.

Early measurements by Iura and Rannie [21] in a four-stage low-speed compressor indicated that regions or "zones" of propagating stall exists in a compressor when it operates in rotating stall. These measurements were compared with predicted information about propagating stall in a two dimensional cascade from theories based on single airfoil stalling developed by Sears [22] and Marble [23]. The comparisons indicated rotating stall speed in compressors may not be accurately predicted by theories based on isolated airfoil stalling responses. The rotating stall performance theories developed by Sears and Marble along with those developed by Stenning et al. [24], Emmons et al. [25], and more recently by Sexton and O'Brien [26] were developed primarily in an effort to determine the rotating stall propagation speed from blade geometry. These theories are based on the knowledge that the stalled

and unstalled zones exists within the compressor annulus during rotating stall operation.

Takata and Nagano [27] developed a two-dimensional, nonlinear, inviscid, incompressible flow theory that predicts stall cell numbers and propagation velocity. The nonlinear theory addressed the hysteresis associated with unstalling a blade row. Research into hysteresis extent in multistage compressors will be discussed further in the next subsection.

Because of the zonal operation of the compressor while in rotating stall, compressor unsteady performance has been modeled such that zones of the compressor operate differently in rotating stall. The approach is an extension to the one-dimensional control volume approach, in that another, circumferential dimension exists.

Dunham [28] proposed that the overall stalled flow of a compressor could be determined from its two-valued pressure rise characteristic. This was a two-dimensional approach to determining compressor stalled performance. This approach has been extended to multistage theories for determination of compressor stalled flow levels. It was reported by Dunham [28] that throttle movements alter only the extent of the stalled region, and that the fluid

velocity within the region was unchanged. Intersection of the throttle characteristic determines the operating region.

Mazzawy [29] proposed that performance of a multistage, axial-flow compressor could be considered as consisting of two characteristics during in-stall operation and that a multiple segment parallel compressor model could be used to predict in-stall performance. This model was initially developed to predict compressor performance with circumferential flow distortion. This concept was subsequently used as the basis for in-stall performance prediction, since the stalled region in a compressor is like a rotating flow distortion.

Koff et al. [7] utilized the parallel compressor model in developing a zonal analysis for the prediction of multistage compressor performance and recoverability during rotating stall operation. The stalled compressor annulus was divided into four circumferential control volumes, unstalled flow, stalled flow, and two transition regions on the leading and trailing planes of the stalled flow. These transition regions were found to be critical for setting the pressure rise in rotating stall. By varying model parameters, such as back flow characteristics, they concluded that a steeper backflow characteristic would result in a higher pressure rise level rotating-stall

performance characteristic and therefore a more recoverable design. A steeper backflow characteristic can be obtained by larger blade stagger angles.

Detailed measurements of a three stage compressor operating in deep rotating stall were obtained by Day [30] and Day and Cumpsty [31]. Their results indicated fundamental flow field characteristics of rotating stall in a low speed multistage compressor. It was reported that the stall cell extends over the full span of the rotor-stator and axially from compressor entrance to exit. Their measurements also indicated the stalled region was not a wake region where flow could not pass, but instead a region where flow would be drawn through from cell exit to entrance by the rotor. In addition, the notion of a parallel or "zonal" compressor model was supported by measurements made. That is, the unstalled region of flow can be considered to operate as an unstalled compressor creating the same exit static pressure as the stalled region. The compressor can be considered to operate on two branches of the characteristic, one the stalled branch and the other the unstalled branch. Both branches will produce matching exit static pressure. This information spurred new theories about rotating stall and has since been used as the basis for most model comparisons.

The low speed test results by Day and Cumpsty [31] supported the assumption that the axial extent of the zones, either stalled or unstalled, were the full length of the compressor. Therefore analysis to date has not considered a variation in the axial direction. Hosny et al. [1] reported that the rotating stall was confined primarily to the rear stages of the compressor in the energy efficient engine compressor test. Giannissis et al. [20] found in a mismatched three stage axial flow compressor that the first stage operated free of stall while the second and third were operating in stall. The downstream stall was seen by the first stage as a rotating distortion. The notion that the stall cell may not extend the full length of the compressor is supported by the results of the 10-stage compressor data presented in Section VII.

Temperature variations both axial and circumferential are important to the understanding of stalled compressor performance. Research in determining the temperature variations in a compressor operating in rotating stall has been limited. Small and Lewis [12] reported from their high-speed three-stage compressor test that the highest internal temperature due to rotating stall was at the trailing edge of stator one, not at the compressor exit as suggested from low speed results. Na'covska' [32] also

concluded from four-stage axial-flow compressor test data that while operating in rotating stall the compressor discharge temperatures were lower than temperatures between blade rows within the compressor. The results on temperature rise through the compressor presented by Small and Lewis, and Na'covska' are supported by the 10-stage test compressor results presented in Section VII.

In addition to different temperature zones within a compressor operating in rotating stall, there has also been reported that zones of flow in the reverse direction exist. Test results by Small and Lewis [12] in a high-speed compressor and by Day and Cumpsty [31] in a low-speed compressor both indicate there are zones of high reverse flows within a compressor operating in rotating stall. These trends provide support for the 10-stage test results presented in Section VII.

The research reviewed in this subsection suggests that rotating stall in a multistage compressor is a zonal phenomena. The research on the 10-stage compressor presented in this dissertation clarifies the critical influence of these zones of stalled flow on the recoverability of a compressor. The recovery hysteresis is affected by the performance of the stalled zone.

D. Recovery Hysteresis

Huppert and Benser [18] pointed out that double branch performance curves (hysteresis loops as defined in Section I) had been obtained for a multistage compressor having a small discharge volume. Recovery hysteresis is primarily associated with high-speed multistage compressor operation, although it does occur in low-speed compressors also. The extent of the recovery hysteresis can, however, be large in high-speed multistage compressors. Therefore it is important to determine what influences hysteresis extent in multistage compressors.

Theories developed from low-speed compressor tests by Day et al. [13] suggested that compressors will unstall when the blockage due to the stall cell drops below 30 percent. The blockage is determined from the intersection of the parabolic throttle line between the stall point on the compressor characteristic and the origin with the horizontal line between shutoff pressure rise and the compressor characteristic as detailed in Figure 2.1. If, when a compressor enters rotating stall, the blockage is greater than 30 percent, Day et al. predicted that the hysteresis will extend until the blockage drops below 30 percent. They considered important parameters affecting recovery hysteresis to be the number of stages and the

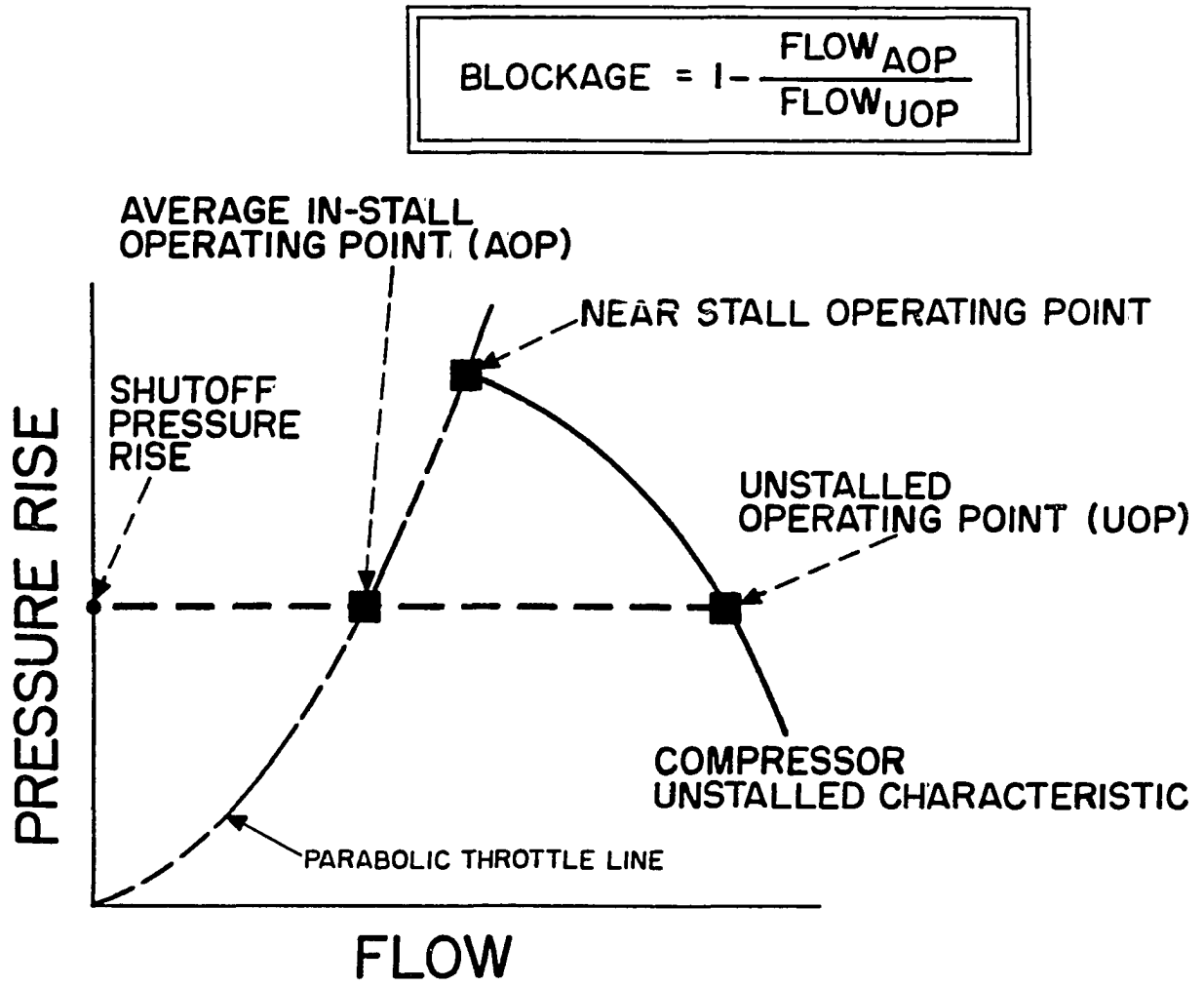

Figure 2.1 Detail of Day's stall cell blockage estimation method

design flow coefficient. The larger the number of stages and design flow coefficient, the greater the recovery hysteresis was.

Recent high-speed test results from Small and Lewis [12] and Hosny and Steenken [17] support the notion that recovery does occur at approximately a 30% annulus blockage due to the stall cell. This may not be true for all compressors as the 10-stage tests results reported herein will show.

Hosny and Steenken [17] also reported high-speed multistage test results that indicate that, based on mass flow levels corrected to the exit to the compressor, recovery hysteresis reduced as speed increased. The influence of speed on recovery hysteresis for multistage compressors is expanded by the results from the 10-stage compressor test considered presently.

E. Active Controls

An alternative approach to designing compressors for maximum recoverability is to use active controls to initiate recovery after the compressor stalls. Active controls can also be used to delay stalling.

Research in the direction of active controls was carried out by Ludwig et al. [33] and Ludwig and Nenni [34]. An active control system for a low-speed compressor stage was developed and tested. The system was able to keep the stage out of stall for throttle settings that would normally produce stall. More recently, Epstein [35] proposed a method to actively control rotating stall growth by creating a disturbance to counteract the non-uniform disturbance that initiates rotating stall.

Active control is a possible approach to minimize stalling problems, but it carries the penalty of additional complexity and weight; both are undesirable in modern aircraft gas turbine design philosophies.

F. Summary

The results of the literature review can be summarized as follows:

Parameters have been developed from low-speed low-pressure tests to predict compressor behavior (either surge or rotating stall) after initial stalling. These parameters required further improvement to predict stalling behavior of high-speed multistage compressors.

Most compressor stall performance prediction models require as input the unstalled, in-stall and reverse flow

pressure rise and temperature rise characteristics of the compressor.

Theories developed from low-speed low-pressure compressor tests predicting the in-stall compressor pressure rise characteristics fail to predict correct characteristics for high-speed multistage compressors.

Stage interactions in multistage axial flow compressors alter in-stall characteristics from those of an isolated stage.

Axial flow compressors have internal zones of stalled and unstalled performance which allows parallel compressor theorie to be used as a stall performance prediction tool. These zones may not extend over the full axial length in high-speed multistage compressors where stage matching will vary with speed.

Compressor tests indicate recovery from in-stall performance will occur when annulus blockage levels from the rotating stall cell drop below 30 percent.

Active controls have been explored to a limited extent for the prevention of compressor stall, thereby reducing the need to design compressors for high stall recoverability.

III. TEST FACILITY

A 10-stage axial-flow compressor test program was accomplished in the Wright-Patterson Air Force Base, Aero Propulsion Laboratory, Compressor Research Facility (CRF). The CRF is designed for exploration of the steady-state and transient behavior of full scale, multistage gas turbine engine fans and compressors. An overall layout of the CRF is shown in Figure 3.1. The facility actually involves space in 3 different buildings. The test building houses the computer and control rooms, the operations building contains the test chamber and signal conditioning room and the electrical power conditioning equipment is located in the electrical power conditioning building. CRF tests are controlled from the facility control room. Commands to execute the test program are sent from the control room to four control computers, located in the signal conditioning room, through a monitor computer located in the computer room. The control computers provide input to the electrical power conditioning equipment which power the drive motors. The control computers also control services that support variable geometry devices on the test compressor.

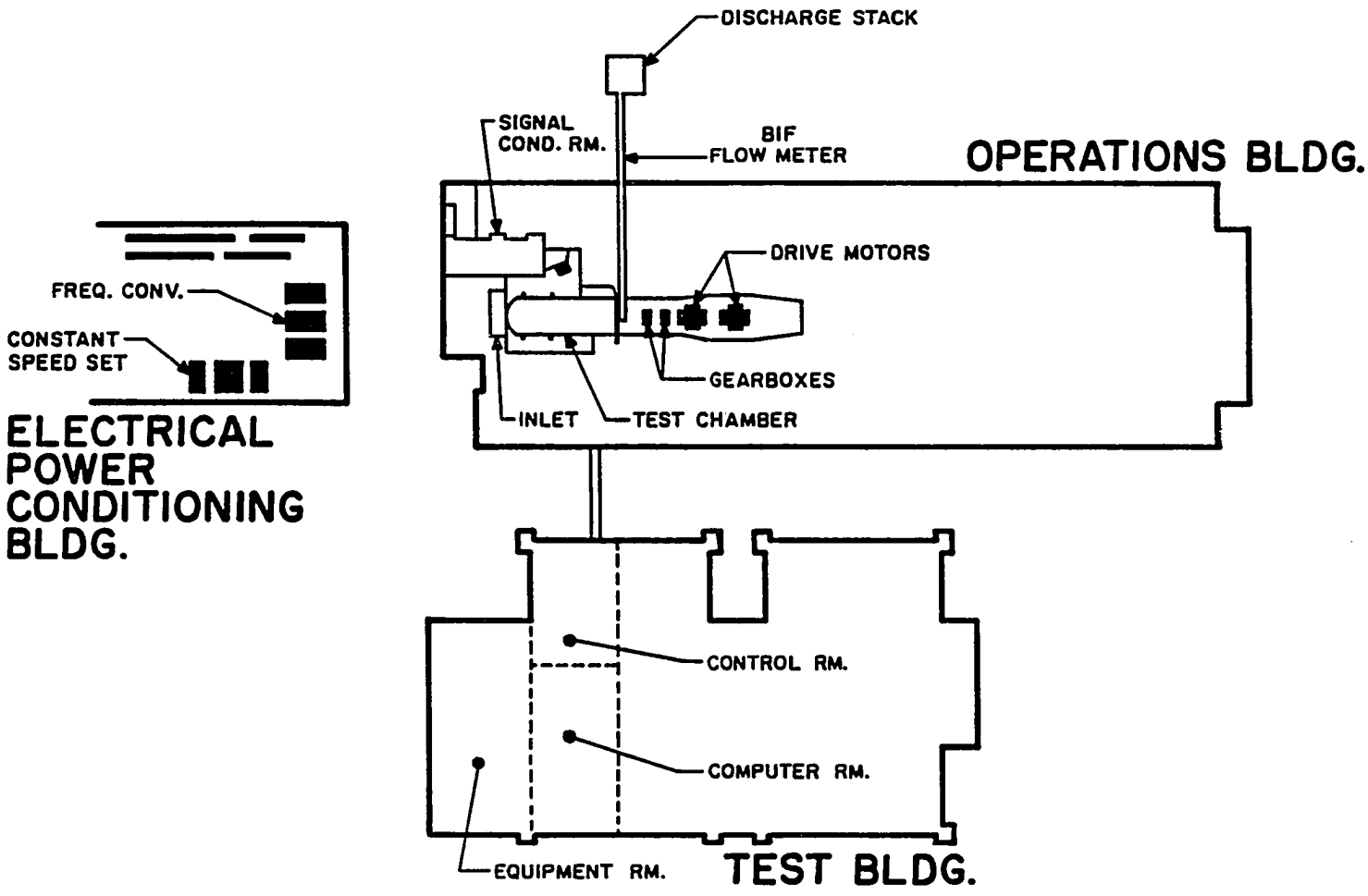

Figure 3.1 Compressor research facility

A. Facility Computer Control System

The four control computers (Modcomp Model# II/45) are designated as the facility control computers (FCC1 and FCC2) and the test article control computers (TAC1 and TAC2). The control computer configuration is shown in Figure 3.2. Each of the primary computers, FCC1 and TAC1, has a backup, FCC2 and TAC2, that shares tasks and executes a safe shutdown if the primary computer fails. The TAC computers accept input from the test operator through a supervisory computer (Modcomp Classic Model# 7860) designated the monitor computer. For the 10-stage compressor tests, inputs to the TAC computers included change requests for test article variable geometry, throttle valve, and bleed valves. The TAC computers initiated changes to the 10-stage compressor through feedback control logic algorithms. Position was sensed by three feedback potentiometers for each variable device on the test compressor. These changes were either preprogrammed as a function of test compressor speed or requested directly during the test program. FCC1 and FCC2 also receives input from the test operator through the monitor computer. These computers provide inputs to a

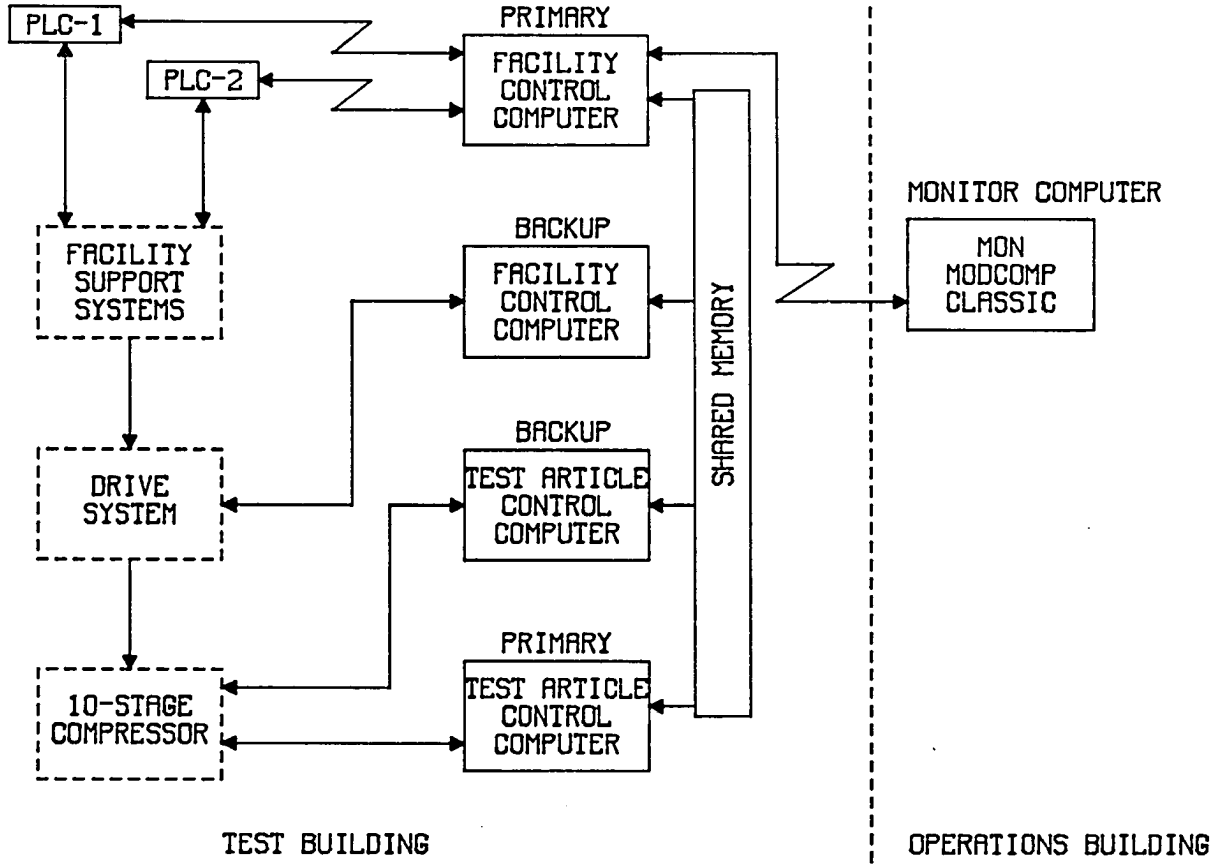

Figure 3.2 Control computer configuration

frequency converter system used to vary the frequency of the 60 Hz line current to change the speed of the synchronous drive motors. FCC1 also receives input on facility status through Allen-Bradley Model 1774 programmable logic controllers (PLC). If the status indicated by the controllers was outside of preset limits the FCC1 and FCC2 initiated appropriate automatic actions to bring the facility and the test compressor to a safe condition.

B. Facility Power Conditioning and Drive Systems

The facility power conditioning equipment consists of a 12,400 hp (9.25 MW) constant speed motor, direct current generator, direct current motor and a frequency converter. The 12,400 hp (9.25 MW) motor drives the direct current generator. Current generated by the DC generator is varied to change the speed of the direct current motor. The direct current motor drives a variable speed frequency converter. This frequency convertor changes the frequency of 60 cycle line power in order to change the speed of the 30,000 hp (22.37 MW) synchronous electric drive motors. A schematic of the power conditioning equipment is provided in Figure 3.3.

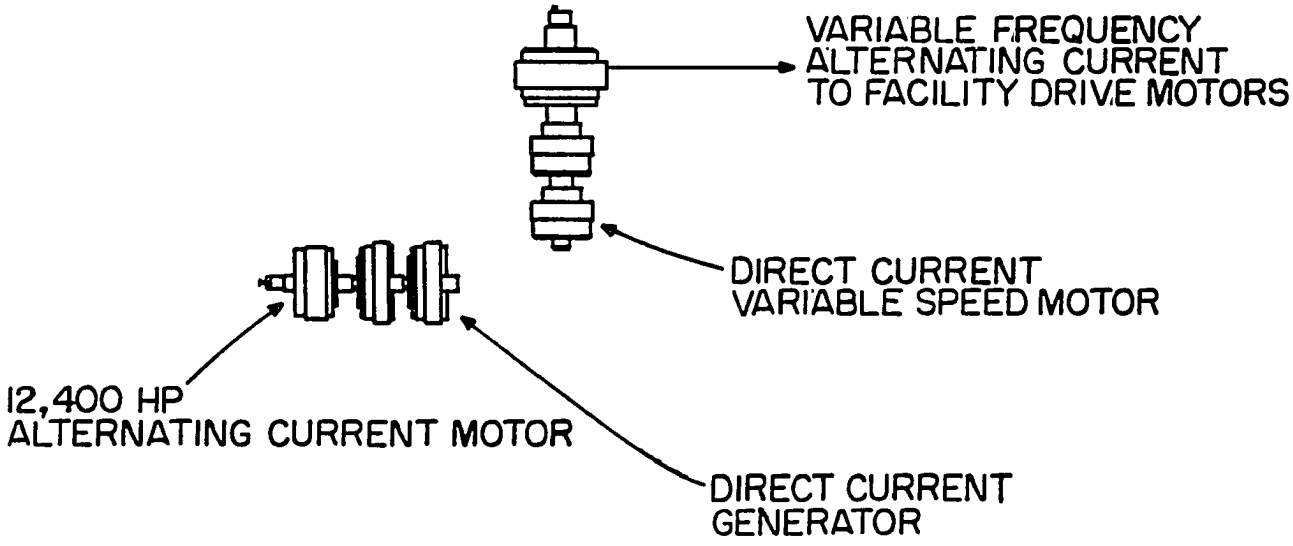

Figure 3.3 CRF power conditioning equipment

The power to drive a test compressor is obtained from a 30,000 hp (22.37 MW) synchronous electric drive motor. The test article speed ranges were provided through two speed increasing gear boxes. A speed range of 3,000 to 15,000 RPM was available for the 10-stage compressor tests. Test compressor speed changes are achieved by varying the frequency of the current supplied to the drive motors. This is accomplished from the control room by changing speed commands to the monitor computer. The drive configuration for the 10-stage compressor tests is shown in Figure 3.4.

C. Facility Flow Conditioning and Measurement Hardware

The 10-stage compressor was mounted, as shown in Figure 3.5, inside a 20.0 ft (6.096 m) diameter test chamber. Filtered air was drawn by the compressor from the atmosphere into the test chamber plenum through 5 inlet pressure control valves. These valves were not utilized for inlet throttling during the test as inlet pressures

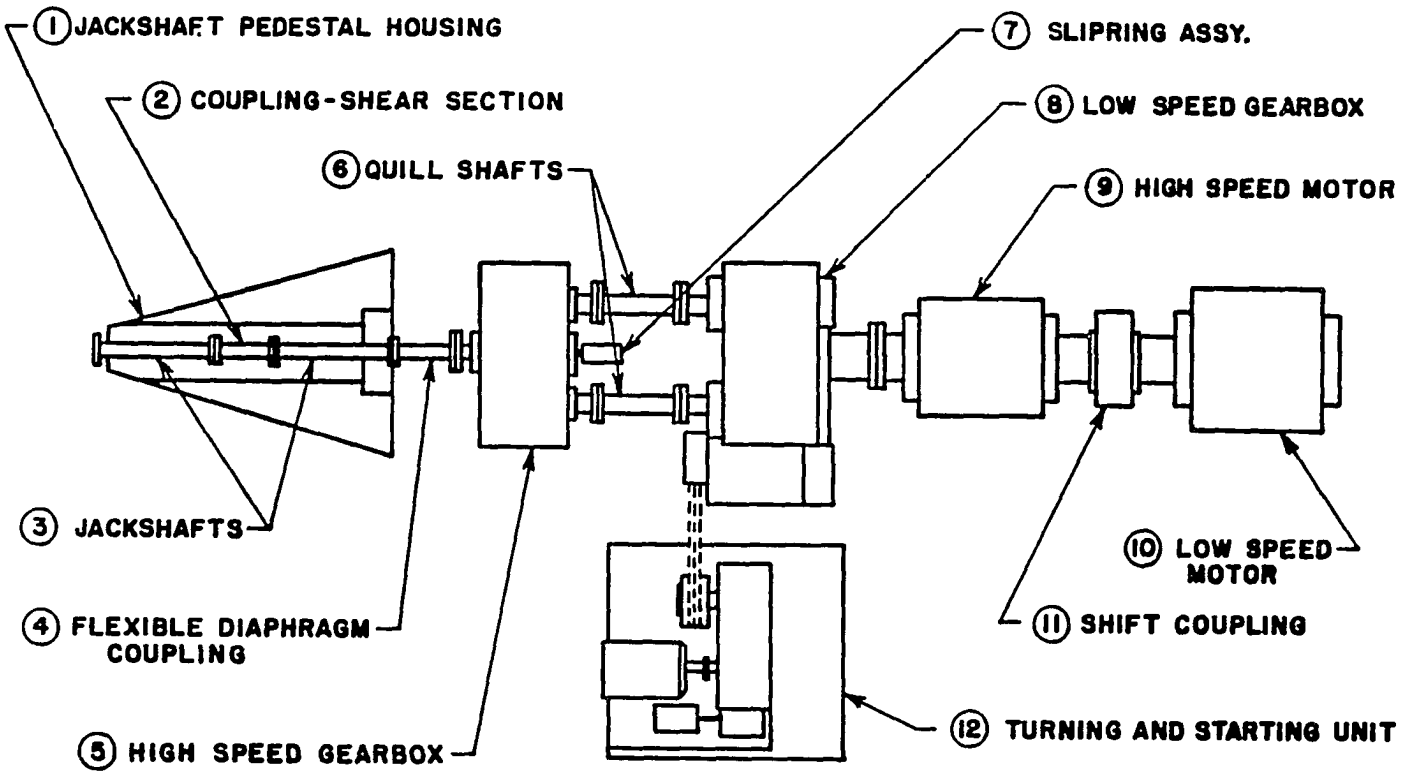

Figure 3.4 CRF drive configuration

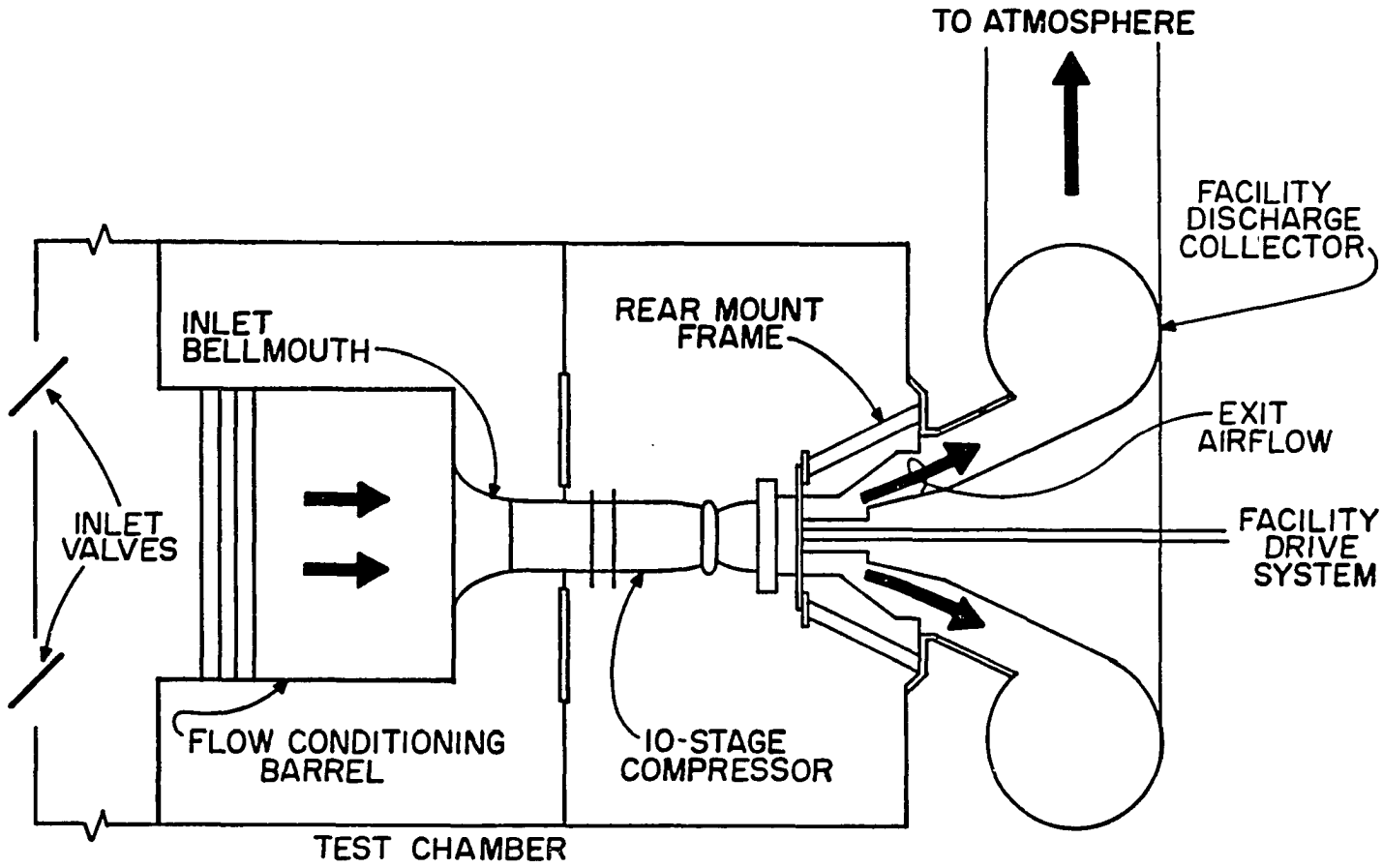

Figure 3.5 10-stage test compressor installation

below atmosphere were not required. Flow conditioning elements, shown in Figure 3.6, are mounted in the plenum to reduce the free stream turbulence intensity to levels below one percent. Each flow conditioning element consists of 2 screens, a honeycomb, and a support structure. A strut sting arrangement was positioned within the plenum upstream of the test compressor (see Figure 3.6). This strut allowed passage of pressurized air and freon to the compressor slip ring. It also provided a route from the test compressor for information from the front mounted slip ring.

Air was discharged from the test compressor discharge throttling valve to the atmosphere through a facility discharge collector and discharge ducting (see Figure 3.5). The 10-stage compressor exit flow was measured with a 19 in. (48.26 cm) throat diameter venturi positioned in the discharge ducting approximately 100 ft (30.48 m) (25 pipe diameters) downstream of the compressor exit. The 10-stage test compressor in-stall mass flow rate was determined with this venturi.

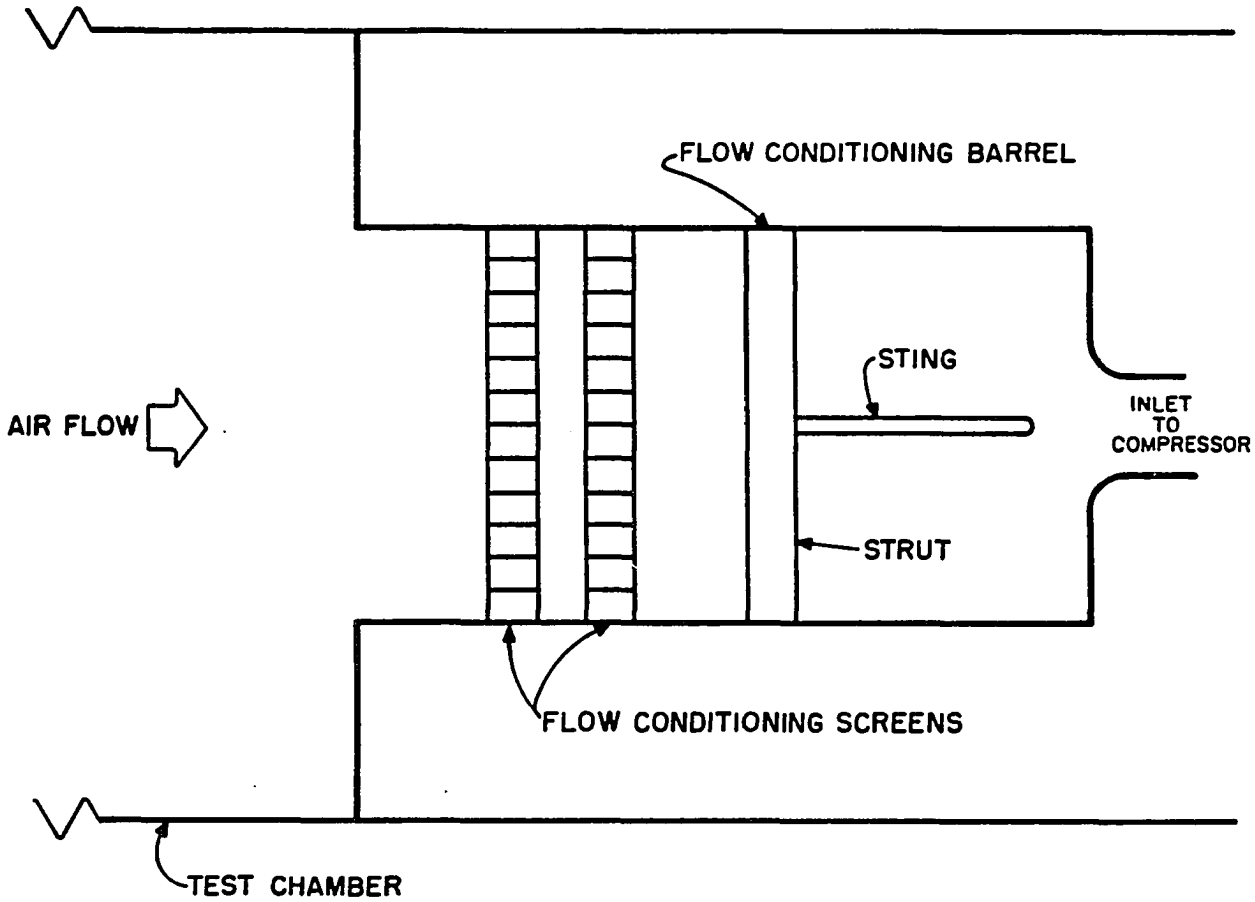

Figure 3.6 CRF flow conditioning screens

D. Facility Data Acquisition System

Data acquired from the test compressor were obtained by requesting the desired data type, time-averaged or close-coupled, from the control room through the monitor computer. The request was transferred from the monitor computer to the data acquisition computer (DAC). The DAC is a Modcomp Classic Model# 7860 computer located in the signal conditioning room. The DAC interfaces with the Preston high performance data acquisition system (HPDAS) which provides for excitation, signal conditioning and sampling of the time-averaged and close-coupled measurement transducers. The HPDAS acquires data from its analog-to-digital converter and associated multiplexer at a rate of 50,000 samples per second across 640 available channels. The digitized data in raw form were transferred through the DAC and the auxiliary computer to the main computer, an IBM 4341, in the computer room. The main computer's primary task is to transfer raw data to digital tape for post test reduction. As processing time was available during testing, the main computer converted samples of the data into engineering units for display on 6 IBM 3277 display terminals. A schematic of the CRF data acquisition system is shown in Figure 3.7. Further details about the data acquisition system for the 10-stage

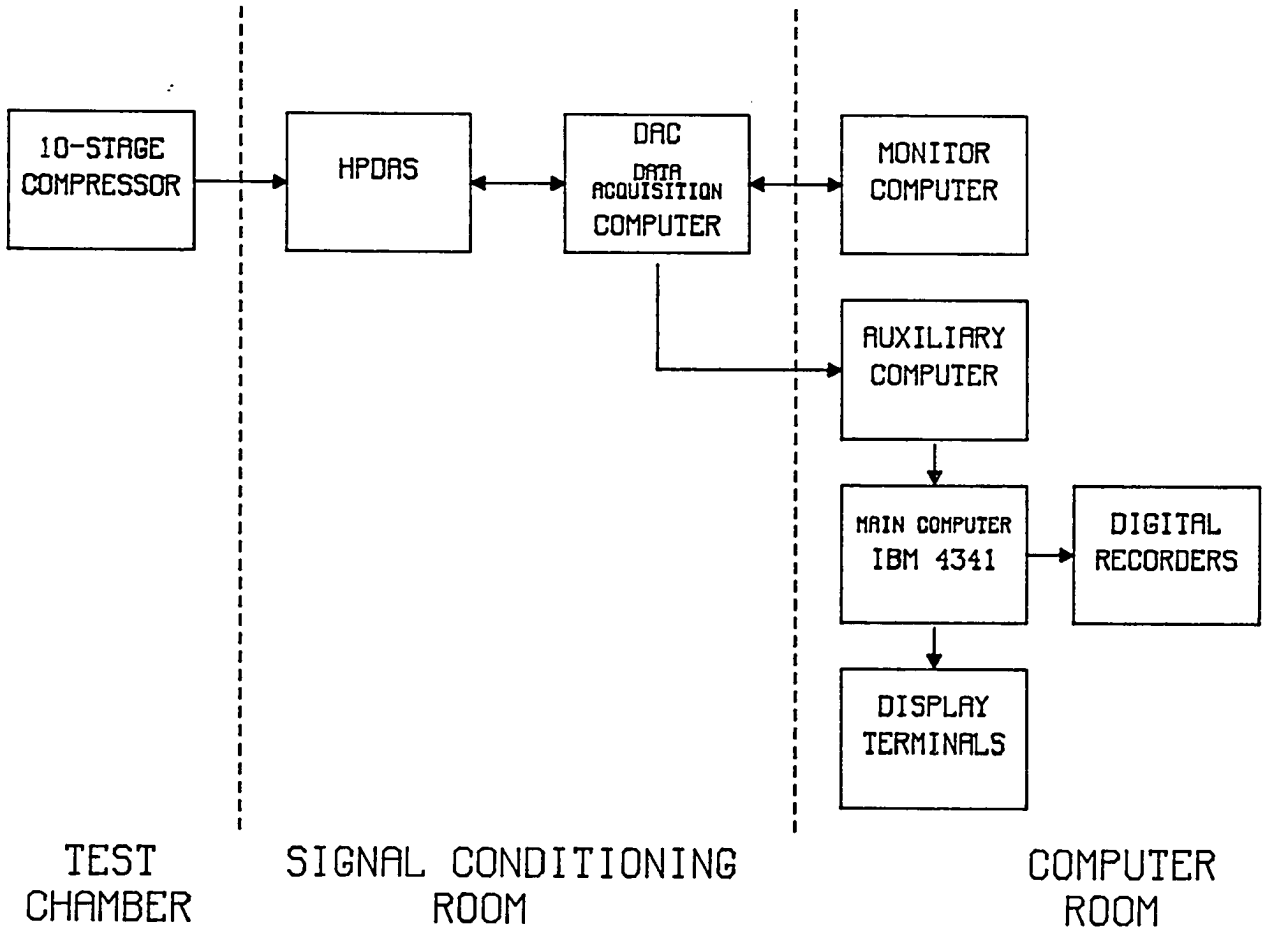

Figure 3.7 CRF data acquisition system

compressor test program are provided in Section V.

In addition to data acquisition, the HPDAS was utilized to obtain automatic zero calibration of amplifiers and pressure calibration of pressure transducers. Calibration standard pressures are provided from quartz pressure controllers. Temperature measurements are obtained through the HPDAS utilizing universal temperature reference (UTR) blocks as cold junction references for thermocouples. The UTR block temperature was determined with resistance temperature detectors. The UTR block temperature equivalent voltage was added to the thermocouple voltage to determine temperature.

Analog measurements were obtained through the facility analog recording system. High-response data from the test compressor were filtered and amplified by signal conditioners located in the signal conditioning room. These data were then displayed and recorded at the aeromechanics station in the control room. This station had 144 monitoring oscilloscopes for analog data monitoring during test periods. Analog recording was accomplished as required by manually starting the tape recorders located at the aeromechanics station in the control room.

IV. TEST COMPRESSOR

The compressor used in the test program was a 10-stage axial-flow high-pressure compressor from a modern high-performance aircraft gas turbine engine. To avoid confusion when comparisons are made with other test vehicles the compressor used in the test program will be referred to as the CRF test compressor or test compressor. The CRF test compressor had a design pressure ratio of 8.3, a design corrected speed of 10,913 rpm, and a design corrected mass flow of 54.44 lb/sec (24.69 kg/sec). The test compressor was a refurbished compression component of an aircraft gas turbine engine that was removed from service. The inlet and discharge sections of the test compressor were custom designed to interface the engine compression section to the CRF and still provide flow conditions similar to those within the engine. The CRF test compressor is shown in Figure 4.1. The description of the test compressor will be presented in two sections, compressor hardware, and compressor instrumentation.

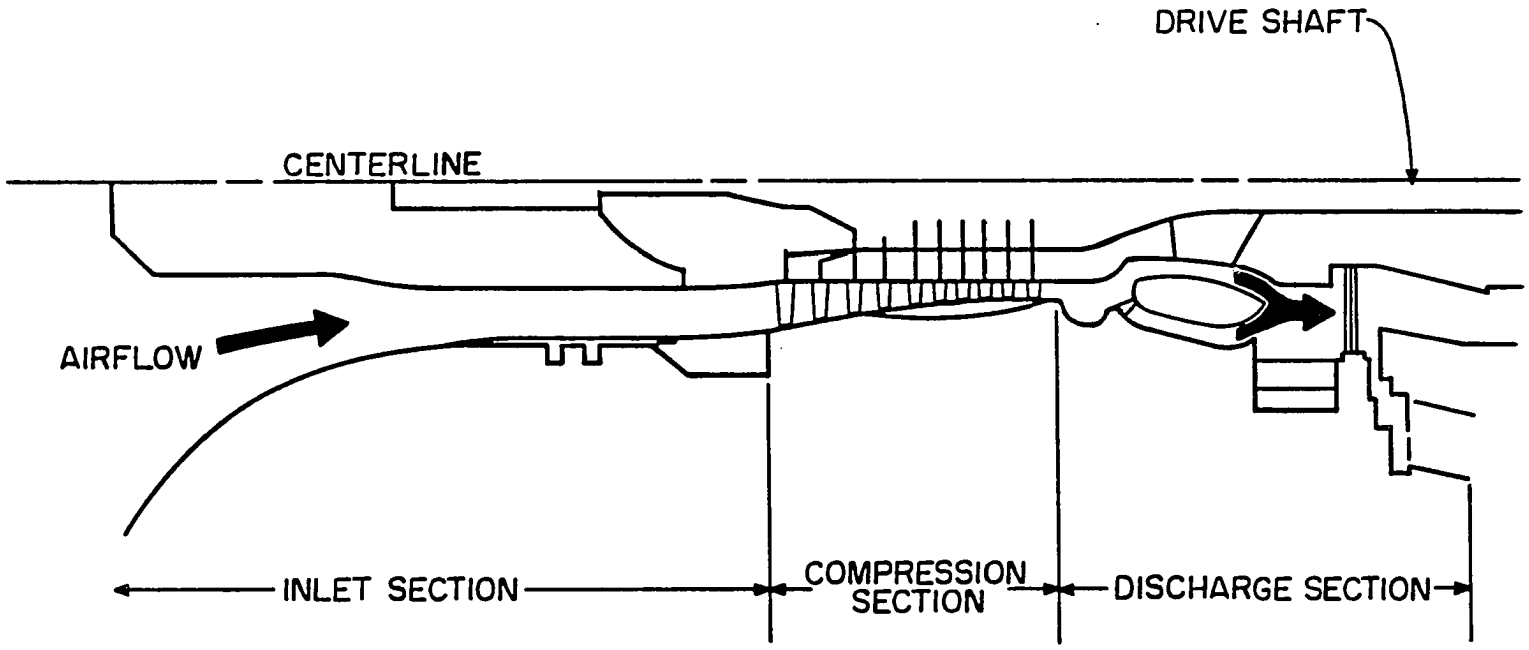

Figure 4.1 CRF 10-stage test compressor

A. Compressor Hardware

The CRF test compressor was designed with three primary sections, inlet, compression section, and discharge (see Figure 4.1). The inlet and the discharge were custom designed to interface with the CRF test chamber, while the compression section was from the aircraft gas turbine engine. Each section will be described individually below.

1. Inlet

The inlet to the test compression section was made up of four primary components, bellmouth, radial distortion screens, preswirl vanes, and inlet adapter duct. The inlet section is shown in detail in Figure 4.2. The bellmouth section consisted of a fiberglass long-throat ASME elliptical design bellmouth and an inner flowpath assembly. The inner flowpath assembly provided a smooth outer casing for the slip-ring assembly. Compressor rotor blade strain measurements were routed through the front mounted slip-ring. The radial distortion screen and preswirl vane assembly were attached to the exit of the bellmouth section. The screens and preswirl vanes were designed to create a radial distortion of total pressure and flow swirl angle that was similar to upstream fan exit distortion

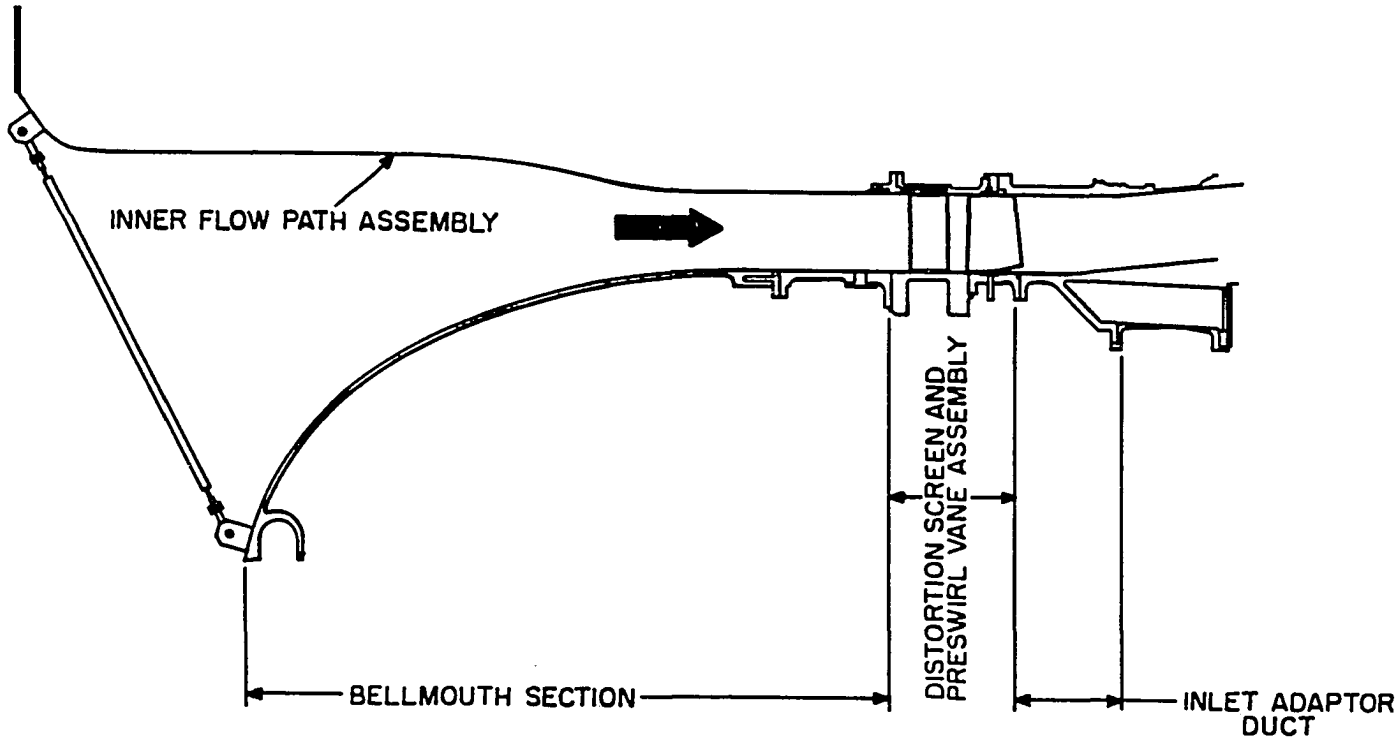

Figure 4.2 Test compressor inlet section

patterns in the engine at design speeds. Details about the screen and preswirl vane configuration can be found in Ref. [36]. The inlet adapter duct was designed to provide for a smooth transition for the flow into the compression section inlet.

2. Compression section

The test compression section was assembled from gas turbine engine hardware. The engine was designed with a three-stage fan, ten-stage high-pressure compressor, compressor bypass ducting, compressor diffuser section, combustor, turbine and exhaust nozzle. The 10-stage test compression section, as shown in Figure 4.3, consisted of the inlet case section, the high-pressure compressor, diffuser, and combustor section from the engine. The inlet case section from the engine, defined as the intermediate case, was designed with a flow splitter to split the fan flow between the engine high-pressure compressor and the bypass ducting. The splitter acted as the outer annulus flow path wall for the CRF test compressor, as bypass flow was not simulated. The splitter and front bearing housing were supported by 8 airfoil shaped struts evenly spaced around the circumference of the intermediate case. At the exit of the intermediate case, inlet guide vanes (IGV) were positioned to establish the air flow angle into the test

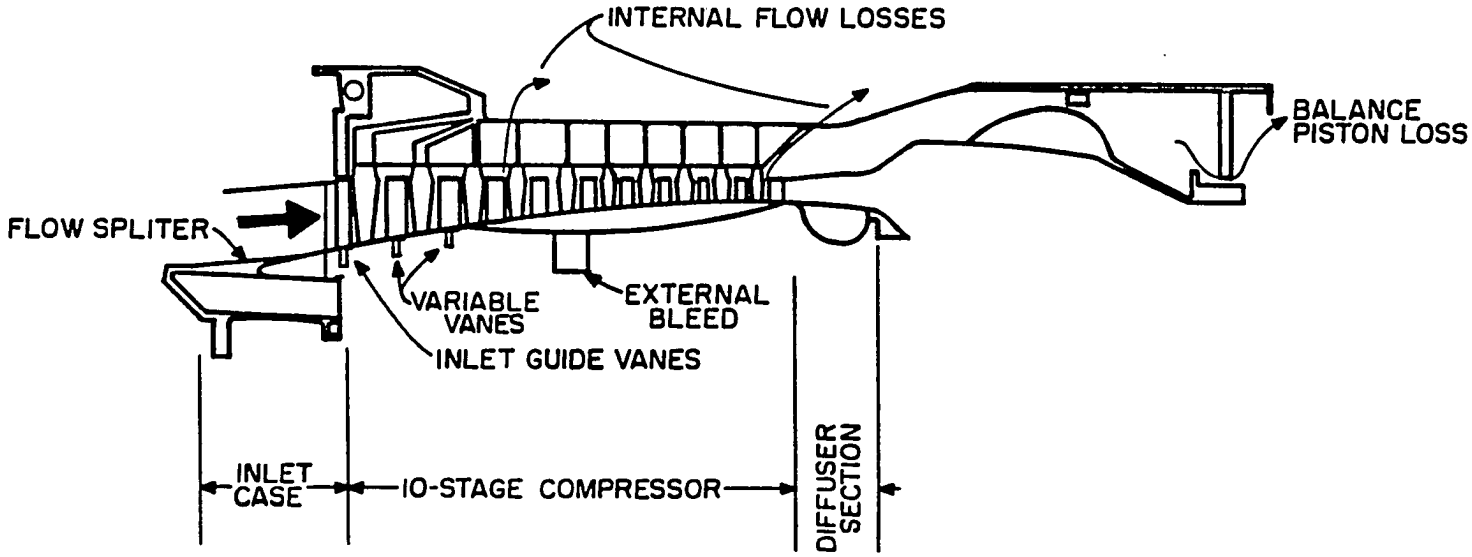

Figure 4.3 Test compressor compression section

compressor. Each vane was connected to a sync-ring assembly, thereby assuring uniform positioning of all vanes. The position of the IGVs was determined from three potentiometers connected to vane shafts. Their position was controlled through the test facility position control system described in Section III. Mechanical problems with two of the IGV potentiometer couplings required that control be determined from a single potentiometer.

The 10-stage compressor was positioned behind the inlet guide vanes beginning with the first stage rotor. The first and second stage stators were connected with a sync-ring assembly like the inlet guide vanes were. The sync-ring assemblies for the IVGs, stator one, and stator two could be varied independently of each other. The first and second stage stator vane positions were determined with three potentiometers each.

The test compressor had both internal and external airflow bleeds. The internal bleed flows were designed for cooling internal engine components. These bleed flow losses were from the third and tenth stages (see Figure 4.3). An additional internal flow loss existed due to the passive thrust balance system. Flow was lost across the seals between the rotating piston and stationary case. The thrust balance system was designed with a balance piston pressurized with discharge air, to overcome rotor thrust.

The flow from the internal stage bleeds and the balance piston were not actively controlled during the test. Flow losses were determined through calibrations of the orifices and seals, conducted prior to the test program. The flow lost overboard from these bleeds was on the order of five percent of the total flow. An external bleed flow valve from the fourth stage was actively controlled and the flow was measured through ASME standard nozzles. This bleed valve was held closed during the CRF 10-stage compressor test described here.

Figure 4.4 defines the stage description for the CRF test compressor. Stage performance is obtained from a stator-rotor combination rather than the conventional rotor-stator definition. Defining the stage characteristics from the stator-rotor performance was required because the instrumentation was mounted on stator leading edges. All stage characteristics presented follow the grouping of stator-rotor as defined in Figure 4.4.

3. Discharge

The discharge section was attached to the compression system exit. This assembly, shown in Figure 4.5, consisted of the diffuser, combustor, variable volume adapter, discharge valve, facility mounting hardware and discharge flow ducting. The diffuser and combustor were

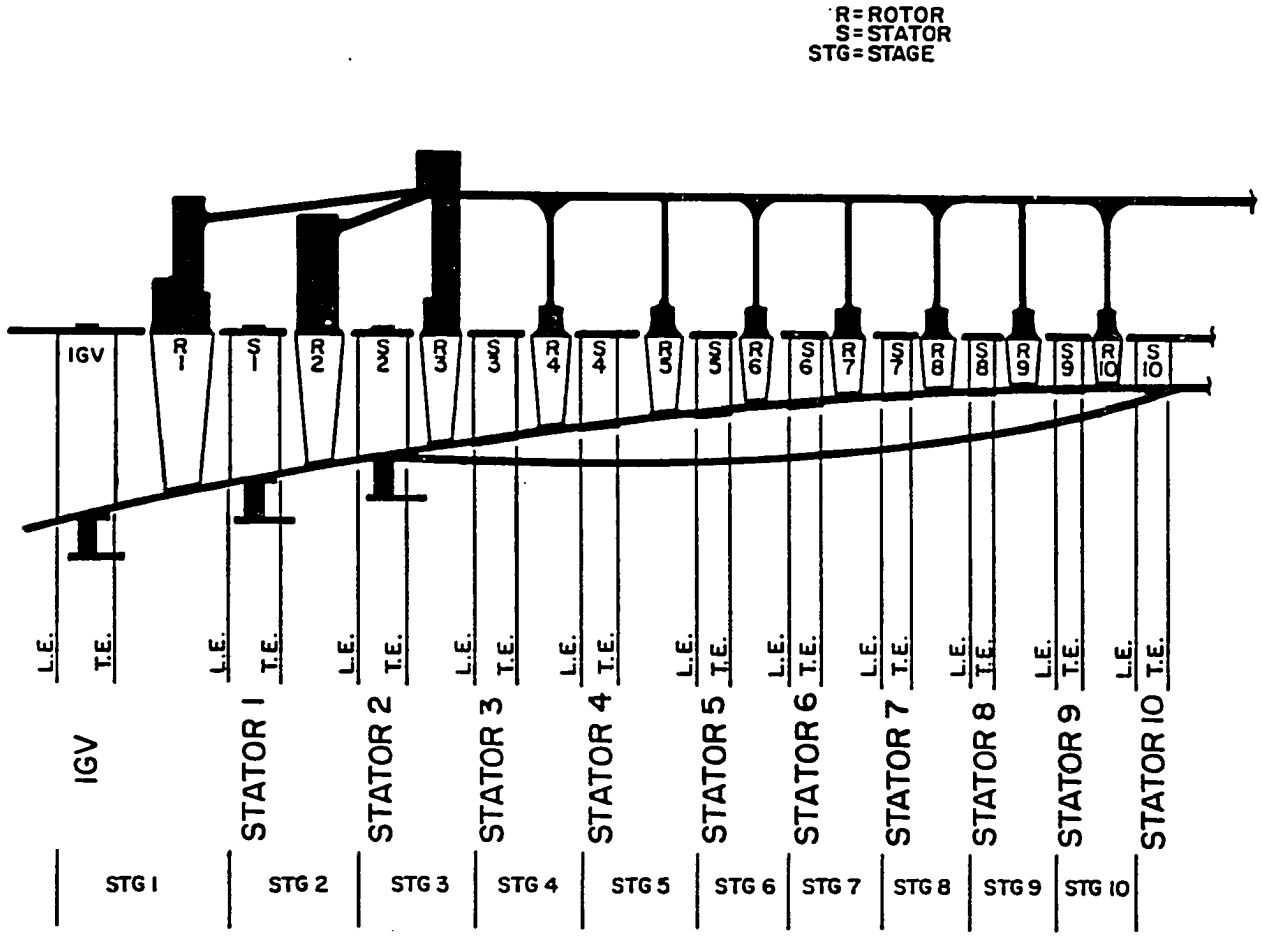

Figure 4.4 Test compressor interstage instrumentation axial locations

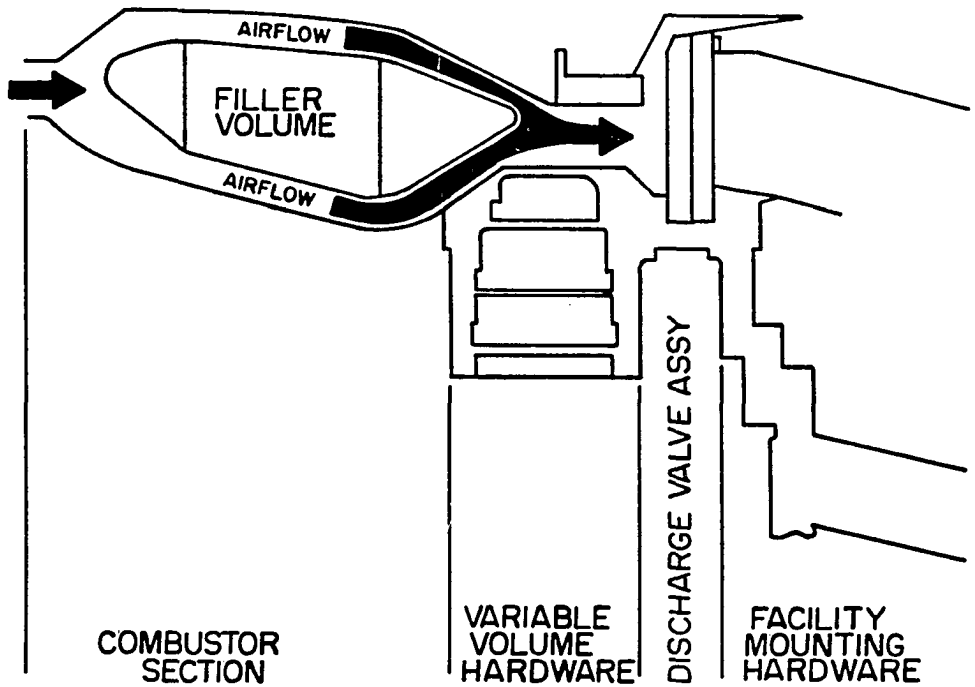

Figure 4.5 Test compressor discharge section

located downstream of the test compressor. The actual engine combustor was replaced with a filler volume. The filler volume was used to reduce the total exit volume of the test compressor to below 30% of engine nominal volume levels. The filler volume was designed to simulate the correct air flow path into the combustor, and reduce actual engine combustor volume level.

The variable volume adapter was designed to allow for exit volume changes without removing the CRF test compressor from the facility. The variable volume adapter in conjunction with the filler volume allowed for testing with volumes of nominal and $\pm$ 20 percent of the engine volume level. The discharge valve was connected to the variable volume adapter and was designed in a shutter type arrangement, with two parallel radially slotted plates. One plate was rotated relative to the other to change discharge flow areas. The valve position was measured by three linear potentiometers, and controlled by the facility discharge valve control system. The mounting hardware was designed to align the test compressor to the facility drive system and support one half of the total compressor weight. The remaining load was supported by a facility front mount ring at the front of the compression section. The exit air ducting was designed to route the compressor airflow from the discharge valve to the facility collection torus.

B. Compressor Instrumentation

The CRF test compressor was instrumented to obtain total pressures, static pressures, and total temperatures at inlet, interstage and exit locations. These measurements were obtained to document the performance of the test compressor. Instrumentation was also included for the measurement of compressor health parameters, such as oil flow rates and temperatures, compressor blade strains, and service cavity pressures and temperatures. Three data acquisition methods were utilized for performance measurements, time-averaged, close-coupled and high-response. They will be described in detail in Section VI. The performance instrumentation on the CRF test compressor will be described in the following subdivisions.

1. Inlet instrumentation

Inlet instrumentation was located at three different axial planes in front of the 10-stage compression system, namely, flow conditioning screen exit, bellmouth throat, and compressor inlet. These axial locations are shown in Figure 4.6. Table 4.1 summarizes the inlet measurements for the CRF test program. Forty-nine thermocouples were located at the exit of the flow conditioning screens in

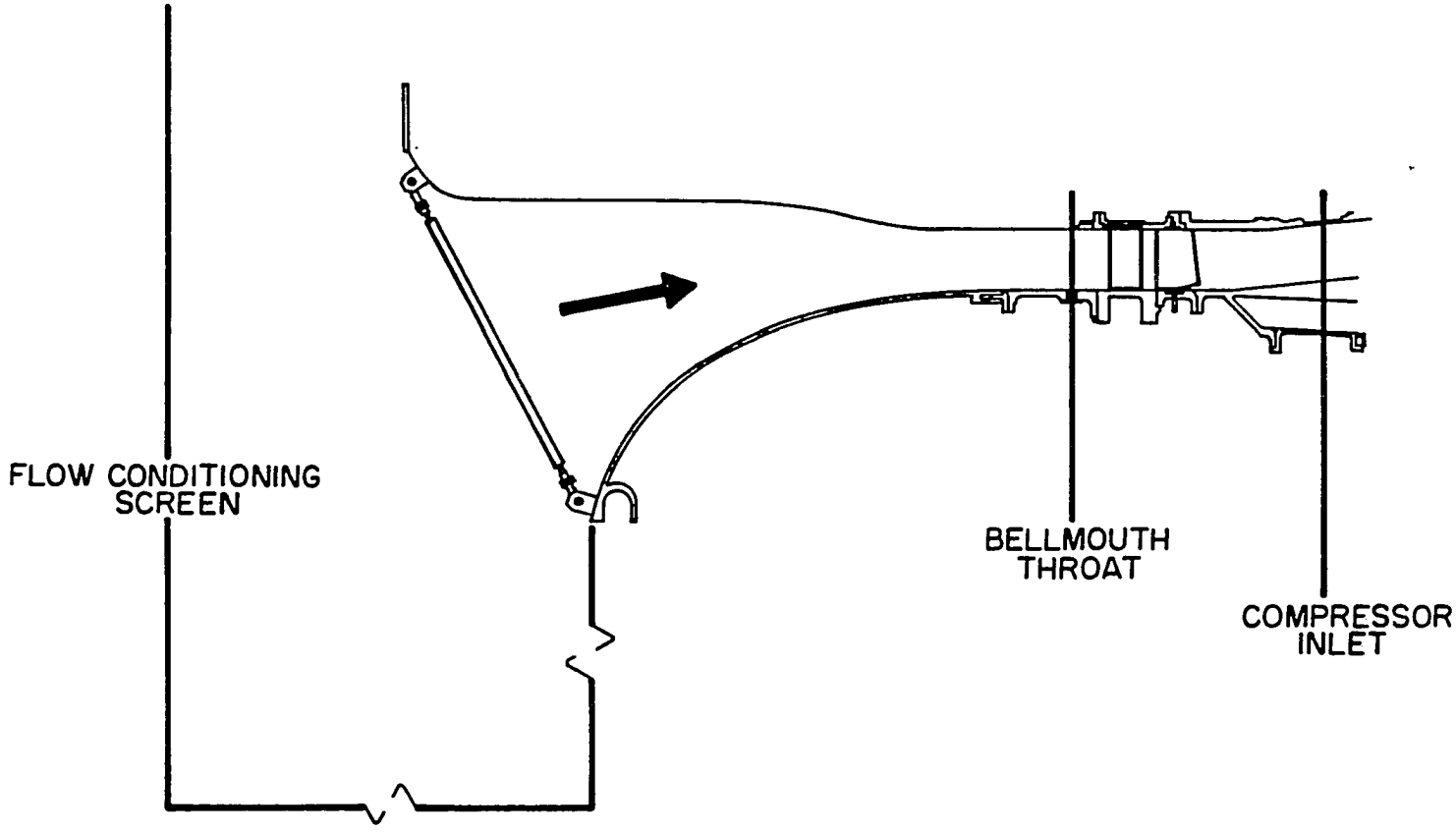

Figure 4.6 Test compressor inlet instrumentation axial locations

Table 4.1 Inlet instrumentation

AXIAL LOCATION	RADIAL LOCATION	PROPERTY MEASURED	#	ACQUISITION
EXIT OF FLOW CONDITIONING SCREEN	CEA[a]	TOTAL TEMPERATURE	49	Ta[b]
THROAT BELLMOUTH	OD[c]	STATIC PRESSURE	7	Ta, CC[d]
	ID[e]	STATIC PRESSURE	8	Ta, CC
	MS[f]	DIFFERENTIAL PRESSURE	4	Ta, CC
COMPRESSOR INLET	OD	STATIC PRESSURE	3	HR[g]
	OD	STATIC PRESSURE	8	Ta
	ID	STATIC PRESSURE	8	Ta

[a] Located at centers of equal area.

[b] Time-averaged type acquisition.

[c] Located at the outside diameter.

[d] Close-coupled type acquisition.

[e] Located at the inside diameter.

[f] Located at the midspan.

[g] High-response type acquisition.

Table 4.1 Continued

AXIAL LOCATION	RADIAL LOCATION	PROPERTY MEASURED	#	ACQUISITION
COMPRESSOR INLET	CEA	TOTAL PRESSURE	15	Ta, (10)CC[h]
	CEA	TOTAL TEMPERATURE	10	Ta
	MS	FORWARD FACING TOTAL PRESSURE	2	Ta, CC
	MS	FORWARD FACING TOTAL PRESSURE	3	HR
	MS	AFT FACING TOTAL PRESSURE	2	Ta, CC
	MS	AFT FACING TOTAL PRESSURE	3	HR
	MS	TOTAL TEMPERATURE	3	Ta, CC
	MS	COMPRESSOR SURGE	1	

[h] Number in parentheses represents portion of total number of measurements.

the inlet flow conditioning barrel of the facility as detailed in Appendix A, Figure 12.1. These measurements were used during tests to determine the inlet air flow temperature for bellmouth mass flow rate determination. Static pressures and total pressures were measured at a second axial plane, at the compressor bellmouth throat. Static pressure was measured directly from wall pressure taps positioned circumferentially, while total pressure was calculated from differential measurements between the static taps and kiel type total pressure probes. Transducers used for these measurements were located on the outside of the bellmouth within two inches of the measurement port.

Total pressure, static pressure and total temperature were measured at the third inlet axial plane located after the inlet screens and preswirl vanes. In addition to the static pressure taps and impact probes, two special probes were positioned at different circumferential locations. Each probe was designed for one total temperature measurement and four pressure measurements. A schematic sketch of one of these probes is shown in Figure 4.7. The four pressure measurements were obtained with two upstream facing impact tubes and two downstream facing impact tubes. High-response Kulite model# XCQ-25 pressure transducers were located inside one upstream and one downstream impact

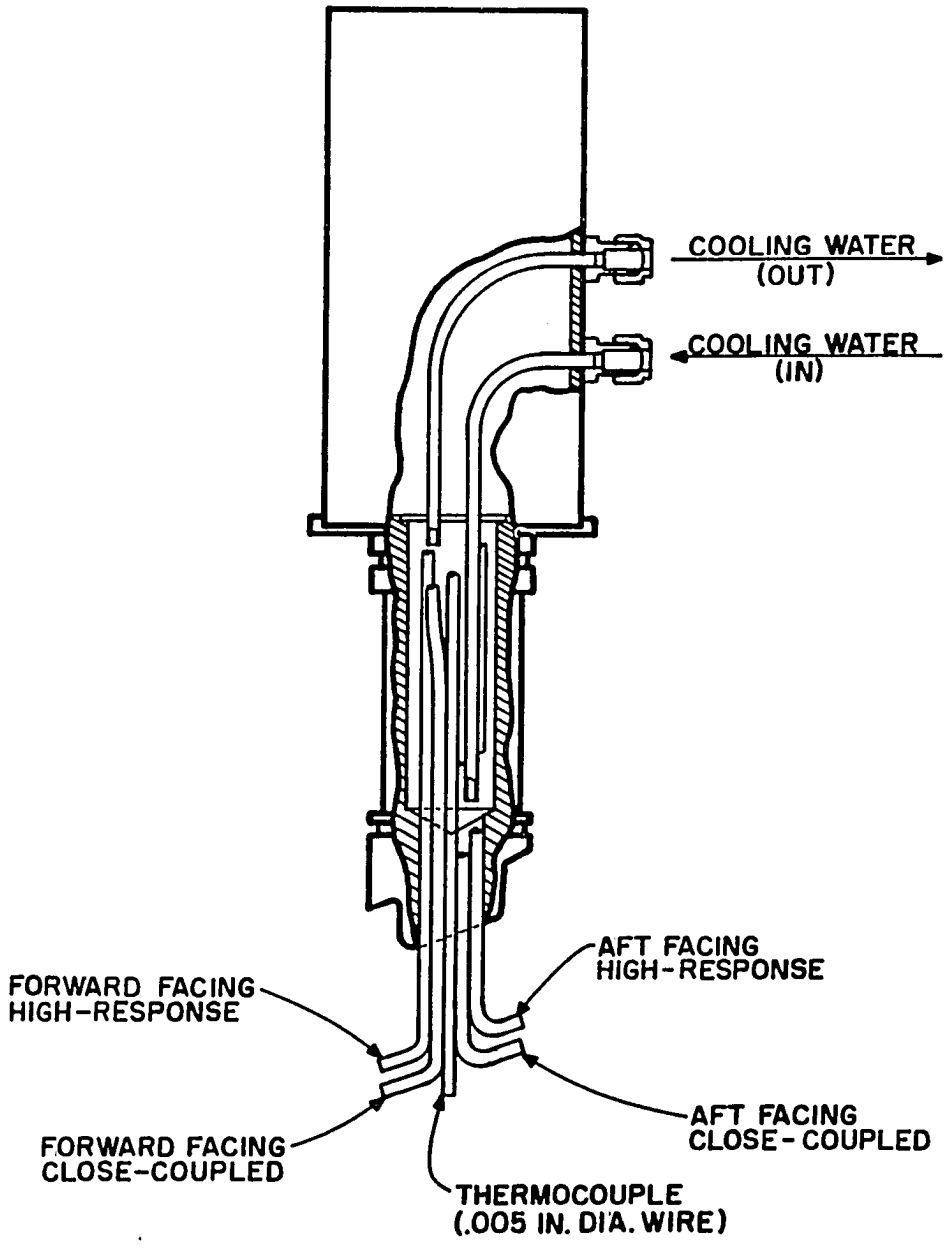

Figure 4.7 Forward and aft facing pressure probe

tube. The probe assembly was designed for water cooling of these transducers. The other upstream and downstream impact tubes were connected to transducers located on the inlet casing. The temperature sensor on the probe was a thermocouple made from 0.006 in. (0.152 mm) diameter chromel-alumel wire. In addition to these special probes, three high response pressure transducers were connected to static pressure taps positioned at different circumferential locations on the outer annulus wall. Detailed circumferential locations of inlet instrumentation at the bellmouth throat and the compressor inlet are provided in Appendix A, Figure 12.2.

2. Compressor system instrumentation

The compressor interstage instrumentation was located at the 22 different axial locations (see Figure 4.4). The total pressure, static pressure and total temperature instrumentation at each axial location are identified in Table 4.2. Total pressures at each axial location were measured from kiel head probes located at five different radial centers of equal annulus area. These sensors were located in pairs on the leading edge of the CRF test compressor stators; three on one stator blade and two on the adjacent blade. Temperatures were measured from a probe configuration similar to the total pressure design.

Table 4.2 Compressor instrumentation

AXIAL LOCATION	RADIAL LOCATION	PROPERTY MEASURED	#	ACQUISITION
INLET GUIDE VANE L.E.	ID	STATIC PRESSURE	3	Ta
	OD	STATIC PRESSURE	3	Ta
INLET GUIDE VANE T.E.	ID	STATIC PRESSURE	3	Ta
	OD	STATIC PRESSURE	3	Ta
STATOR 1 L.E.	OD	STATIC PRESSURE	3	HR
	OD	STATIC PRESSURE	1	Ta
	CEA	TOTAL PRESSURE	5	Ta
	CEA	TOTAL TEMPERATURE	5	Ta
STATOR 1 T.E.	OD	STATIC PRESSURE	1	Ta

Table 4.2 Continued

AXIAL LOCATION	RADIAL LOCATION	PROPERTY MEASURED	#	ACQUISITION
STATOR 2 L.E.	OD	STATIC PRESSURE	3	HR
	OD	STATIC PRESSURE	1	Ta, CC
	CEA	TOTAL PRESSURE	5	Ta, CC
	CEA	TOTAL TEMPERATURE	5	Ta
STATOR 2 T.E.	OD	STATIC PRESSURE	1	Ta, CC
STATOR 3 L.E.	OD	STATIC PRESSURE	3	HR
	OD	STATIC PRESSURE	1	Ta
	ID	STATIC PRESSURE	1	Ta
	CEA	TOTAL PRESSURE	5	Ta
	CEA	TOTAL TEMPERATURE	20	Ta
STATOR 3 T.E.	OD	STATIC PRESSURE	1	Ta
	ID	STATIC PRESSURE	1	Ta

Table 4.2 Continued

AXIAL LOCATION	RADIAL LOCATION	PROPERTY MEASURED	#	ACQUISITION
STATOR 4 L.E.	OD	STATIC PRESSURE	3	HR
	OD	STATIC PRESSURE	2	Ta (1)CC
	ID	STATIC PRESSURE	2	Ta (1)CC
	CEA	TOTAL PRESSURE	10	Ta (5)CC
	CEA	TOTAL TEMPERATURE	19	Ta
STATOR 4 T.E.	OD	STATIC PRESSURE	2	Ta (1)CC
	ID	STATIC PRESSURE	2	Ta (1)CC
STATOR 5 L.E.	OD	STATIC PRESSURE	3	HR
	OD	STATIC PRESSURE	1	Ta
	ID	STATIC PRESSURE	1	Ta
	CEA	TOTAL PRESSURE	5	Ta
	CEA	TOTAL TEMPERATURE	5	Ta

Table 4.2 Continued

AXIAL LOCATION	RADIAL LOCATION	PROPERTY MEASURED	#	ACQUISITION
STATOR 5 T.E.	OD	STATIC PRESSURE	1	Ta
	ID	STATIC PRESSURE	1	Ta
STATOR 6 L.E.	OD	STATIC PRESSURE	3	HR
	OD	STATIC PRESSURE	1	Ta,CC
	ID	STATIC PRESSURE	1	Ta,CC
	CEA	TOTAL PRESSURE	5	Ta,CC
	CEA	TOTAL TEMPERATURE	5	Ta
STATOR 6 T.E.	OD	STATIC PRESSURE	1	Ta,CC
	ID	STATIC PRESSURE	1	Ta,CC

Table 4.2 Continued

AXIAL LOCATION	RADIAL LOCATION	PROPERTY MEASURED	#	ACQUISITION
STATOR 7 L.E.	OD	STATIC PRESSURE	3	HR
	OD	STATIC PRESSURE	1	Ta
	ID	STATIC PRESSURE	1	Ta
	CEA	TOTAL PRESSURE	10	Ta
	CEA	TOTAL TEMPERATURE	20	Ta
	MS	TOTAL TEMPERATURE	2	CC,Ta
	MS	TOTAL PRESSURE	1	HR
STATOR 7 T.E.	OD	STATIC PRESSURE	1	Ta
	ID	STATIC PRESSURE	1	Ta

Table 4.2 Continued

AXIAL LOCATION	RADIAL LOCATION	PROPERTY MEASURED	#	ACQUISITION
STATOR 8 L.E.	OD	STATIC PRESSURE	3	HR
	OD	STATIC PRESSURE	2	Ta,(1)CC
	ID	STATIC PRESSURE	2	Ta,(1)CC
	CEA	TOTAL PRESSURE	10	Ta,(5)CC
	CEA	TOTAL TEMPERATURE	20	Ta
STATOR 8 T.E.	OD	STATIC PRESSURE	2	Ta,(1)CC
	ID	STATIC PRESSURE	2	Ta,(1)CC
STATOR 9 L.E.	OD	STATIC PRESSURE	3	HR
	OD	STATIC PRESSURE	1	Ta
	ID	STATIC PRESSURE	1	Ta
	CEA	TOTAL PRESSURE	5	Ta
	CEA	TOTAL TEMPERATURE	5	Ta

Table 4.2 Continued

AXIAL LOCATION	RADIAL LOCATION	PROPERTY MEASURED	#	ACQUISITION
STATOR 9 T.E.	OD	STATIC PRESSURE	1	Ta
	ID	STATIC PRESSURE	1	Ta
STATOR 10 L.E.	OD	STATIC PRESSURE	3	HR
	OD	STATIC PRESSURE	1	Ta
	ID	STATIC PRESSURE	1	Ta
	CEA	TOTAL PRESSURE	5	Ta
	CEA	TOTAL TEMPERATURE	5	Ta
STATOR 10 T.E.	ID	STATIC PRESSURE	1	Ta

The thermocouple was made from 0.010 in. (0.254 mm) diameter cromel-alumel wire which was routed from the probe location to outside the test compressor. Static pressures were determined from taps at inside and outside annulus wall locations at both the stator leading and trailing edges for each stage. All 10 stages were instrumented with high-response pressure transducers (Kulite Model# XTEL-190) connected to outside annulus wall static pressure taps. Three static pressures were located at different circumferential locations at every stator row leading edge. The circumferential spacing between the three ports was nonuniform to assist in stall cell speed and cell number characterization. In addition to the instrumentation described above, stages 4 and 7 were also each instrumented with a high-response pressure transducer connected to a kiel head probe located on a vane leading edge. The exact number and circumferential position details of the instrumentation at each axial location is available in Appendix A, Figures 12.3 through 12.13.

3. Discharge instrumentation

Instrumentation was located in the discharge of the test compressor at two axial locations as shown in Figure 4.8. Table 4.3 identifies the instrumentation at the exit of the compression section of the CRF test compressor. At

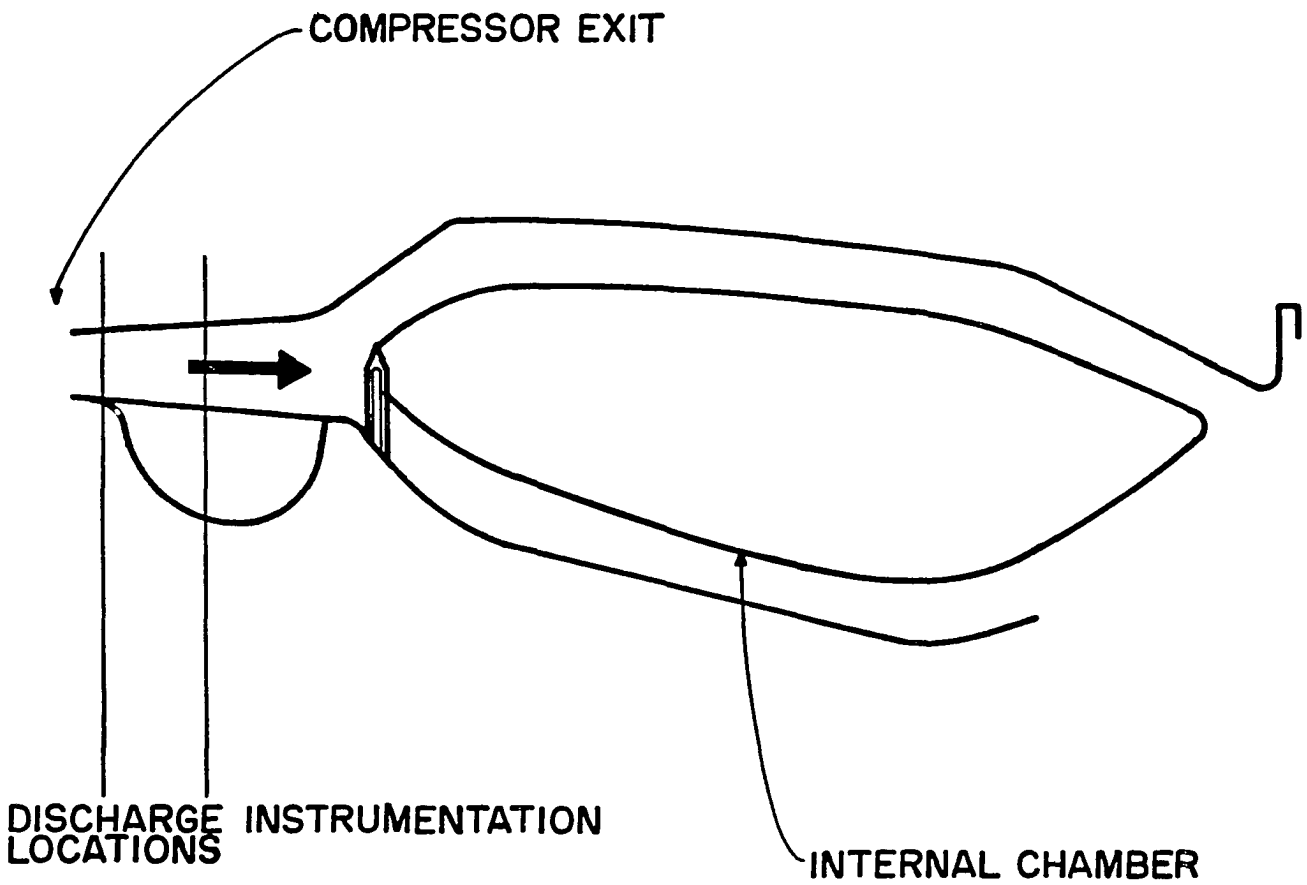

Figure 4.8 Test compressor discharge instrumentation axial locations

Table 4.3 Compressor discharge instrumentation

AXIAL LOCATION	RADIAL LOCATION	PROPERTY MEASURED	#	ACQUISITION
COMPRESSOR EXIT 1	OD	STATIC PRESSURE	7	HR
	OD	STATIC PRESSURE	8	Ta
	ID	STATIC PRESSURE	8	Ta
COMPRESSOR EXIT 2	CEA	TOTAL PRESSURE	15	Ta,(10)CC
	CEA	TOTAL TEMPERATURE	15	Ta
	MS	FORWARD TOTAL PRESSURE	2	HR
	MS	REARWARD TOTAL PRESSURE	2	HR
	MS	TOTAL TEMPERATURE	2	Ta,CC

the first axial position, static pressure taps were located at both the flow path inner wall and outer wall. In addition, 7 pressure taps at the outer flow path wall were connected to high-response pressure transducers. Total pressure and temperature sensors were located at the second axial location. Pressures and temperatures were measured at 5 different radial centers of equal annulus area. In addition, two forward and aft facing probes similar to those used at the compressor inlet section were positioned at different circumferential locations. The small span of the annular flowpath prohibited the positioning of two upstream and two downstream facing impact tubes. Therefore only a single upstream and downstream high-response measurement was available per probe. Temperature instrumentation on these probes were the same as those used in the inlet section. Detailed circumferential locations of the discharge instrumentation are shown in Appendix A, Figure 12.14.

V. DATA ACQUISITION CONFIGURATION

The data acquisition configuration and methods described in this section were utilized to measure time-averaged pressures and temperatures and unsteady pressure variations in the CRF test compressor operating in-stall. In-stall operation data are extremely difficult to obtain. Operating a high speed multistage compressor in a stalled condition is only accomplished with significant risk of damage to the test compressor and the facility. Therefore, prior to testing the compressor in-stall, a great deal of effort was spent to ensure that the desired information would be correctly acquired in a minimum amount of time. The data acquisition components and procedures necessary to yield data containing appropriate frequency, amplitude and phase information were obtained from the compressor operating in rotating stall are described in detail below. The specialized instrumentation and processing equipment used to obtain these data are also defined.

The pressure data acquired during the tests can be categorized as, high-response, time-averaged and close-coupled measurements. The design of the test article and the availability of transducers prohibited utilization of a single measurement method to obtain the desired

information. The test article was designed with limited access for positioning transducers near measurement locations. To obtain all of the desired unsteady information some measurements had to be made further away from the actual pressure port than others. Therefore, two methods to acquire unsteady pressure were devised. The measurement systems and setup procedures were defined to obtain time-averaged and time-resolved fluctuating pressure data at a fundamental frequency of approximately 50 Hz. Two independent systems were utilized to obtain the data. A primary benefit in using two separate measurement methods is that comparisons of common data could be made between the two systems to reinforce data validity and define frequency response limitations.

A. High-Response Pressure Measurements

The high-response system provided for higher frequency response than the close-coupled system which is described later. The higher frequency response resulted in a more accurate characterization of pressure fluctuations. A limitation of the high-response system was that the transducers involved were fragile and not well suited for placement in the test environment. Fifty-two channels were

designated as high-response measurement channels having a nominal frequency response of 200 Hz each. Approximately seventy high-response transducers were available for high-response measurements. This allowed for spares if sensors failed during testing. High-response channel data were acquired in analog form and stored on tape through FM recording. Data obtained through high-response measurement channel are identified in Table 5.1. Locations of the measurements within the compressor are shown in Figure 5.1. Details about radial positions of the high-response measurements are provided in Appendix A, Figures 12.2 through 12.14.

To obtain the desired frequency response with the high-response channels, special instrumentation ports were required because the test compressor was designed with a flow path outer wall that involved an inner and outer casing as shown in Figure 5.2. Transducers could not be practically mounted directly onto the outer wall of the inner casing. Thus, pressure measurements were made through a fixed length tube connected from the tap or probe pressure sensing hole to a boss located where access was possible through the outer casing. Access locations through the outer casing were limited by the large number of penetrations required, the compressor variable geometry, bleed ducts, and service locations. The length of this

Table 5.1 High-response measurements

MEASUREMENT LOCATION	MEASUREMENT TYPE	NUMBER
COMPRESSOR INLET OD	WALL STATIC PRESSURE	3
COMPRESSOR INLET	FORWARD FACING TOTAL PRESSURE	3
COMPRESSOR INLET	AFT FACING TOTAL PRESSURE	3
INTERSTAGE OD	WALL STATIC PRESSURE	30
INTERSTAGE	TOTAL PRESSURE	2
COMPRESSOR DISCHARGE OD	WALL STATIC PRESSURE	7
COMPRESSOR DISCHARGE	FORWARD FACING TOTAL PRESSURE	2
COMPRESSOR DISCHARGE	AFT FACING TOTAL PRESSURE	2

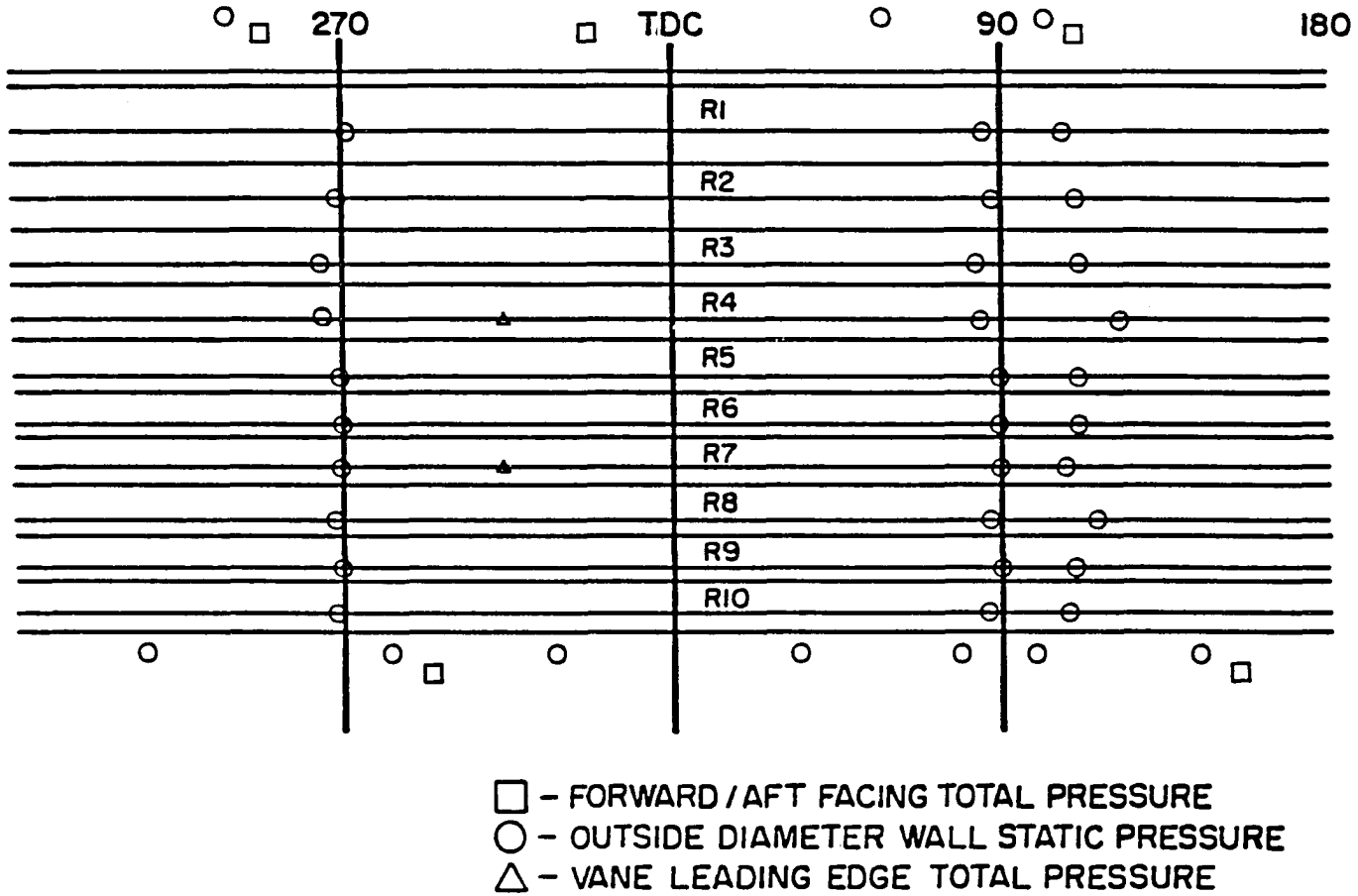

Figure 5.1 High-response instrumentation axial and circumferential locations

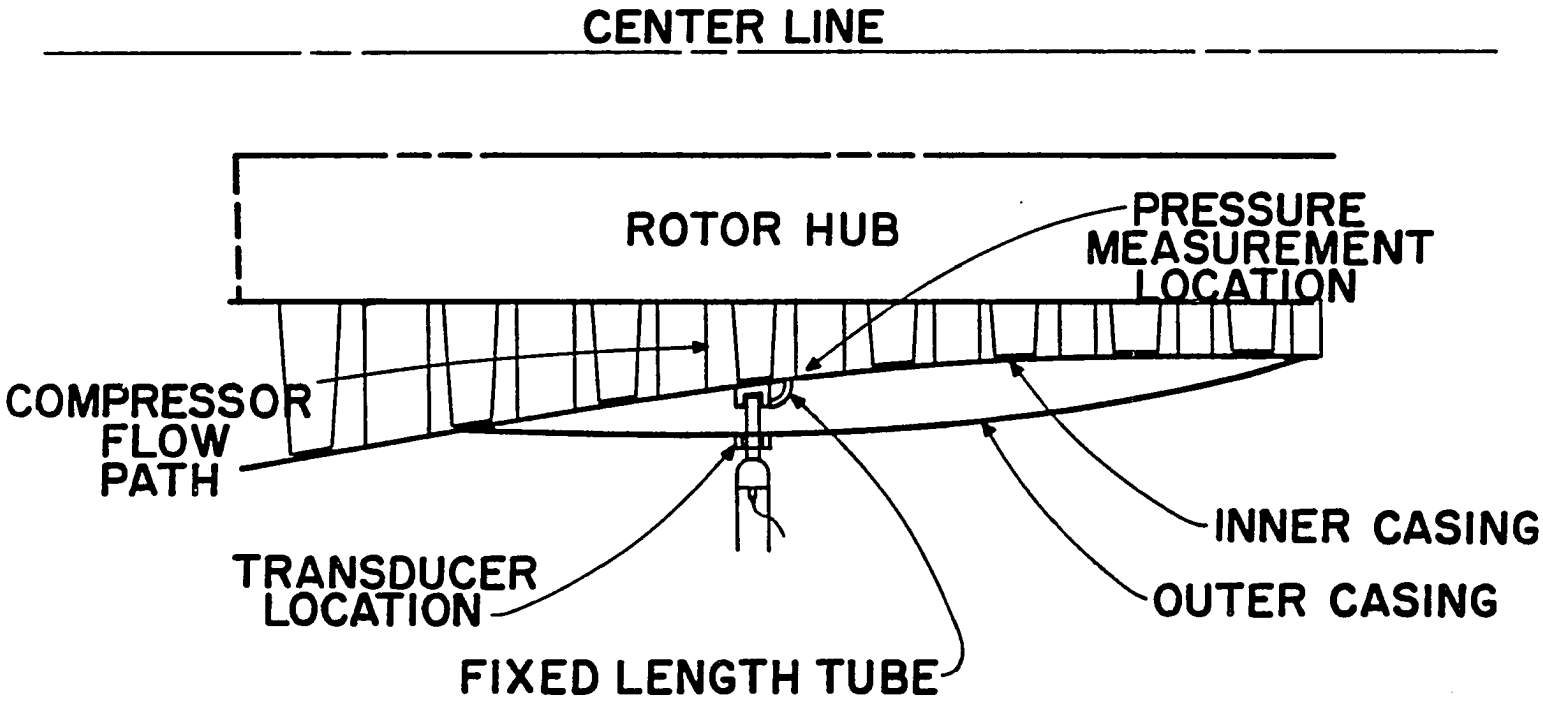

Figure 5.2 Test compressor inner and outer case configuration

tubing, 5.2 in. (13.21 cm), was based on the longest length required to get from the pressure sensing hole to the pressure transducer. The tube inside diameter was 0.020 in. (0.508 mm). Transducer cooling was used to ensure survival and stability of the pressure transducer for test article temperature levels over 250° F (121.1° C). For this purpose, a special cooling jacket surrounding the pressure transducer was designed. All measurements identified in Table 5.1 except those made at the compressor inlet were obtained with this tube configuration. For pressure measurements at the inlet to the compressor, tube lengths were minimized by locating these transducers directly above the measurement port. These tube lengths were appreciably less than 5.2 in. (13.21 cm).

Fluctuating pressure data acquired through small diameter tubing is subject to modification because of oscillatory resonance of the fluid contained in the tube. A computer algorithm was therefore used to model the effects of the tube and transducer volume on the pressure measurement. This algorithm was developed by Nyland et al. [37] of NASA. It utilizes a frequency response theory developed by Bergh and Tijdeman [38] to determine pressure amplitude ratio and phase angle as a function of frequency for a given set of conditions, tube length, volume, mean pressure, and temperature. Extensive tests were

conducted by Coleman [39] to verify the validity of the NASA algorithm for high-response pressure measurement application. Transfer functions were experimentally determined for several lengths of 0.020 in. (0.508 mm) inside diameter tubing over a frequency range of 0.0 to 200 Hz. Experimental results were compared with results from a system modeled using the algorithm. This comparison indicated that the algorithm could predict pressure amplitude response of the tube system to within 3 to 12 percent of the experimental value, while phase shift could be predicted to within 6 to 14 degrees. The more accurate results were obtained with the shorter tube lengths. Test results indicate that the algorithm can be reliably utilized for determining the transfer function, frequency and phase, of the fluctuating pressures for the high-response instrumentation used with the CRF test compressor.

The transducers used to convert the fluctuating pressures to voltage fluctuations were manufactured by Kulite (model XTEL-190). These transducers are capable of responding to frequencies up to 70 KHz with no appreciable amplitude modification. Transducer pressure ranges were based on predicted maximum pressures within the compressor for speeds up to 87% of the design corrected speed. The small size of the transducers made them ideal for measuring

pressures where minimal tube lengths are required. A transducer installed in the cooling jacket holder and mounted to the compressor boss is shown in Figure 5.3.

The high-response pressure data required special conditioning and recording methods to assure data integrity. The special conditioning and recording were required because of measurement transducer temperature sensitivity. Calibrations of the high-response transducers with pressures measured by temperature stable transducers were necessary to obtain absolute dynamic pressure levels. In addition, assurances were made to obtain desired measured frequency response and phase relationships as these were important to data analysis requirements. The measurement path for the high-response pressures is shown in Figure 5.4.

The transducer signals were amplified by Pacific (Model # 8255) signal conditioners. The signal conditioners provided the excitation voltage to the pressure transducers and handled transducer output signal filtering and amplification during unsteady pressure measurement. When obtaining dynamic pressure measurements, the modifications being made to the transducer output signal by the signal conditioner were carefully monitored. The conditioner provided for the option of transducer output voltage filtering at specified preset frequency

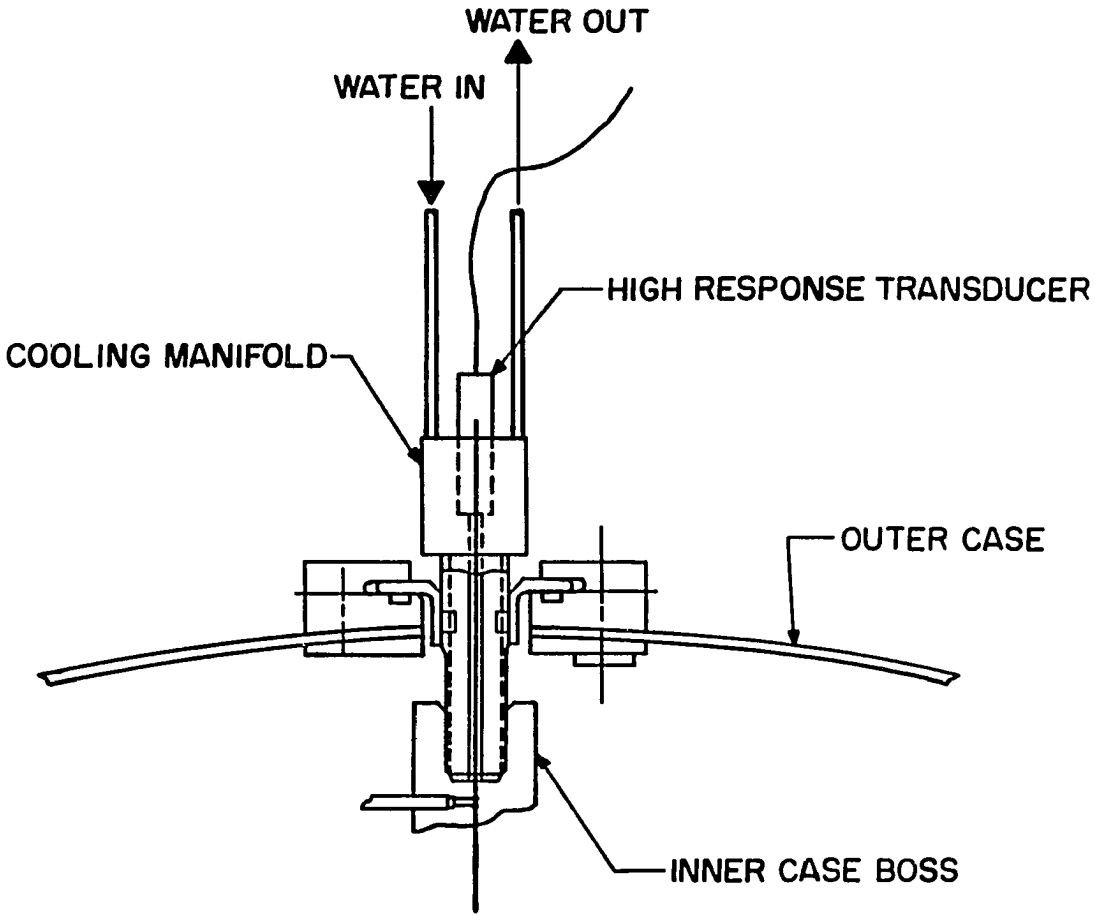

Figure 5.3 High-response pressure transducer measurement configuration

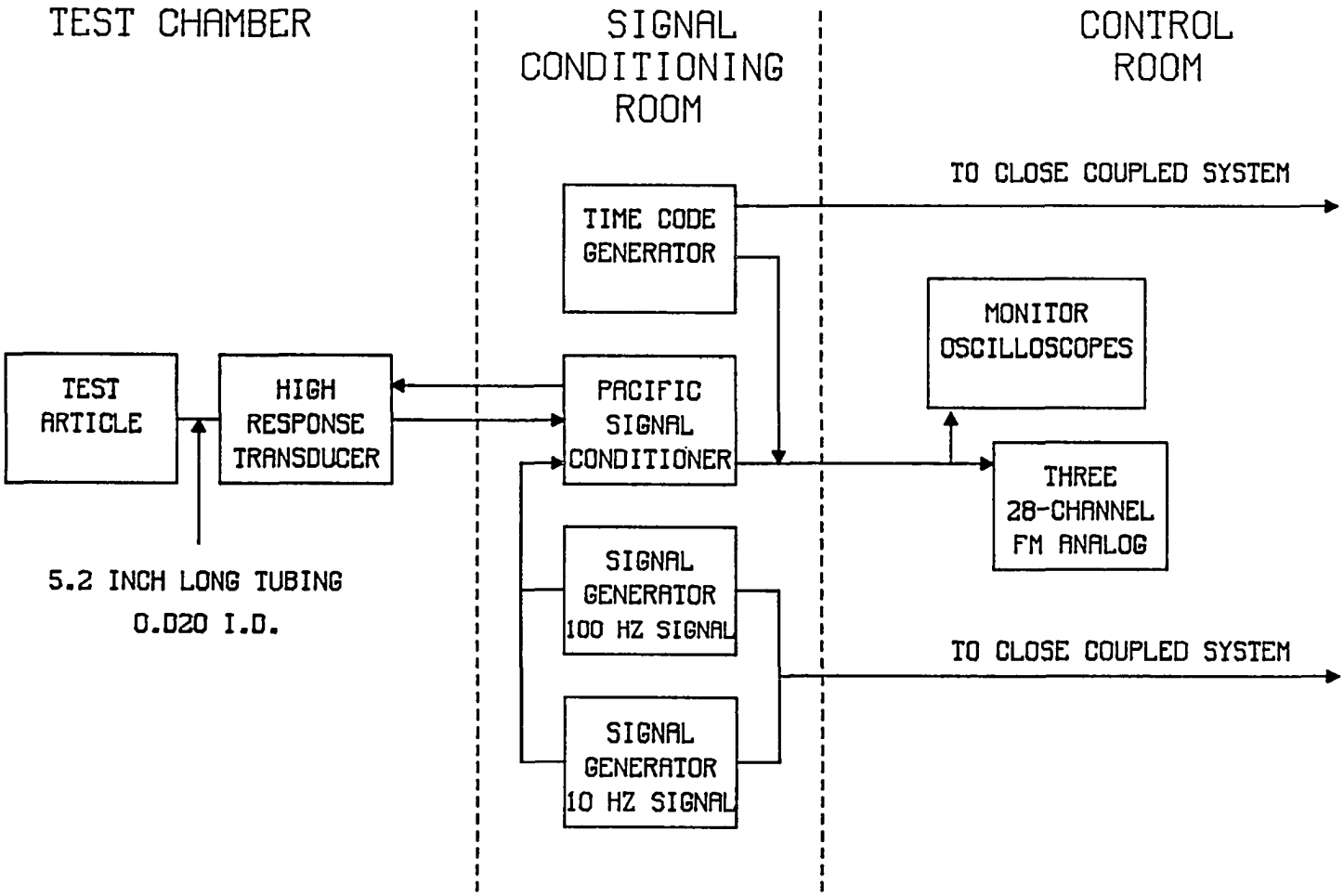

Figure 5.4 High-response data acquisition system schematic

levels of 10 Hz, 100 Hz, 1 KHz. The transducer output voltage was attenuated by a two pole Bessel filter with a -3 db attenuation at the filter frequency selected. The cutoff frequency for the compressor tests was set at 1 KHz to assure that the desired frequency response of 200 Hz would be obtained with the high-response channels. The amplifiers also allowed for either AC or DC coupling; the DC option was selected. The DC component of the pressure measurement was used as a single point calibration with a known steady state pressure level provided. With this on-line calibration the transducer zero offset drift from the bench calibration value could be determined. Thus compensation of bench calibration results due to temperature related zero offset variations could be accomplished during tests. This on-line calibration allowed absolute pressure levels to be determined during post test analysis. Since the amplifiers were DC coupled, each amplifier gain had to be set to avoid saturation of the amplifier by the DC component of pressure. Consideration was also given to setting the gain of each amplifier so as to avoid saturation of the recording devices involved.

The high-response pressure data were recorded on three 28-channel recorders (Datatape Model #2808). The recorders

were configured for frequency modulated (FM) recording. Each pressure channel was assigned to one channel of the recorder and data were recorded at a center frequency of 75.6 KHz. The frequency deviation was adjusted to allow for a maximum input signal level of 5 volts. The recorders were operated at a speed of 15 in./sec (38.1 cm/sec) which provided for a data frequency response of 10 KHz as defined in Ref. 40. This value of 10 KHz was well above the desired response of 200 Hz and minimized the amount of tape used. Where phase correlation was desired, data from the channels involved were placed on the same tape drive head stack. Thus, information from channels for which inter-channel phase information was desired was either placed on all even tracks or all odd tracks. This minimized the effects of phase error due to comparing data recorded on different head stacks.

After all options were selected on the signal conditioners and the recorders, a procedure to insure data level validity was carried out. This procedure required that three known pressures, up to the maximum range of the transducer, be applied to the transducer. The output of the transducer prior to amplification was recorded. Output from the signal conditioner and the output of the recorders were also documented. This procedure was completed for all channels of high-response data, and it assured that the

transducer output signal would not saturate the amplifier or the tape recorder during tests. The amplified transducer output signals were monitored on individual oscilloscopes during tests to assure that they did not drift to saturation levels because of instrument temperature fluctuations.

In addition to pressure data being recorded, other important information was also stored on tape. This additional information was recorded to assist in verification of accurate phasing of data during data analysis. One track of each tape was reserved for recording of an IRIG A time code. This time code allowed for timing resolution of 0.1 ms. Another track of each tape was reserved for recording of the tape drive servo signal. The servo signal is generated during tape operation and used during playback to set the playback speed. Any fluctuations in tape speed during recording was duplicated during playback. This minimized phase errors caused by differences between recording and playback speeds. A third track on each tape was used for recording of a standard signal. This standard signal was the sum of 10 and 100 Hz sine waves (see Patterson [41]). The standard signal is used during post test analyses, to assist in alignment verification when data is digitized from different tape decks. The standard signal is also

useful in comparisons of high-response and close-coupled data.

To assure data validity throughout the three-month test period involved, a fixed procedure, described below, was followed on every test day. This procedure was considered necessary to allow comparisons between data obtained during the first day of testing with data obtained on any other day of testing.

After allowing signal conditioners enough time to warm-up, a standard square wave signal was applied to the input of the amplifiers. This signal was recorded on the analog tape recorders and the amplitude of the signal was noted in a log book. The gain of each amplifier and the attenuation by each tape recorder were documented on each day of data acquisition. In addition, the frequency content of the summed sine wave was verified with a spectrum analyzer. The exact frequency content was recorded in a log book. This frequency content was compared to the frequency content of the digitized signal to validate the post test digitization process. The tape recorders were checked to verify that IRIG time was being recorded and could be decoded. At selected times during testing, the 10-stage compressor was brought to a fixed operating condition. This condition was set at a fixed speed and pressure ratio of the compressor. At this

"checkpoint" the DC output levels of the high-response pressure transducers were recorded. This information was utilized to identify the stability of each transducer. If a change in the output of the transducer was seen for a fixed pressure input it was noted. Transducer output stability was not a problem.

High-response pressure data were recorded during unsteady operation of the 10-stage compressor. Also, prior to compressor stall, high-response pressure data were recorded for post test calibration. The high-response transducers were calibrated with steady state time averaged pressure data obtained from a nearby physical location. With this information, transducer offset and sensitivity were determined for the test point just prior to the dynamic event of interest.

The uncertainty associated with the high-response measurements was determined from the uncertainty of the time averaged measurements (bias), as they were used as the calibration standard, and the precision error introduced by the measurement transducer, signal conditioning and recording devices. The method used to determine measurement uncertainties for the high-response and close-coupled data acquisition systems described in this

dissertation was defined by Abernethy and Thompson [42]. The bias and precision errors are combined using the following equation

$$U_m = \pm(B_m + t_{95} S_m)$$

where (B_m) are the bias errors and (S_m) are the precision errors associated with the measurement. The student T distribution (t_{95}) weighting factor is determined based on the number of samples taken to make up a measurement average. For time-resolved measurements such as the high-response and close-coupled measurements the student T value is 12 because only single samples are recorded. Time averaging thirty samples results in a weigthing factor of two. Based on Abernethy's uncertainty procedure, the high-response measurement uncertainties are ± 5 percent of transducer full scale. This uncertainty band is not unusual for measurements of this type.

B. Time-Averaged Pressure and Temperature Measurements and Close-Coupled Pressure Measurements

In addition to the analog signal recording of high response pressure data, time-averaged pressure and temperature measurements were acquired. Four hundred and one channels of pressure and temperature measurements were

used to obtained time-averaged steady-state properties. Close-coupled and time-averaged channel data were acquired through real-time digital conversion and stored on digital tape. The close-coupled and time-averaged system involved rugged and therefore suitable transducers for the test environment.

The measurement uncertainty of the time-averaged data was much improved over the high-response data uncertainty because of the very accurate calibration standards used and the large number of samples (30) that were averaged to make the measurement. The uncertainty of the time averaged pressure measurements was nominally ± 0.5 percent of transducer full scale. The time-averaged temperature uncertainty was ± 1.0°.

The time-averaged data were in digital form which allowed for easier conversion to engineering units. Frequency response for this system was limited by the on-line digitizing rate as well as pressure tube lengths. Thus, data aliasing had to be considered prior to acquiring data[1]. These measurements were digitized as part of the recording process. A time-averaged measurement is defined as an arithmetic average of 30 samples of each channel

[1]Aliasing results when digital sampling frequency levels are too low compared to the measured signal frequency levels. Frequencies in the measured signal above one half the sampling rate will appear as false lower frequencies on the digitized data. See Ref. 43.

sequentially at the maximum rate possible for analog to digital conversion. For 30 samples the length of time over which each individual channel average spans is 195 ms. The data obtained through time averaging were detailed in Tables 4.1,4.2 and 4.3.

A subset of the time-averaged measurements are close-coupled pressure and temperature measurements. Close-coupled measurements were obtained from the same transducers as were the time-averaged measurements. The difference between the two types, close-coupled and time-averaged, was the number of averages taken to make up the measurement and the rate the data were obtained. Because the close-coupled measurements involved only single samples the student T weighting factor is 12, resulting in a close-coupled pressure measurement uncertainty of $\pm$ 1.5 percent of full transducer range.

Eighty-six channels with a nominal frequency response of 70 Hz for pressures and 5 Hz for temperatures were designated as close-coupled measurement channels. The designation of close-coupled was selected to represent measurements that were acquired at a lower frequency than for the high-response measurements (200 Hz) but at a higher frequency than for the time-averaged measurements (0.5 Hz). Close-coupled means the transducer is as close to the pressure port as physically possible on the 10-stage test

compressor. The typical sensing tube length between the pressure port and the transducer was 20 in. (50.8 cm). Close-coupled temperatures of 5 Hz response were obtained with bead type thermocouples constructed from 0.006 in. (0.152 mm) diameter chromel-alumel thermocouple wire. The close-coupled measurements were scanned separately at a much higher rate than the time-averaged measurements and with no time delay between samples of close-coupled channels. A scan was defined as a single sample of all close-coupled channels simultaneously. This is the primary difference in time-averaged and close-coupled measurements. Transducers, signal conditioners and recording methods are the same for both forms of data acquisition. A schematic of these acquisition systems is shown in Figure 5.5.

The nominal frequency response for the close-coupled pressure measurements was 70 Hz and for the close-coupled temperature measurements, 5 Hz. Table 5.2 identifies those measurements of unsteady pressures which were recorded digitally. Detailed locations within the compressor are shown in Figure 5.6

Table 5.2 indicates that the close-coupled data included total pressure measurements at compressor inlet, interstage and exit locations and static pressure measurements at inlet and interstage locations. The

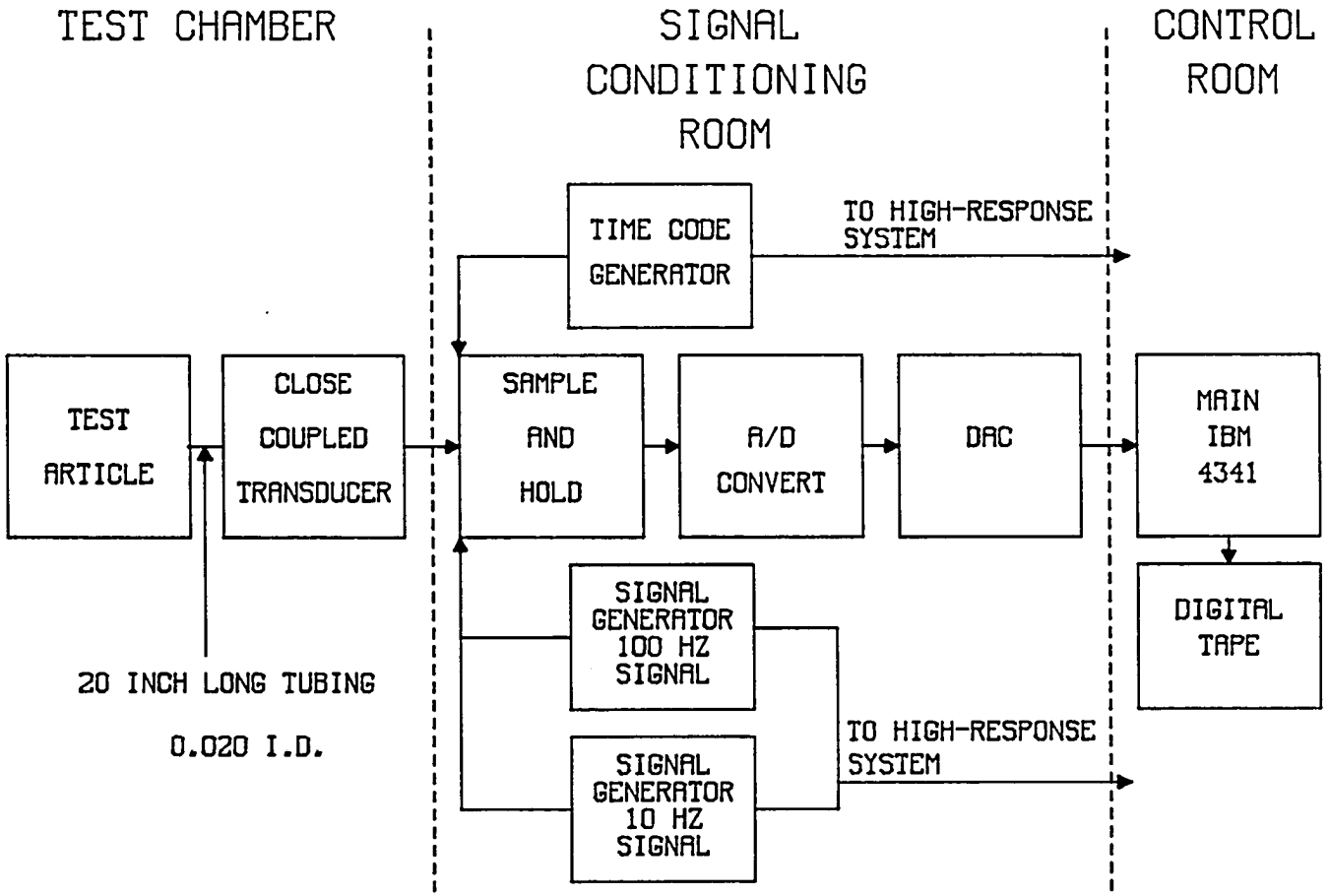

Figure 5.5 Close-coupled data acquisition system schematic

Table 5.2 Close-coupled measurements

MEASUREMENT LOCATION	MEASUREMENT TYPE	NUMBER
INLET BELLMOUTH ID	STATIC PRESSURE	8
INLET BELLMOUTH OD	STATIC PRESSURE	7
INLET BELLMOUTH	TOTAL TO STATIC DIFF.	4
COMPRESSOR INLET	TOTAL PRESSURE	10
COMPRESSOR INLET	FORWARD FACING TOTAL PRESSURE	2
COMPRESSOR INLET	AFT FACING TOTAL PRESSURE	2
COMPRESSOR INLET	TOTAL TEMPERATURE	3
INTERSTAGE VANE LE	TOTAL PRESSURE	20
INTERSTAGE VANE LE	TOTAL TEMPERATURE	4
INTERSTAGE ID	STATIC PRESSURE	6
INTERSTAGE OD	STATIC PRESSURE	8
COMPRESSOR DISCHARGE	TOTAL PRESSURE	10
COMPRESSOR DISCHARGE	TOTAL TEMPERATURE	2

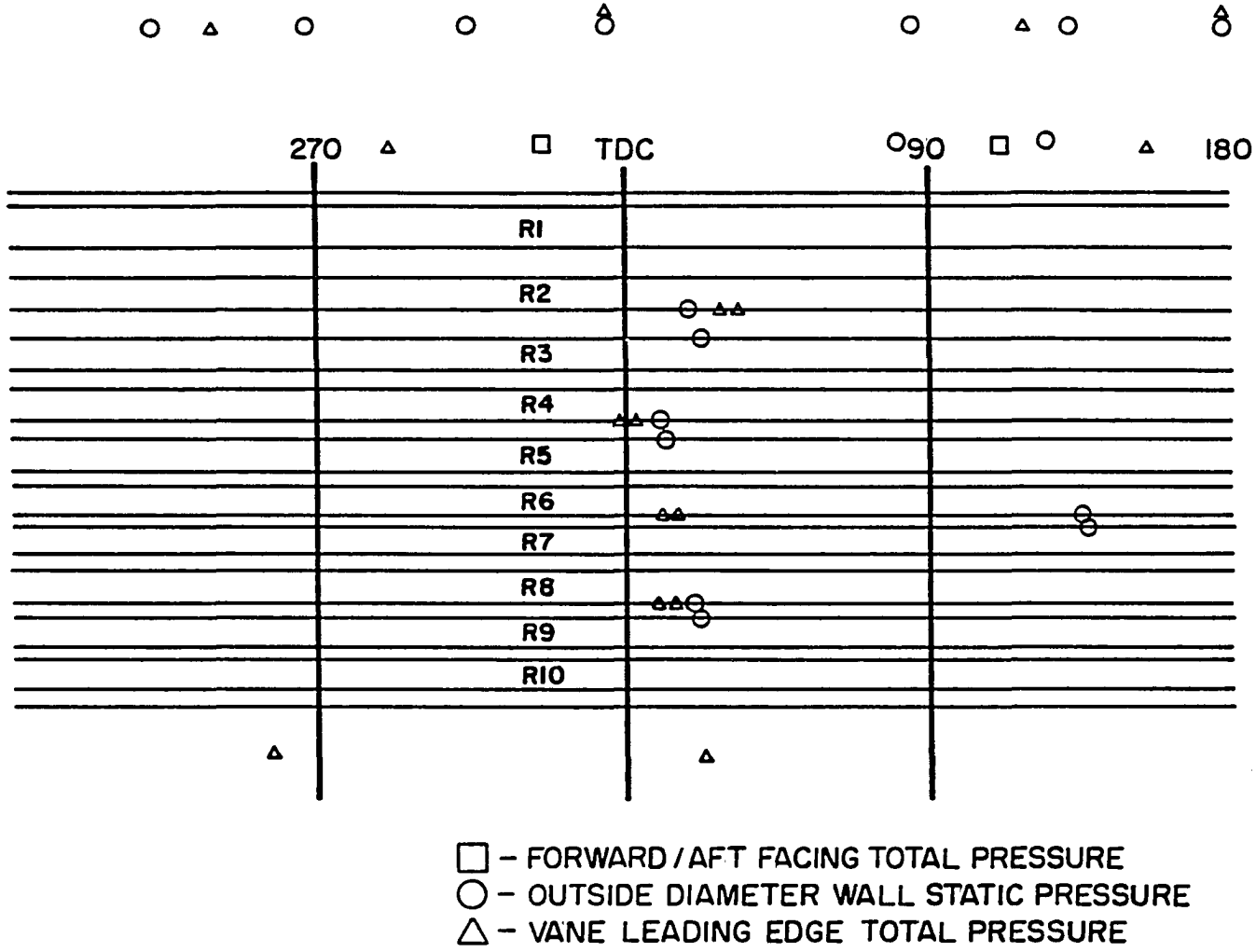

Figure 5.6 Close-coupled instrumentation axial and circumferential locations

close-coupled data obtained during the 10-stage compressor tests described in this dissertation were similar to those described by Hosny et al. [1] for their in-stall test of the GE/NASA Energy Efficient Engine compressor. In the tests described by Hosny and Steenken [17], measurements were made at the compressor inlet and exit with rakes that allowed transient mass flow rate to be determined. Also, static pressure taps at inlet, exit and interstage locations in their compressor were used. In addition to the type measurements described by Hosny and Steenken, close-coupled measurements of interstage total pressures in the CRF 10-stage compressor test described in this dissertation were obtained at five different radial immersions in 4 different stages. This interstage total pressure information is essential for characterizing the unsteady pressures that occur within a compressor during rotating stall operation. Data obtained from these locations were used in the validation of an analytical multistage compressor model developed by Davis [44]. These data were also used to determine the axial extent of a rotating stall cell within the 10-stage test compressor. In addition, the interstage total pressure measurements obtained at different immersions and the inside diameter (ID) static pressure data were useful for determining the radial extent of the stall cell related pressure

disturbances. Measurement of the parameters described in Table 5.2 provide the information necessary to further the understanding of the in-stall performance of a multistage compressor.

As with high-response measurements, assurances were made with the close-coupled pressure measurements to obtain an appropriate frequency response. The tube length for each close-coupled measurement was recorded. The nominal tube length was 20 in. (50.8 cm) and each tube had an inside diameter of 0.02 in. (0.508 mm). The algorithm described in Ref. [39] suggests that the frequency response of the transducer tube system is affected by the temperature and pressure of the air within the tubes. The mean pressure within the tube during pressure measurement is known and therefore can be correctly modeled. The temperature in the measurement tubes is not known. Therefore its effect must be determined. The results of a study of temperature effects on pressure attenuation are shown in Figure 5.7. In addition errors in phase angle were also determined by this algorithm as shown in Figure 5.8. These results indicate that care must be taken in interpretation of the close-coupled results. Direct comparisons with the high-response measurements were used to determine the attenuation effects on the close-coupled measurements. Knowing these effects resolves the question

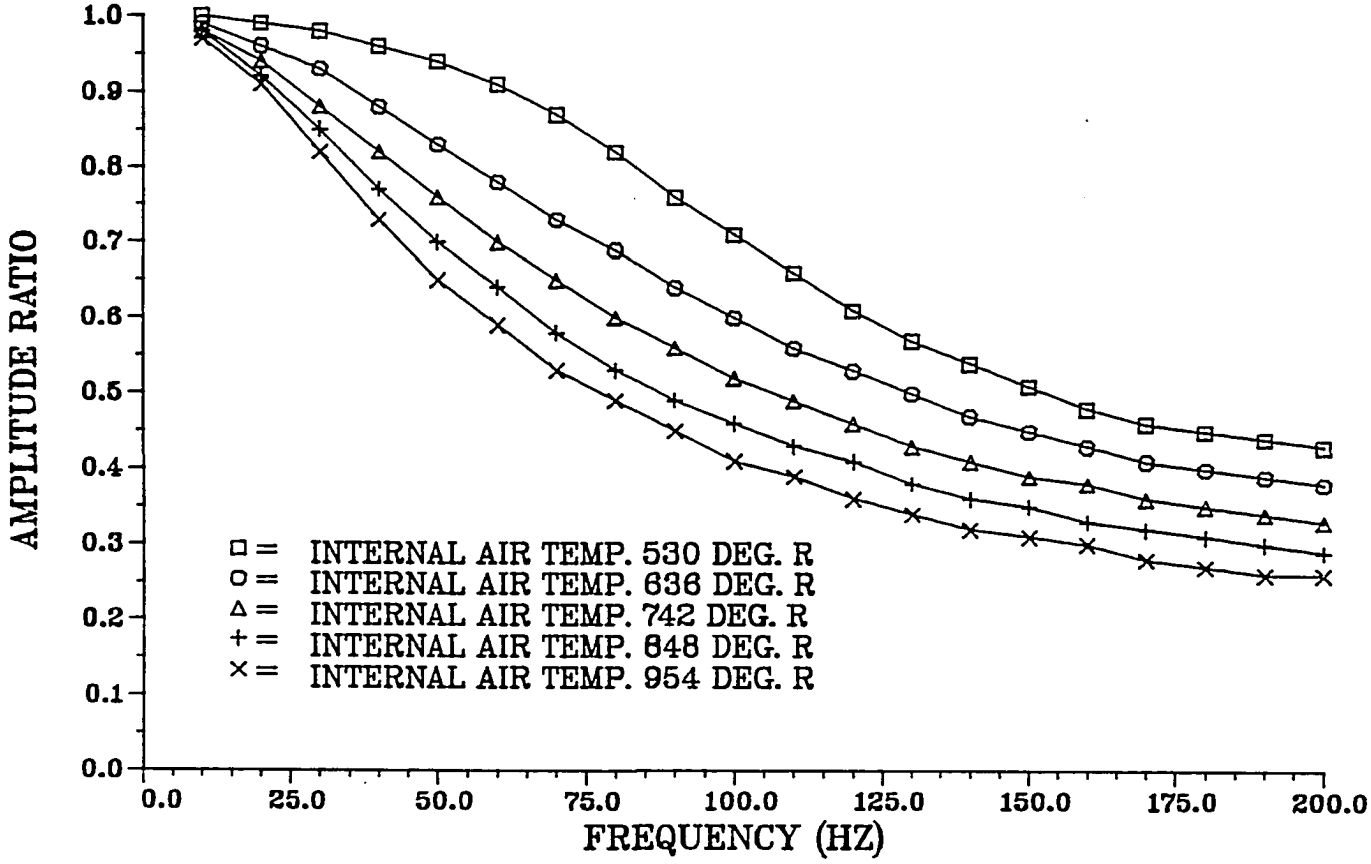

Figure 5.7 Pressure attenuation characteristics of close-coupled measurements

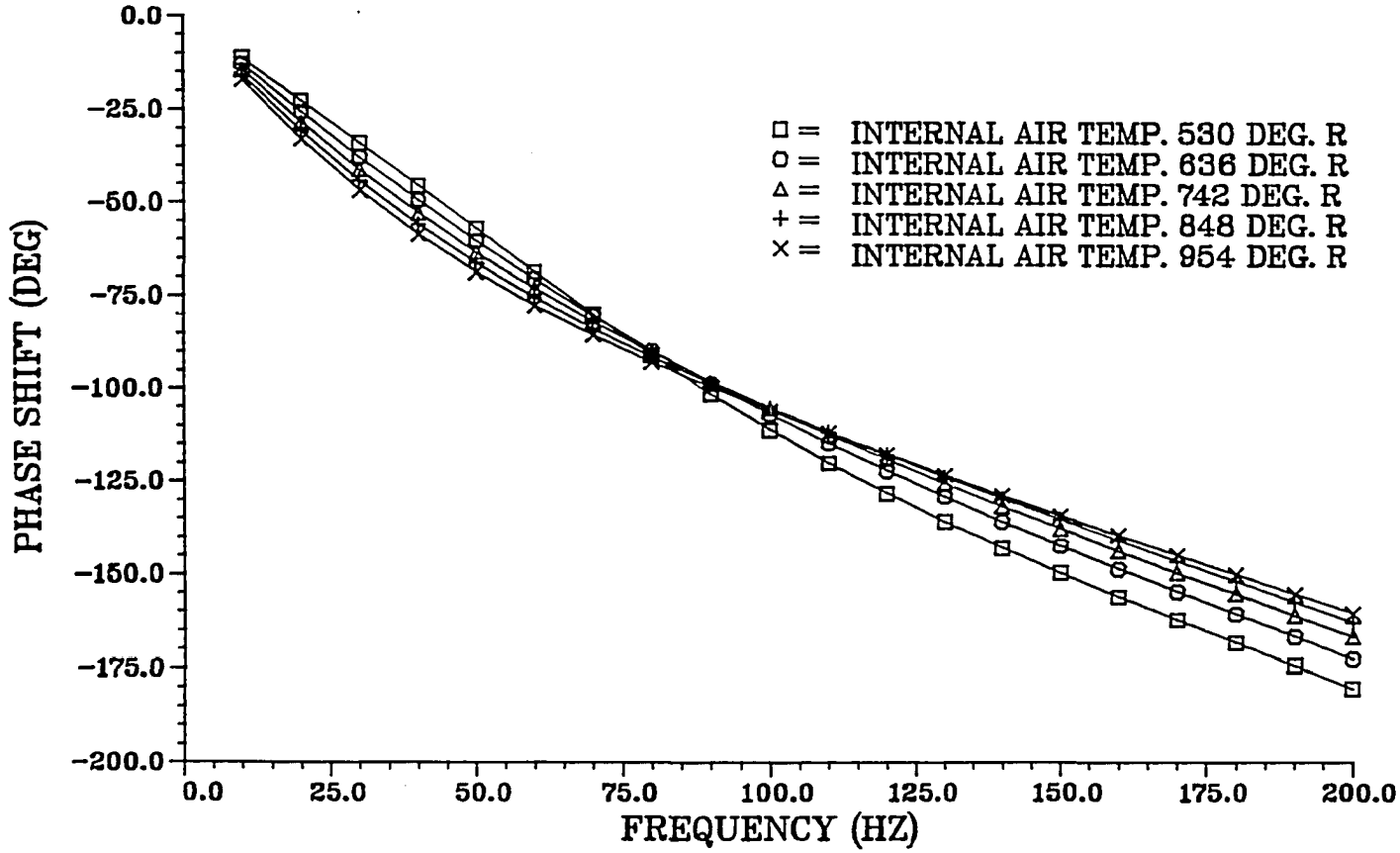

Figure 5.8 Phase shift characteristics of close-coupled measurements

of whether of not a theoretically determined transfer function from the algorithm must be applied to the data during post test analysis to determine the true characteristics of the fluctuating pressure.

Transducers utilized for the close-coupled measurements were Scanivalve model ZOC-14 (Zero-Operate-Calibrate) pressure transducers. The ZOC transducers were maintained at a constant temperature with cooling water maintained at 70° F (21.1° C) with a closed loop cooling system. Temperature control resulted in calibration, zero offset and sensitivity stability.

Pressure transducer signals were input to a Preston (model 8300-XWBRC) amplifier. The gain setting for each of the amplifiers used for time-averaged and close-coupled measurements was dependent on the transducer output for a particular channel. Although the amplifiers were capable of outputting a 10 volt signal, the analog to digital (A to D) converter saturated at 5 volts. Therefore, the appropriate gain was selected to insure that the maximum output for a channel was as close to 5 volts as possible. The signal was amplified in order to increase the ratio of signal to line noise from the amplifiers to the A to D converter. Each amplifier had a three pole Butterworth-Thomson filter with selectable cutoff frequencies of 10 Hz, 40 Hz, 120 Hz, 400 Hz, and 1200 Hz.

The cutoff frequency chosen for the test was 400 Hz. The filters have a transfer characteristic of -3 db at 200 Hz and -4 db at 250 Hz and -8 db at 400 Hz. The attenuation due to the filter combined with the attenuation due to the tube lengths and transducer volumes made all signals at frequencies greater than 250 Hz insignificant. Since the sampling frequency of the close-coupled digital data system was 692 scans/sec, aliasing did have to be considered. For a 692 scan/sec sample rate, the Nyquist rate is 346 Hz. Signals between 346 and the filter cutoff frequency of 400 Hz were folded back onto signals with frequencies of 292 to 346 Hz. This implies that any signals at or above 290 Hz were contaminated by aliasing and therefore could not be considered valid information. Since the signals were attenuated greatly after 250 Hz, this aliasing did not effect the results and the nominal desired response was obtained. The fixed filter settings of the amplifiers would not allow the desired frequency response to be obtained for any setting other than 400 Hz, because of either aliasing or attenuation. All filters for the time-averaged measurements were set at 10 Hz, as the higher frequency response was not required.

Although the phase response of the Preston amplifiers (used for the close-coupled measurements) and Pacific

amplifiers (used for the high-response measurements) were considered individually, the phase shift between high-response and close-coupled data was accounted for by using the 10 and 100 Hz sine wave sum defined previously. This sine signal was sent through the digital close-coupled data system as well as to each analog high-response tape recorder. This signal was also used during post processing to eliminate phase shift errors between high-response and close-coupled data.

All 86 channels used for close-coupled measurements were equipped with sample and hold electronics. Time-averaged channels were not equipped with the sample and hold electronics. In each close-coupled channel, the sample and hold electronics converted a continuous signal into discrete values. Data acquisition with the sample and hold electronics occurred with no phase lag between channels because all channels were sampled simultaneously. All sampled signals were held until they could be digitized and subsequently recorded. The total time required to sequentially transfer the held information was dictated by the speed of the analog-to-digital converter. Thus, a sample of all close-coupled channels was held for 1/692 second while the previous sample was being converted into digital values. The actual time to acquire a sample was approximately 10 micro seconds. This technique eliminated

the phase errors caused by sequential reading of data from individual channels of close-coupled data.

Errors can result with sample and hold electronics if the voltage level of the channels sampled "droops" during the time it takes them to be transferred sequentially to the analog to digital converter. Also the gain stability of the electronics can result in errors if not verified. If gain electronics are not stable they may produce false variations in output levels for stable input signal levels. Gain instabilities in the frequency range of interest could be perceived as false input pressure signal fluctuations. The specification for the droop rate and gain stability is 1 mv/ms and 0.1% of full scale respectively. In order to verify these specifications, tests were designed to determine the droop rate and gain stability of the sample and hold electronics. One test involved paralleling the same sine wave into all of the sample and hold channels. The output was reviewed for each channel to verify that the sample and hold electronics were functioning identically. This test also allowed precision errors in the equipment to be determined. A second test consisted of applying 5 volts to all sample and hold channels and reading the voltage at the output of one channel. Then several other channels were read for 1 ms. Finally the original channel was read again in order to determine the drop in voltage. Both of

these tests were performed at the beginning of a test day to insure the integrity of the sample and hold equipment over the entire test period.

When acquiring close-coupled digital data, each scan was read by the data acquisition computer in digital counts corresponding to the transducer output voltage. A scan is one sample of all close-coupled channels. The information was then transmitted to the main frame computer, an IBM 4341, to be recorded and displayed. The main frame computer did not convert every scan of information to engineering units during a test period, since this would drastically slow down acquisition time. Therefore, data were stored on digital tape in raw form as counts data. In order to monitor close-coupled channels on-line during transient data acquisition, a scan of some data was taken from the entire stream of data and converted into engineering units and displayed. During this time, all raw counts data were being sent to tape. Once one scan of data was converted and displayed another scan was acquired from the stream of data for reduction and display. Approximately one scan per second of all close-coupled channels was acquired for display from the 692 scan per second stream. The displayed data allowed for monitoring of the close-coupled data while they were being acquired. This also assured that data obtained were not saturated and

therefore useless for post test analysis. Monitoring close-coupled data reduced unnecessary repetition of test points.

All scans of close-coupled transient data could not be converted into engineering units until a standard format tape was created from counts data. This conversion could not occur until after testing was completed and it involved the input of counts data into engineering units reduction software in the main frame computer at a slower rate than acquired. It took approximately 20 minutes to process 1 second of transient data.

The close-coupled measurements defined in Table 5.2 were acquired following set procedures during the test. While operating the compressor at a quasi-steady in-stall condition, a time-averaged data point was acquired. Immediately following this, a 5 second close-coupled data scan was obtained. This included approximately 3375 scans of each of the 86 channels defined in Table 5.2. The five second data acquisition time provided approximately 250 cycles of periodic pressure data. Immediately following the 5 second scan, another time-averaged data point was obtained. The time-averaged data points included information from the 86 channels that were close-coupled along with the other pressures and temperatures that were detailed in Section IV. The time-averaged data were taken

to determine the average values of the dynamic data. These time-averaged data were utilized to assist in validation of the close-coupled data obtained. The time-averaged data were also used to determine the quasi-steady in-stall compressor pressure and temperature characteristics.

VI. TEST PROCEDURES AND DATA ACQUISITION

Two primary goals were set for the CRF 10-stage compressor tests. The first goal was to determine the time-averaged performance of the compressor under unstalled and in-stall operating conditions. The steady unstalled and quasi-steady in-stall compressor performance characteristics were measured with the time-averaged data acquisition method described in Section V. The time-averaged measurements were obtained to characterize overall compressor performance and the performance of each of the 10 stages within the test compressor. The second goal of the tests was to obtain time-resolved performance data for the compressor during its transition into rotating stall, and while it operated in rotating stall. These time-resolved performance parameters were measured with the close-coupled and high-response data acquisition systems also described in Section V. Overall compressor and selected individual stage time-resolved performance measurements were obtained. The procedures followed to obtain the time-averaged, steady and quasi-steady performance, and time-resolved performance data for the test compressor are described in the following subsections.

A. Steady and Quasi-steady Procedures

Specific procedures were followed to determine the performance of the compressor while it operated in a steady, unstalled condition and also in a quasi-steady, rotating stall condition. These procedures were defined to assure data accuracy and test compressor health during the tests. The test procedures were defined to assure correct compressor parameter measurement without prolonging risk to the test compressor. The procedures were also designed to allow for complete definition of how critical parameters such as compressor speed and compressor blade geometry may affect the steady and quasi-steady performance. The data acquisition procedures and test variables are described in the following paragraphs.

1. Data acquisition procedures

Of primary importance when measuring the compressor steady and quasi-steady performance is compressor operation in a condition that does not vary with time. Prior to obtaining any performance data, a test was completed to determine the time required for the compressor to settle into a steady operating condition. The speed and throttle position of the compressor were changed from a low speed, and low throttle level to a high speed and high throttle

level. Time-averaged data (described in Section V) were obtained at one minute intervals after the high speed high throttle condition was established. The results suggested that the overall and stage performance of the compressor settled to within 99 percent of its final steady level within 3 minutes after the new operating condition was established. Therefore, for the remainder of the test program a 3 minute delay at a fixed operating condition was established prior to obtaining a time-averaged data point.

The repeatability of the operation of the data acquisition and facility control systems over a day was verified by obtaining time-averaged data points at fixed compressor operating conditions prior to and after each test day. In addition to this procedure, selected test points were repeated on different test days to assure CRF test compressor performance repeatability from day to day.

2. Test variables

Data were obtained at different compressor operating conditions to define the effects of speed and inlet guide vane (IGV), first stator, and second stator setting angle values on compressor steady and quasi-steady performance as well as compressor recoverability. The test program was defined to determine unstalled and in-stall

operating characteristics for the CRF test compressor from 49.8% of the compressor design corrected speed up to a speed near the point where the stall instability was surge. This rotating stall/surge point was found by throttling the compressor to the stall point and then determining if the subsequent instability was surge or rotating stall (see Figure 1.4).

The type of instability that occurred subsequent to compressor stalling was determined with the use of two compressor discharge high-response static pressures. These measurements, defined in Section IV, were located at two different circumferential locations in the same axial plane. Compressor surge was accompanied by an axisymmetric blowdown of pressure at the discharge of the compressor. Rotating stall manifested itself as a disturbance rotating circumferentially around the compressor discharge flow path. This difference between surge and rotating stall allowed for precise determination of the compressor instability phenomena. The signals from circumferentially spaced high-response transducers were subtracted from each other. In a surge event the pressure fluctuations for circumferentially spaced transducers were in phase with each other. The difference of the two signals (one minus the other) was a constant output not varying with time. If the nature of the compressor instability was rotating

stall, the difference in the two signals varied with time because the two circumferentially spaced transducer signals were periodic and out of phase with each other. The highest compressor speed for which rotating stall information was obtained was 78.5% of the design corrected speed. Above 80.0% speed the compressor instability was surge.

At test compressor speeds between 49.8% and 78.5% design speed, operating points for which data acquisition could occur were limited by the natural resonance of compressor mechanical systems. A compressor resonant condition did not allow data acquisition at 70% of design corrected speed. Therefore the speeds where in-stall performance was documented for the CRF 10-stage compressor test were 49.8%, 59.7%, 67.7%, 74.5% and 78.5% of design corrected speed.

Throttle positions for these speeds were limited to a predefined low operating line position greater than design operating throttle on one end to a throttle closure position (in stall) where internal compressor blade temperatures were at maximum limits for compressor health.

The procedure followed at each speed was to obtain time-averaged data at a throttle point, on the unstalled characteristic, near stall. In some cases additional data were acquired at throttle settings between the design

throttle point and the near stall throttle point. The near stall throttle point was predetermined from an earlier portion of the test program. After the near stall time-averaged data were obtained, the throttle was closed at a rate of 0.5% closure per second until the compressor stalled. The exit throttle point at which the test compressor stalled was determined by monitoring high-response pressure signals and rotor strain gage signals. A sharp increase in pressure fluctuation and rotor strain indicated that the 10-stage compressor was in rotating stall. At the initial in-stall point a time-averaged data point was immediately obtained. A second point at the same throttle location was then obtained after the 3 minute stabilization time had lapsed. While the compressor was operating in stall, internal temperatures and blade stresses were monitored to assure health limits that would endanger the compressor were not exceeded.

After the initial in-stall point data were obtained, the throttle was trimmed to a more closed position. Nominally this position was chosen to be 2% more closed than the initial in-stall position. After a 3 minute stabilization period at this throttle condition two sets of time-averaged data were obtained. Between the two sets of time-averaged data a 5 second time-resolved close-coupled

data scan was obtained. The reason for this scan will be clarified in the next subsection. The throttle was closed at 2% increments and time-averaged data obtained as described above until internal temperature upper limits were encountered. After the most closed throttle data point was obtained, the throttle was again opened at 2% increments and data were again obtained as defined above.

Due to the compressor in-stall hysteresis (defined in Section I) in-stall time-averaged data were obtained at throttle positions more open than the near stall throttle position. Time-averaged data were obtained at 2% exit throttle opening increments until the compressor recovered from the stalled condition. Recovery was identified as the operating point where high-response pressure and rotor strain gage levels no longer indicated rotating stall operation. Some difficulty in obtaining the near recovery points was encountered at 78.5% and 74.5% of design corrected speed, because of the high stress conditions that existed as the compressor throttle was opened while the compressor operated on the in-stall hysteresis curve. Therefore, the near recovery point was established as accurately as possible for the given high stress conditions. The accuracy of near recovery operating points is discussed further in the Section VII.

After the compressor recovered from the in-stall condition, time-averaged data on the unstalled characteristic were obtained for exit throttle settings corresponding to those for in-stall operation. Care was taken to assure that the data were obtained after approaching exit throttle positions from the same direction as for the in-stall positions. Approaching the desired throttle setting by opening the throttle eliminated discharge throttle mechanical linkage hysteresis effects.

In addition to measuring the steady and quasi-steady CRF test compressor unstalled and in-stall performance as a function of speed, variable geometry effects were also examined. The compressor was designed with three sets of variable vanes as defined in Section IV. These vanes were set to preprogrammed positions as a function of compressor speed. Their position was fixed up to a speed of 79.6% of design corrected speed. Tests were completed for all speeds defined above with the preprogrammed schedule. The tests were then repeated for the vanes at a 7 deg. more open condition. All procedures for data acquisition as defined above were followed. The quasi-steady in-stall data could not be obtained for 78.5% of design corrected speed because the nature of the stall instability changed

from rotating stall to surge when the vanes were scheduled more open. This result is discussed further in Section VII.

Variable discharge volumes, as defined in Section IV, were available for use during the test program. Although the volume was different for portions of the tests described above, it was determined that discharge volume had no effect on the steady or quasi-steady compressor performance. Therefore, volume is not considered in the CRF test compressor data analysis.

B. Time-resolved Performance

A second goal of the test program was to document the time-resolved performance of the CRF test compressor during its transition into stall and while it was in rotating stall. This performance was documented with the use of the close-coupled and high-response acquisition systems described in Section V. Fixed procedures were followed during this phase of the test program. These procedures are defined in the following paragraphs.

1. Data acquisition procedures

The procedure followed to obtain time-resolved performance data for the test compressor required the use

of both the close-coupled and high-response data acquisition methods. Prior to throttling the compressor into stall a time-averaged data point was obtained at the near stall condition The test compressor discharge throttle was closed from the near stall position at a rate of .5% per second until the compressor stalled. During this transition the high-response data were recorded by manually starting the FM tape recorders. In addition, the close-coupled acquisition system was started and set to continue taking data until the stall transition and subsequent instability was documented. To assure data repeatability, time resolved data points for the same set of compressor conditions were repeated. In addition the time response of the two acquisition systems were compared to assess system amplitude attenuation and phase shifts. This comparison is defined in more detail in Section VII.

2. Test variables

Time-resolved data were obtained for the same speeds as for the time-averaged steady and quasi-steady data. Results of the data obtained at 59.7% and 78.5% of design corrected speed are detailed in Section VII. The procedure followed for scheduling the discharge throttle requires definition as it is important when comparing the experimental results with theoretical results.

The throttle was closed from the test operators console at a rate of 0.5%/sec from the near stall condition until stall occurred. For the time-resolved test, stall was determined by an automatic sensing probe at the inlet to the compressor. The probe was the same as the forward and aft facing probe detailed in Section IV Figure 4.7. The pressures sensed by the forward and aft impact probe were pneumatically connected to each side of a delta pressure transducer. The voltage output of the transducer was monitored by an electronic circuit. When the transducer output voltage switched from positive to negative, indicating flow reversal, the circuit indicated stall. When stall was sensed, a message was sent to the TAC computer (defined in Section VII Test Facility) to begin opening the discharge throttle at a rate of 50% of full open per second. The discharge throttle continued to open until the stall was no longer sensed by the inlet probe. Nominally, the delay from sensing stall until clearing required slightly more than one second for a rotating stall. One second was adequate for characterizing the transition from an unstalled to an in-stall condition. The time required to establish a nonvarying condition is discussed further in Section VII.

VII. DATA ANALYSIS AND RESULTS

Data analysis is discussed in three different sections. The first section involves a description of a state-of-the-art multistage compressor dynamic performance model developed by Davis [44] and a review of the test cases used to validate the model. The second section includes an analysis of the time-averaged, steady and quasi-steady, in stall performance of the CRF test compressor described in Section IV. The third part covers analysis of the in-stall time-resolved, close-coupled and high-response data obtained in the CRF test compressor during its transition from an unstalled condition into rotating stall. Analysis of the experimental results includes the use of these data with the multistage model developed by Davis, and comparison of test results with results generated by the model. In addition, in-stall hysteresis is discussed and methods to minimize in-stall hysteresis levels are presented.

Prior to describing the data obtained during tests, a brief description of the multistage compressor model developed by Davis will be presented. This multistage compressor model represents the state-of-the-art in

high-speed multistage compressor dynamic performance modeling. Validation of the Davis model has been heretofore limited due to the lack of multistage high-speed compressor dynamic and quasi-steady in-stall data. The data presented in this report are suitable for further validation of the Davis model, and are therefore used to prescribe model improvements.

A. Multistage Model Description

The model developed by Davis is the only model in the open literature that predicts multistage compressor stalling performance from stage characteristics. This model is a one-dimensional, compressible, unsteady, stage-by-stage compressor dynamic performance model. It describes the system behavior of a multistage compressor during events such as surge and rotating stall. The model follows a control volume approach similar to the one used with low-speed models by Greitzer [3]. A numerical technique is utilized for solving the non-linear equations of mass, momentum and energy conservation for each component control volume. The compressor is divided into component control volumes beginning with the compressor

bellmouth. Each individual stator and rotor combination (stage) is considered to be a distinct control volume. The exit ducting is also divided into individual control volumes. Each component volume must be small enough to preserve the dynamic characteristics of the multistage compressor. Forces acting on the fluid in each control volume containing blades, i.e., forces due to the effects of compressor blading and the walls of the compressor annulus, are input as an axial force distribution (FX). Heat input (Q), and shaft work (SW), both per unit length, are also input into the control volume. For the experimental comparisons provided herein heat input was not considered, i.e., the flow was assumed to be adiabatic. Therefore heat transfer is not included in the description of the model presented in this dissertation.

The blade forces and shaft work must be provided to the model in the form of measured stage pressure and temperature characteristics. Stage characteristics are defined such that stage pressure rise and temperature rise can be determined for a given corrected speed, overall mass flow rate, and inlet total pressure and total temperature conditions. Stage temperature rise is needed to determine the stagnation enthalpy rise within the stage, from shaft

work (SW), necessary for energy conservation concerns. The stage pressure rise is required to determine the pressure forces (FX) acting on the fluid due to the compressor rotor. These pressure forces must be considered to assure momentum conservation.

The inlet boundary conditions of pressure and temperature for the control volume are time-dependent. The exit boundary conditions are either specification of static pressure, or of a unity Mach number. The governing equations for the control are described below.

1. Governing equations

Mass conservation for one-dimensional, unsteady, compressible flow can be expressed as

$$\left\{ W + \frac{\delta W}{\delta x} dx + W_B dx \right\}_{leaving} + \left\{ \frac{\delta(\rho A dx)}{\delta t} \right\} = W_{entering}$$

where

$$W = \rho u A$$

and

$$W_B = bleed\ flow$$

The model allows for introduction of a bleed flow, (W_B), in the continuity equation. During tests of

the 10-stage compressor, bleed flows were minimal and considered negligible. Therefore the appropriate model continuity equation can be rewritten as

$$\frac{\delta(\rho A)}{\delta t} = -\frac{\delta W}{\delta x}$$

The axial forces acting on the fluid in the control volume for conservation of axial momentum consideration include pressure and the blade forces (F_B), as defined by the following equation. The blade forces and pressure forces were input from measured stage characteristics.

$$\sum F_x = F_B dx - \frac{\delta(P_s A)}{\delta x} dx + P_s \frac{\delta A}{\delta x} dx$$

The total rate of change of axial momentum of the fluid in the control volume is identified as

$$\frac{\delta}{\delta t}(u \rho A dx) + \rho u^2 A + \frac{\delta(\rho u^2 A)}{\delta x} dx - \rho u^2 A$$

The conservation of momentum equation reduces to

$$\frac{\delta W}{\delta t} = -\frac{\delta(IMP)}{\delta x} + FX$$

where $$IMP = Wu - P_s A$$

and $$FX = P_s \frac{\delta A}{\delta x} + F_B$$

The energy equation for the fluid in the control volume is

$$SW\,dx = \frac{\delta}{\delta t}\left[\left(e + \frac{u^2}{2}\right)\rho A\,dx\right] - \frac{\delta}{\delta x}[\rho u A(h)]dx$$

which reduces to $$SW = \frac{\delta(EA)}{\delta t} - \frac{\delta H}{\delta x}$$

where $$H = Wh$$

$$E = \rho\left(e + \frac{u^2}{2}\right)$$

$$h = C_p(T_T - T_{ref})$$

Shaft work (SW) is determined from measured stage characteristics as defined previously.

2. Stage characteristics

The stage characteristics required by the model must be provided in terms of flow coefficient defined as

$$\phi = \frac{\left\{\left[\frac{W\sqrt{T_T}}{P_T A}\right]\left[\frac{\left(\frac{N}{\sqrt{\theta}}\right)_{design}}{\left(\frac{N}{\sqrt{\theta}}\right)_{actual}}\right]\right\}}{0.5318}$$

temperature coefficient defined as

$$\psi^T = [TR - 1]\left[\frac{\left(\frac{N}{\sqrt{\theta}}\right)_{design}}{\left(\frac{N}{\sqrt{\theta}}\right)_{actual}}\right]^2$$

and pressure coefficient defined as

$$\psi^P = \left[PR^{\frac{\gamma-1}{\gamma}} - 1\right]\left[\frac{\left(\frac{N}{\sqrt{\theta}}\right)_{design}}{\left(\frac{N}{\sqrt{\theta}}\right)_{actual}}\right]^2$$

where

$$\theta = \frac{T_T}{T_{ref}}$$

To model the dynamic characteristics of the stage during the stalling process, blade forces are lagged through the use of a first-order lag function. Lagging the blade forces simulates the dynamics of a compressor during

its transition into rotating stall or surge. Test results [1] have shown the existence of a transition time associated with compressors during the stalling event. This is the time required to stabilize into a steady in-stall or surge condition. The time constant for the lagging function in the model is a variable which can be adjusted to vary model results. The first order lag function for the blade forces is defined as

$$F_x = FX_{ss} - \tau \frac{dF_x}{dt}$$

where τ is the first order lag time constant.

3. Solution methods and model validation

The model governing equations are mathematically hyperbolic and therefore require specification of initial and boundary conditions. The solution for a mathematically hyperbolic set of equations is computed by marching outward in time while satisfying the boundary conditions. The governing equations were solved by Davis using the MacCormack second-order finite-difference scheme [45].

Because the model poses a boundary value problem as well as an initial value problem a method for treatment of the boundaries was required. The model utilizes the method-of-characteristics (MOC) for unsteady compressible flow, neglecting body forces and heat sources for determination of the compressor inlet boundary conditions. The compressor exit boundary conditions are either determined with the MOC scheme for unchoked flow or with an isentropic sonic nozzle scheme for choked flow.

Davis [44] reported that his model was validated with two test cases. One test case involved a low-speed, three-stage, axial-flow compressor [46]. The other test case involved a nine-stage, high-speed, axial-flow compressor [17]. A brief description of these test cases will be provided. This description will clarify the limitations of the validation.

a. Three-stage low-speed case As described previously, the model requires experimentally determined stage characteristics that yield blade forces and stage work inputs for each control volume. For the three-stage test case, data were available as reported by Greitzer [4] and Gamache and Greitzer [16] and Gamache [46]. Individual

stage and overall pressure rise characteristics were measured for their test compressor. These characteristics were determined for the unstalled compressor, the compressor operating in-stall, and the compressor operating in the reverse flow region. These data represent a complete set of pressure characteristics for the multistage Davis model. Temperature characteristics were only measured for the overall compressor. Therefore, stage temperature characteristics for the model were assumed to be the same for each stage while producing the measured overall temperature rise characteristic. The model results were compared with the measured [4] overall dynamic stall and surge performance of the low-speed, three-stage compressor. The multistage model predicted the same performance trends as were measured. Davis concluded that the model correctly matches the dynamics of a low-speed compressor in surge and rotating stall. Further validation involving a high-speed, nine-stage compressor was sought to determine the usefulness of the model for predicting stall and surge events for high-speed multistage compressors.

b. Nine-stage high-speed compressor case

High-speed multistage compressor stage data were not available to Davis in the open literature. Results reported by Hosny et al. [1], from the 10-stage energy efficient engine compressor test, detailed unstalled and in-stall characteristics for the overall compressor but not for the individual stages. Therefore, Davis synthesized unstalled stage characteristics for a nine-stage compressor configuration from a stage-stacking model described in [47]. In-stall characteristics and reverse flow characteristics were estimated based on previously described low-speed compressor characteristics. Model results were compared qualitatively with measured results obtained by Hosny and Steenken [17] for the high-speed, 10-stage energy efficient engine compressor test described in Section II. Only qualitative comparisons could be made between the Davis predictions and the energy efficient engine compressor data as the model geometry was for a different compressor (nine-stage unstalled stage-stacking model) from the energy efficient compressor. Qualitatively, the model did predict dynamic events similar to those seen in the tests described by Hosny. No quantitative comparisons were made and therefore, a more

complete validation of the models ability to predict high-speed compressor behavior was not possible. The data defined in the next section provide the information necessary for a high-speed compressor quantitative evaluation of the Davis model.

B. Steady Unstalled and Quasi-steady In-stall Performance

The data obtained from the CRF 10-stage compressor test program provide the information needed to more thoroughly validate the multistage model developed by Davis. In addition, these test data provide some insight into the differences in quasi-steady in-stall performance and recovery that exists between low-speed multistage compressors and high-speed multistage compressors.

The data that describe the unstalled and in-stall performance of the CRF test compressor were obtained as described in Section VI. In addition a special procedure, described below, was followed in obtaining the data set for 78.5% speed. With the compressor operating in-stall and the throttle open to the operating point nearest to causing the compressor to unstall, the throttle was closed at fixed increments and data obtained. These data duplicated the

in-stall performance data, thereby indicating that once on the in-stall portion of the characteristic, throttling the compressor resulted in performance along the in-stall characteristic.

The stage pressure and temperature characteristics can be used to determine stage work and blade force input for the Davis multistage model. The stage characteristics were ascertained from the equations defined in the model description. The in-stall portion of the characteristic, measured during the CRF compressor test, is representative of the time-averaged change in pressure and temperature across the stage during quasi-steady rotating stall operation and therefore is not in the truest sense a steady state characteristic as is the unstalled characteristic. The in-stall characteristic is a repeatable representation, for a given operating condition, of the average change in pressure and temperature across a stage during rotating stall operation. Parallel compressor theory, discussed in Section II, suggests that while in rotating stall the stage is actually operating with part of the annulus on an unstalled chatacteristic and the other part on a zero or negative flow characteristic. Parallel compressor theory does not require a time-averaged representation of stage

pressure and temperature rise while operating in rotating stall. For the one-dimensional model developed by Davis the time averaged temperature across the stage is necessary, therefore the in-stall characteristic as defined above was measured and provided as input to the model.

The measured stage, pressure and temperature, characteristics are presented as a function of flow coefficient. Both overall compressor and individual stage characteristics are presented. The effects of compressor speed and variable geometry on overall compressor and individual stage characteristics are also displayed.

1. Compressor speed effects

The overall compressor pressure rise characteristics for the compressor operating at the five design corrected speeds mentioned in Section VI with variable vanes set at nominal positions are presented in Figure 7.1. Detailed overall compressor data at each speed for the compressor operating prior to stall, at the initial in-stall point, for different throttle settings in-stall, and after the stall was cleared from the compressor are provided in Appendices B,C,D,E, and F, Figures 13.1, 14.1, 15.1, 16.1,

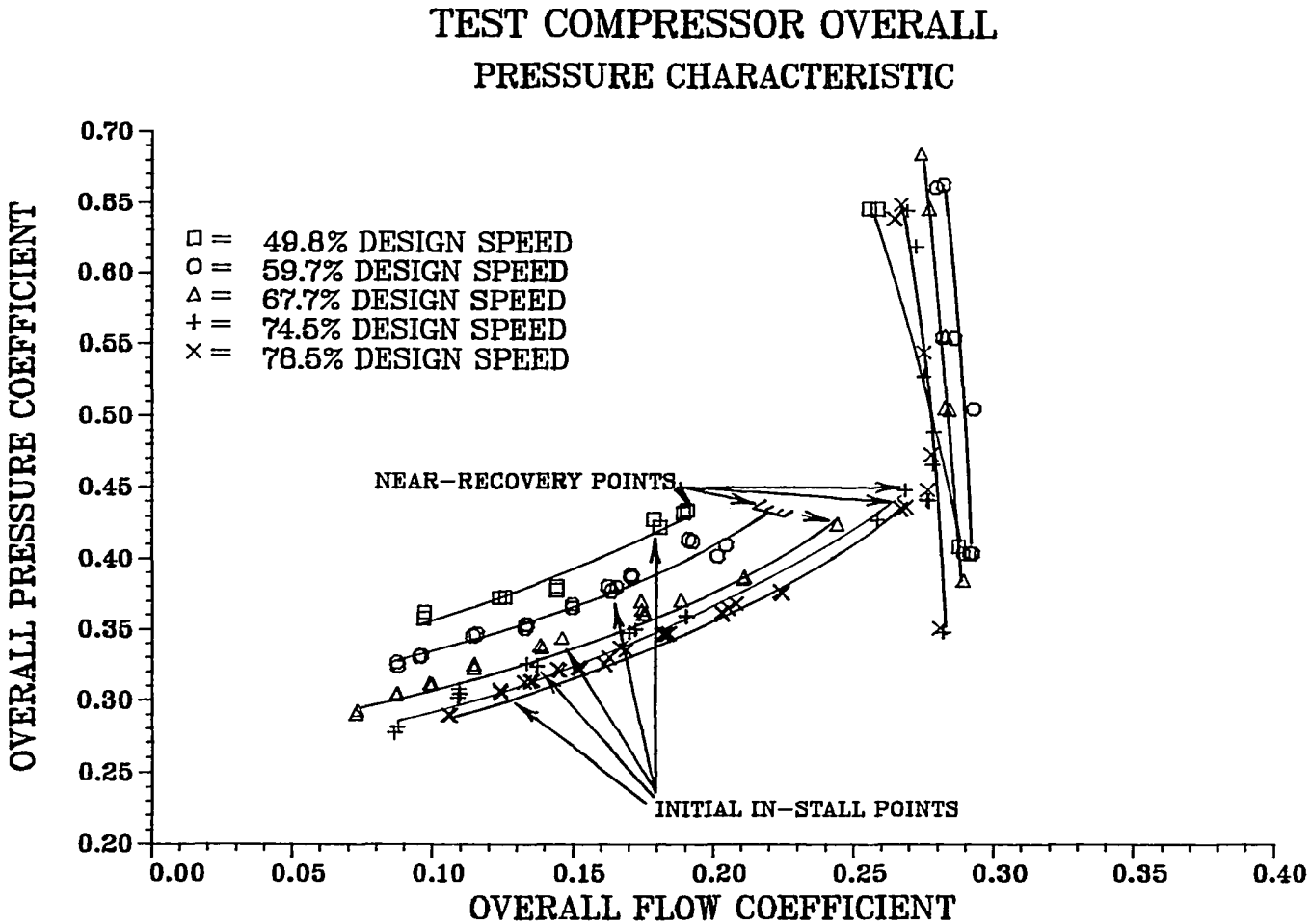

Figure 7.1 CRF test compressor overall pressure characteristics

and 17.1 respectively. The in-stall data include information obtained in the in-stall hysteresis region. During compressor stalling and recovery data were obtained at a rate of 147 samples/second for all data channels. These data were arithmetically averaged over time to obtain a more precise near-stall and near-recovery conditions. These operating conditions are noted on the overall compressor characteristic with hatched lines. This method for determining the near-stall and near-recovery conditions was followed, if required, for all overall compressor data presented in this section. At most speeds this method was not required because time-averaged data were obtained at the near-stall and near-recovery operating point.

The compressor overall characteristics (Figure 7.1) indicate that, for all speeds, the in-stall compressor performance characteristics were lower in pressure coefficient and flow coefficient than before stall. The initial in-stall operating points for each shaft speed are pointed out. The initial in-stall point flow coefficient is progressively lower with increases in speed level. This reduction in initial in-stall point flow coefficient with increased shaft speed level is true for all individual

stages also, as is indicated by the detailed characteristics in Appendices B,C,D,E and F.

Details of the stalling event will be discussed in the next subsection on dynamic performance of the compressor. Figure 7.1 also indicates that in-stall characteristics have the same basic slope at all speeds, but are offset to lower pressure coefficient values as speed increases. This reduction in overall pressure coefficient with increase in shaft speed is discussed further with stage performance results.

Also the in-stall hysteresis, as defined in Section I, appears to be limited by a pressure coefficient of near 0.44 for the CRF test compressor. For all speeds, the compressor recovers from a in-stall operating condition when the overall pressure coefficient reaches approximately 0.44. For 74.5% and 78.5% design speed the in-stall performance line extends almost all the way to the unstalled characteristic. At these higher speeds, the transition from in-stall operation to stall recovery is not a rapid increase in flow and pressure as was the case at lower speeds. Instead, at these higher speeds, a small

increase in flow and pressure occurs during the transition from in-stall operation to stall recovery. Some recovery strategies based on this observation are presented later.

The extent of the CRF test compressor in-stall hysteresis can be represented by the following equation,

$$H_f = 1 - \frac{\phi_{IIP}}{\phi_{NRP}}$$

where H_f is a measure of compressor in-stall hysteresis.

For a compressor having a near-recovery flow coefficient (ϕ_{NRP}) equal to the flow coefficient at the initial in-stall condition (ϕ_{IIP}), the hysteresis would be zero. The lower the hysteresis factor (H_f), the more recoverable the compressor is. Figure 7.2 details the hysteresis factors for all compressor speeds tested. In addition hysteresis factors have been calculated from data presented by Hosny et al. [1] for the 10-stage energy efficient engine compressor they tested. Figure 7.2 indicates that hysteresis levels in the CRF test compressor increase as speed levels increase. The high hysteresis level at 78.5% design speed for the CRF test compressor reflects poor compressor in-stall recoverability.

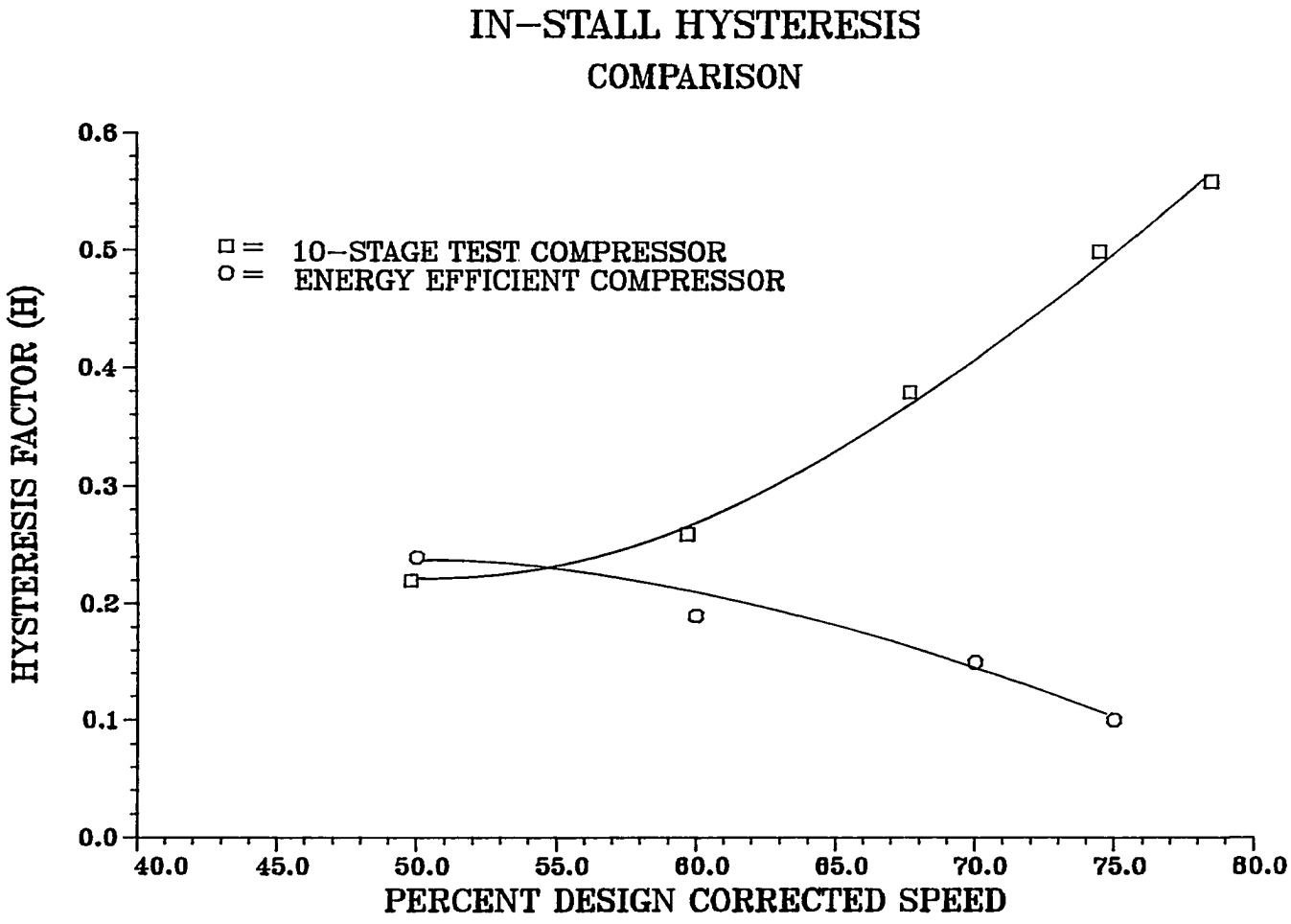

Figure 7.2 Speed effects on multistage compressor in-stall hysteresis

Figure 7.2 also shows that the CRF test compressor has greater in-stall hysteresis levels than the 10-stage energy efficient compressor and that the trend for the energy efficient compressor of hysteresis levels dropping with speed are opposite in the CRF test compressor. Overall performance data for the energy efficient compressor (E3) and the CRF test compressor are presented in Figure 7.3. These data clearly show the high level of in-stall hysteresis experienced by the CRF 10-stage test compressor. Analysis of the individual stage characteristics for the CRF test compressor provides a possible reason for the large amount of in-stall hysteresis associated with the CRF 10-stage test compressor.

The overall temperature characteristic of the CRF 10-stage compressor, shown in Figure 7.4, indicates a continuously rising temperature coefficient with reduction in flow coefficient. Details of the stage temperature characteristics show that this trend of rising temperature with reduction of flow is not true for all stages in the CRF 10-stage compressor.

Overall pressure characteristics are similar, trendwise to those obtained by Day et al. [13], and Urasek et al. [19] with low-speed, low pressure ratio compressors.

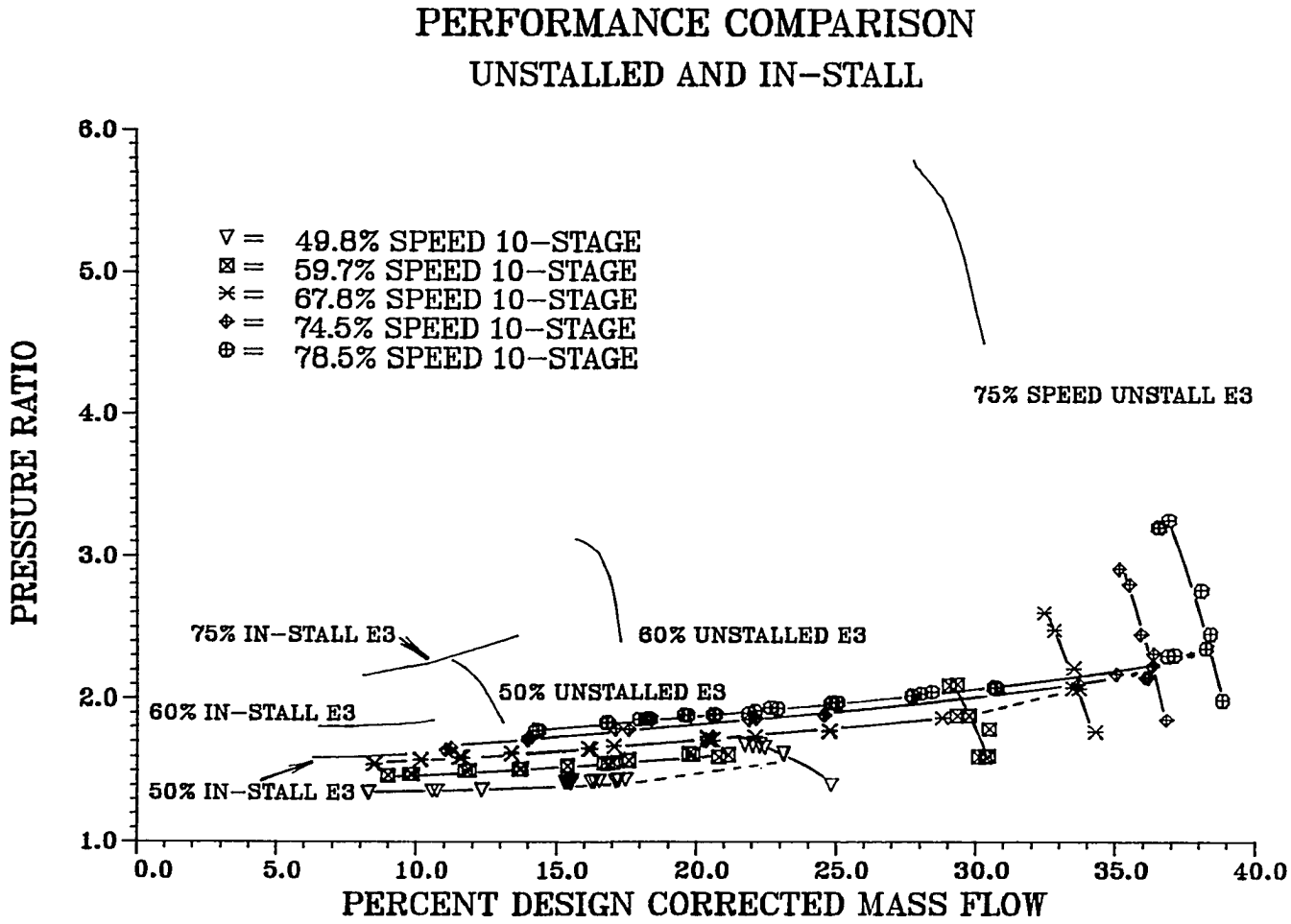

Figure 7.3 Performance comparison of multistage compressors

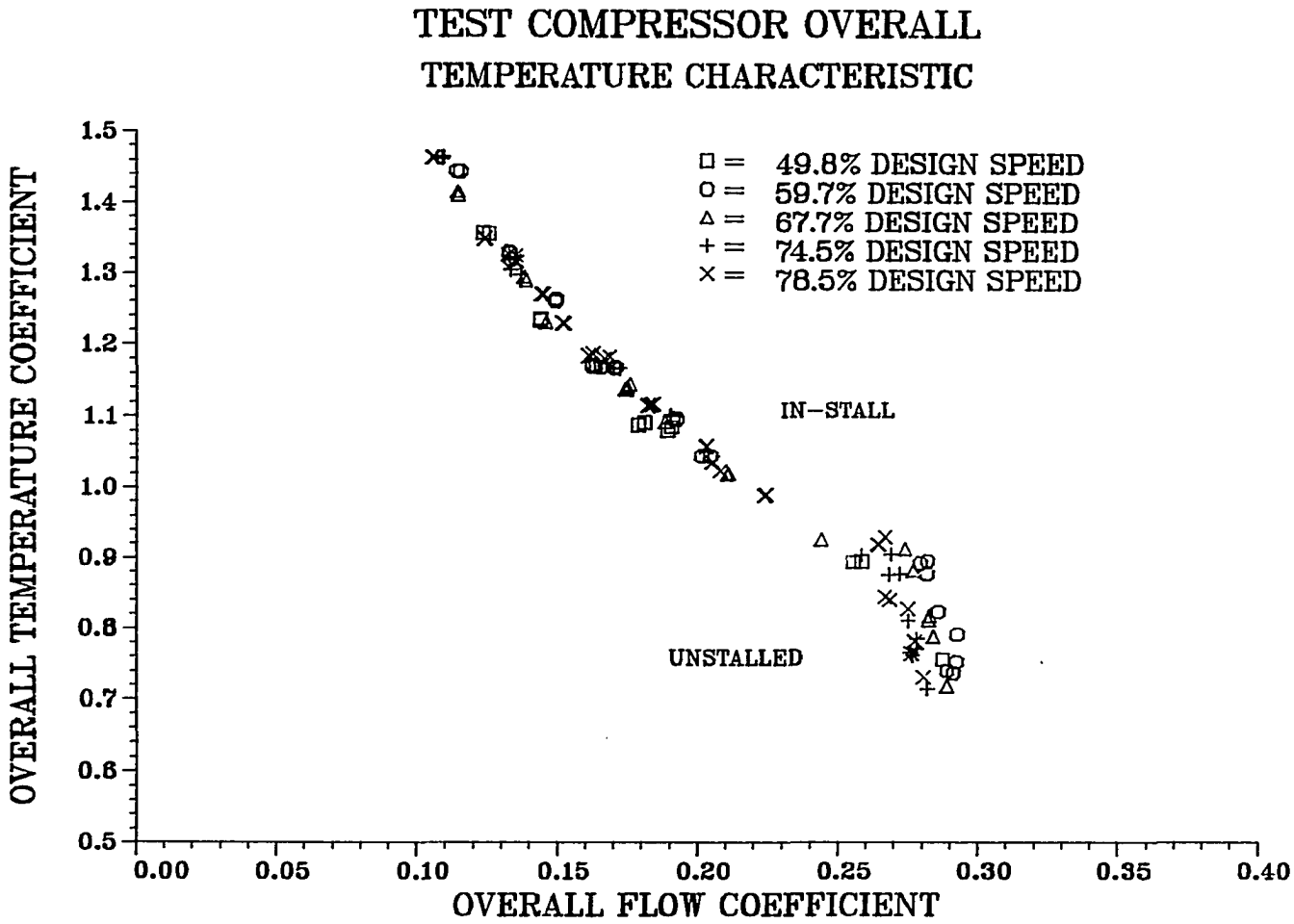

Figure 7.4 CRF test compressor overall temperature characteristics

Further investigation into the CRF 10-stage compressor individual stage results indicate that complex interactions exist between stages because of mismatching.

It is appropriate at this point to discuss the significance of pressure characteristic slope to the operation of a compressor stage as it is important to the analysis presented in this dissertation. Three-stage compressor low speed results reported by Day [30] indicated for low C_x/U designs it was possible to have a negative sloping overall characteristic with rotating stall present within the compressor. For the compressor configured with a design C_x/U of 0.35 a multi-cell tip-stall was detected over a small flow coefficient range on the negatively sloped portion of the characteristic. This portion of the negatively sloped characteristic with rotating stall present was preceded by compressor operation on a positive portion of the characteristic where four rotating stall cells, spanning the hub region of two stages, were present. No rotating stall was detected prior to operation on the four cell positive slope portion of the characteristic. This suggests that initial stalling was indicated with a change in slope of the characteristic from negative to positive. It is on this basis that a continuous negatively

sloping characteristic is assumed to represent unstalled stage operation. For a second low speed compressor configuration (see Ref. [31]) with a design C_x/U above 0.35 no evidence of rotating stall was found while operating on the negatively sloped portion of the characteristic. Since the CRF test compressor is a high speed compressor with a design C_x/U much above 0.35, and because of time-resolved stage pressure information to be presented later it was assumed that continuous negatively sloped pressure characteristics represent unstalled operation of a stage. Unstalled operation is defined to represent the absence of a full span single cell rotating stall. It is possible that some portion of the rotor may be operating under a multi-cell rotating stall condition while the stage is operating on the negatively sloped portion of the characteristic. Further discussion relating to detection of stall within a stage will be provided with the time-resolved CRF 10-stage compressor test results.

The first stage pressure characteristics of the CRF test compressor for all speeds tested are presented in Figure 7.5. Details of the pressure and temperature characteristics of all stages for all speeds are provided

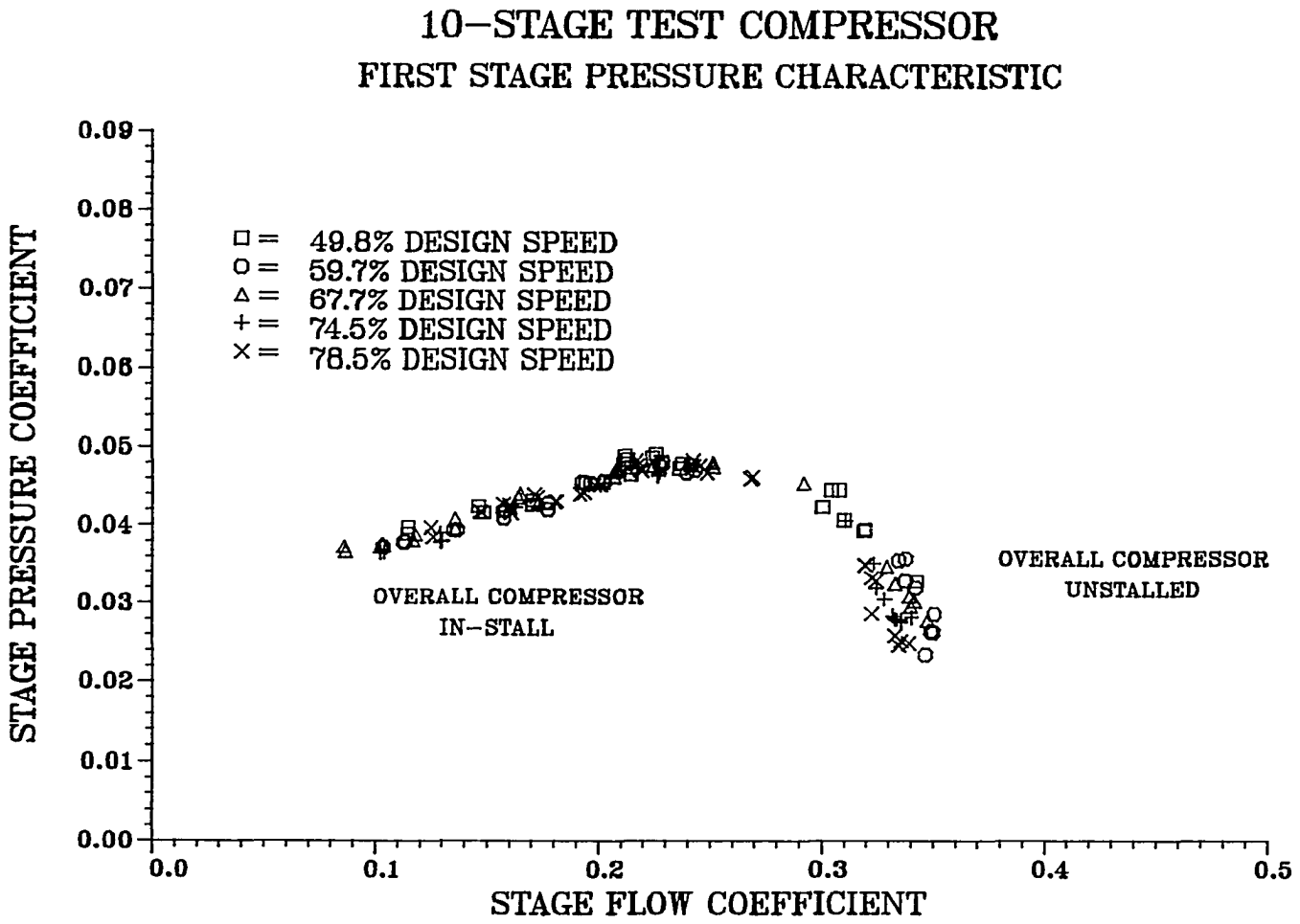

Figure 7.5 Test compressor first stage pressure characteristics

in Appendices B,C,D,E, and F. The data in Figure 7.5 show that the pressure characteristic of the first stage is essentially the same for all speeds. The data also indicate that individual stage pressure coefficient levels may increase when the overall compressor stalls as the slope of the characteristic is positive after overall compressor unstalled operation.

Figure 7.5 shows that after overall compressor stall the first stage produces a greater pressure rise than when the overall compressor was unstalled because the slope of the characteristic is still negative. At lower flow coefficients (0.2) the first stage does appear to be in-stall since the slope of its characteristic is positive. The characteristic is similar in nature to single stage undergoing progressive stall defined in Ref. [48]. Progressive stall is a gradual increase in blocked annulus area due to stall, resulting in a continuous positively sloped characteristic. Reference [49] indicated that progressive stall was prevalent in inlet stages of a multistage compressor. Figure 7.6 indicates by the dashed line that the stage did not gradually become blocked by the stall cell as defined for progressive stall. Instead, an abrupt drop in flow coefficient occurred when

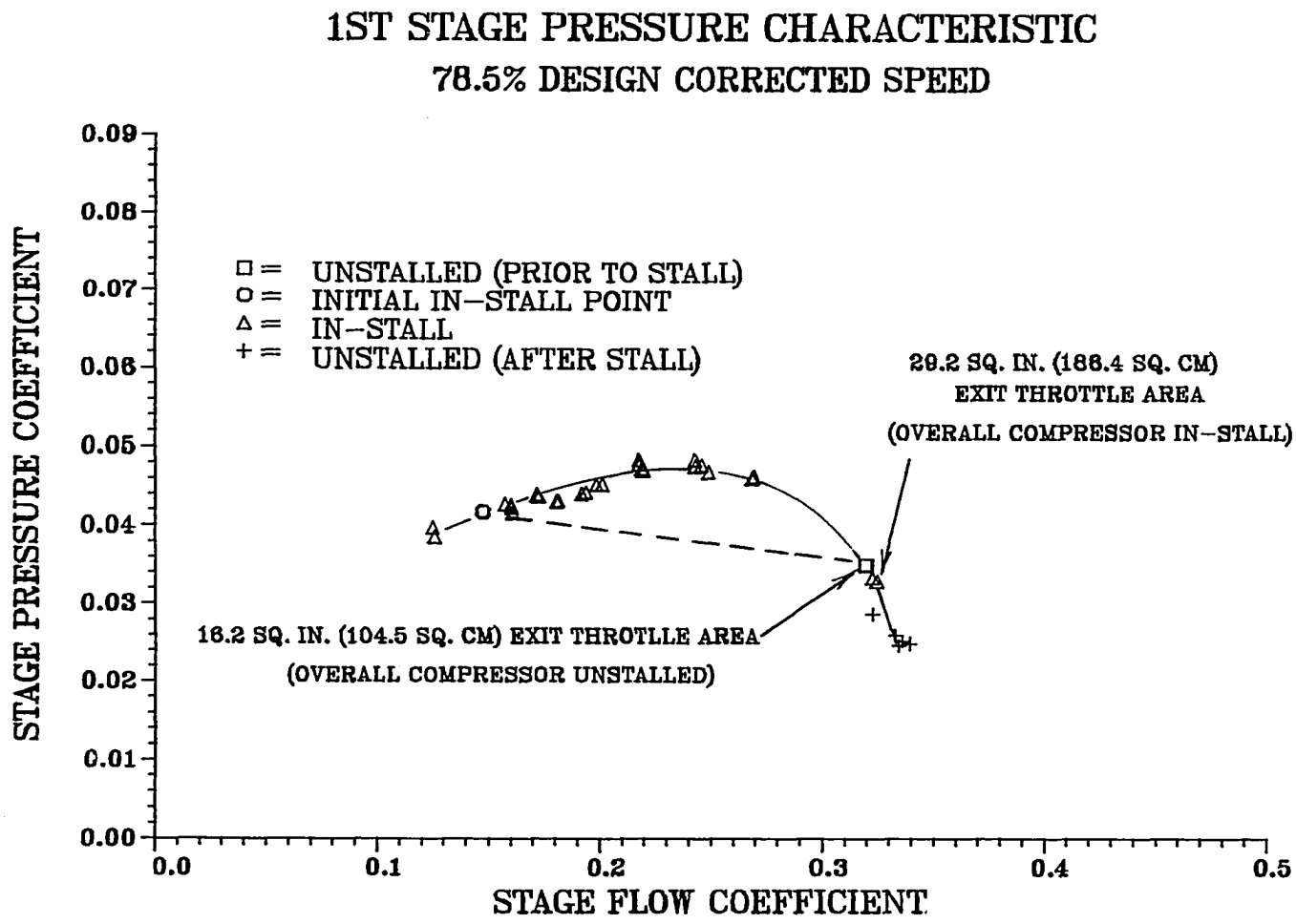

Figure 7.6 Rotating stall cell effect on first stage characteristic

the middle stages stalled resulting in overall compressor stall. Then, as overall compressor recovery was initiated by opening the compressor exit throttle, the continuous progressive stall nature of the first stage characteristic was exposed. The legend labeling for Figure 7.6 is defined for the overall compressor operation. Therefore, the symbols for unstalled operation are for the overall compressor operating condition. The occurrence of some stages operating unstalled while others are in stall was observed by Giannissis et al. [20] in a three stage mismatched compressor test. Mismatching of stages within the CRF test compressor resulted in some stages operating unstalled while the overall compressor exhibited stalled performance levels.

Stages at the front of the compressor perceive the stall cell in the middle stages of the compressor as a throttle, and therefore operate at higher pressure coefficients levels, than they would without the middle stages stalling. Additional support for the notion that rear stages operating in rotating stall act as a throttle to front stages in the CRF test compressor will be presented with the time-resolved results. Data shown previously in Figure 7.6 provide further evidence that the

stall cell in the middle stages of the CRF test compressor acts as a throttle for the first three stages. At 78.5% of design corrected speed the first stage characteristic has two identical operating points for different compressor exit throttle settings. The exit throttle area of 16.2 in^2 (104.5 cm^2) for the overall unstalled compressor operation produces the same operating point as an exit throttle area of 29.2 in^2 (188.4 cm^2) for overall compressor in-stall operation. This similarity of operating point for two distinct throttle areas also occurred in the second and third stages as shown in Appendix F, Figures 17.3 and 17.4. Additional evidence of individual stages of the CRF test compressor operating on the unstalled part of their characteristic while other stages are operating in-stall are provided later in this section and also when time-resolved data are analyzed in the next section of this dissertation.

Increased pressure rise in individual stages after overall compressor stalling has not been observed in low-speed, low-pressure-rise compressor in-stall tests and therefore must be an important consideration in high-speed multistage modeling.

Figure 7.7 details the pressure characteristics of the second stage of the CRF test compressor for all test speeds. Unstalled pressure coefficient levels range from 0.0 to 0.4 with the characteristic nearly vertical. When stage pressure characteristics are near vertical the stage is operating at high flow conditions far from stall (see Figure 1.2, Section I). As the characteristic becomes more nearly horizontal (zero slope) stalling is more likely. At zero or small positive slopes stalling occurs.

Data shown in Figure 7.7 indicate that the second stage is operating far from stall in the overall compressor unstalled operating region. When the overall compressor stalls, overall flow levels are reduced and the second stage moves up to a higher pressure rise operating location on the negative sloped portion of the characteristic. The second stage, like the first stage, appears also to be operating unstalled when the overall compressor is operating on the in-stall portion of its characteristic. Unlike the first stage which eventually stalls, the second stage does not stall, even when passing very low flow. Large flow fluctuations, as a result of a middle stage of the compressor stalling, would normally cause a nearby stage to stall if it were operating near to its stall

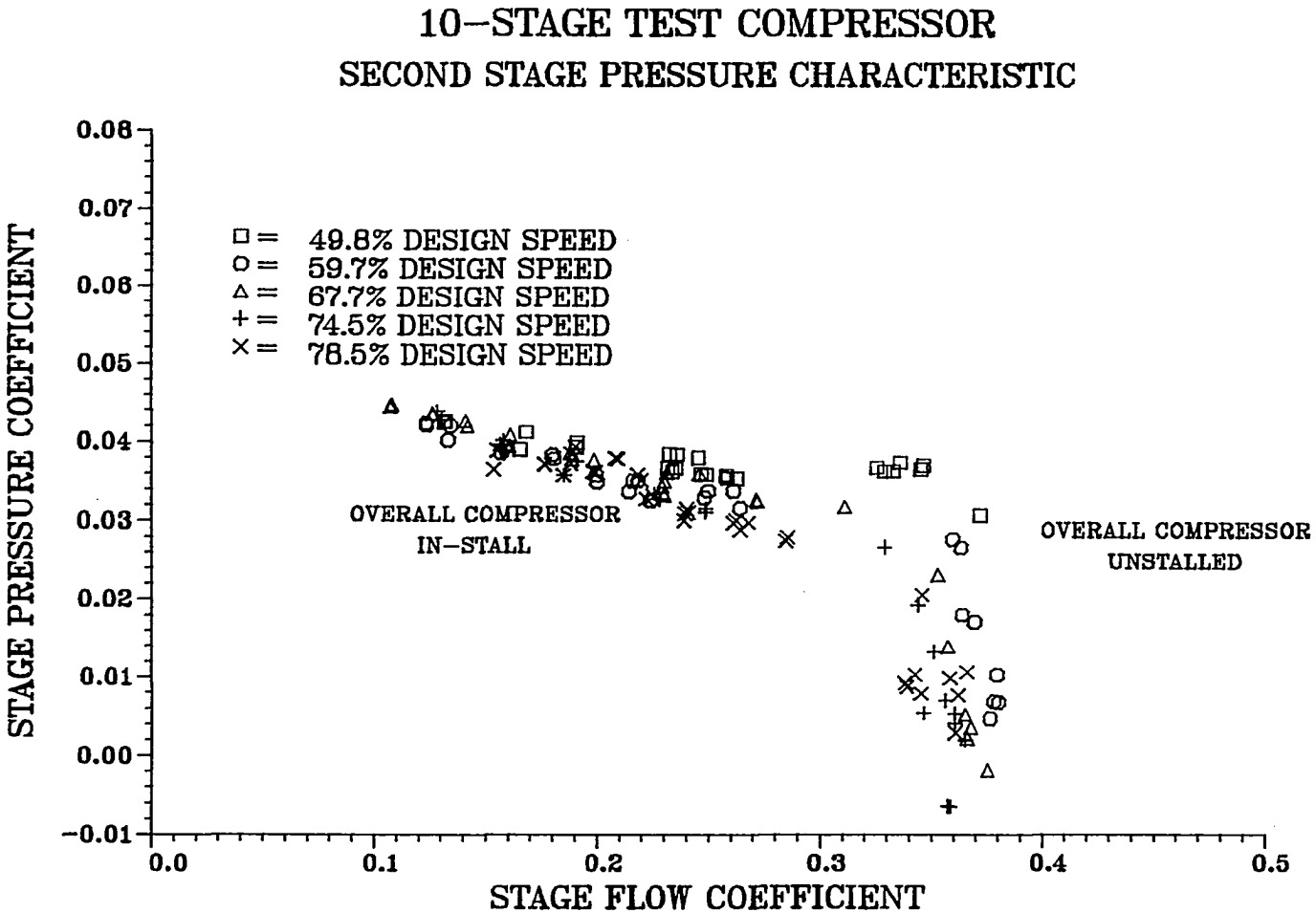

Figure 7.7 Test compressor second stage pressure characteristic

point. Stages operating at flow coefficients appreciably above the value for stall or near their choke limit, however, tend to decrease the amplitude of flow fluctuations resulting from rotating stall in other stages and therefore may not stall (see Ref. [49]). The large flow coefficient range (0.1 to 0.35) of second stage unstalled operation, detailed in Figure 7.7, may be a result of the pressure fluctuations being imposed upon it from the rear stalled stages. Epstein [35] reported that it is possible to conteract the disturbance that initiates rotating stall by creating an imposed disturbance. This is one possible explanation for the large flow coefficient range of unstalled operation of stage 2, and stage 3 to be discussed next. The data in Figure 7.7 also indicate that unlike the first stage, the second stage produces higher pressure coefficient levels in the overall compressor in-stall operating region, at lower speeds levels.

The data in Figure 7.8 for the third stage also indicate this second stage trend of lower pressure coefficient at higher speeds. At speeds above 59.7% design corrected speed the third stage of the CRF test compressor suffers losses that are large enough to result in a negative pressure coefficient during overall unstalled

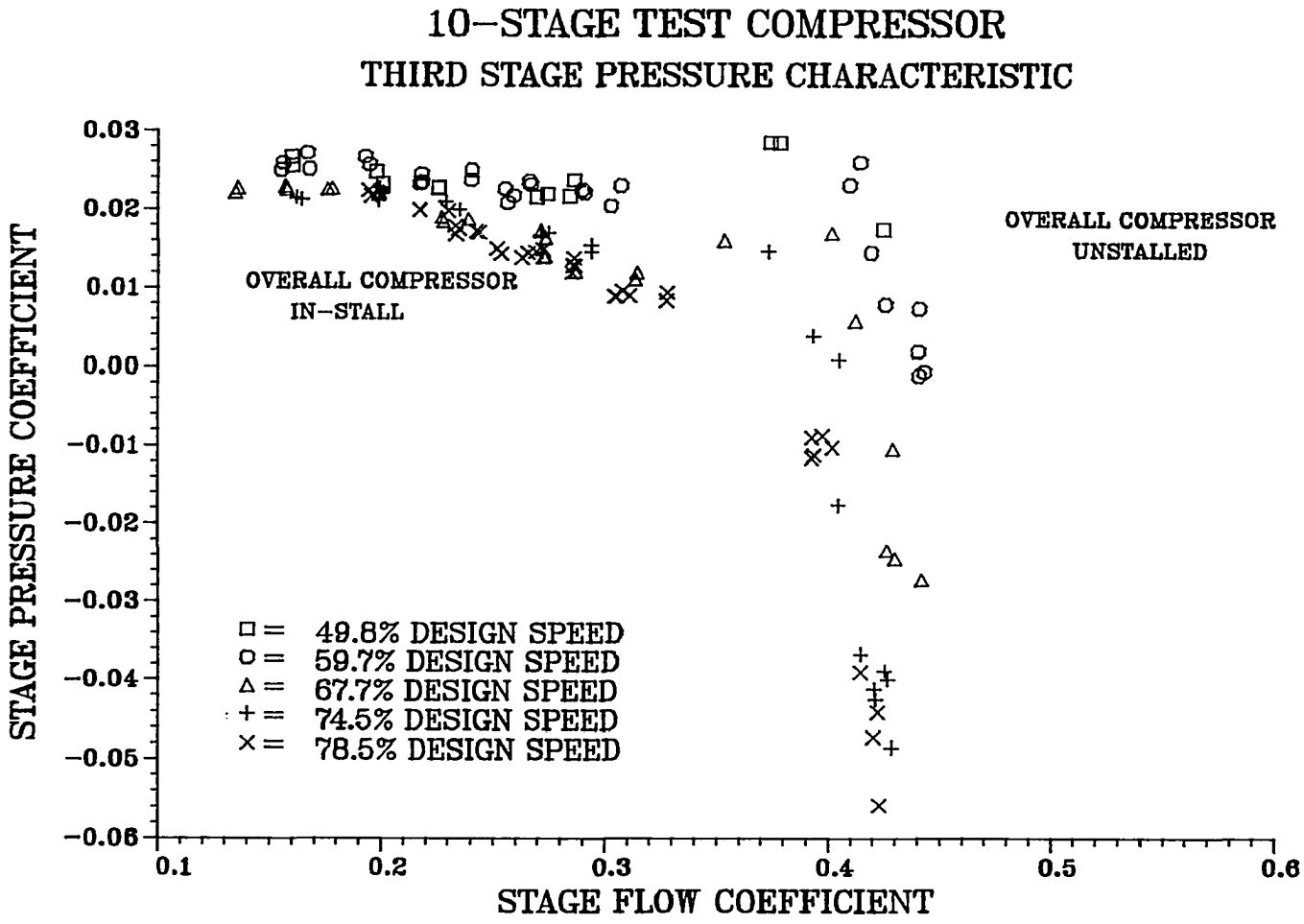

Figure 7.8 Test compressor third stage pressure characteristic

operation. The third stage also exhibits a characteristic that indicates unstalled operation while the overall compressor is operating on the in-stall portion of its characteristic. Stages 2 and 3 do not appear to be stalled during overall compressor in-stall operation.

The reduced values of pressure coefficient for stages 2 and 3 associated with the overall compressor operating in-stall are the primary reason for the lower overall compressor in-stall characteristic at higher speeds (see Figure 7.1). If the pressure rise from stages 2 and 3 could be increased by altering vane positions with no other stage affected, the overall in-stall characteristic could be raised to higher pressure rise levels. This alteration could also result in a more recoverable compressor.

Data shown in Figure 7.9 represent the fourth stage characteristics of the CRF test compressor for all speeds tested. The slope of the characteristics for both unstalled and in-stall operation of the compressor does not vary with speed. The level of the unstalled pressure characteristic (0.08) is much higher than the levels obtained by stages 1 thru 3 (0.02 to 0.045), indicating a much higher loading of the fourth stage compared to the first three stages. The high loading of stage four and low

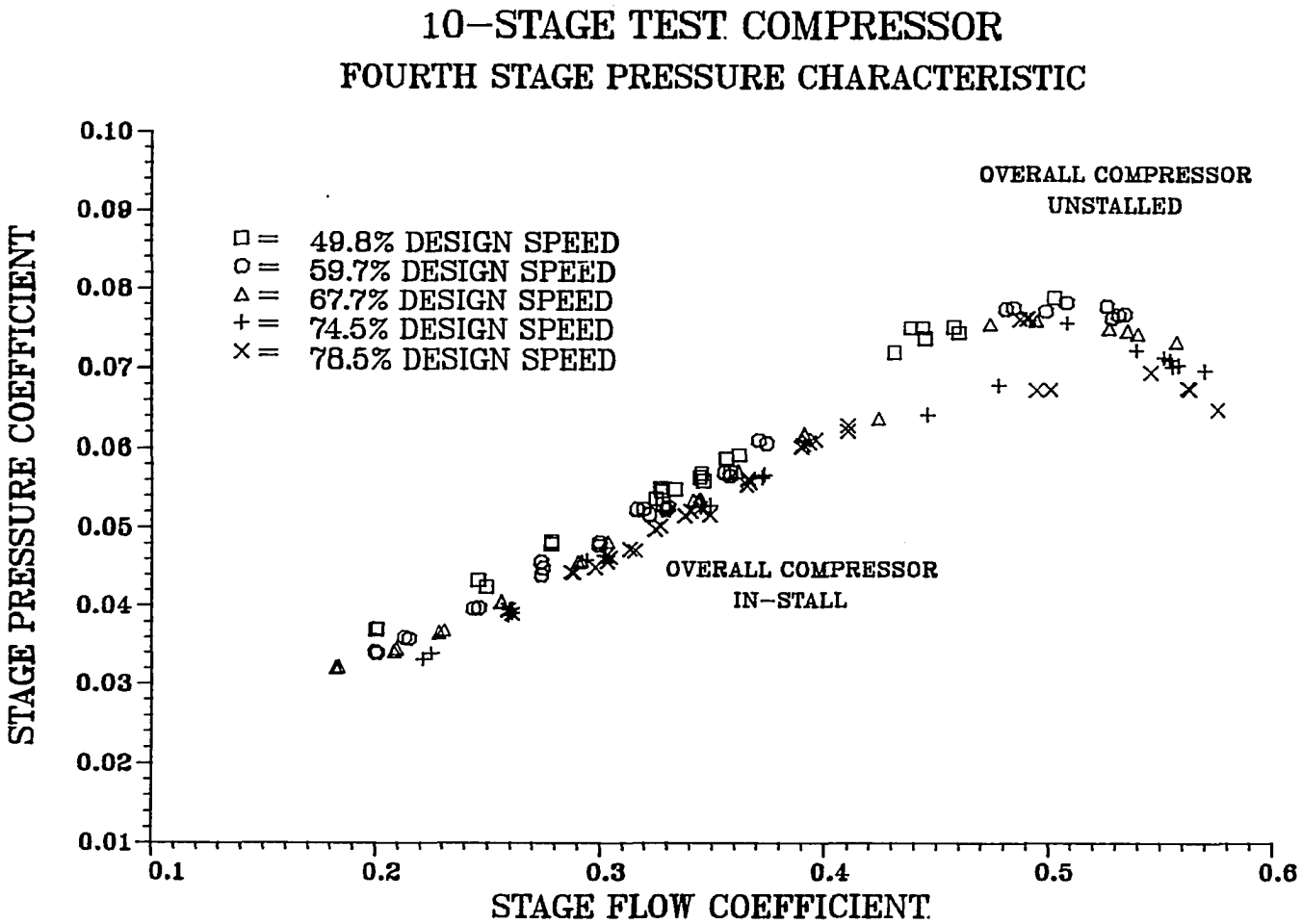

Figure 7.9 Test compressor fourth stage pressure characteristic

loading of stages one through three results in a mismatching between stages three and four at the speeds tested. The fourth stage operates near stall while the first three stages are still operating far from stall. At 49.7% speed, the unstalled fourth stage characteristic extends well into the positive slope region prior to the overall compressor stalling. No other unstalled stage characteristic reaches a positive slope at 49.7% of design speed prior to compressor stalling. Therefore, it is suggested that at 49.7% speed the fourth stage initiates overall compressor stalling.

The mismatching between stages three and four results in the CRF test compressor operating as if it consisted of two compressors, one compressor made up of the first three stages that are unloaded, and the other, a seven-stage compressor with a front stage (stage four) loaded to near stall at 49.7% speed. This observed mismatching is important for understanding the reason for the large in-stall hysteresis levels associated with the CRF 10-stage compressor. This type of mismatching, unloading the first three stages at low speeds to increase their stall free range, tends to produce high overall compressor flow rates

and high stall margins at part design speed (see Ref. [49]). In normal design practice, at part design speed, the front stages of a multistage compressor would be highly loaded to create high pressures for the back stages to help them avoid choking. These highly loaded front stages are then operating near stall and they are therefore very susceptible to stalling from inlet distortions. In aircraft engines that have fan stages in front of the compressor, tolerance to fan exit flow distortions is desired. This tolerance to distortion can be achieved by unloading the first three compressor stages and moving their operating point far from stall to their high flow regions. Further analysis in this dissertation will show that this design strategy of unloading the front stages of a multistage compressor may result in reduced compressor recoverability.

The in-stall characteristic of the fourth stage (see Figure 7.9) is positive sloped, like results obtained from low-pressure-rise, low-speed compressor tests. The fourth stage does not generate the increase in pressure rise with reduction in flow as did the first three stages. Instead, the pressure rise decreases with decreasing flow when the overall compressor is operating on its in-stall

characteristic. The overall compressor in-stall portion of the stage characteristic at 78.5% design corrected speed extends to flow coefficients, 0.49 and above, where two values of pressure coefficient are possible.

The fifth stage pressure characteristics are shown in Figure 7.10. The in-stall characteristics for the fifth stage vary slightly with speed. As was the case with the third stage, the fifth stage in-stall pressure coefficients are lower at the higher speeds. Also, for 74.5% and 78.5% design speeds, there exists doubled valued operating zones for the unstalled and in-stall characteristics. This is true for stages 5 though 10 at speeds of 74.5% and 78.5% design speed and as mentioned earlier for stage four at 78.5% design speed. These double valued characteristics for the stages reflect the large in-stall hysteresis of the CRF test compressor at higher speeds.

The sixth stage characteristics are shown in Figure 7.11. The unstalled portion of the characteristic has a near zero slope for all speeds, indicating high load operation for all speeds. The in-stall characteristic is positive sloped similar to the fifth stage.

The seventh stage characteristics are provided for all speeds in Figure 7.12. The slope of the in-stall portion

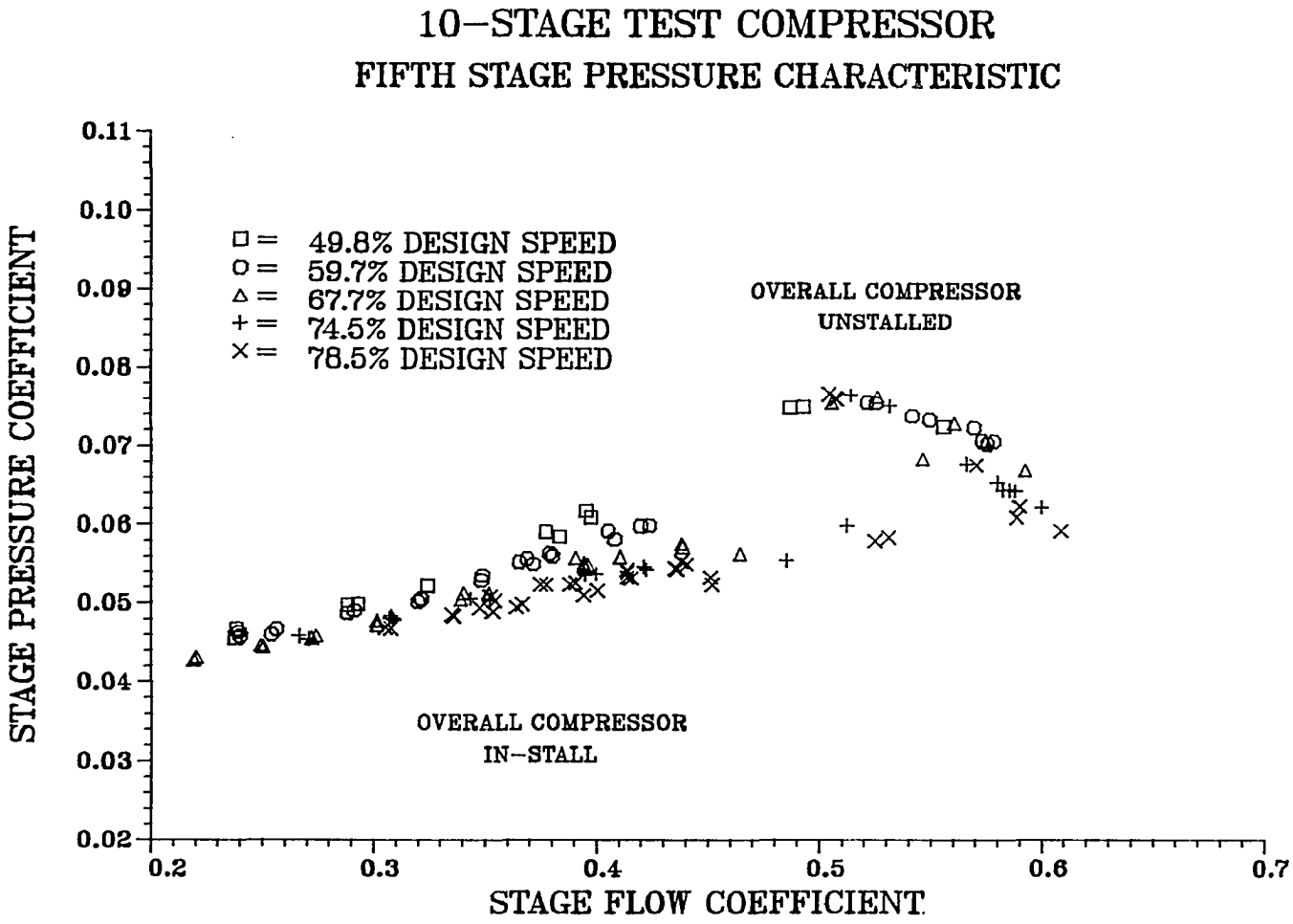

Figure 7.10 Test compressor fifth stage pressure characteristic

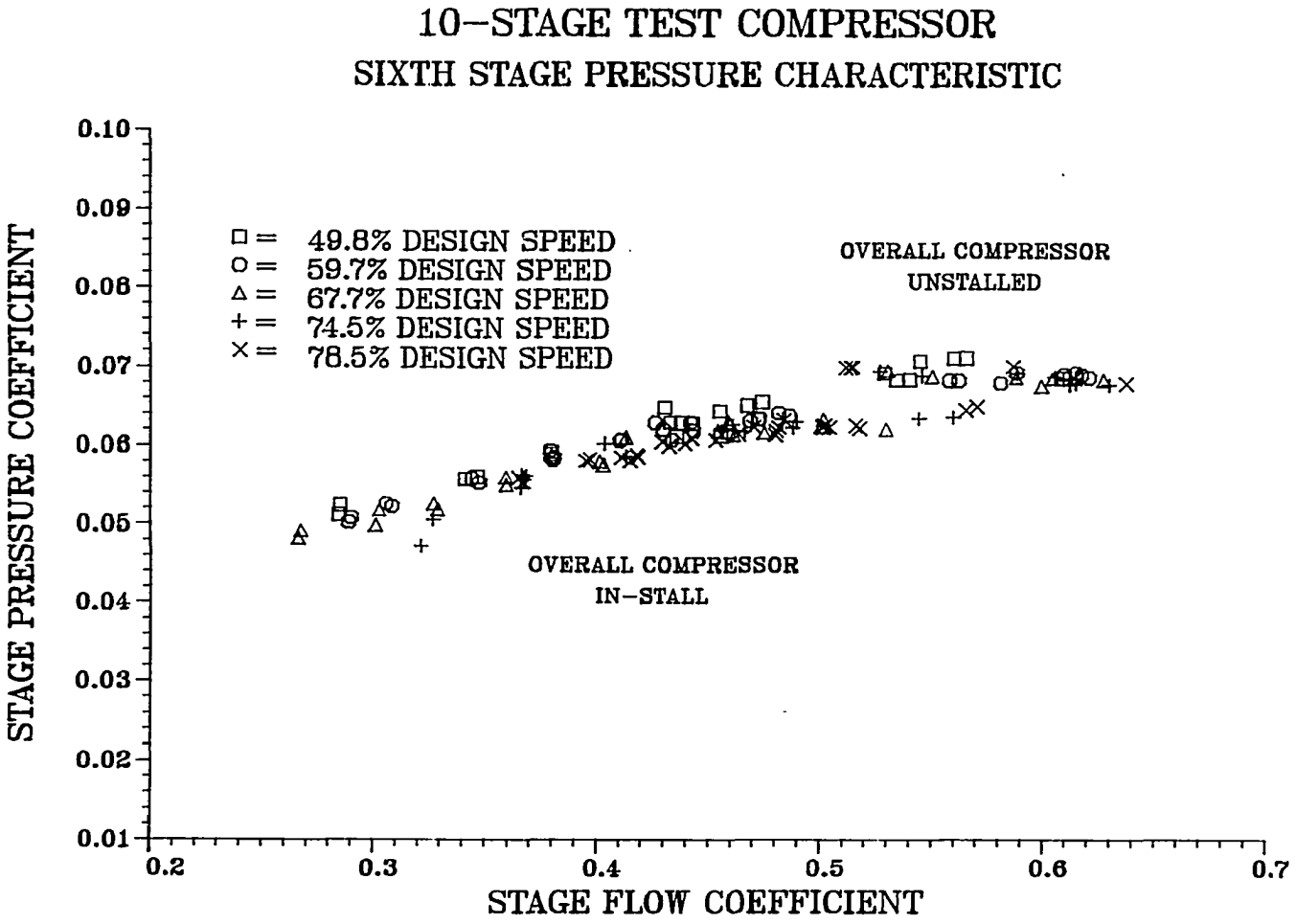

Figure 7.11 Test compressor sixth stage pressure characteristic

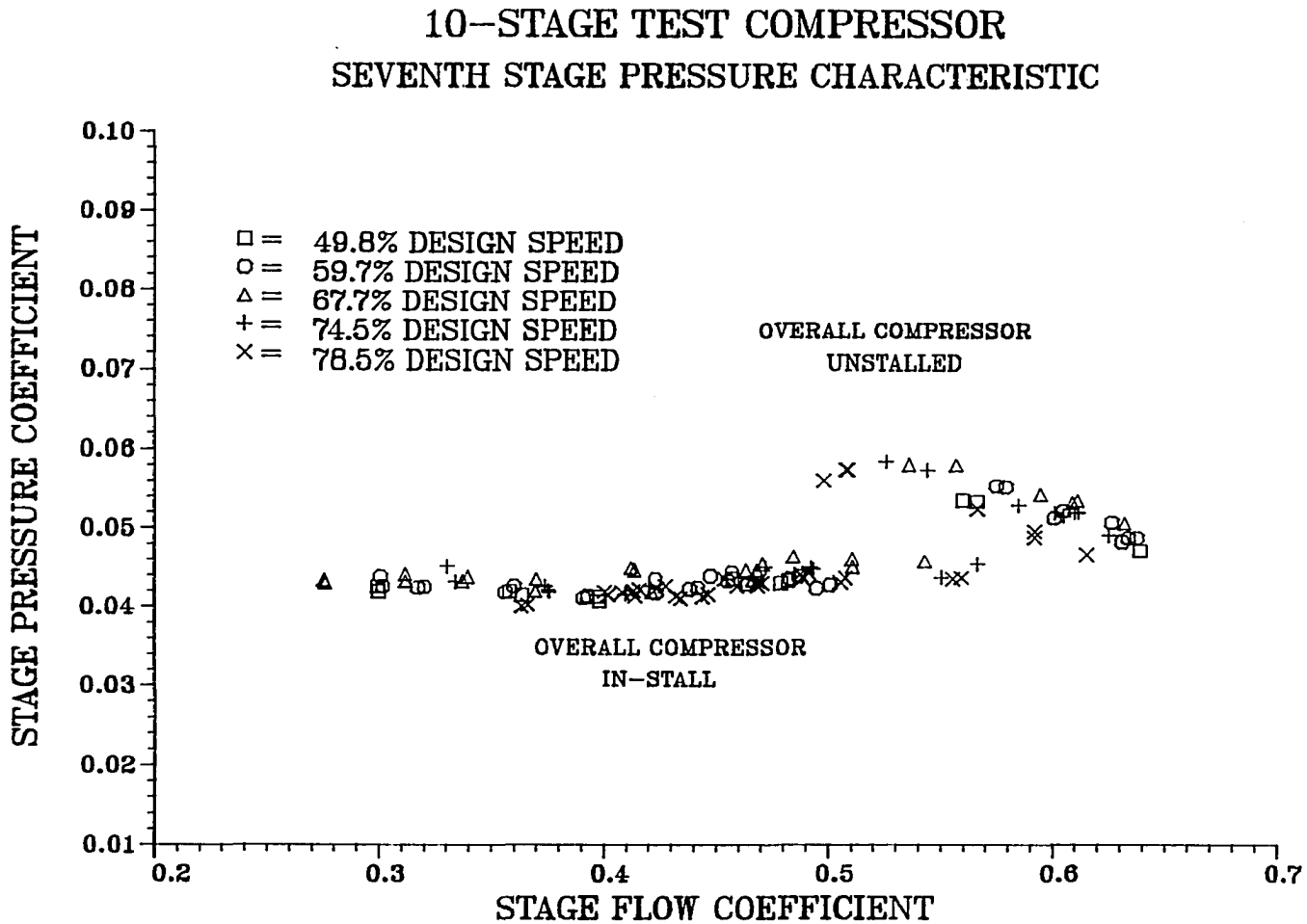

Figure 7.12 Test compressor seventh stage pressure characteristic

of the seventh stage characteristic is near zero for all speeds. The unstalled portion of the characteristic reaches positive slopes at 78.5% design corrected speed. No other stage characteristic reaches a positive slope at 78.5% design corrected speed. Therefore, at 78.5% design speed overall compressor stalling is initiated by the seventh stage, not the fourth stage as was the case for 49.7% design speed. This is because of the reduced pressure rises of the first three stages at 78.5% design speed compared to those at 49.8% design speed. The reduced pressure coefficients, and resulting lower exit fluid density, for the first three stages at 78.5% design speed cause the fourth stage to operate at higher flow coefficient operating points (lower pressure coefficient operating points) than at 49.8% design speed for the same throttle setting. This allows the compressor exit throttle area to be reduced further until the seventh stage reaches its stalling flow coefficient before the fourth stage does.

The difference in the stalling stage for different speeds may also have an effect on the overall compressor in-stall hysteresis. This is explored further in the discussion of the time-resolved test compressor results.

The eighth stage characteristics provided in Figure 7.13 shows that the unstalled characteristics remains negatively sloped for all speeds, indicating that this stage does not initiate compressor stalling. This is true for stages 9 and 10 also. The in-stall characteristics do show higher pressure coefficient levels for the higher speed of 78.5% of design corrected speed, but it is not enough to result in higher overall compressor pressure coefficients at the higher speeds.

The ninth stage pressure characteristics are shown in Figure 7.14 and indicate that the in-stall portion of the characteristics are slightly negative sloped, until above flow coefficient levels of 0.52. This type of characteristic has been reported by Day and Cumpsty [31] for a high design C_x/U low-speed 3-stage compressor. The data in Figure 7.14 also indicate that more double valued operating points exists between unstalled and in-stall operation.

The tenth stage pressure characteristics are detailed for all speeds in Figure 7.15. The characteristics for both unstalled and in-stall operation do not vary significantly with speed. The unstalled characteristics are near vertical at the lower pressure coefficients,

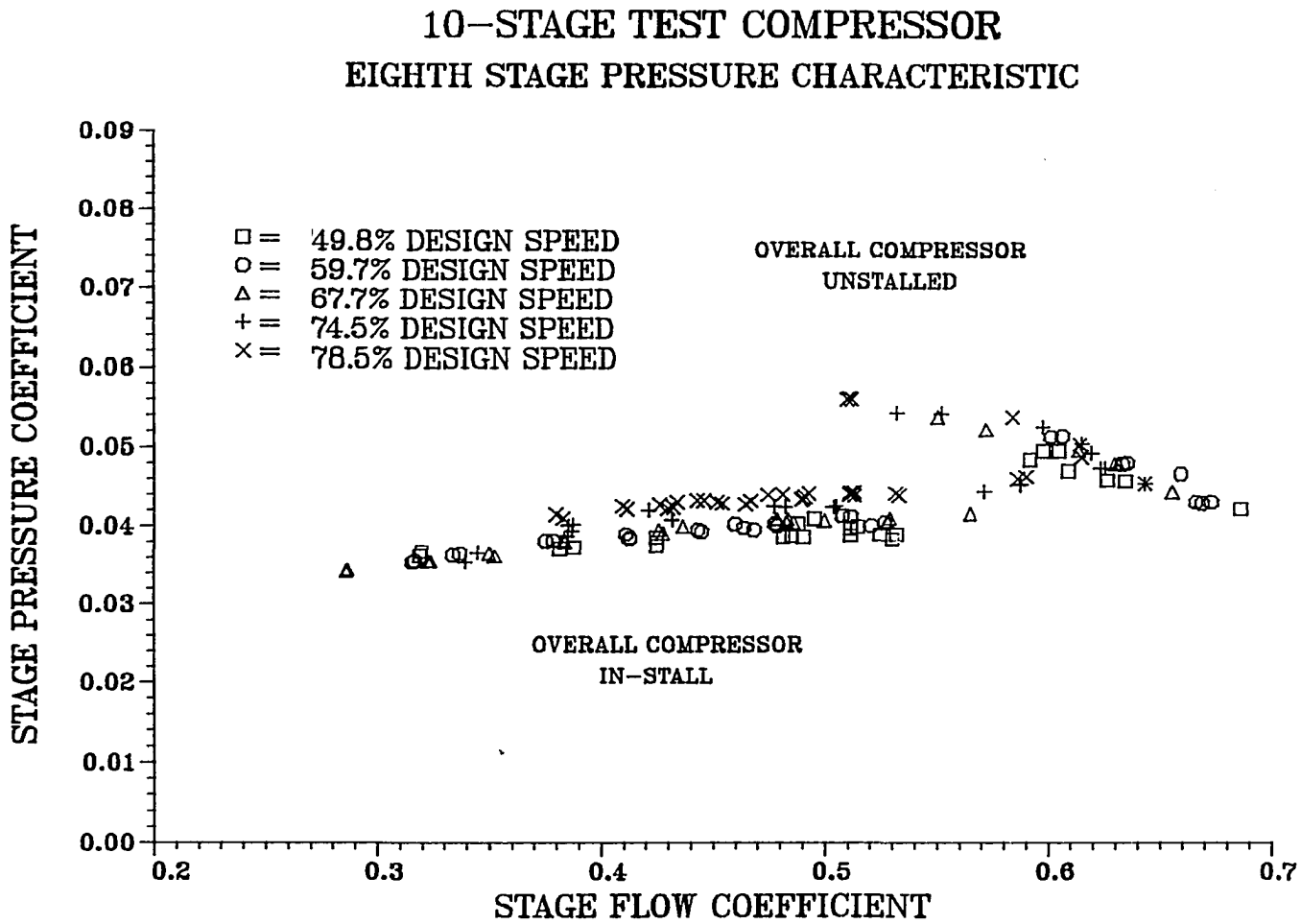

Figure 7.13 Test compressor eighth stage pressure characteristic

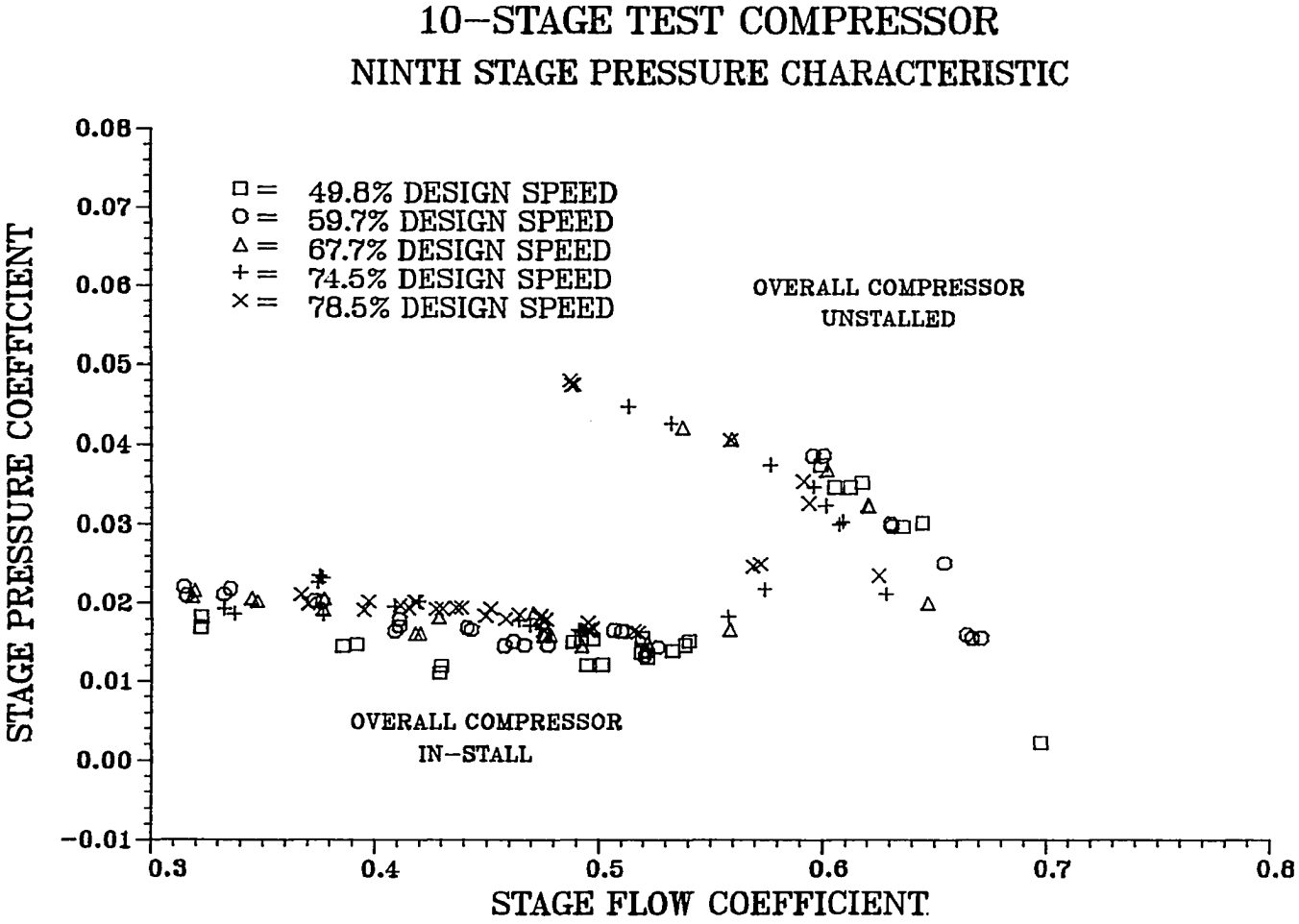

Figure 7.14 Test compressor ninth stage pressure characteristic

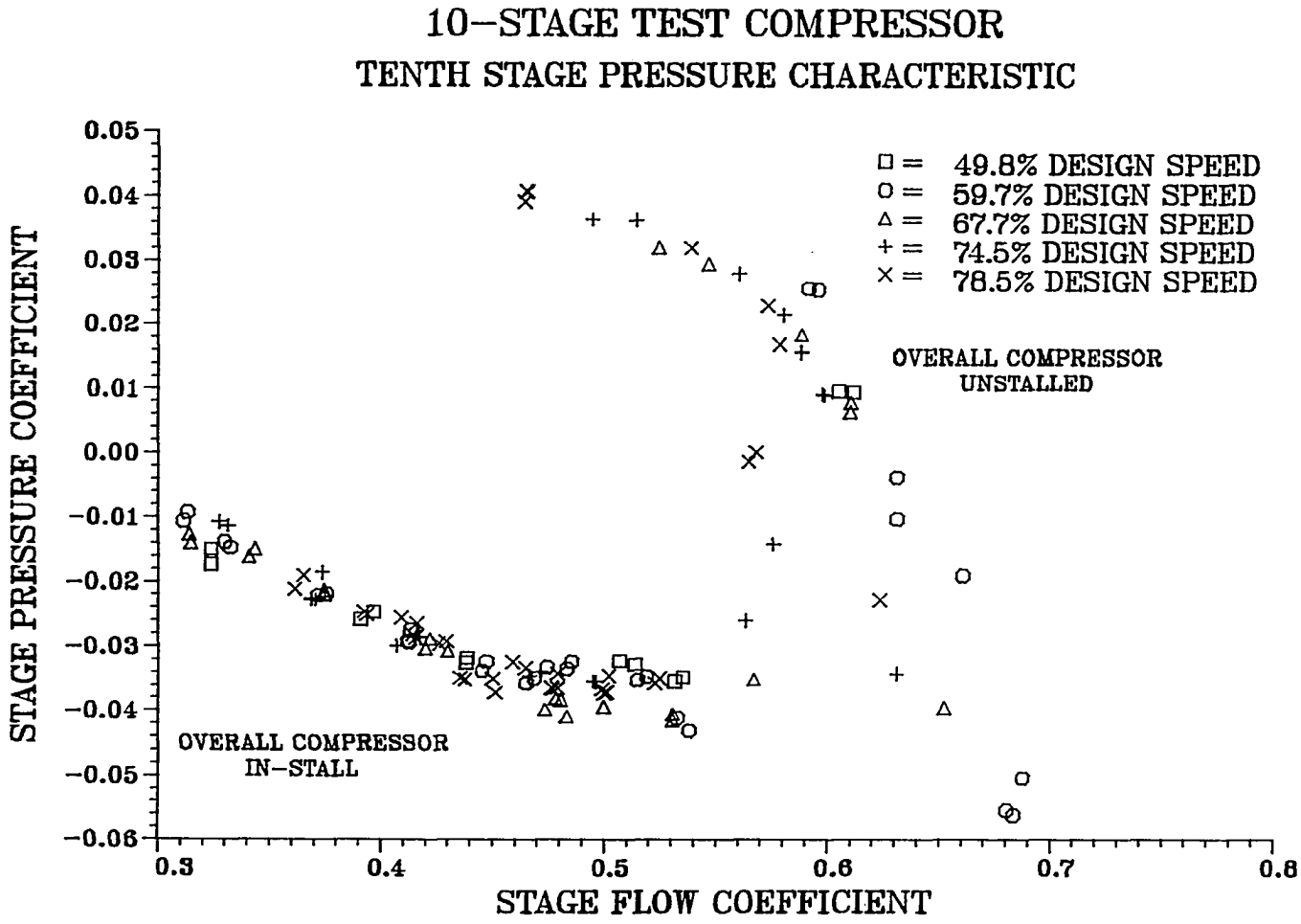

Figure 7.15 Test compressor tenth stage pressure characteristic

indicating high flow levels. This is typical for rear stages of a multistage compressors while operating at the low shaft speeds as defined in Ref. [48]. The unstalled pressure coefficient curve extends to negative values for more open throttle settings. The tenth stage is extracting work at these low speeds for the more open throttle settings. Stall margin of the overall compressor at design speed is normally controlled by the stall margin of the rear stage (see Ref. [49]). Matching the rear stage with the front stages so it passes very high flows with negative pressure coefficients at 78.5% design speed allows for much greater overall compressor stall margin when the compressor is operating at 100% design speed. Therefore mismatching of the first three stages, as discussed earlier, and mismatching of the tenth stage result in high stall margin over the complete range of operating speed of the compressor. However, this mismatching results in high hysteresis levels and low recoverability as is discussed in the next subsection where the time-resolved data are reviewed.

The in-stall characteristic for the tenth stage shown in Figure 7.15 involves negative pressure coefficient

levels for all speeds and all operating points. Characteristics obtained from low-speed, low-pressure-rise compressor tests have not involved negative pressure coefficient levels during overall compressor in-stall operation. The negative values are caused by the low pressure rise created by stages one through nine when the compressor is operating in stall. The low pressure rise and elevated temperatures, which are discussed next, result in low density air entering the tenth stage. The result is higher than anticipated velocities even when the overall compressor is operating in stall. Further evidence of high velocities through the tenth stage when the overall compressor is operating in stall are presented in the next subsection on time-resolved data. The in-stall characteristic is negatively sloped until a flow coefficient of 0.55 is obtained by opening the throttle. The overall compressor did not operate in stall at tenth stage flow coefficients higher than 0.55 except at 67.7%, 74.5% and 78.5% of design corrected speed. It is possible that for tenth stage flow coefficients above 0.55, the flow velocities in the blockage free part of the annulus are very high resulting in choking. The rotating stall cell in the middle stages of the compressor forces the air to flow

through the unblocked portion of the annulus. Even though the exit mass flow rate is reduced upon stalling, it is still high enough to cause high velocities through the unblocked portion of the tenth stage. The drop in pressure and increase in temperature, as shown in Figures 7.16 and 7.17, after stalling the overall compressor results in lower density and higher velocities at the tenth stage. The data in Figures 7.16 and 7.17 were obtained by closing the throttle as indicated by the arrow along the exit throttle axis.

After the compressor has stalled and the throttle is opened, the flow increases as seen on the in-stall characteristic of the tenth stage in Figure 7.15. The tenth stage losses also increase as made evident by the negative sloping in-stall characteristic.

Even though the time averaged in-stall total pressure does rise with throttle opening as shown in Figure 7.18, thereby increasing the fluid density, the fluid density is still not large enough to reduce rotor ten velocity levels. The data in Figure 7.18 were obtained by opening the throttle as indicated by the arrow along the exit throttle area axis. The negatively sloping tenth stage characteristic (see Figure 7.15) causes stage operation to

PRESSURE PROFILE

78.5% DESIGN CORRECTED SPEED

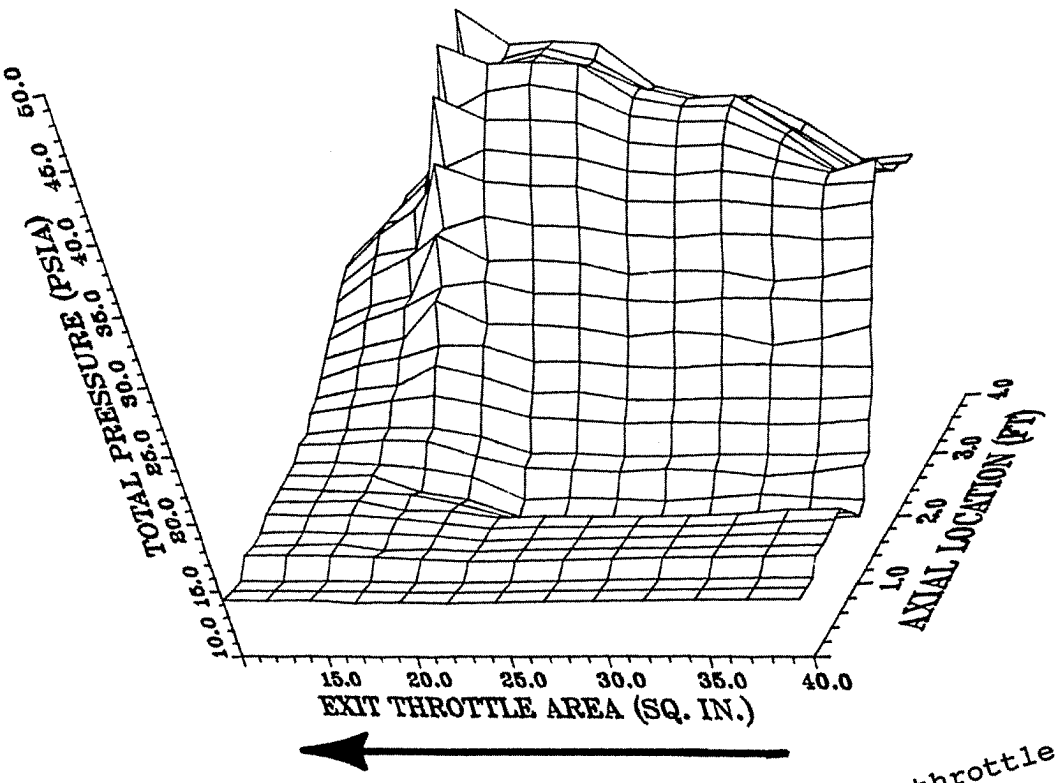

Figure 7.16 Test compressor pressure with throttle closing

TEMPERATURE PROFILE

78.5% DESIGN CORRECTED SPEED

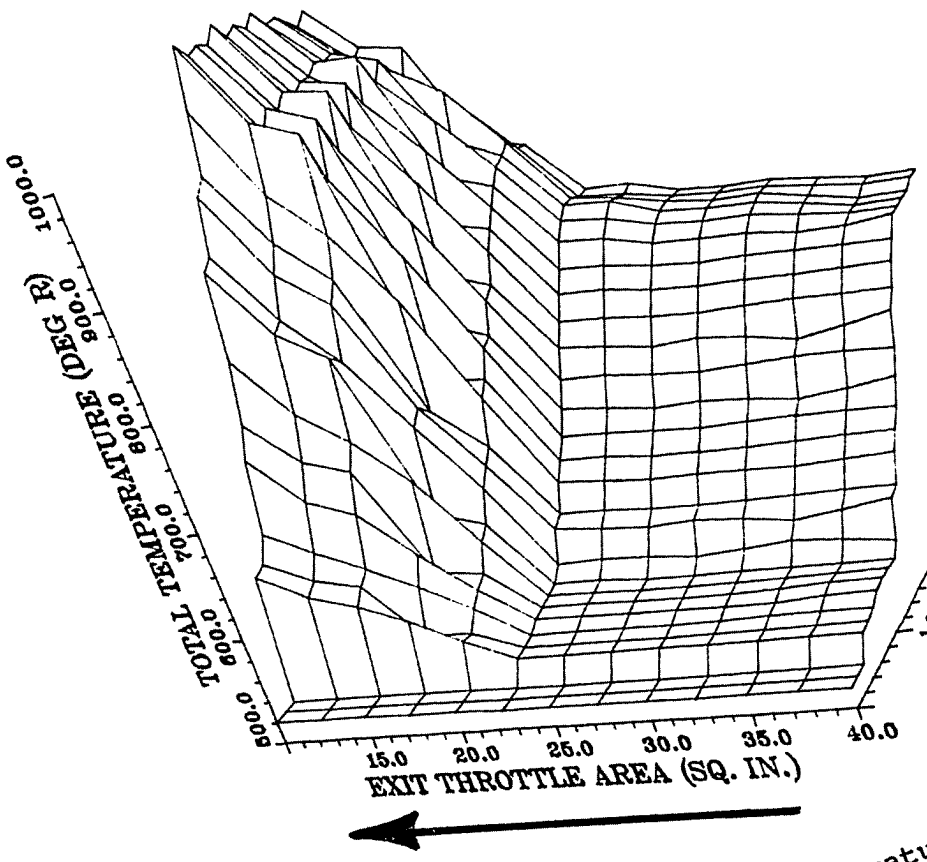

Figure 7.17 Test compressure temperature with throttle closing

IN–STALL PRESSURE
78.5% DESIGN CORRECTED SPEED

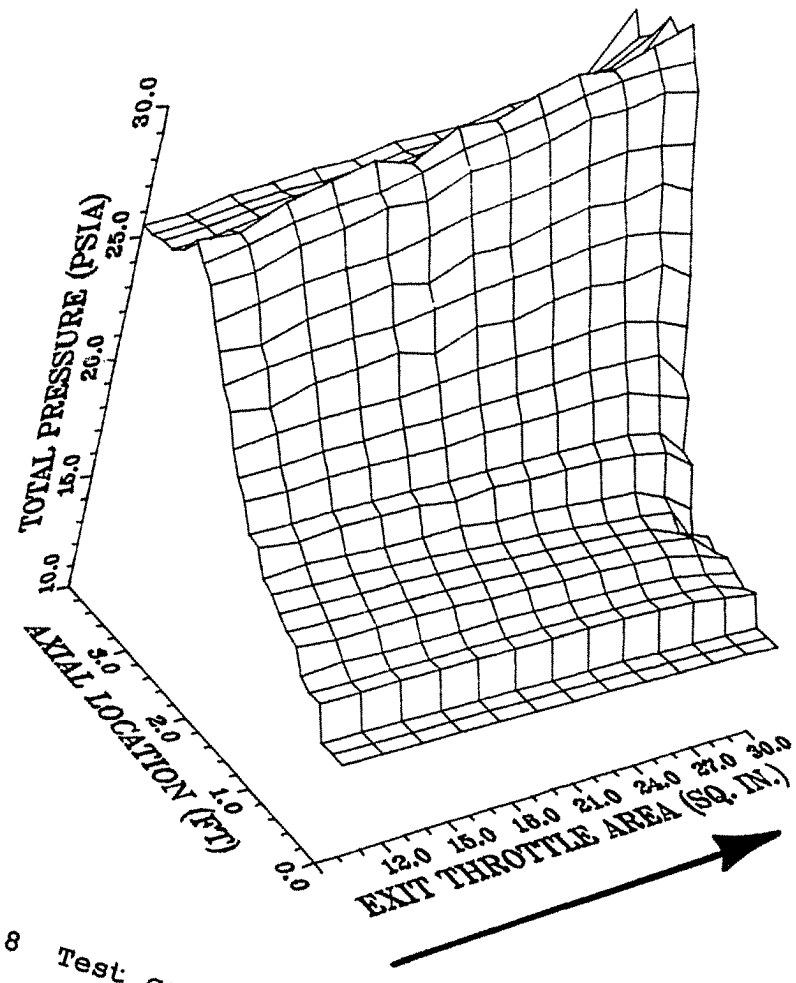

Figure 7.18 Test compressor pressure rise in-stall

diverge from the unstalled characteristic with exit throttle area increase and recovery is not possible.

Tenth stage operation continues down the in-stall characteristic to lower pressure coefficient levels as the throttle is opened up to a throttle area corresponding to a tenth stage flow coefficient of 0.55. At this point, pressure rise by the front stages of the compressor is great enough to increase the fluid density and reduce the velocity level in the unblocked portion of the tenth stage. Tenth stage pressure losses decrease and the in-stall characteristic slope changes from negative to positive. Stall cell size reductions also lessen the level of blockage in the stage, thus further lowering the velocities through the tenth stage. Once the tenth stage is operating on the positive-sloped portion of its in-stall characteristic recovery is rapid. From this throttle setting on only small increases in throttle area were required to increase the pressure rise across the stage because the velocities within the stage are decreasing and losses are dropping. The reason for this extended in-stall operation, resulting in high levels of overall compressor hysteresis, is discussed along with the time-resolved data.

Stage temperature characteristics for stages 1 through 5 of the CRF test compressor for all speeds tested are presented in Figures 7.19 through 7.23. The data show that for stages 1 through 5 the temperature coefficient rises continuously with reduction in flow during overall compressor in-stall operation. Data in Figures 7.24 through 7.28 for stages 6 through 10 indicate that the temperature coefficient drops continuously in the stages with flow reduction while the overall compressor is operating in-stall. Small and Lewis [12] reported this characteristic trend for a three-stage high-speed compressor as did Na'covska' [32] for a four-stage compressor. Positive slope time-averaged temperature characteristics for a compressor while it is operating in rotating stall have not been observed in low-speed compressors and were therefore not considered when simulated characteristics were developed by Davis [44] for the 9-stage analytical model.

To assist in explaining the effect of individual stages on overall compressor performance, an axial profile of total temperature and of total pressure for 49.7% and 78.5% design corrected speed are presented in Figure 7.29. These data detail the pressure and temperature rise for an

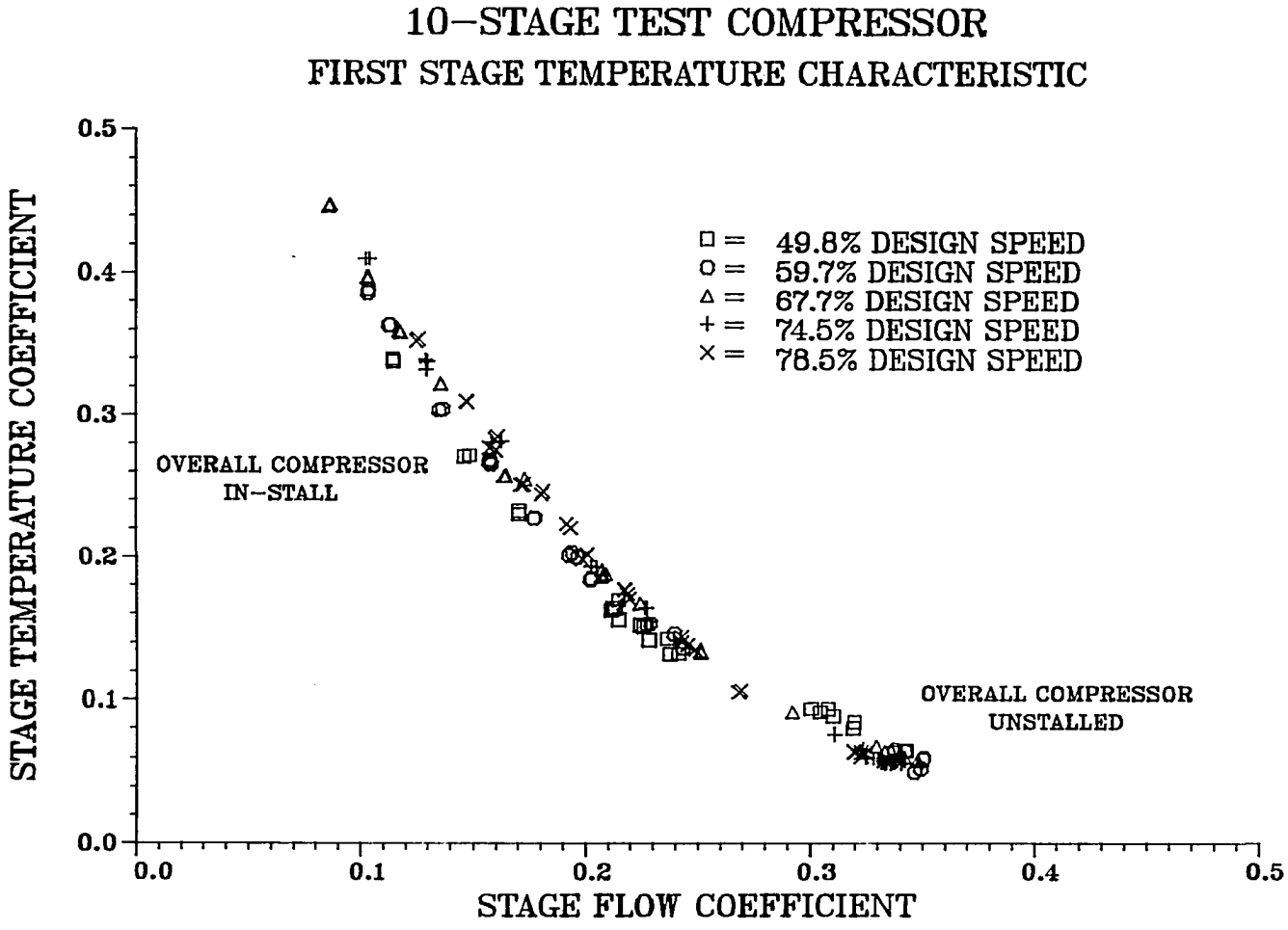

Figure 7.19 Test compressor first stage temperature characteristic

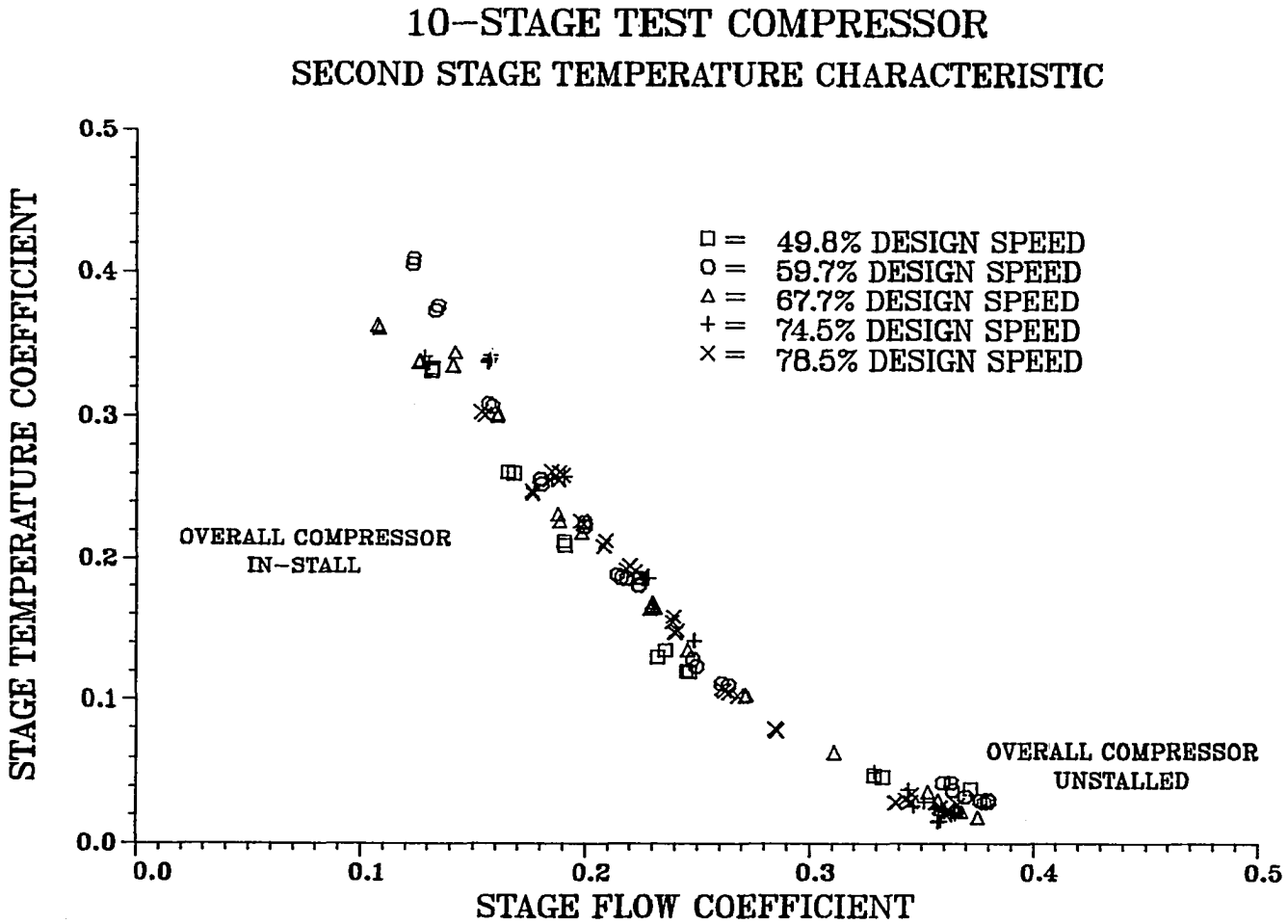

Figure 7.20 Test compressor second stage temperature characteristics

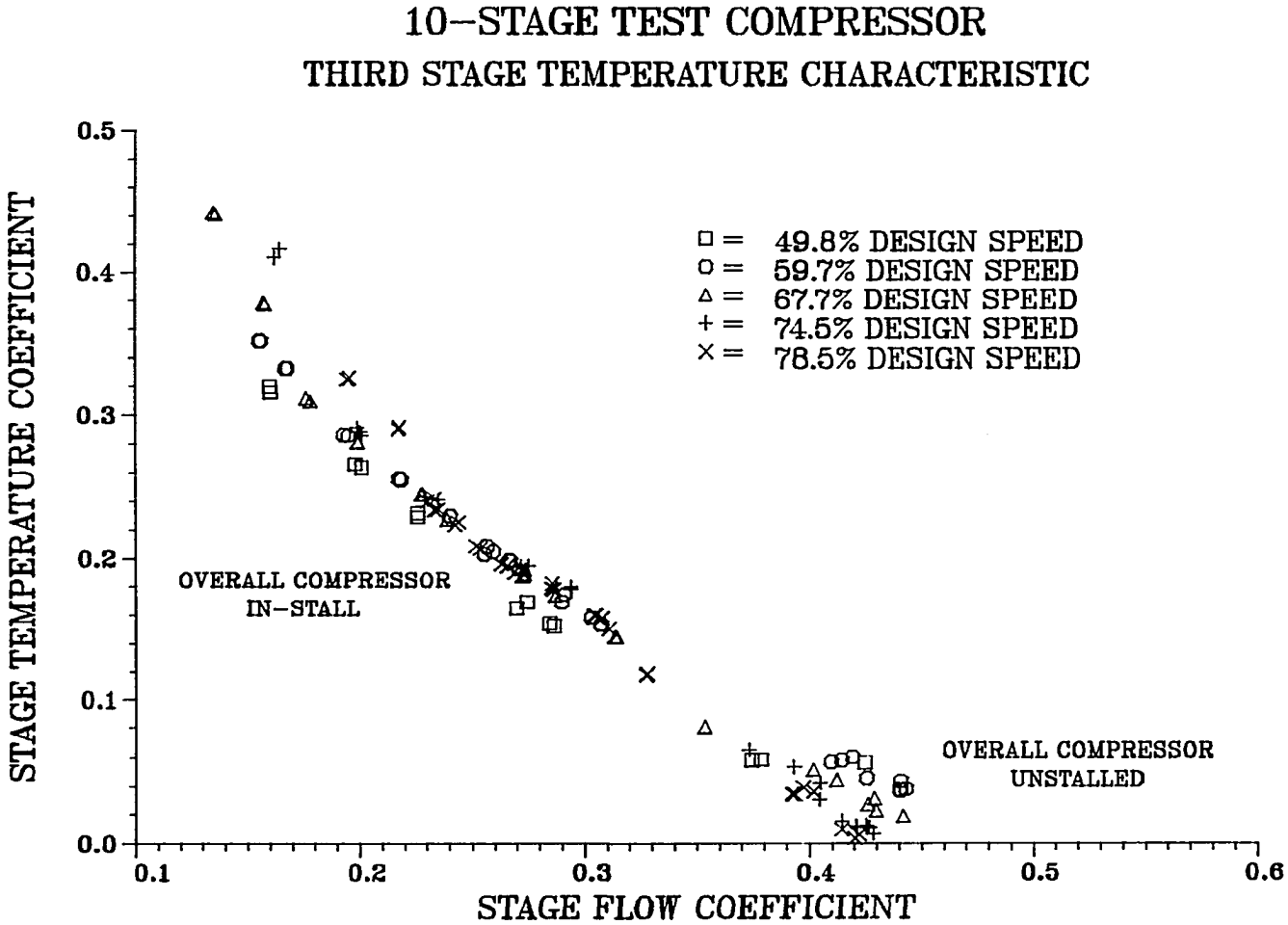

Figure 7.21 Test compressor third stage temperature characteristics

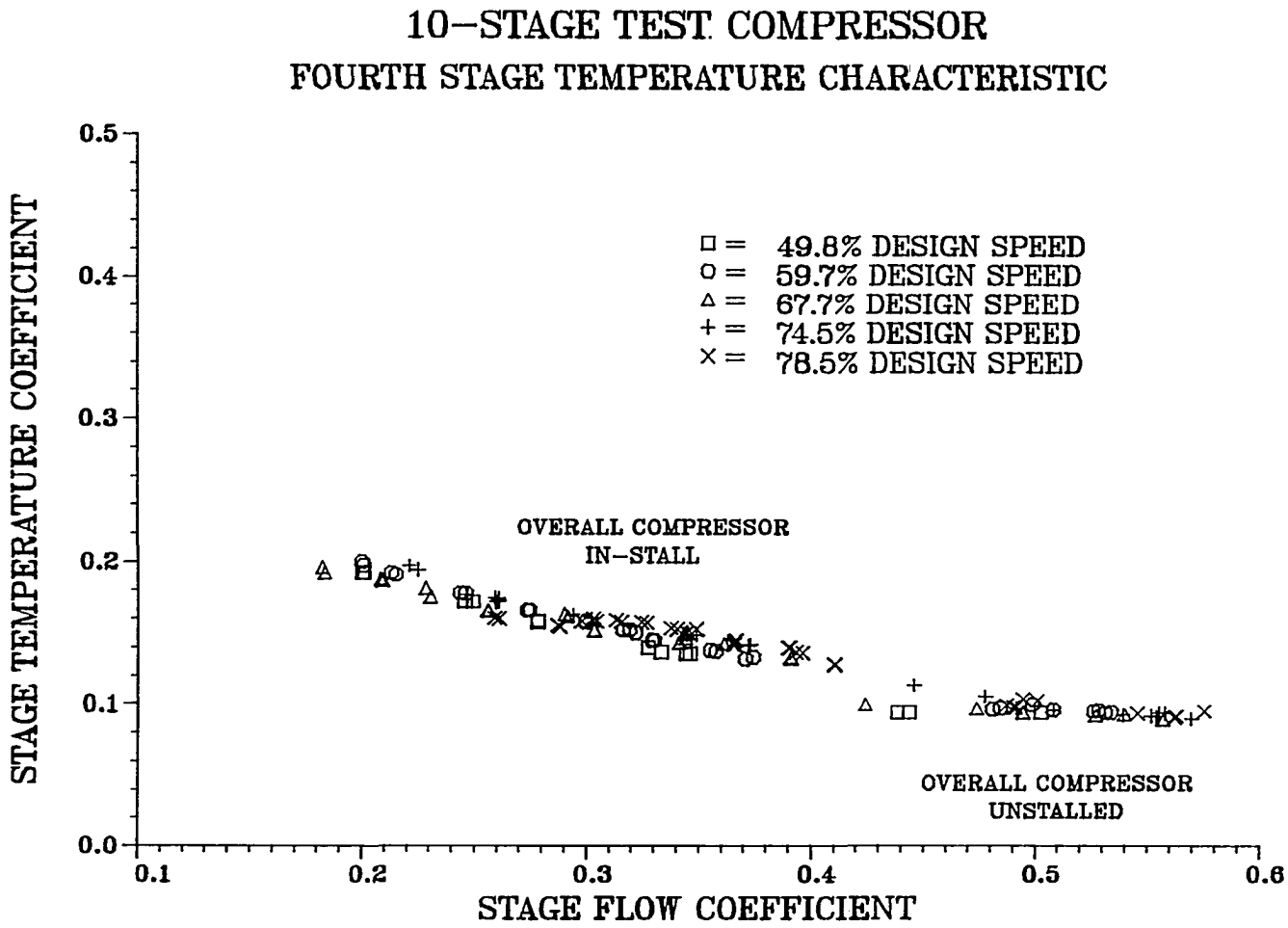

Figure 7.22 Test compressor fourth stage temperature characteristics

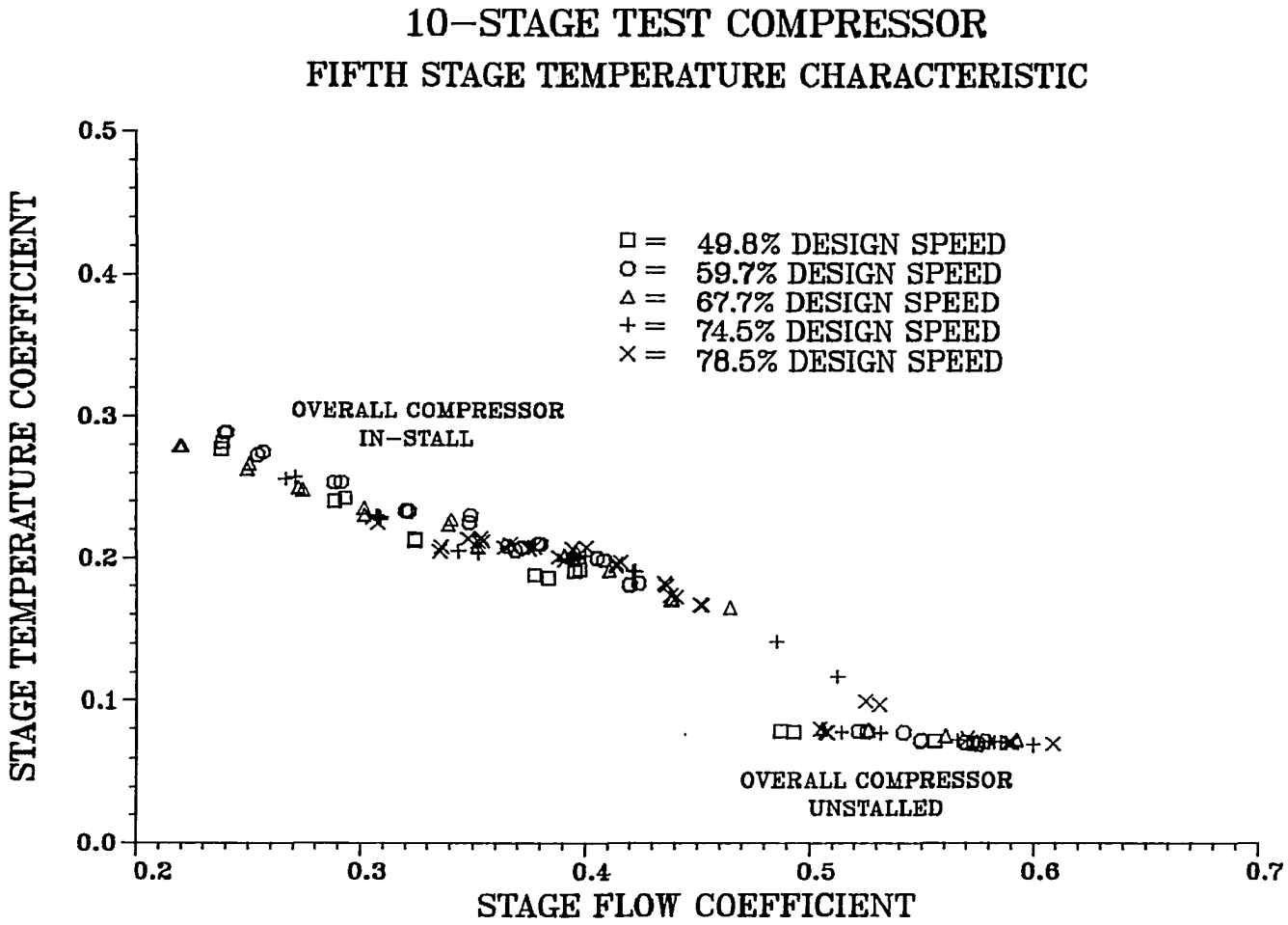

Figure 7.23 Test compressor fifth stage temperature characteristics

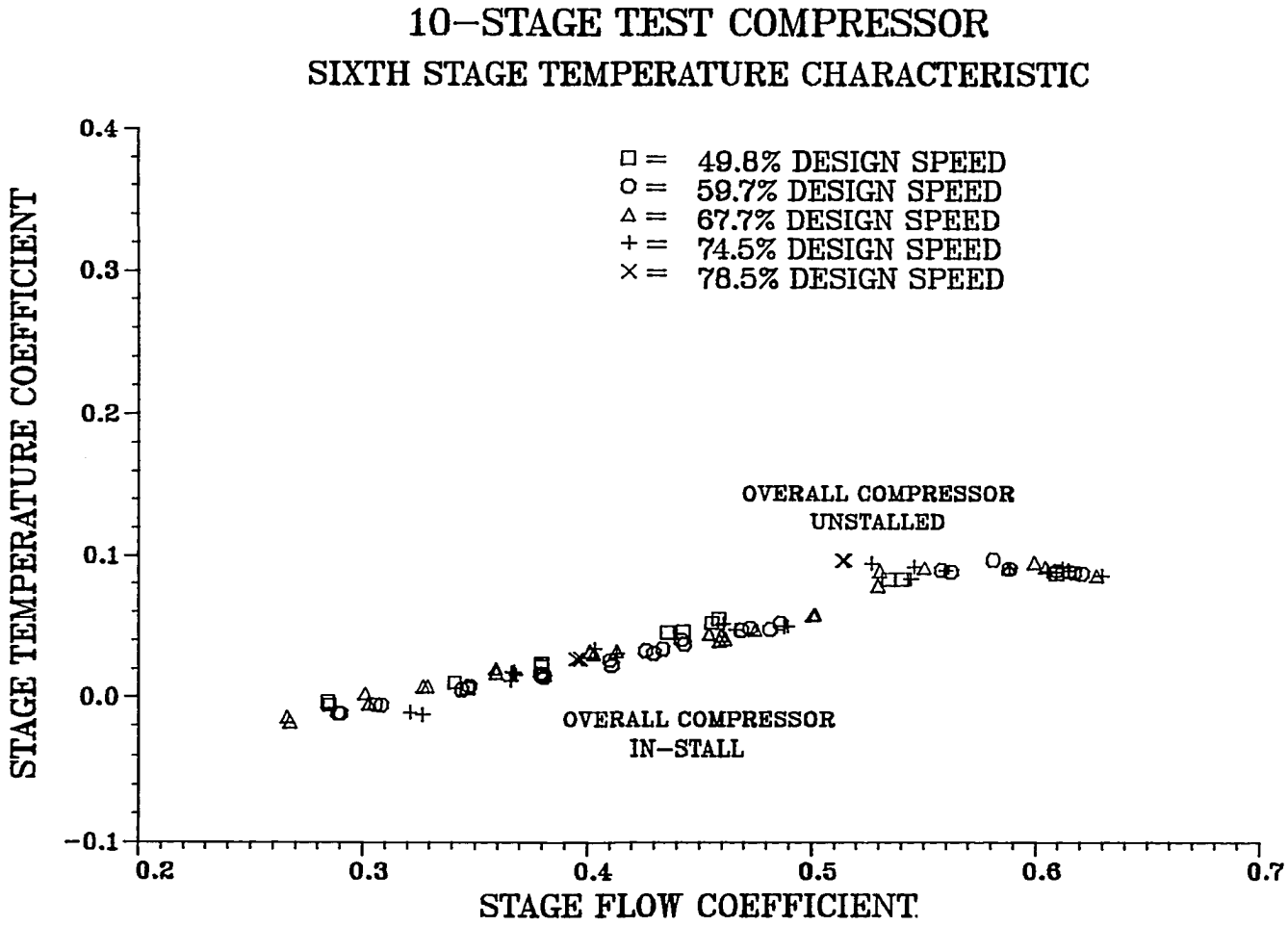

Figure 7.24 Test compressor sixth stage temperature characteristic

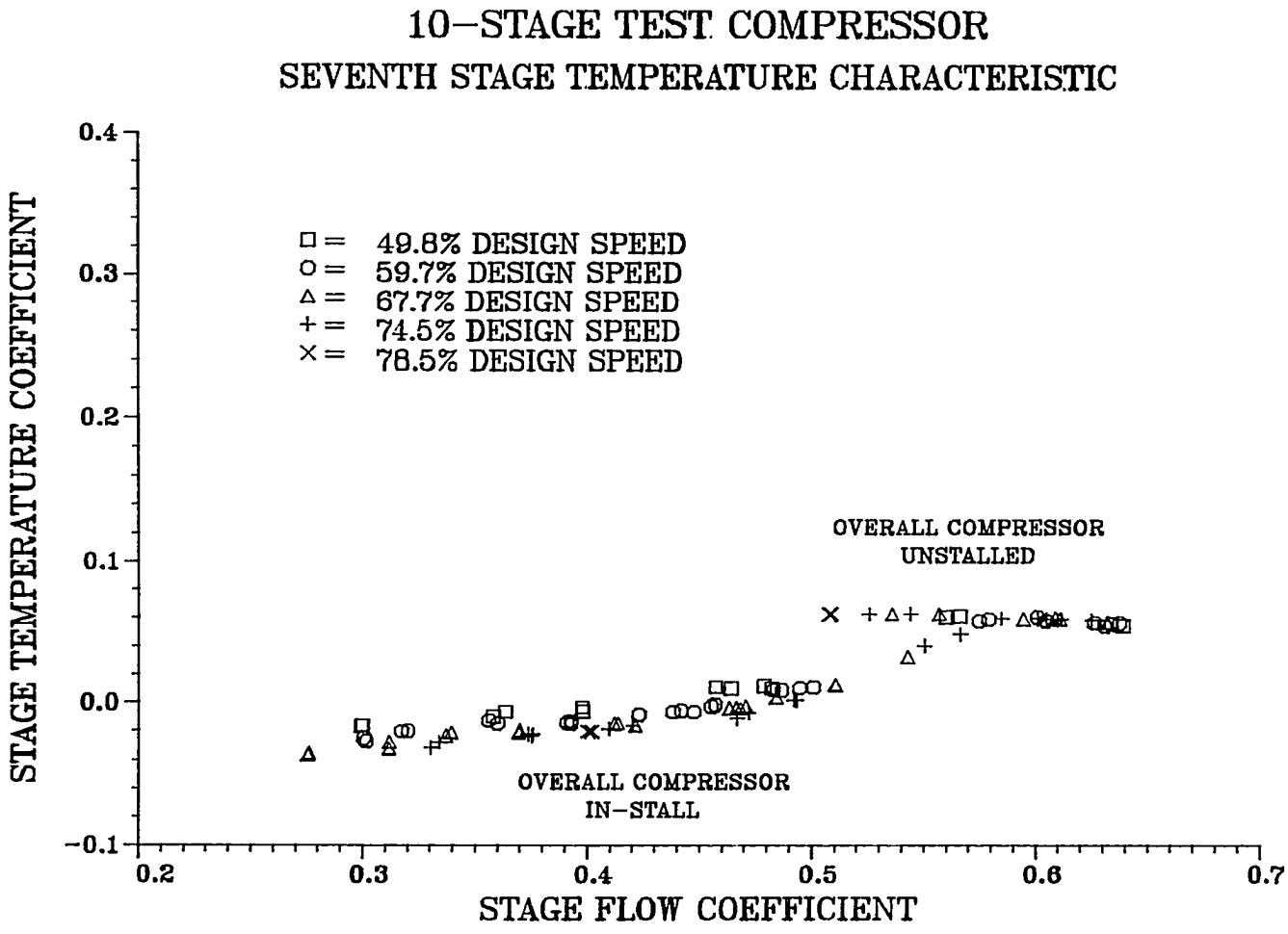

Figure 7.25 Test compressor seventh stage temperature characteristics

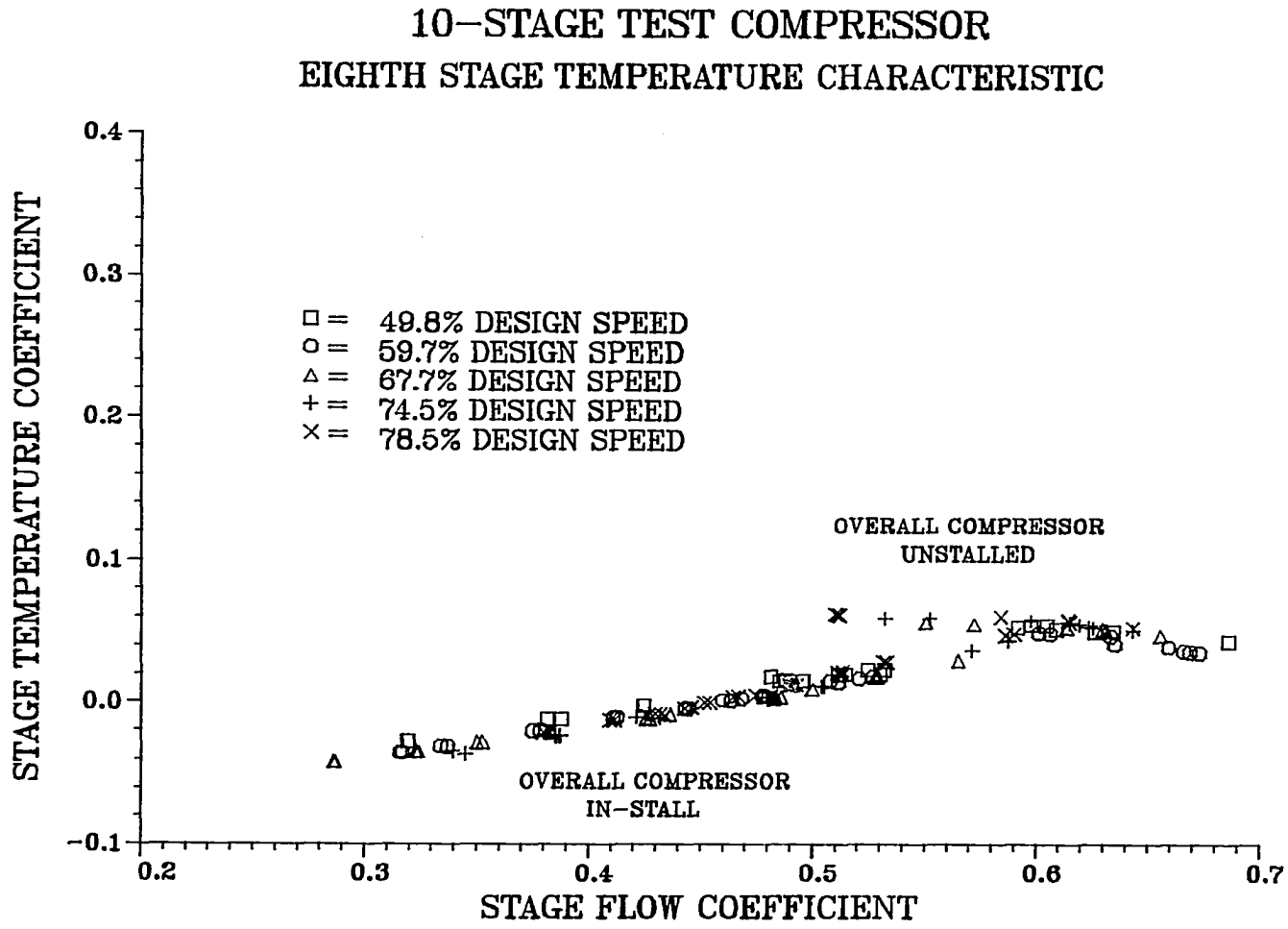

Figure 7.26 Test compressor eighth stage temperature characteristics

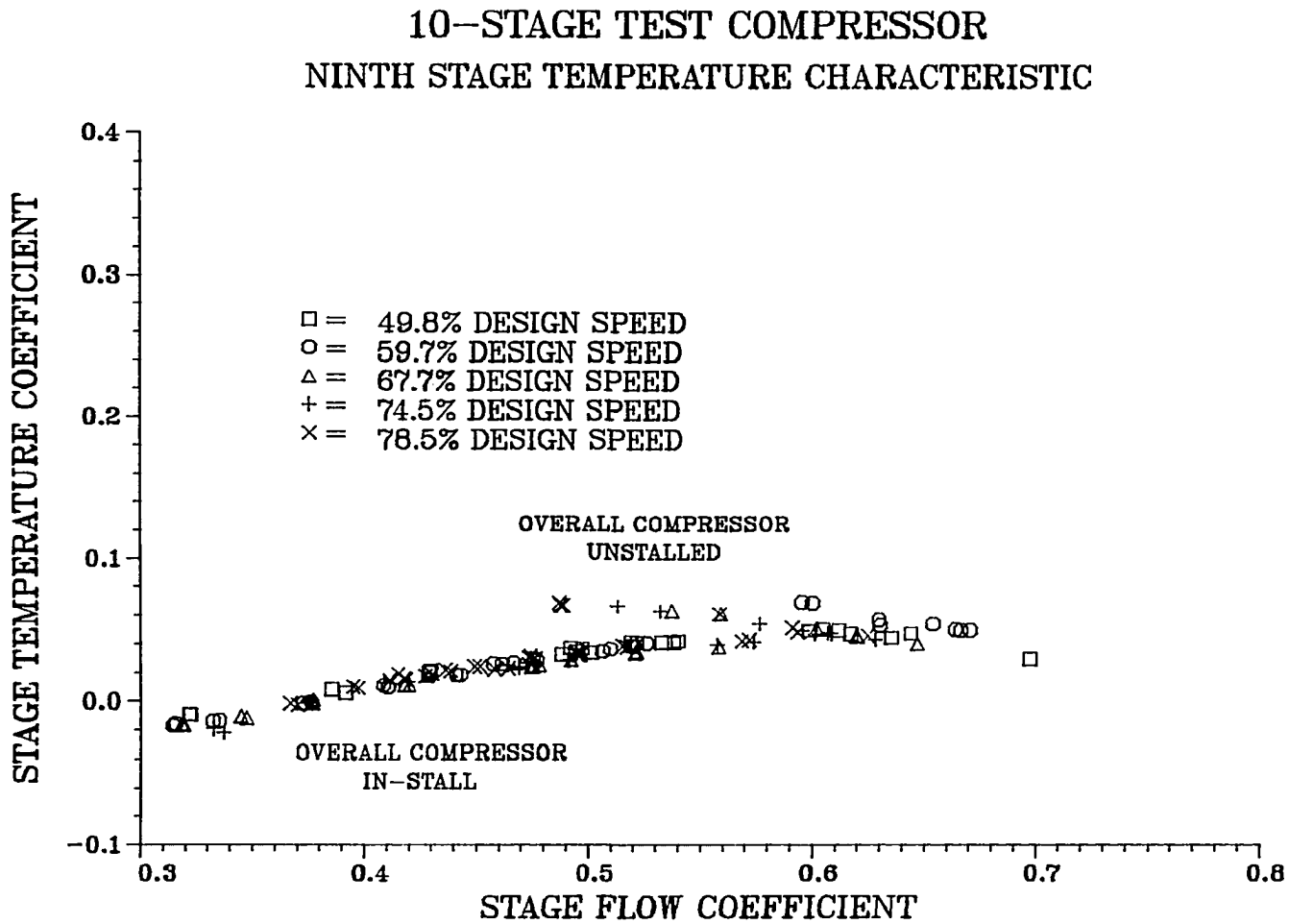

Figure 7.27 Test compressor ninth stage temperature characteristics

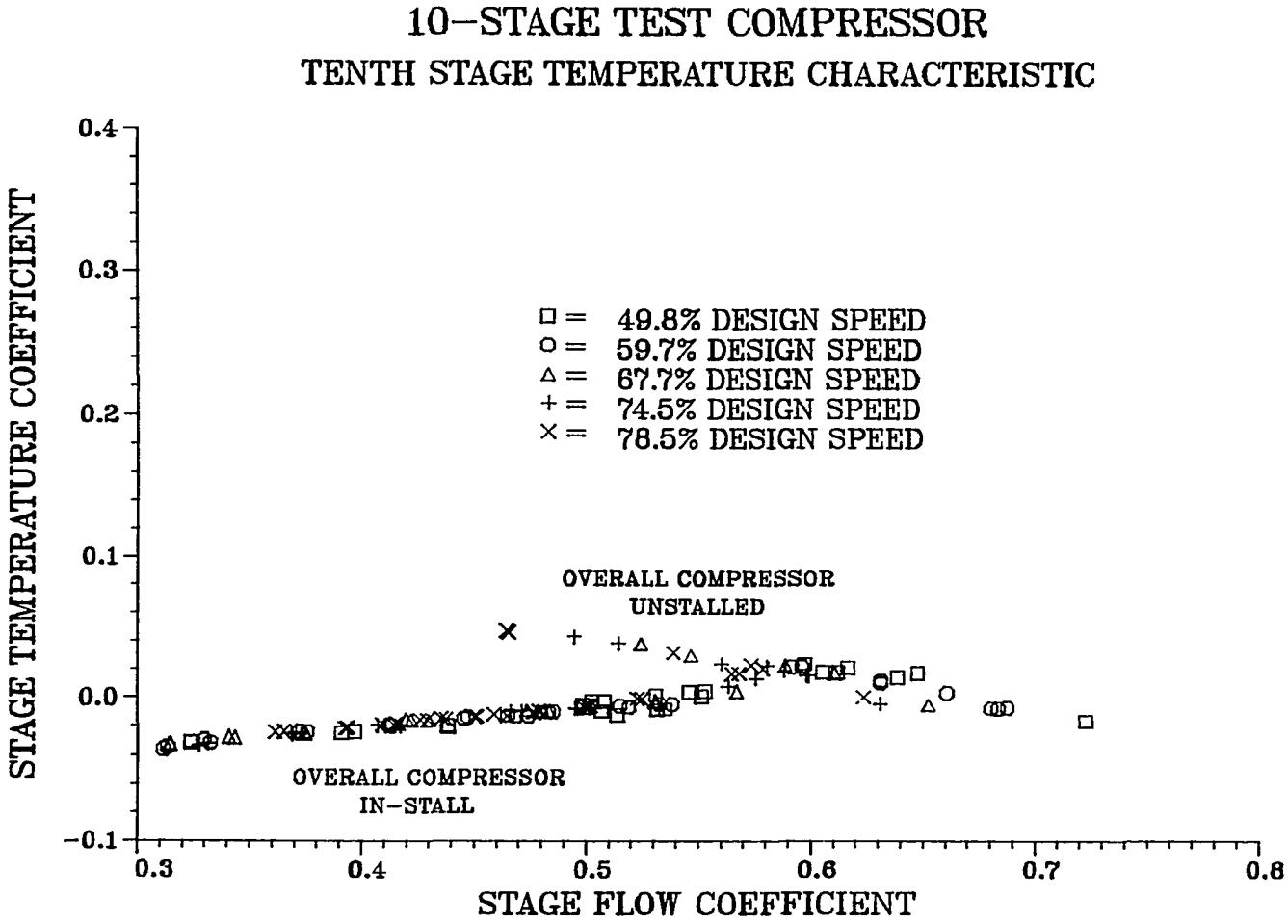

Figure 7.28 Test compressor tenth stage temperature characteristics

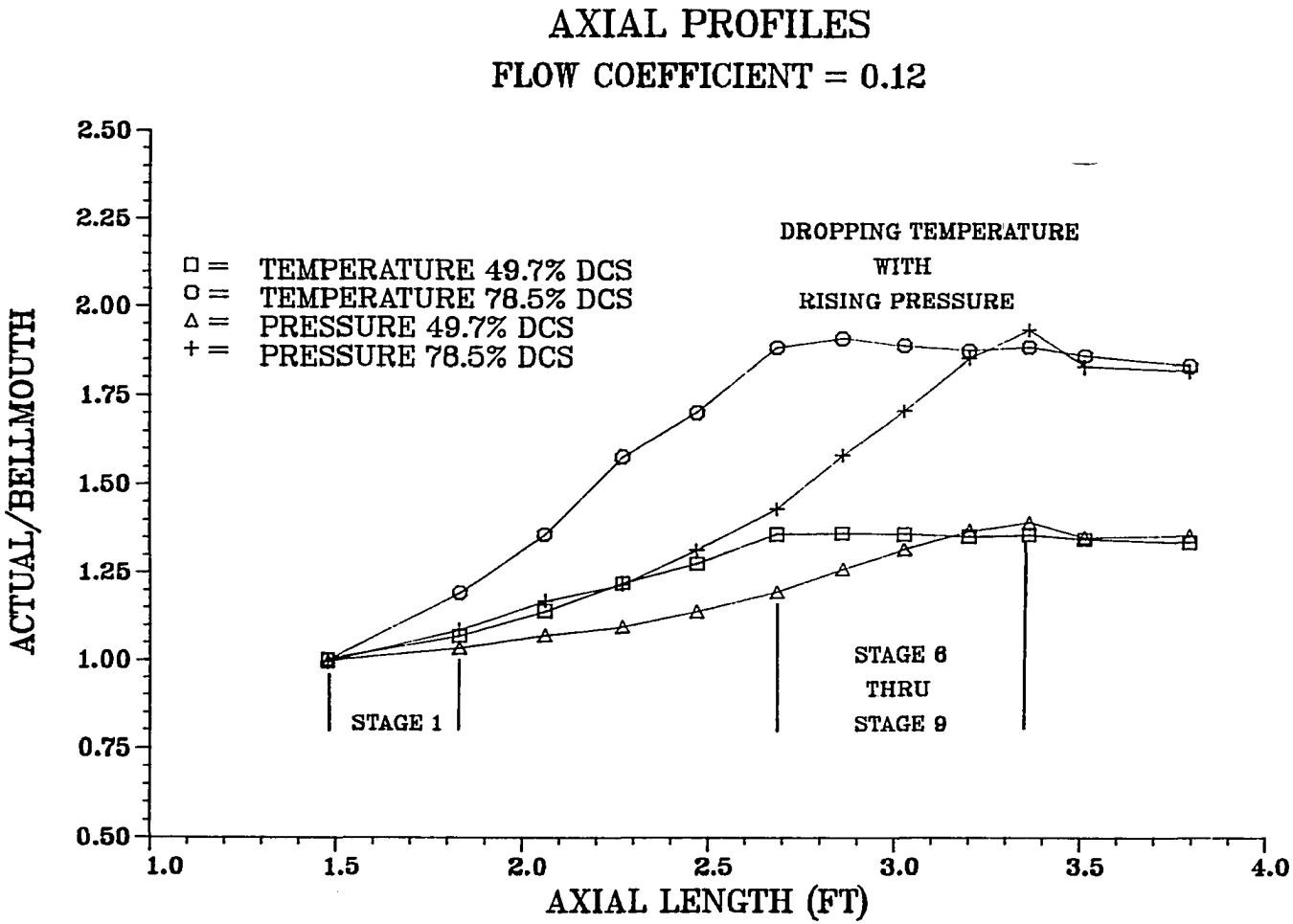

Figure 7.29 Axial total pressure and temperature profiles (in-stall)

overall compressor in-stall flow coefficient of 0.12 for both speeds (for details on this operating point see Figure 7.1). The data in Figure 7.29 indicate that stages 1 through 5 produce an increase in the overall total pressure, but very inefficiently (accompanying high temperature rise). Stages 6 through 9 produce a pressure rise with a temperature drop which violates thermodynamic principals as viewed from a steady state compression process and therefore requires further explanation. The measured temperature rise or drop across any stage is an average value of the time varying temperature across the stage. Measurement instrumentation positioning and instrumentation frequency response, as described in Section IV, prohibited detailed documentation of the time varying temperature caused by rotating stall cell propagation within the compressor annulus. It for this reason that steady compression process thermodynamics do not apply and unsteady theories must be considered. A possible explanation for the measured drop in temperature across a stage with a rise in measured pressure is provided below.

Small and Lewis [12], who also noted the drop in time averaged temperature with a rise in pressure, observed

significant back-flow within a rotating stall cell during their three-stage high-speed compressor tests. Such back-flow, if extensive enough could result in a higher time-averaged temperature at the entrance of a stage than at the exit because of work input to the fluid flowing in the reverse direction. The drop in temperature with rise in pressure in the rear stages of the CRF test compressor operating in stall probably indicates that significant reverse flow existed within stages 6 through 9 during this in-stall condition. These reverse flow conditions within the compressor could not be verified in the CRF 10-stage compressor because of the measurement instrumentation limitations.

Axial variations of total temperature and total pressure are shown in Figure 7.30 for the overall compressor flow coefficient of 0.26 for both 49.7% and 78.5% design corrected speed. This flow coefficient corresponds to an unstalled operating point very near to stall conditions. The data in Figure 7.30 indicate a drop in pressure across the third stage resulting in little pressure rise through the first three stages. It also details a more expected result for a steady compression process of a rise in pressure with rise in temperature

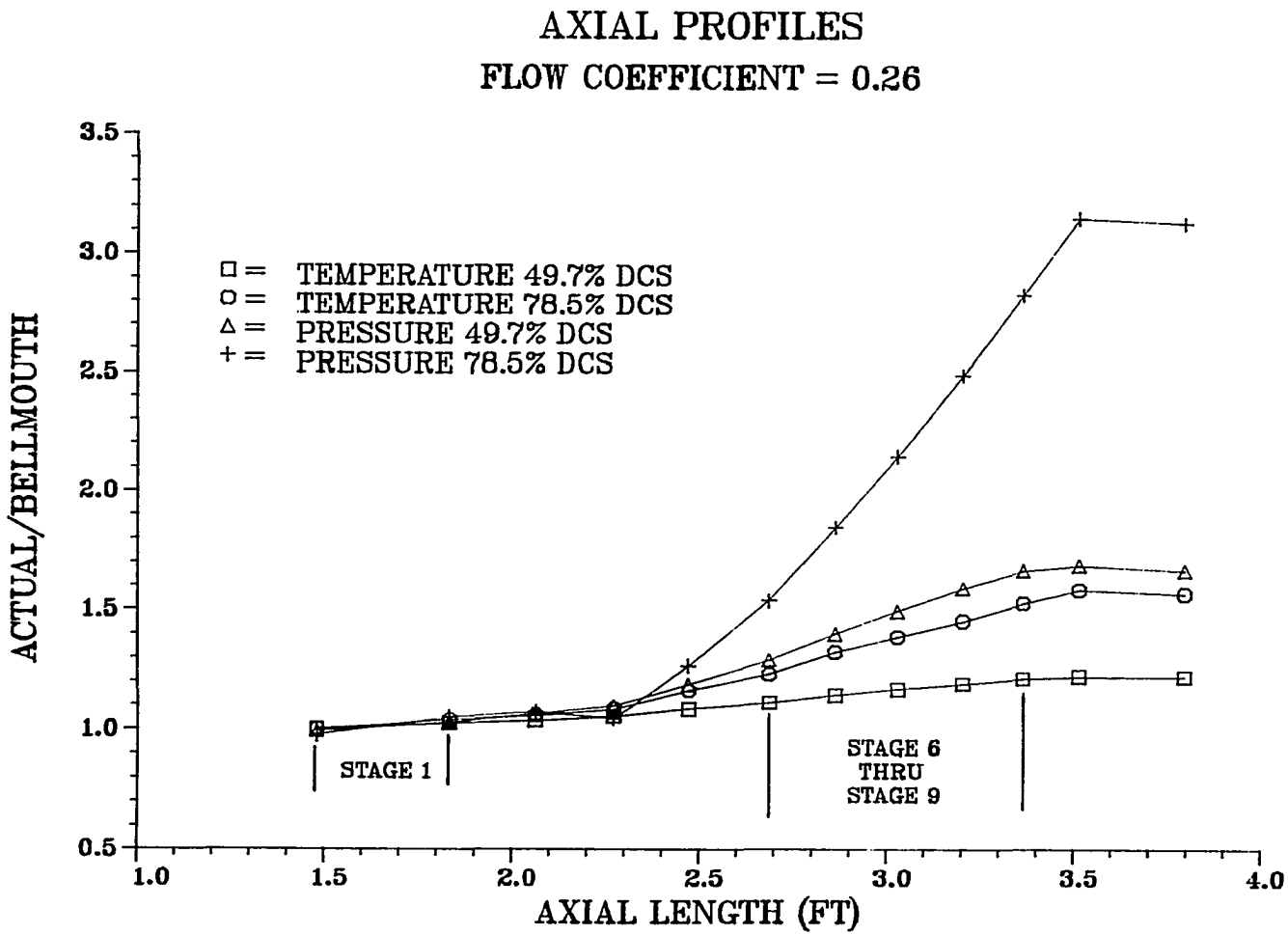

Figure 7.30 Axial total pressure and temperature profiles (unstalled)

across stages 4 through 10. The drop in pressure and temperature between the axial length of 3.5 and 3.9 feet represents the change in conditions across the exit diffuser section of the compressor.

2. Variable geometry effects

The effects of vane setting angle changes in the first three stages were investigated. Two cases will be presented, the first case for the CRF test compressor operating at 74.5% speed with the IGV, stator 1 and stator 2 fixed at setting angles (nominal) used during the 59.7% and the 79.5% speed tests. The second case presented is at 74.5% speed with these three variable vanes opened up by 7 degrees from the nominal position. Data were obtained following the procedures outlined in Section VI.

Data for 74.5% speed were chosen for comparison, because this speed was the highest speed for which compressor instability still led to rotating stall. Surging occurred at speeds above 74.5% with the vanes set at the +7 location. Figure 7.31 shows the CRF test compressor overall pressure rise characteristics for nominal geometry and variable vanes opened by 7 degrees.

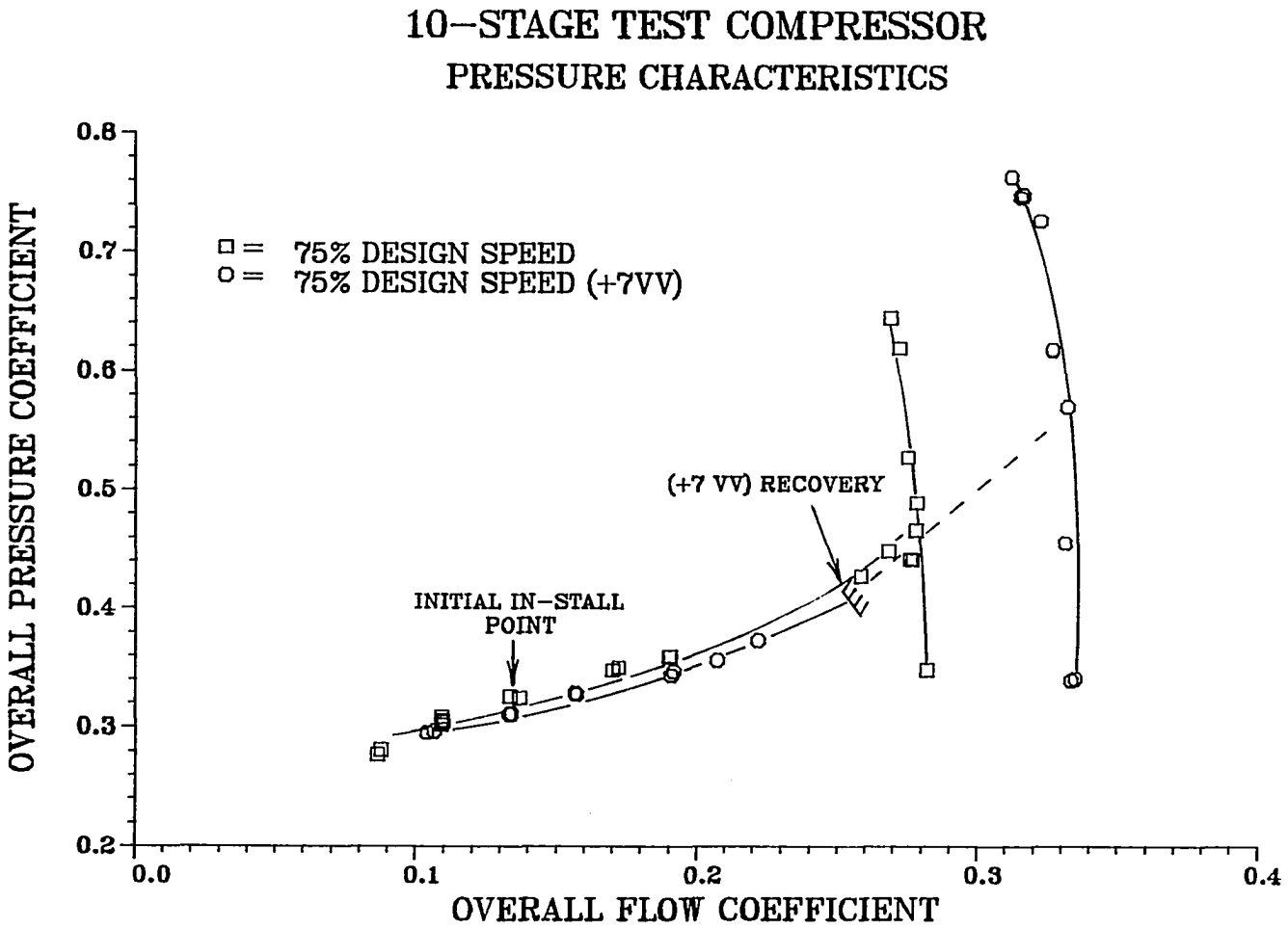

Figure 7.31 Test compressor overall pressure characteristics (variable vane effects)

The information in this figure suggests that the unstalled portion of the characteristic is shifted to a level of higher flow by opening the variable vanes by 7 degrees. The in-stall portion of the characteristic was slightly affected by the change in vane setting angle resulting in a slightly lower characteristic for the vanes at the 7 degrees open position. The flow coefficient for the CRF test compressor at the stall point is the same for both cases. Speed did have an effect on the stall point flow coefficient as previously discussed while vane angle setting did not.

The hysteresis factor (H_f) for the nominal case and for the +7 variable vane case for 74.5% speed are the same because the initial in-stall and near-recovery flow coefficients are nearly identical for both cases. The overall compressor and individual stage temperature and pressure rise characteristics for the two cases are provided in Appendix E, Figure 16.1 and Appendix G, Figure 18.1. The data in these figures also show that variable geometry affects unstalled operation, and has a small influence on the overall in-stall compressor performance.

The in-stall pressure coefficients are only slightly lower for the 7 degrees open variable vane condition because of individual stage effects as explained below.

The first stage pressure characteristics provided in Figure 7.32 indicate that the unstalled characteristic has been shifted to higher flow coefficient levels by opening the variable vanes from the nominal position. This is why the overall characteristic (see Figure 7.31) is shifted to higher flow coefficient levels. The second stage pressure characteristics are detailed in Figure 7.33. The opening of variable vane setting angle has the same effect, as on the first stage, the unstalled characteristic is shifted to higher flow and pressure coefficient levels. For the second stage opening the vanes also altered the in-stall characteristic. The in-stall characteristic is at higher pressure coefficient and flow coefficient levels with the vanes opened by 7 degrees. The data in Figure 7.34 show that the same trends noted for the second stage of both in-stall and unstalled characteristics being altered by opening the first three stationary blade rows, is also true for the third stage.

From the characteristics of the first three stages, it would appear that the overall pressure coefficient of the

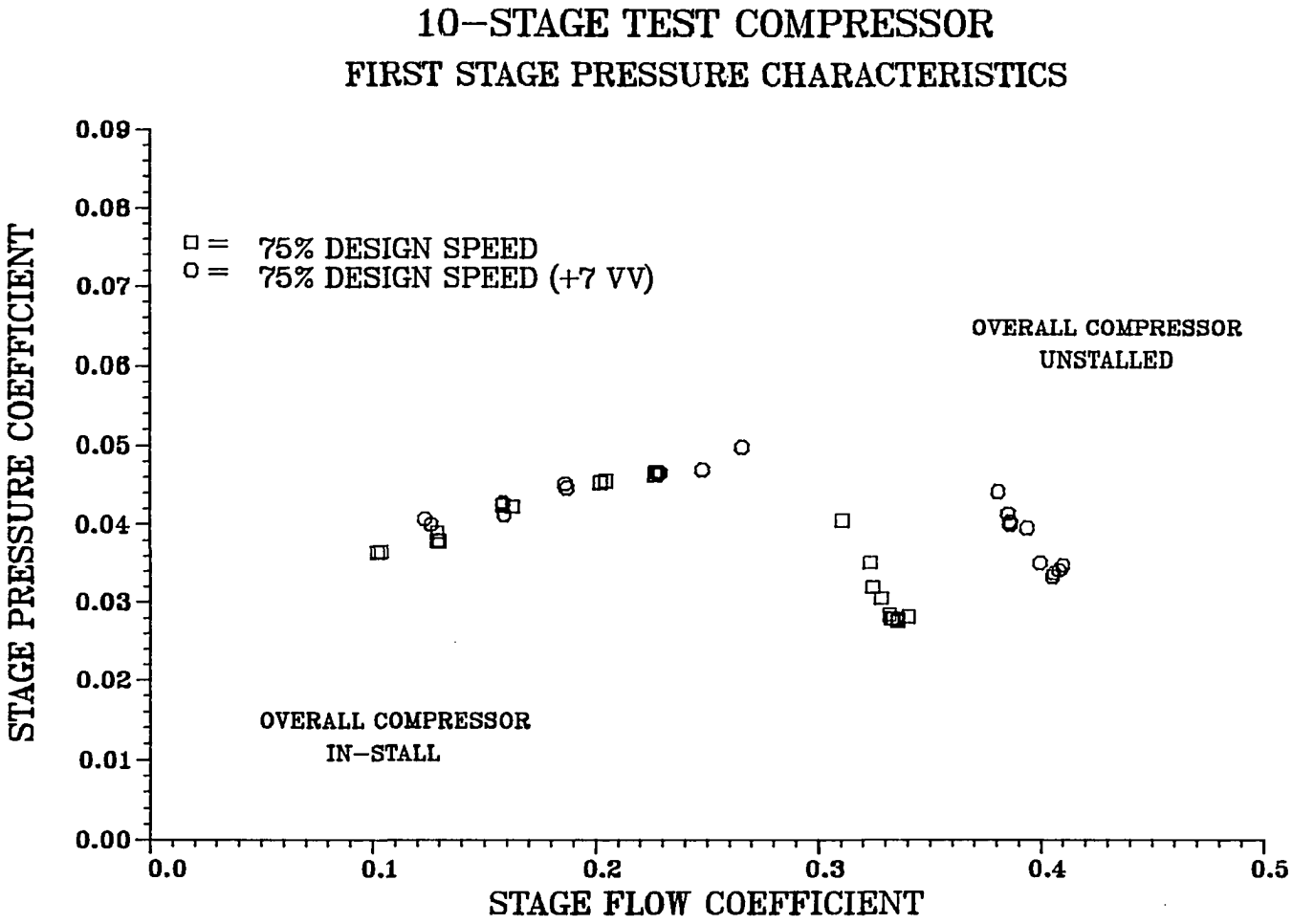

Figure 7.32 Test compressor first stage pressure characteristics (variable vane effects)

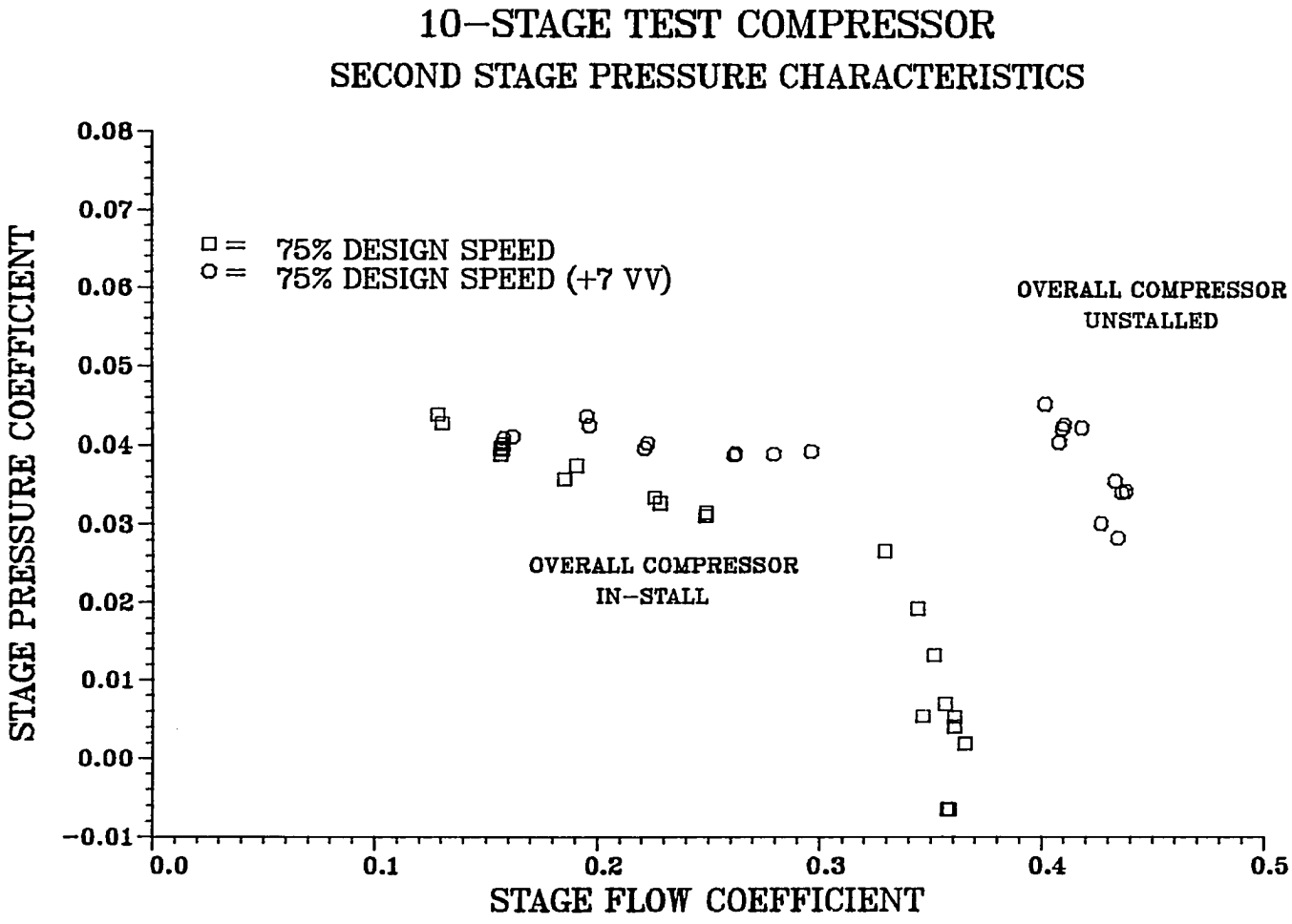

Figure 7.33 Test compressor second stage pressure characteristics (variable vane effects)

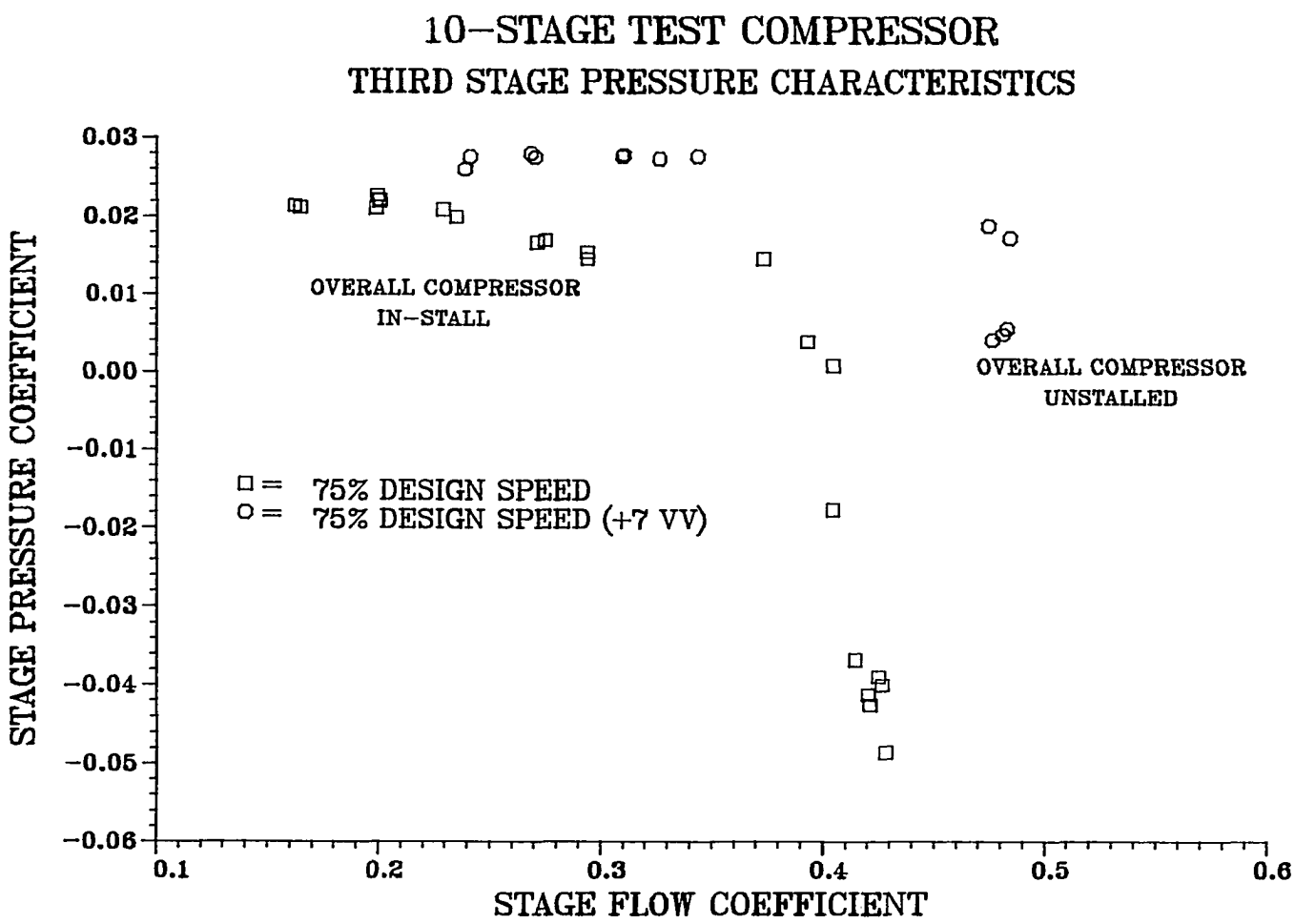

Figure 7.34 Test compressor third stage pressure characteristics (variable vane effects)

CRF test compressor should be at a higher level with the variable vanes set at 7 degrees more open from the nominal position. The data in Figure 7.31 showed that this is not true; instead the overall pressure characteristic is slightly lower. The in-stall characteristics of the remaining seven stages result in a net reduction of the overall compressor pressure coefficient.

The change in variable vane setting angles had little influence on the pressure characteristics of stages four through eight as demonstrated by the data in Figures 7.35 through 7.39. The in-stall characteristic of the ninth stage shown in Figure 7.40, is slightly lower in pressure coefficient level for the vanes at the 7 degrees open setting.

The in-stall characteristic of the tenth stage, shown in Figure 7.41, has been considerably altered by opening the variable vane rows. For a 7 degree more open change pressure losses are greater in the in-stall hysteresis region. Vane position changes of the first three stages have significant impact on the in-stall performance of the tenth stage. The higher flows produced by stages 1 through 3 in-stall at 7 degrees more open vane setting angles (indicated by the higher flow coefficient levels in Figures

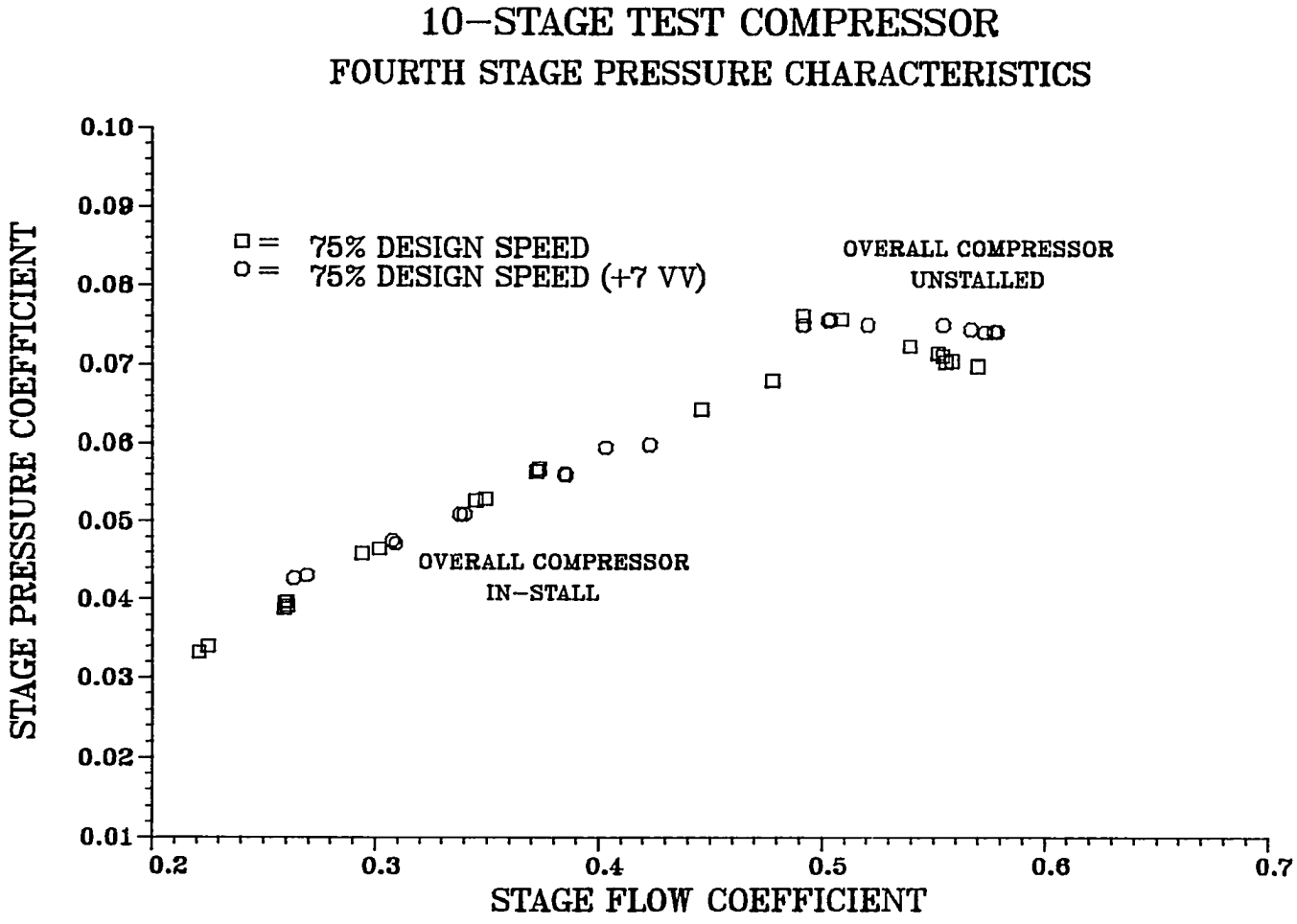

Figure 7.35 Test compressor fourth stage pressure characteristics (variable vane effects)

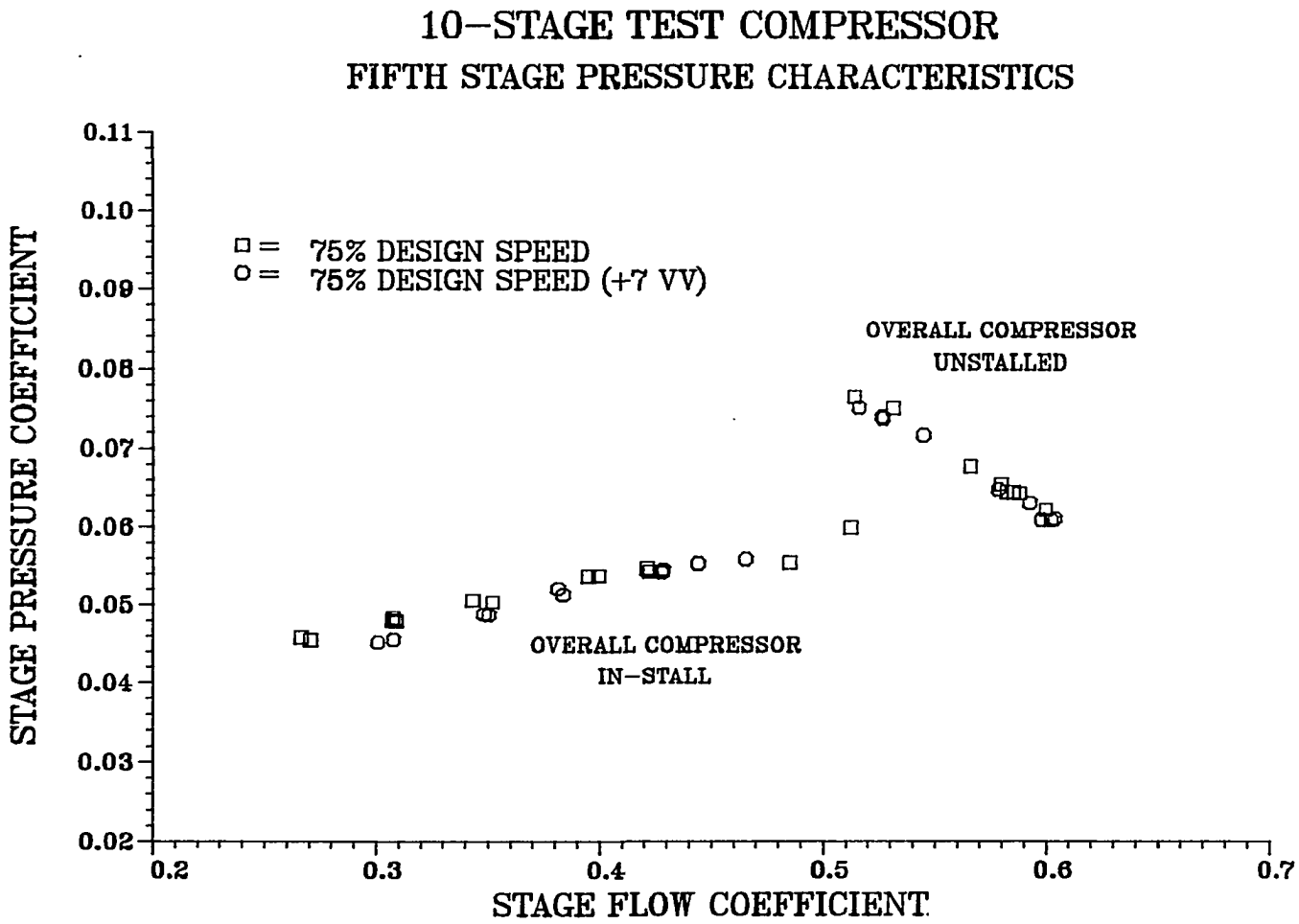

Figure 7.36 Test compressor fifth stage pressure characteristics (variable vane effects)

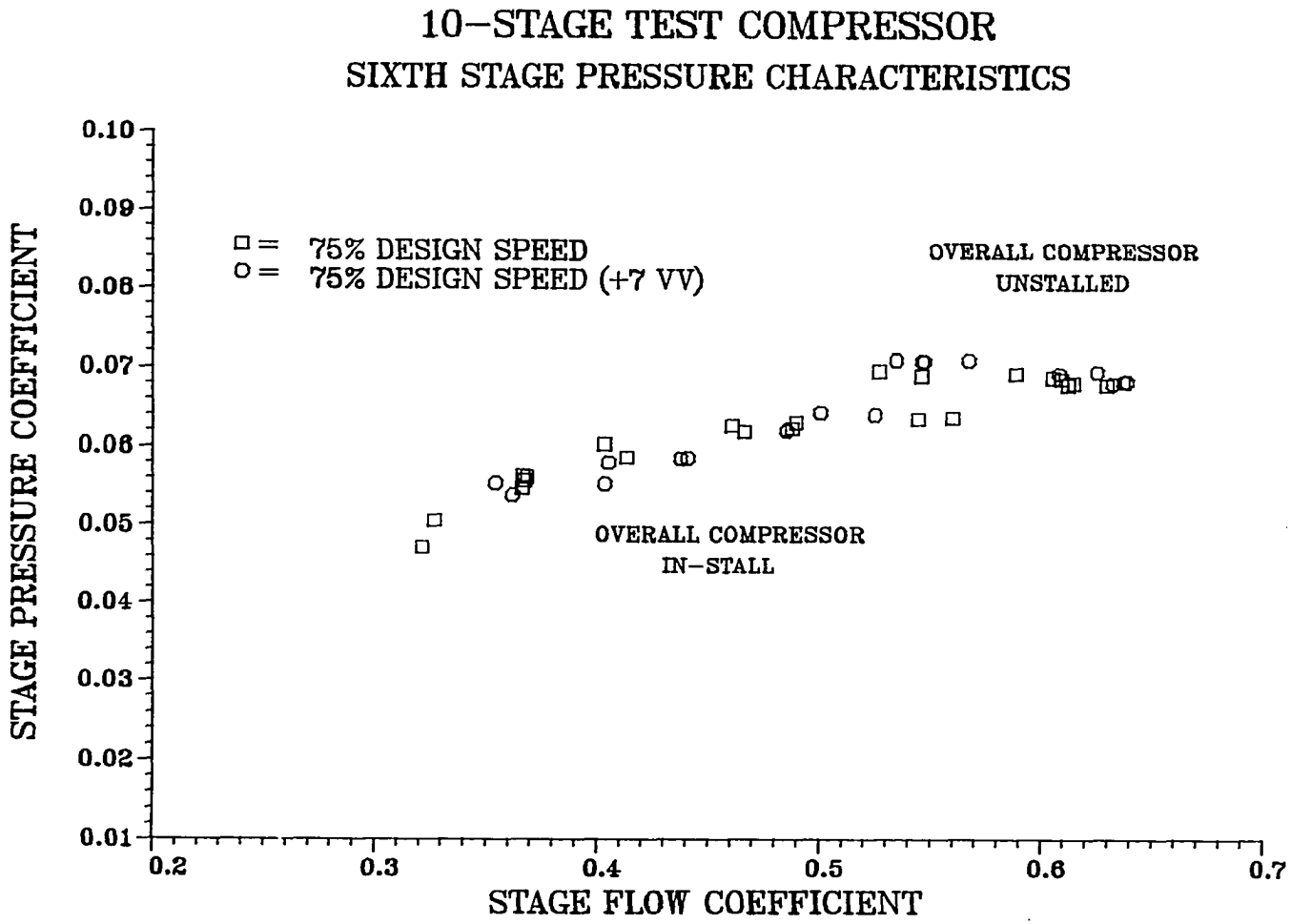

Figure 7.37 Test compressor sixth stage pressure characteristics (variable vane effects)

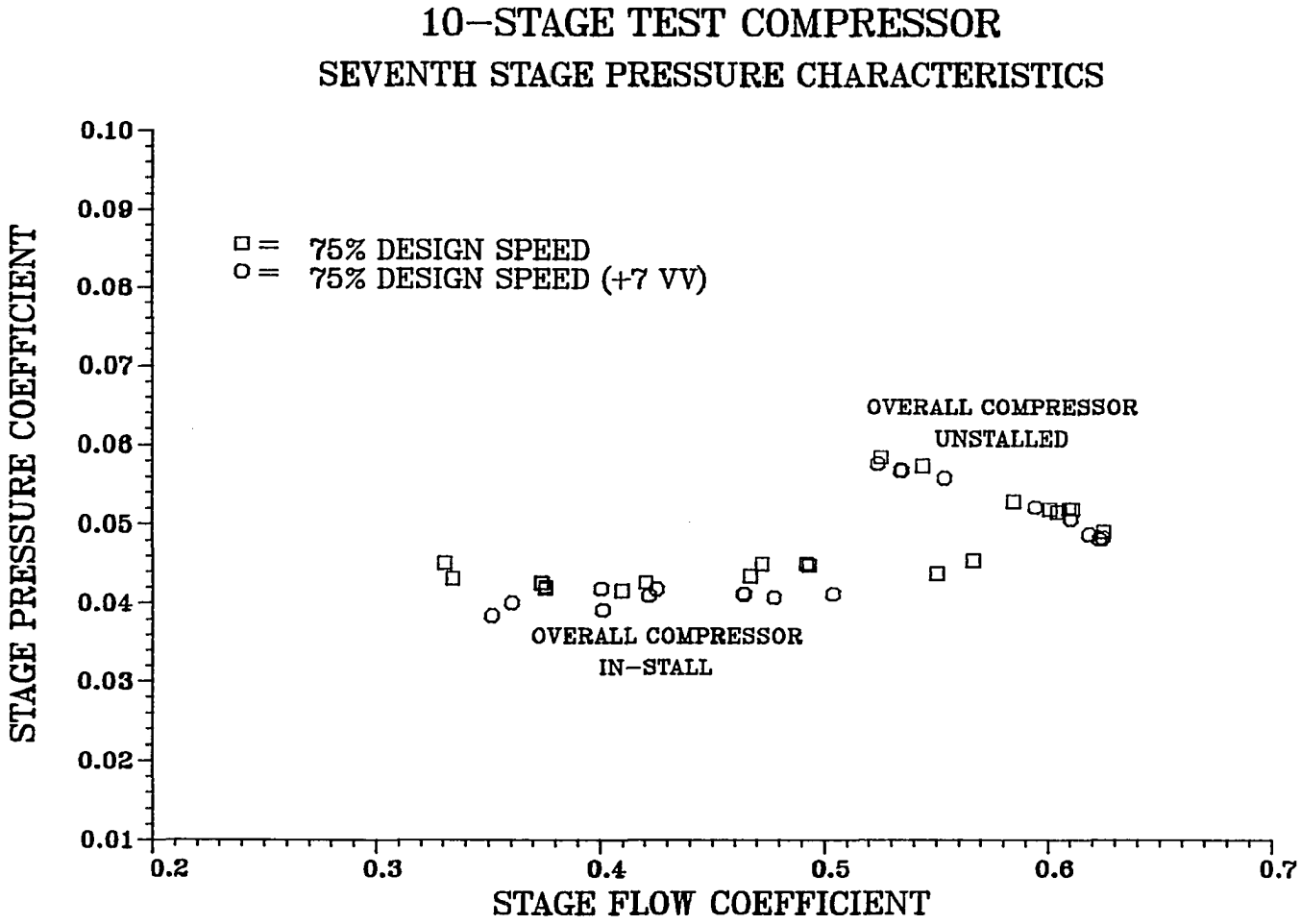

Figure 7.38 Test compressor seventh stage pressure characteristics (variable vane effects)

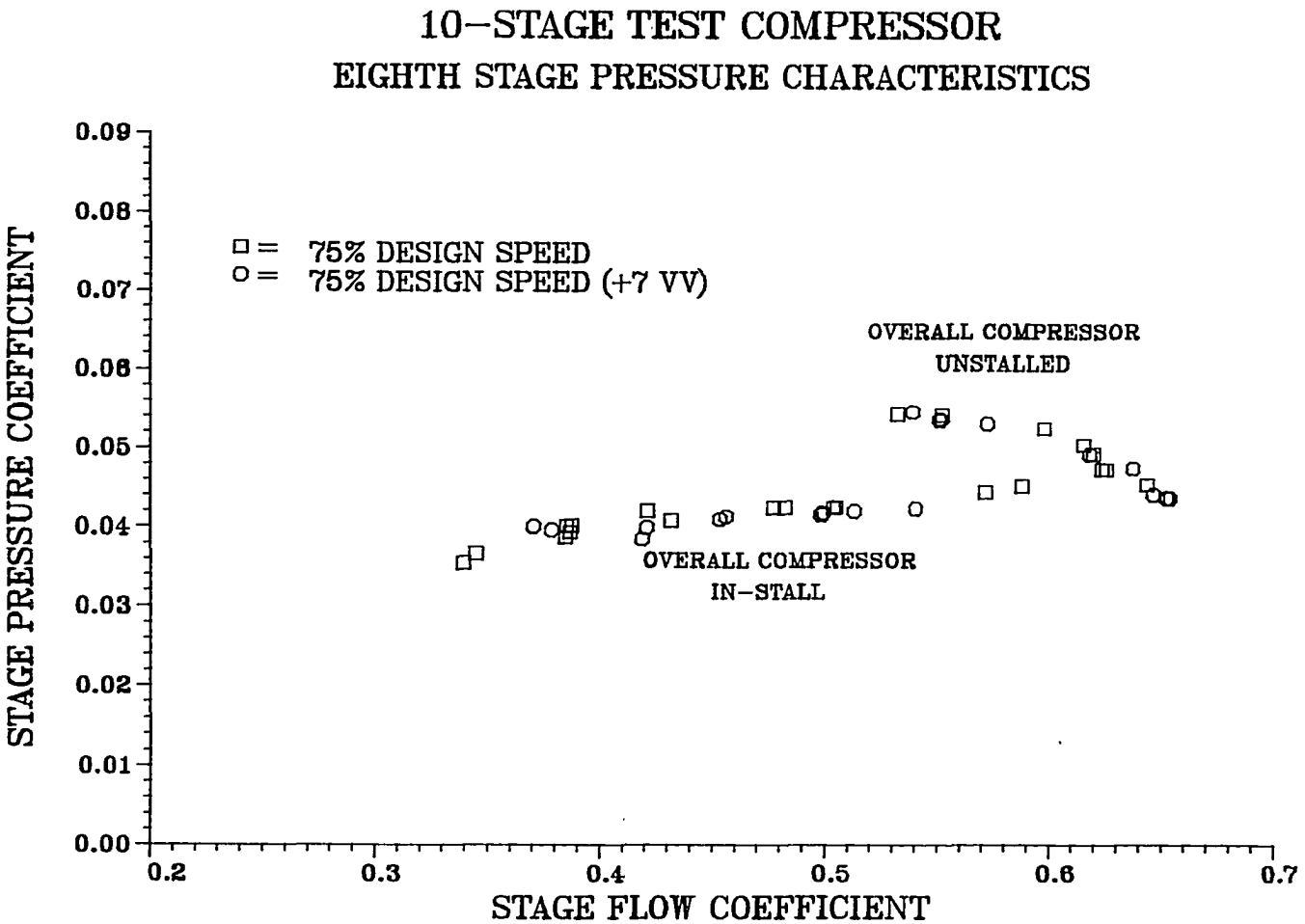

Figure 7.39 Test compressor eighth stage pressure characteristics (variable vane effects)

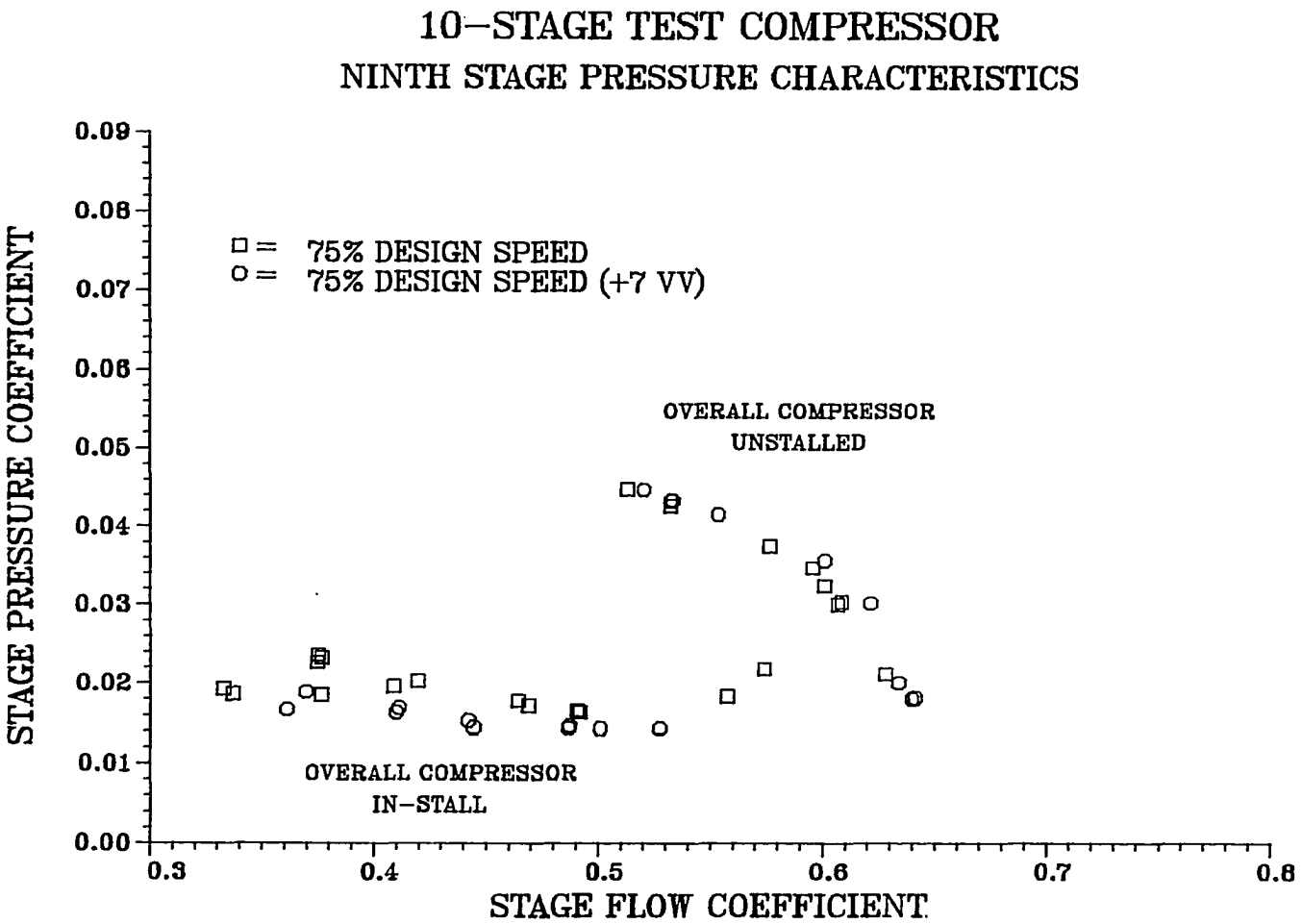

Figure 7.40 Test compressor ninth stage pressure characteristics (variable vane effects)

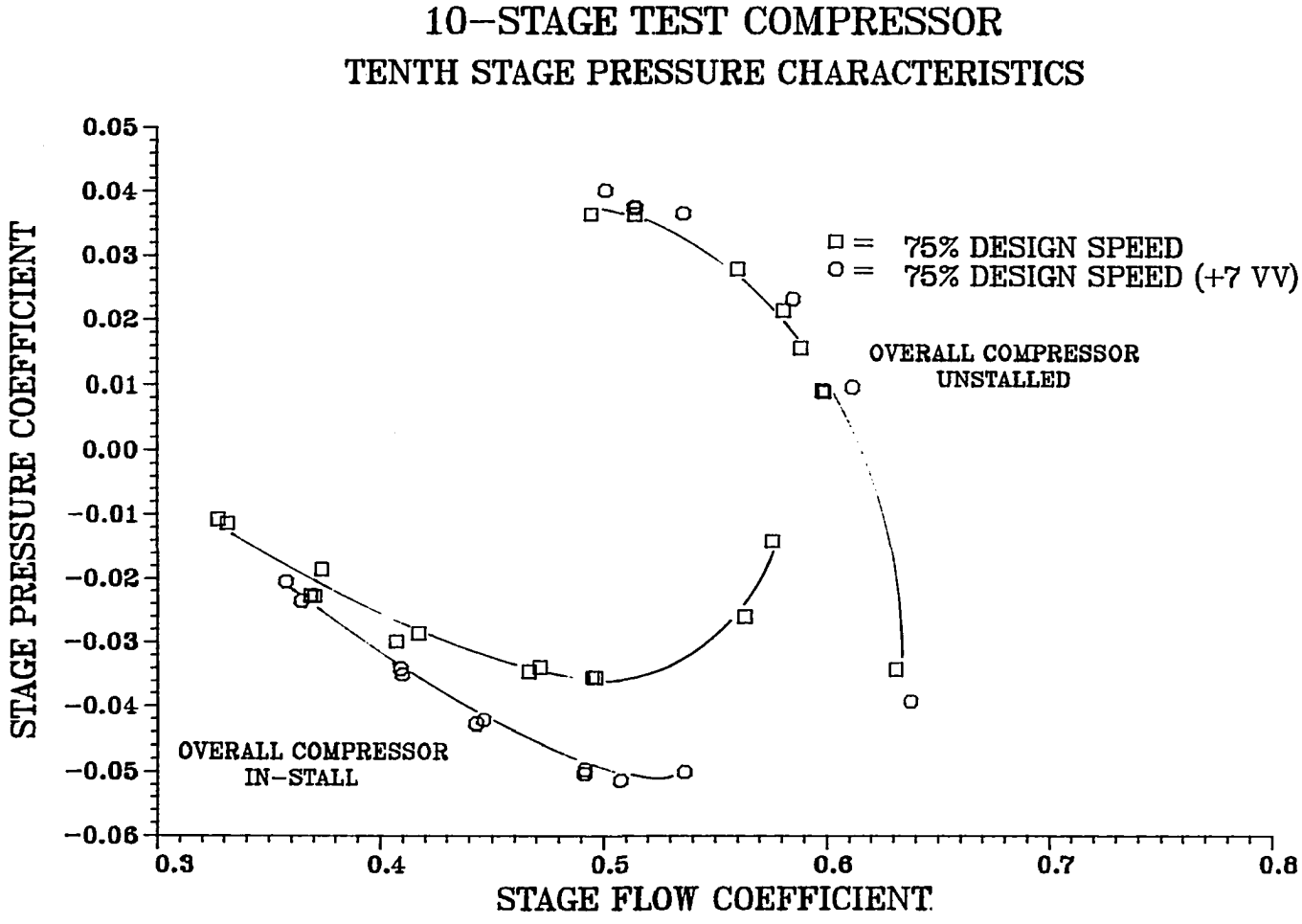

Figure 7.41 Test compressor tenth stage pressure characteristics (variable vane effects)

7.32, 7.33, and 7.34) resulted in higher losses in the tenth stage. These higher losses in the tenth stage are the reason for the slightly lower overall compressor pressure coefficients for the vanes opened by 7 degrees even though the first three stages created higher pressure coefficients. The increase in pressure losses (lowering of the pressure coefficient characteristic) in the tenth stage are due to increases in the velocity of the fluid flowing in the portion of the annulus not blocked by the stall cell. The effect of increased velocity and therefore pressure loss on overall compressor hysteresis is discussed further with the time-resolved in-stall data analysis.

C. Time-resolved Compressor Stall and In-stall Performance

The close-coupled and high-response data described in Section V provide insight into the dynamic performance of the CRF 10-stage test compressor. Information about the details of the rotating stall cell within the CRF test compressor is analyzed to investigate hysteresis extent. In addition, close-coupled data obtained during the transition of the CRF compressor into rotating stall are

compared with predictions by the dynamic compressor model developed by Davis [44].

Comparison of data obtained from the CRF test compressor with Davis model results provide insight for model improvements.

The CRF test compressor time-resolved performance will be described in two subsections. In the first section, the details of the rotating stall cell at 78.5% and 59.7% of design corrected speed are discussed. In the second section, comparisons between the 10-stage compressor model results and CRF test compressor close-coupled data are presented.

1. Compressor stall cell details

Close-coupled and high-response data were obtained as described in Section VI while the test compressor was operating at quasi-steady in-stall conditions. When investigating details of in-stall operation and stall cell blockage, the frequency response of the data is important. In Section V the limitations of the CRF test compressor close-coupled data were discussed. It was necessary to make comparisons between close-coupled data and

high-response data to determine how accurately the close-coupled information described the details of the rotating stall cell. A comparison between data obtained using both acquisition methods from two different exit total pressure probes, located near to each other, is provided in Figure 7.42. The data were obtained at the exit of the CRF test compressor during its transition into rotating stall at 78.5% of design corrected speed. This comparison suggests that the fundamental characteristic of the rotating stall is included in the close-coupled data. Also, the close-coupled data capture the compressor dynamics during transition into rotating stall, and therefore can be used for comparison with analytical models. The details of the sharp rise and drop in local pressure caused by the rotating stall cell are lost because of the limited frequency response of the close-coupled method. For this reason, the close-coupled data were used to describe the basic details of the rotating stall from a global perspective only. They were also used to detail the transition from unstalled operation to rotating stall. Details of stall cell blockage levels were determined from high-response data.

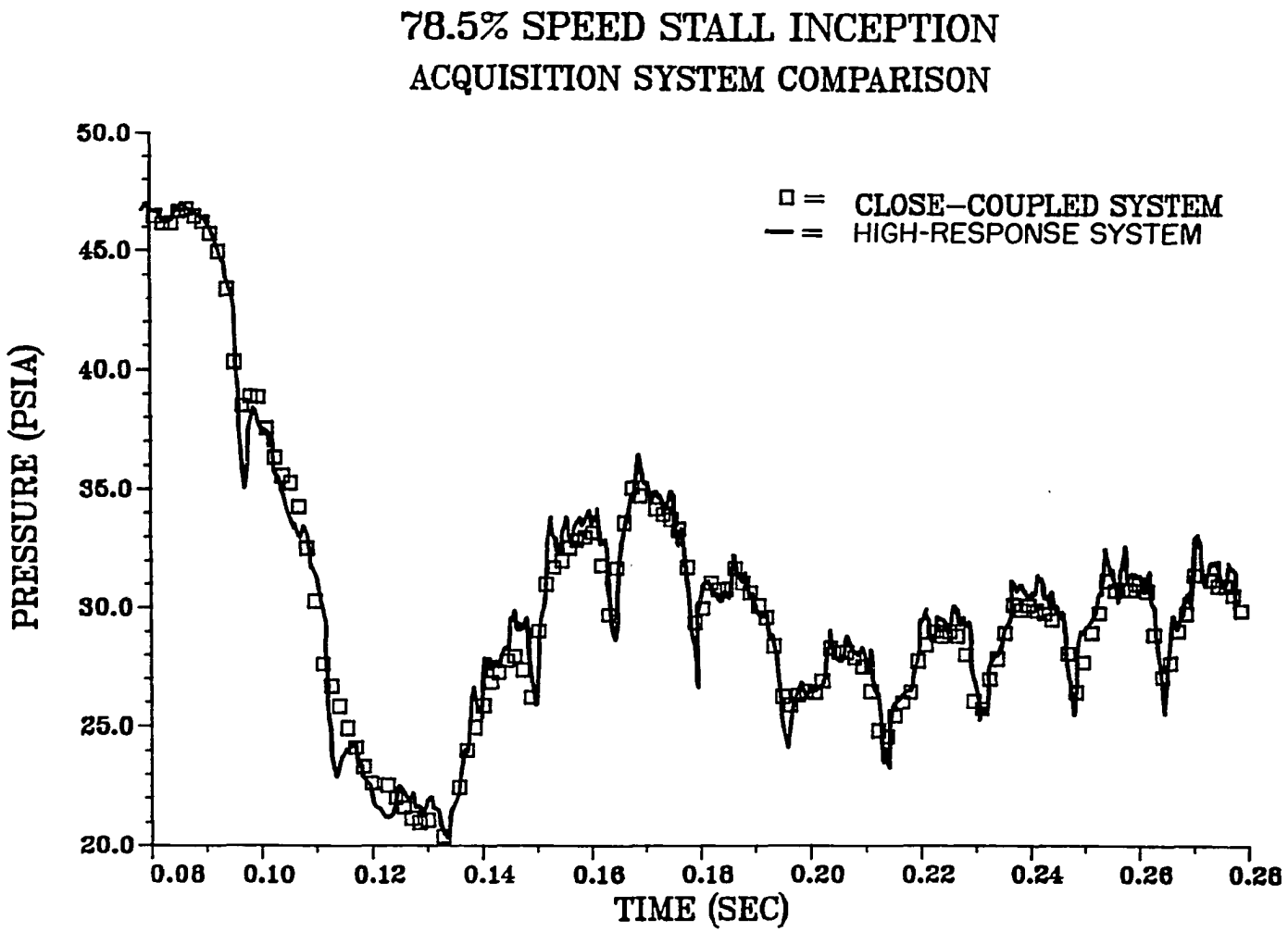

Figure 7.42 High-response and close-coupled data acquisition system response during stalling

Data obtained at 78.5% and 59.7% of design corrected speed were used in the analysis of the rotating stall cell extent, speed and blockage levels. The data in Figure 7.43 show compressor total pressure levels during rotating stall at six different axial locations within the compressor. These data were obtained at 78.5% speed with the overall compressor in stall at a compressor exit throttle opening of 10.0 in^2 (64.5 cm^2), on operating point shown on Figure 7.44.

The data in Figure 7.43 detail the measured pressure fluctuations from the vane mounted probes at the compressor inlet, third stage inlet, fifth stage inlet, seventh stage inlet, ninth stage inlet and the compressor exit at the near hub location. The axial locations of each measurement are indicated with arrows for reference in Figure 7.43. For all axial locations, except at the compressor inlet, the measurements were made at the same circumferential location. The physical location of the inlet measurement was approximately 130 degrees out of phase from measurements at other axial locations. The data were time shifted to account for this location variation. The data in Figure 7.43, although somewhat qualitative, do indicate that the pressure fluctuations are largest in magnitude at

TEST COMPRESSOR IN-STALL

TIME-RESOLVED TOTAL PRESSURE RISE

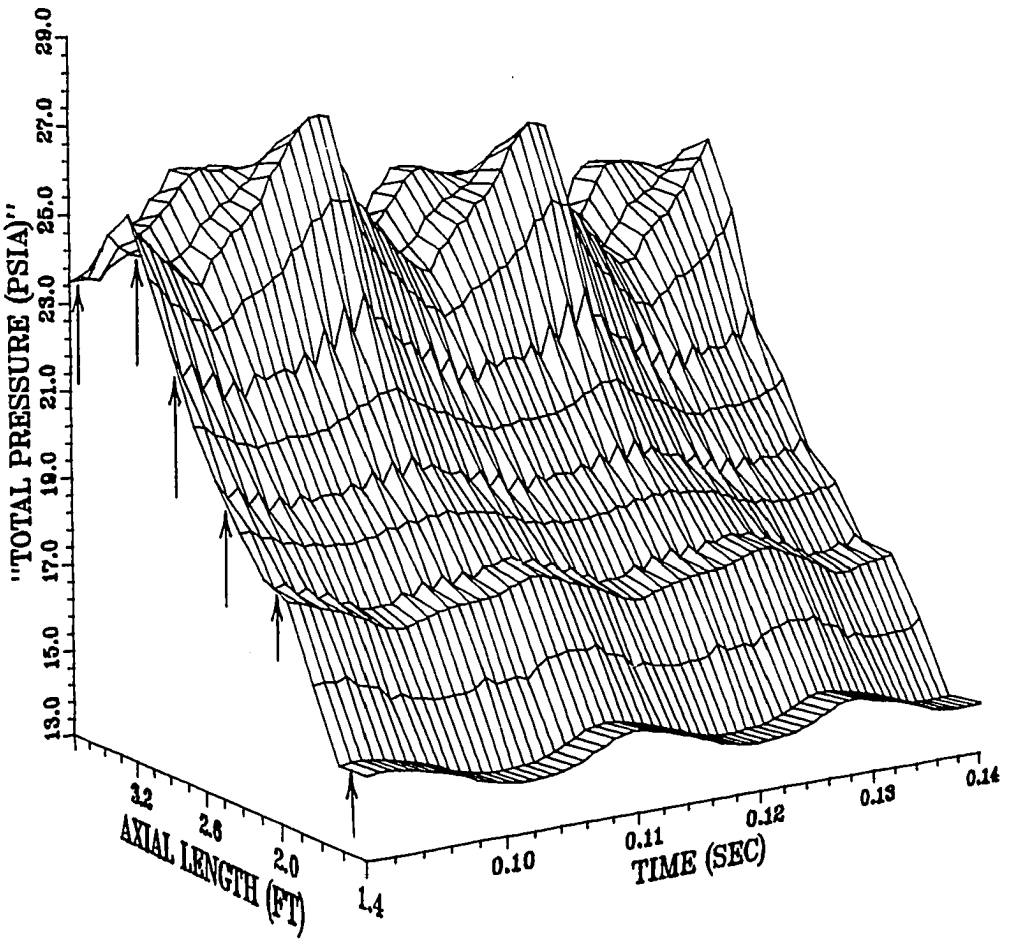

Figure 7.43 Test compressor time-resolved near annulus hub total pressure at 78.5% speed in-stall, exit throttle area 10.0 sq. in. (64.5 sq. cm)

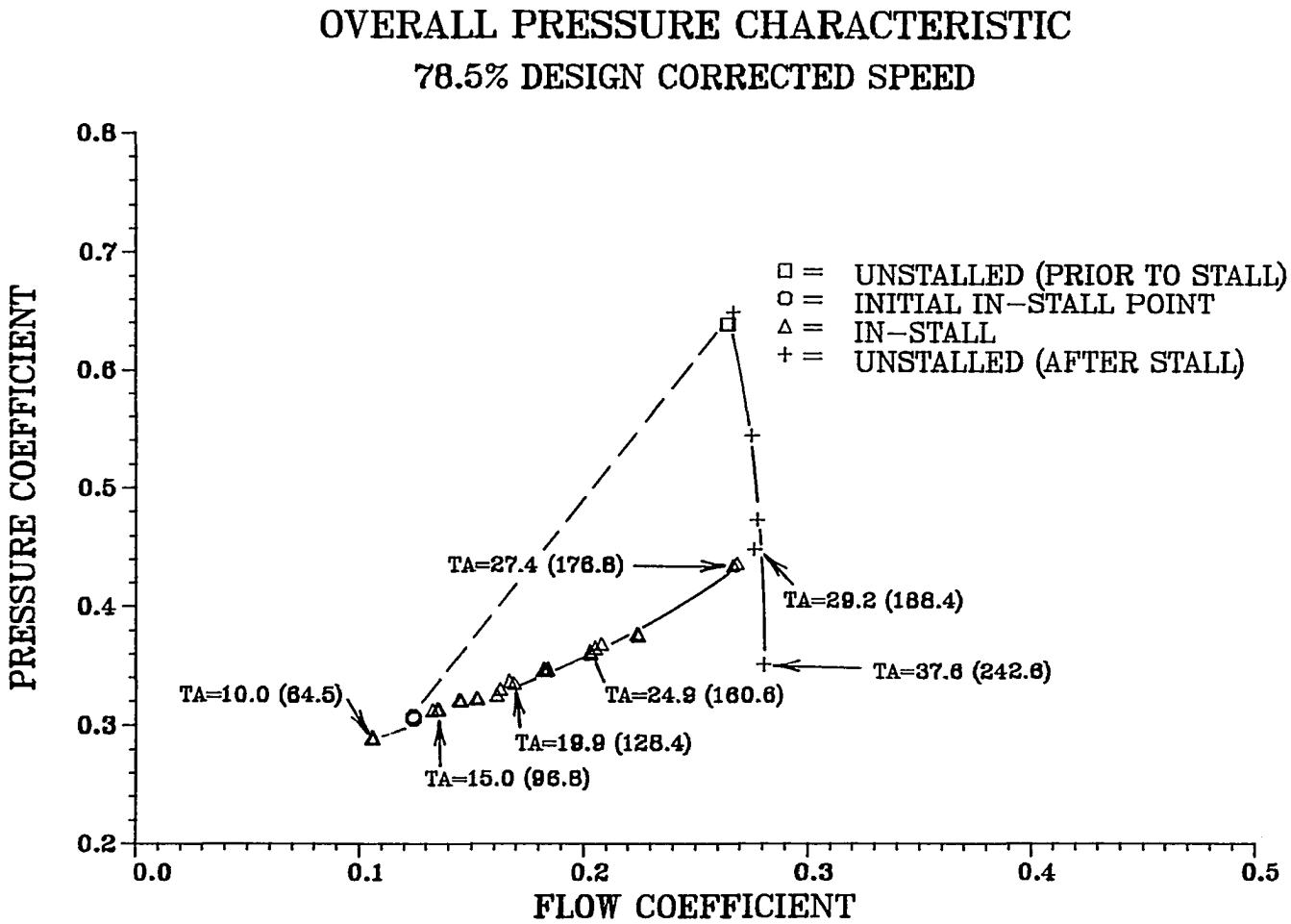

Figure 7.44 Test compressor 78.5% speed overall performance (exit throttle area details)

the ninth stage inlet, and that the pressure variations at the third stage inlet are much smaller than for the ninth stage inlet. At this low throttle area (10 in^2 (64.5 cm^2)) the data in Figure 7.43 suggests that the first stage is operating in rotating stall because the pressure fluctuations are higher at the compressor inlet than at the stage 3 inlet. The low level of total pressure fluctuations at the third stage inlet may be due to the rotating blockage behind the first three stages. As mentioned earlier this blockage acts as a throttle to the flow through the stage and results in a net pressure rise higher than unstalled levels in the first three stages after the compressor stalls. This trend supports the notion presented earlier that the rotating-stall in the CRF test compressor was located within the rear stages of the compressor, and that stages 2 and 3 were not in full span rotating stall as many theories [29] would suggest.

Time-resolved pressures at the entrance to the fifth stage also shown in Figure 7.43, indicate that the stall cell has some influence on the fourth and fifth stages. However, the magnitude of the fluctuations at the entrance to the fifth stage in the hub region are still much below the fluctuation levels at the ninth stage entrance. This

trend supports the previously described proposal that large amounts of reverse flow are present in stages six through nine, as the magnitude of the fluctuations attributable to the rotating-stall cell are the greatest within these stages.

The data in Figure 7.45 detail the static pressure measured on the outside diameter of the test compressor annulus. Static pressure measurements for the inlet to stages 3, 5, 7 and 9 are shown. The entrance to the stages are represented with arrows for reference on Figure 7.45. These data qualitatively show a phase shift of approximately 180 degrees between the static pressure fluctuations at the inlet to the fifth stage and the inlet to the seventh stage.

A more quantitative representation of the total and static pressure variations between the inlet to the third stage and inlet to the ninth stage is detailed in Figure 7.46. The data in this figure suggest that there is a phase shift in static pressure fluctuations between the front and rear stages of the compressor. It also shows that at the entrance to the ninth stage the total and static pressure fluctuations caused by rotating stall are of the same magnitude, while at the inlet to the third

TEST COMPRESSOR IN-STALL

TIME-RESOLVED STATIC PRESSURE RISE

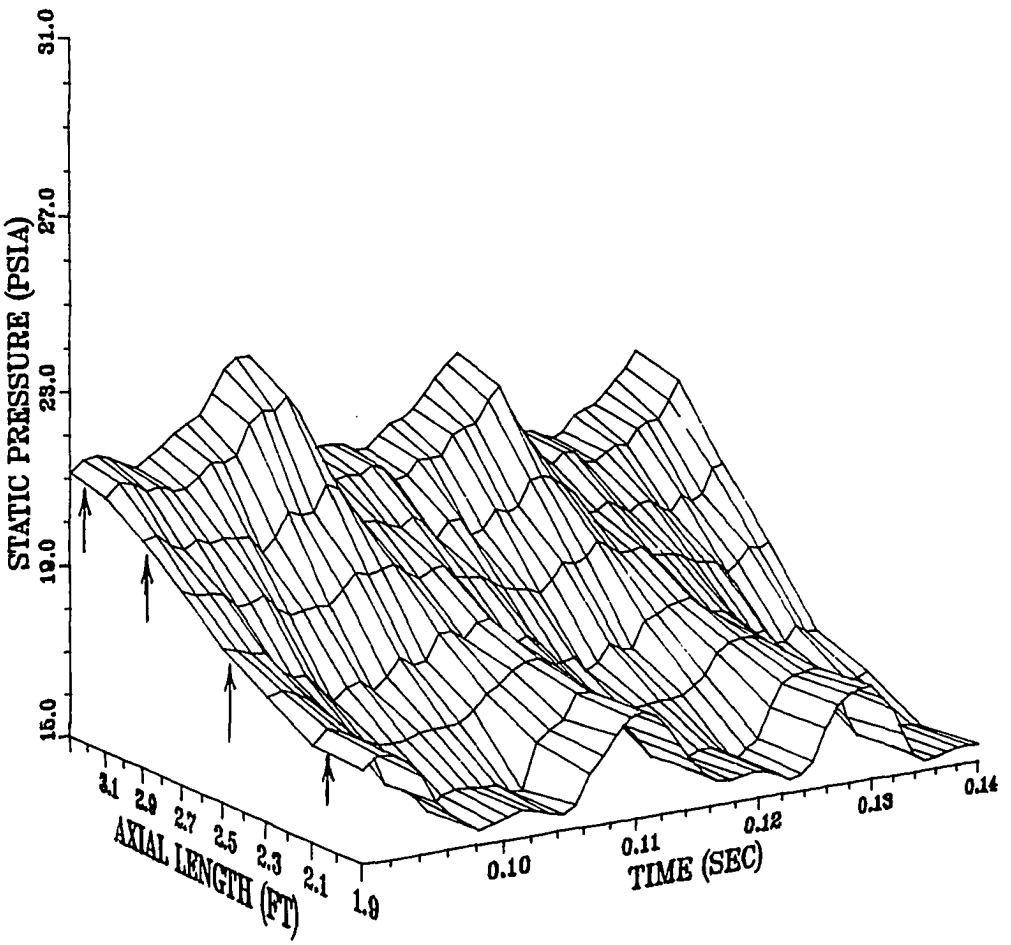

Figure 7.44 Test compressor time-resloved outside annulus static pressure at 78.5% speed in-stall, exit throttle area 10 sq.in. (64.5 sq. cm)

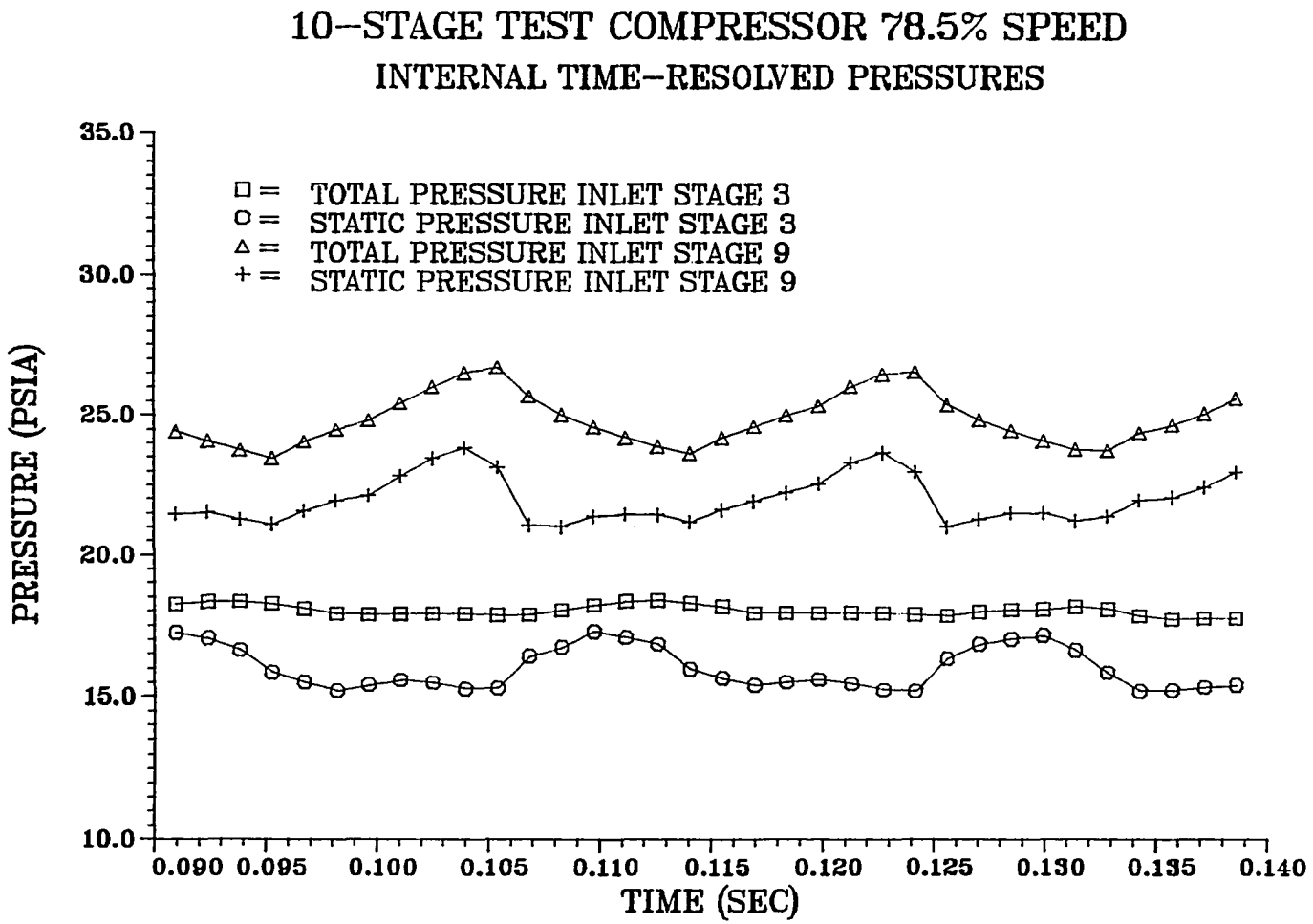

Figure 7.46 Test compressor time-resloved tip region total and static pressure at 78.5% speed in-stall exit throttle area 10 sq. in. (64.5 sq. cm)

stage the static pressure fluctuations are greater than the total. This trend is demonstrated even more clearly in Figure 7.47 where the same information is presented for a more open throttle area of 20 in^2 (129.0 cm^2). The data presented in Figures 7.46 and 7.47 suggest that the third stage is being loaded by the passage of the rotating stall cell in the rear stages of the compressor as indicated by the rise in static pressure (drop in velocity) when the stall cell downstream passes. The rotating stall cell in the rear of the compressor is detailed by the drop in both total and static pressure. The data presented in Figures 7.46 and 7.47 represent the conditions that exist at the tip region of the rotor. Review of further data not presented here indicated that the trends presented in these figures were generally true for the complete span of the compressor annulus. Comparison of the measured outer annulus static pressures by themselves might suggest that the stall cell spirals very sharply around the annulus between stages 5 and 7, but if the total pressures are considered this becomes highly unlikely.

The rise in static pressure with accompanying near steady total pressure at the entrance to third stage

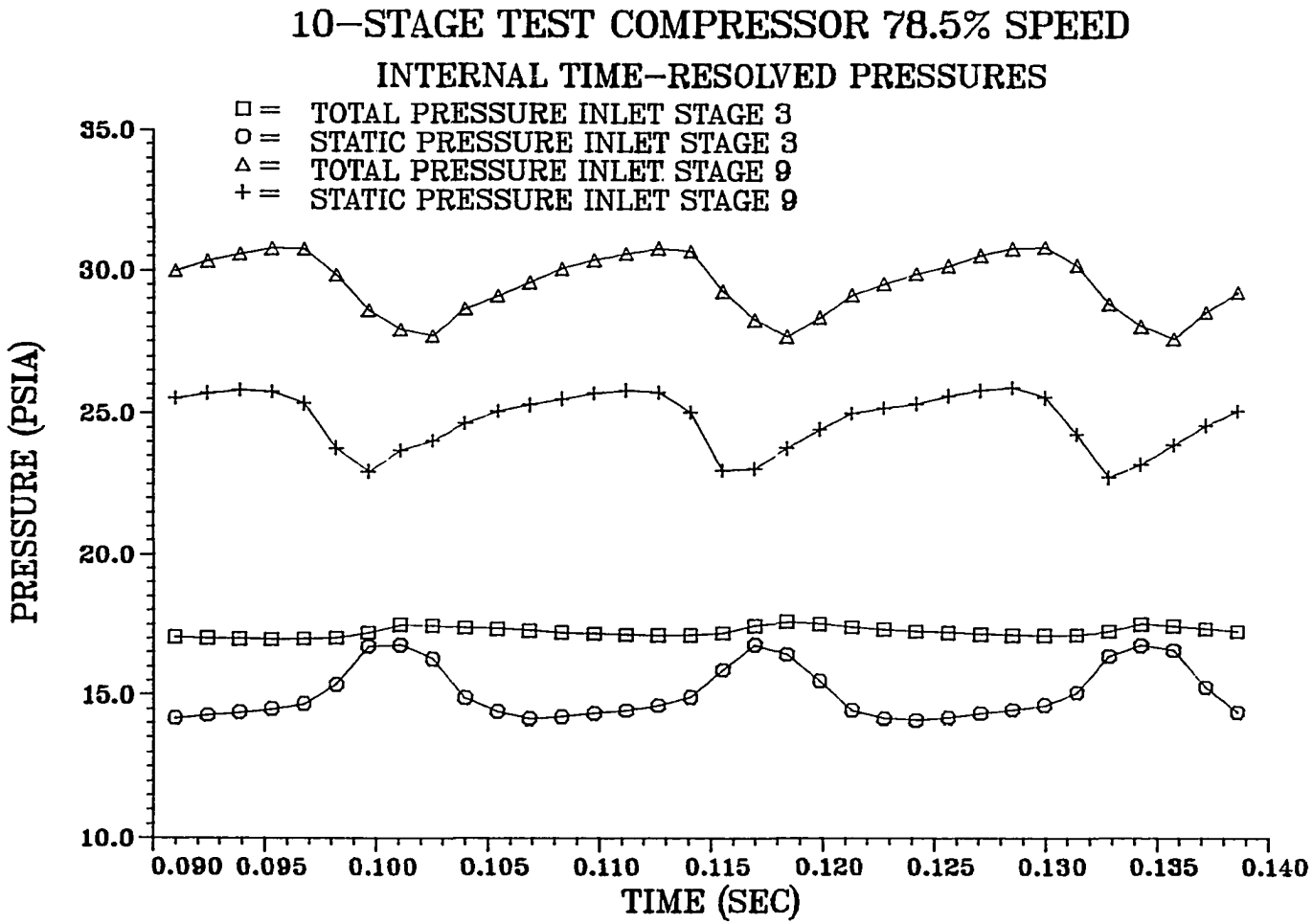

Figure 7.47 Test compressor time-resloved tip region total and static pressure at 78.5% speed in-stall exit throttle area 20 sq. in. (129.0 sq. cm)

supports the notion that this stage is not in a stalled condition, but instead is driven higher up on its characteristic by the rotating stall cell in the rear of the compressor.

It was stated earlier that high velocities probably existed in the unstalled portion of the tenth stage annulus. High-response data obtained at 59.7% and 78.5% design speed were used to estimate the velocity levels that were present in the unstalled portion of the tenth stage annulus. The magnitude of the blockage of the annulus by the rotating-stall cell was determined from high-response data for the exit throttle areas called out previously in Figures 7.44 for 78.5% design speed and in figure 7.48 for 59.7% design speed. The high-response pressure levels obtained from the forward facing and aft facing impact probes (see Figure 4.7 for probe details) at the exit of the compressor for the 15.2 in^2 (98 cm^2) throttle setting at 59.7% design speed is shown in Figure 7.49. These data show that the portion of the annulus blocked to through flow by the rotating-stall cell is 42 percent of the annulus (150 degrees). The rotating blockage leading edge was identified by a sharp and continual drop in pressure measured by the forward probe. The trailing edge of the

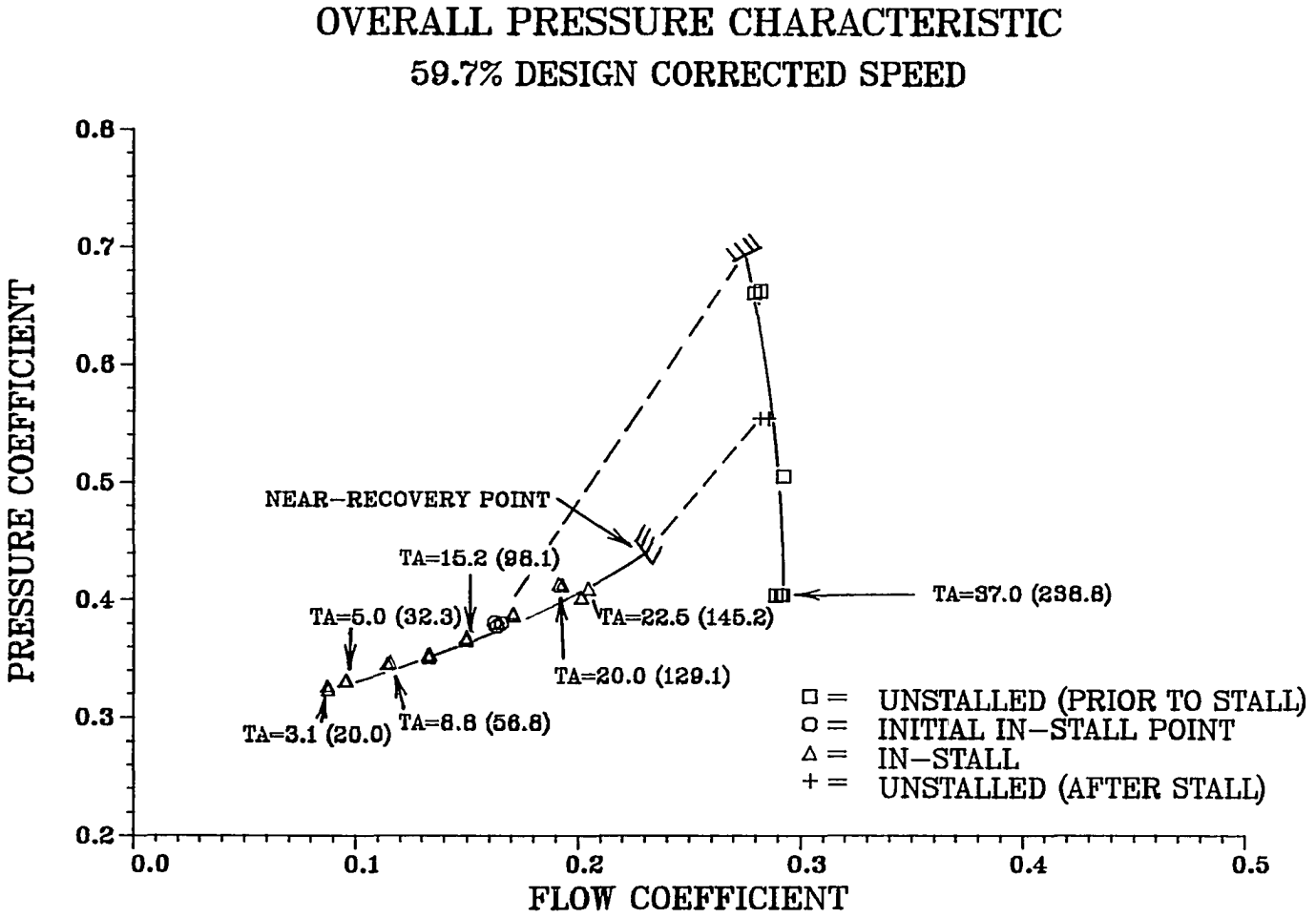

Figure 7.48 Test compressor 59.7% speed overall performance (exit throttle area details)

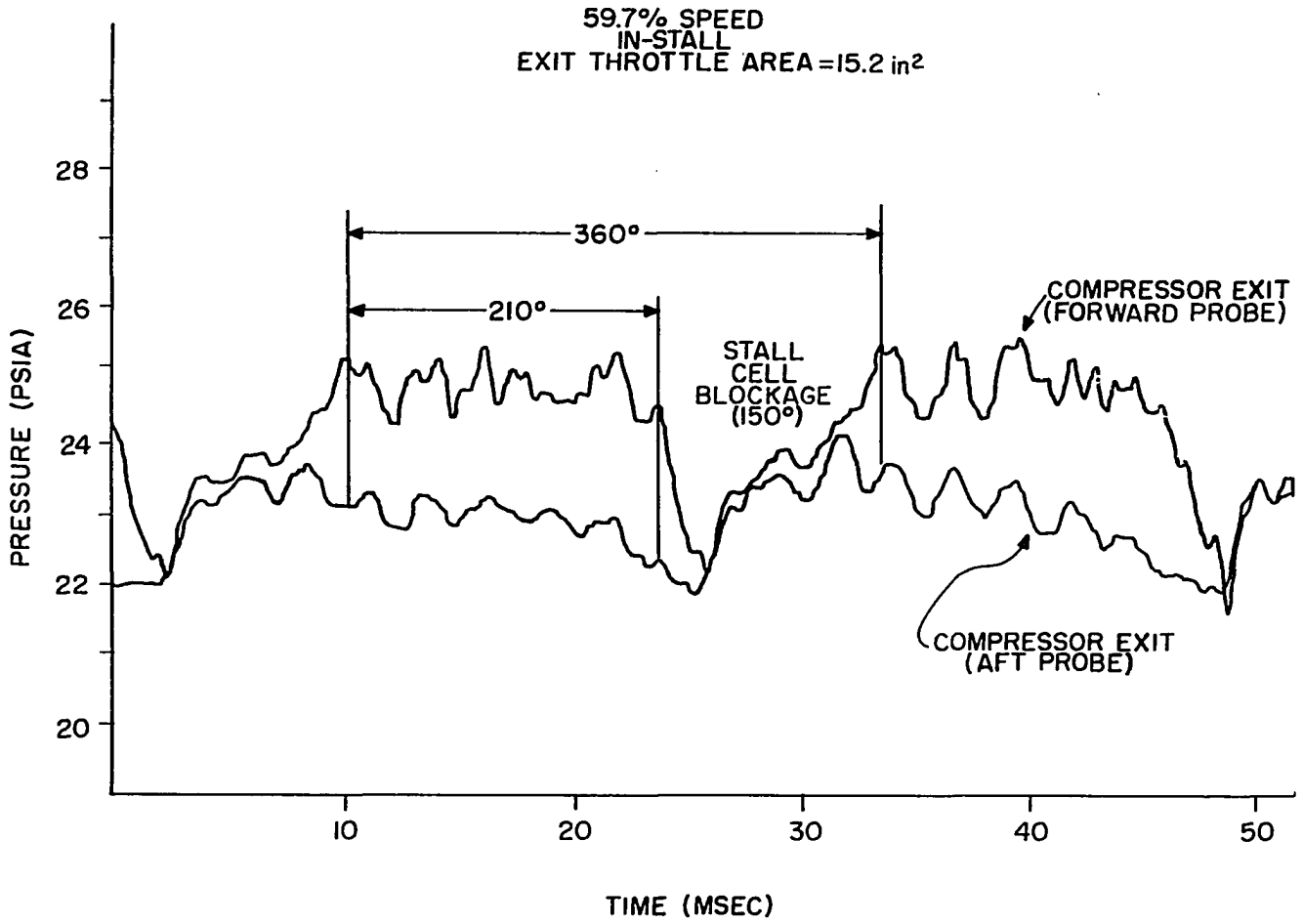

Figure 7.49 Test compressor high-response exit pressures 59.7% speed, exit throttle area 15.2 sq. in. (98.0 sq. cm)

rotating blockage was identified by the peak point after a continual rise in forward probe pressure. At the peak point the aft probe signal drops representing a drop in static pressure and re-establishment of through flow. The aft probe signal can be used to represent static pressure with proper calibrations. The signal represented in the figure has not been compensated by a calibration and therefore does not represent true static pressure. In its uncalibrated form it can still be used to determine stall cell blockage extent because absolute values are not required.

This procedure for identifying blockage extent is not the most accurate method available since flow angle changes are not determined. High-response instrumentation available on the CRF test compressor could not be used to sense flow angle. Thus, small errors in defining the absolute blockage level are possible. Errors in the blockage level approximation will result in errors in relative Mach number calculations very nearly one for one (see Figure 7.50). This procedure was followed consistently for both speeds investigated and therefore comparison of relative blockage levels at the different speeds are valid.

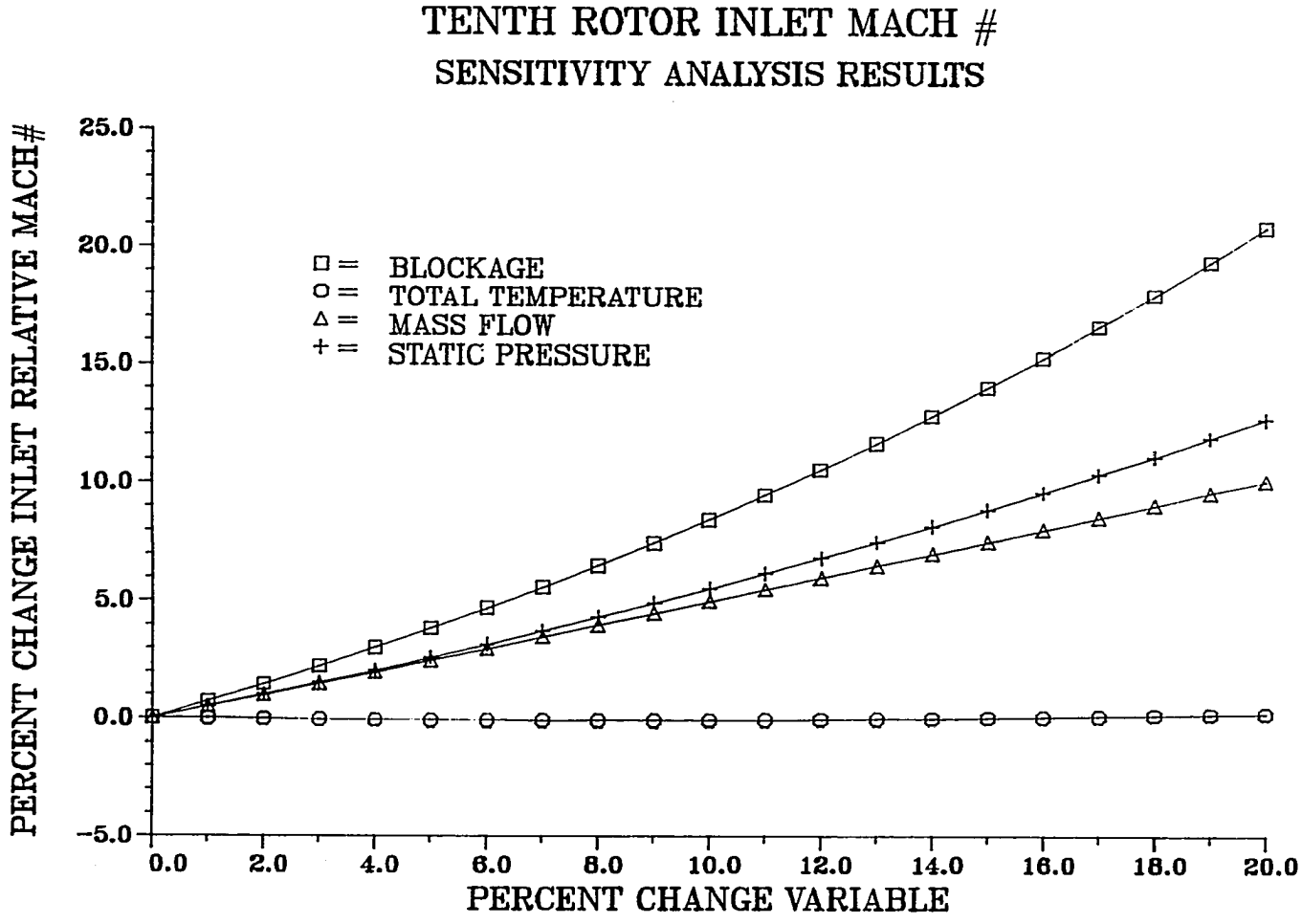

Figure 7.50 Sensitivity of rotor ten inlet relative to properties

High-response pressure signals from the same exit probes (forward facing and aft facing) and exit throttle area 15.2 in^2 (98 cm^2) described above but for 78.5% design speed are presented in Figure 7.51. These data indicate that 180 degrees or 50 percent of the annulus is blocked by the rotating-stall cell. This blockage does differ slightly from the 59.7% design corrected speed blockage extent for the same exit throttle area, but not significantly.

The high-response exit forward and aft facing pressure probe data for five other in-stall operating points called out in Figures 7.44 and 7.48 for both speeds are provided in Appendix H, Figures 19.1 through 19.10. The rotating stall cell blockage levels in the tenth stage for all operating points called out in Figures 7.44 and 7.48 are displayed in Figure 7.52. These data indicate that blockage level does not vary significantly with speed at any given throttle setting. The data also show that blockage extent may be slightly higher at 78.5% speed than 59.7% speed and that the blockage extent decreases as exit throttle area is increased. For 59.7% design corrected speed the compressor recovers from rotating stall at a blockage level of approximately 35 percent of the annulus

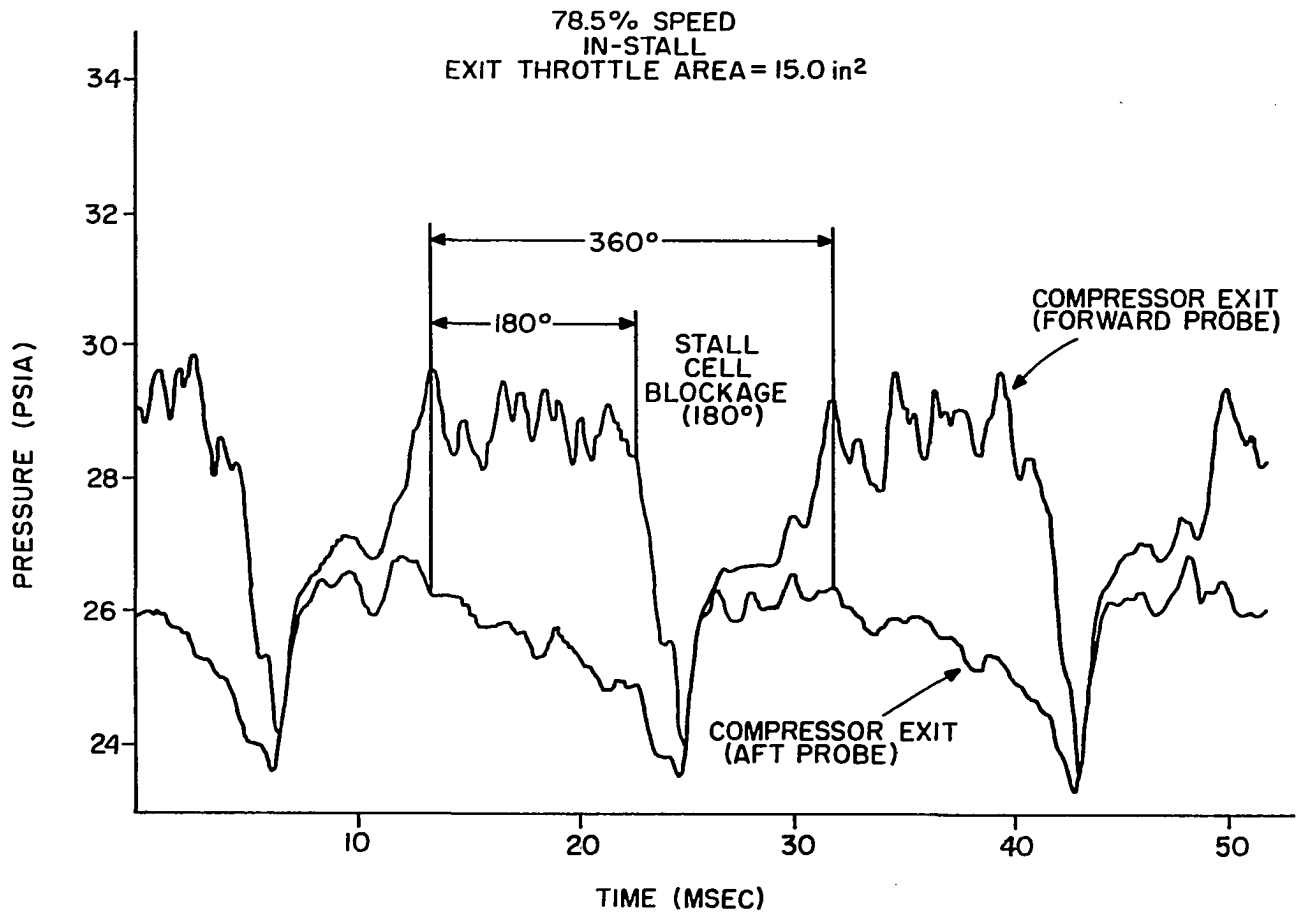

Figure 7.51 Test compressor high-response exit pressures 78.5% speed, exit throttle area 15.0 sq. in. (98.0 sq. cm)

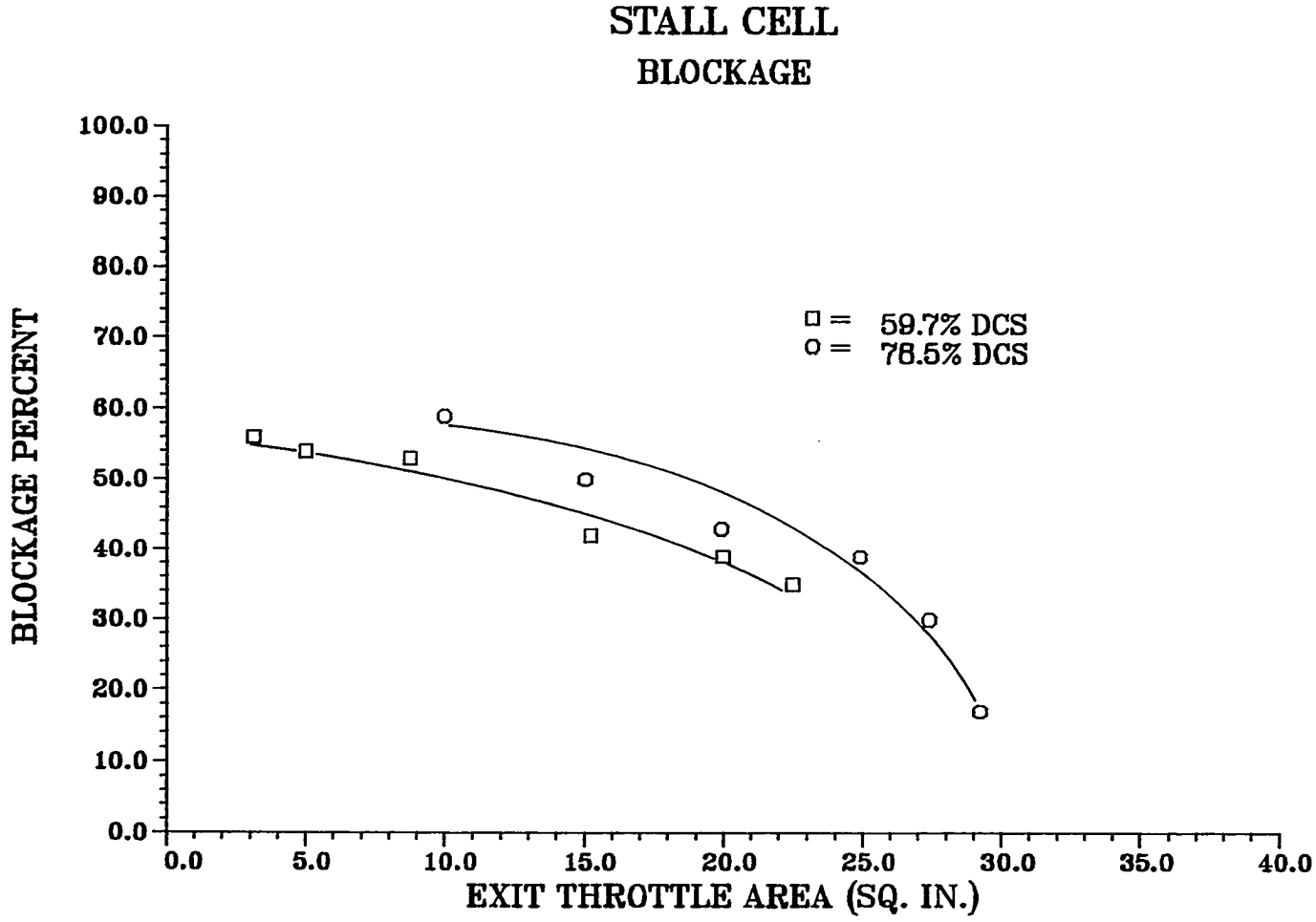

Figure 7.52 Test compressor exit throttle effects on rotating stall cell blockage level

area. This value is almost equal to levels reported by Small and Lewis [12], and Hosny and Steenken [17]. For 78.5% design corrected speed the compressor does not recover from rotating stall until the blockage extent is approximately 17 percent of the annulus area. Blockage extents this small have not been previously reported in the open literature. This difference in recovery blockage extent is discussed further when velocities in the unstalled portion of the annulus are described.

The speed of the rotating stall cell as it travels around the annulus of the stage can also be determined from the high-response pressure levels presented in Figures 7.49 and 7.51, and Appendix H. From the period of the pressure fluctuations the speed of the rotating stall cell can be determined. The speed of the rotating stall cell, defined as percentage of the rotor speed, for 59.7% and 78.5% design corrected speed, are presented in Figure 7.53. These data suggest that the speed of the rotating stall cell is a constant percentage of the rotor speed for a given blockage level. It also indicates that the speed of the rotating-stall cell increases with lower blockage

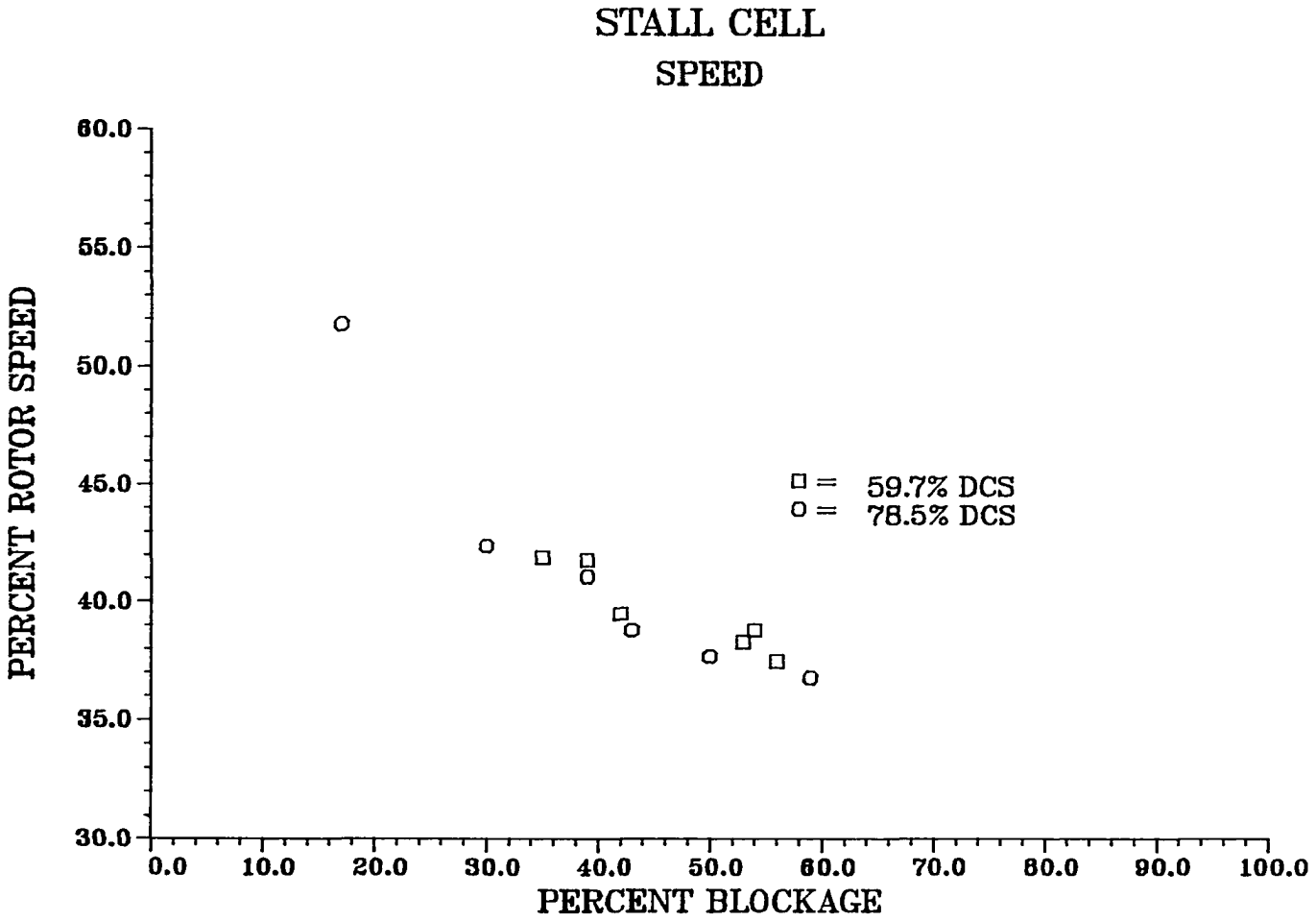

Figure 7.53 Test compressor rotating-stall cell speed variations

levels. For 78.5% design corrected speed at 17 percent blockage the speed of the rotating stall cell is much higher than for all other blockage levels.

To determine the flow velocity in the unblocked region of the annulus it was assumed that little through flow exists within the region blocked by the rotating stall cell. This assumption was based on the observation that the high-response pressure levels of the forward and aft facing probes are nearly equal within the region blocked by the rotating stall cell (see Figure 7.51) thereby indicating zero flow in the axial direction. Therefore the mass flow from the compressor exit measured at the facility venturi station (see Section III for details) must pass through the unblocked portion of the annulus. The axial velocity (C_x) within the unblocked portion of the annulus can be estimated with the following equations involving one-dimensional compressible flow of an ideal gas,

$$W = A(1 - B)\sqrt{\frac{\gamma g_c}{R}}\frac{P_s}{\sqrt{T_T}} M \sqrt{1 + \frac{\gamma - 1}{2} M^2}$$

$$C_x = M \sqrt{\frac{\gamma g_c R T_T}{\left(1 + \frac{\gamma - 1}{2} M^2\right)}}$$

where W is the sum of the mass flow as measured at the exit venturi station, described in section III, and the losses from the balance piston (See Figure 4.3 for details). B is the blockage percentage due to the rotating stall cell, A is the entrance area to the tenth stage, and P_s and T_T are the static pressure and total temperature from the time-averaged measurements at the entrance to the tenth stage.

By using the time-averaged properties for properties within the unblocked portion of the flow some errors are introduced. The static pressure at the outside diameter of the entrance to the tenth stage was measured with the high-response data acquisition system. After comparing the results of the high-response static pressure measurement with the time-averaged measurement it was determined that the time-averaged measurement of static pressure accurately represented the static pressure within the unblocked region of the annulus. Therefore negligible error was introduced by using the time-averaged value of static pressure at the entrance to the tenth stage. A high-response total temperature measurement was not available at the entrance to the tenth stage. A review of the literature on time-resolved temperature measurements obtained from a

compressor stage while operating in rotating stall indicated that little information exists on this subject. Na'covska' [32] reported temperature fluctuations on a multistage axial flow compressor during rotating stall to be ± 1 percent of the mean. She conceded, however, that because of frequency response limitations of her measurement instrumentation, the fluctuations could be larger. Therefore using time-averaged total temperature data does introduce some error, but without details of the time-resolved temperature, the time-averaged temperature can be assumed to be adequate based on a sensitivity analysis which is presented in Figure 7.50. The errors in total temperature will result in negligible error in relative Mach number of the tenth stage rotor flow.

The relative velocity at the inlet of rotor ten was determined from the axial velocity, blade geometry and rotor speed as follows,

$$V_R = \sqrt{U^2 + C_x^2}$$

Figure 7.54 represents the geometry of the blading of the tenth stage. The exit angle of the ninth stator is near axial, therefore the flow entering the tenth rotor is assumed to be axial. Using midspan rotor speed, the relative velocity in the rotor row was determined from the velocity triangle shown in Figure 7.54. The Mach number of the fluid entering the rotor (M_R) was determined from the relative velocity and the total temperature of the air, as defined by the equation below.

$$V_R = M_R \sqrt{\frac{\gamma g_c R T_T}{\left(1 + \frac{\gamma - 1}{2} M_R^2\right)}}$$

The results of this estimation procedure are presented in Table 7.1. Information using this estimation technique was also included in the table for unstalled compressor conditions. The variation of relative Mach number of the flow entering the tenth rotor with speed and exit throttle area is provided in Figure 7.55. The exit throttle areas correspond to the operating points called out for the pressure characteristics in Figures 7.44 and 7.48.

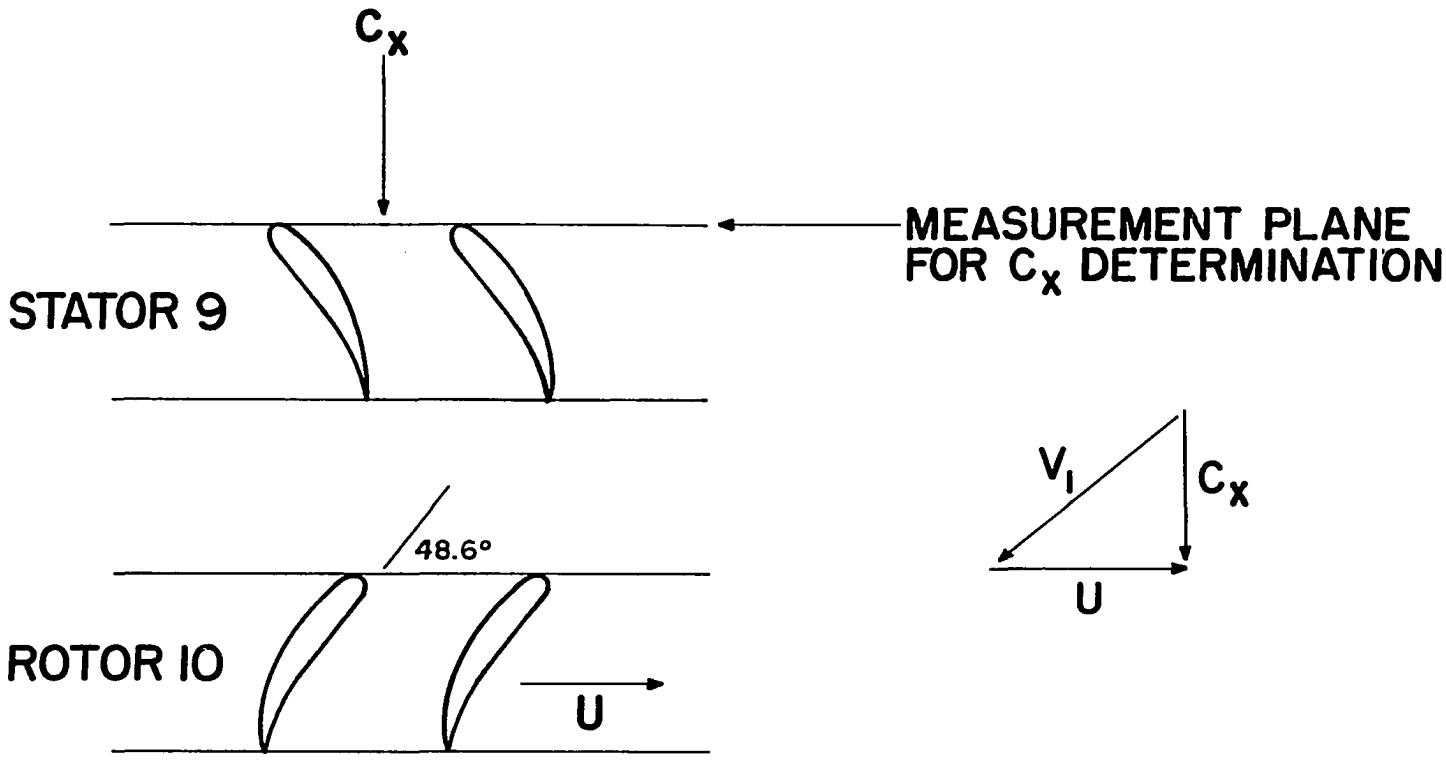

Figure 7.54 Tenth stage blade geometry

Table 7.1 Tenth stage velocity properties

PERCENT SPEED	THROTTLE AREA IN^2	MASS FLOW LBS/SEC	PERCENT BLOCKAGE	STATIC PRESSURE PSIA	TOTAL TEMPERATURE DEG R	AXIAL MACH NUMBER	AXIAL VELOCITY FT/SEC	ROTOR VELOCITY FT/SEC	RELATIVE VELOCITY FT/SEC	RELATIVE MACH NUMBER
59.7	37.0	15.6	0.0	21.8	652.	0.33	404.	507.	648.	0.53
59.8	29.8	15.8	0.0	23.2	658.	0.31	389.	507.	639.	0.52
59.8	26.4	15.2	0.0	24.1	674.	0.29	369.	508.	628.	0.51
59.7	20.6	15.2	0.0	26.0	676.	0.27	342.	507.	612.	0.49
59.7	22.5	10.8	35.0	22.0	718.	0.36	467.	508.	690.	0.54
59.7	20.0	10.3	39.0	22.1	731.	0.37	482.	508.	700.	0.54
59.7	15.2	8.0	42.0	21.2	767.	0.32	430.	509.	666.	0.50
59.7	8.8	6.1	53.0	20.6	804.	0.32	436.	508.	670.	0.49
59.6	5.0	5.1	54.0	20.3	836.	0.28	395.	508.	644.	0.46
59.6	3.1	4.6	56.0	20.1	852.	0.27	386.	509.	639.	0.46
78.7	37.8	20.0	0.0	25.0	747.	0.39	510.	669.	842.	0.65
78.7	29.3	19.6	0.0	27.0	750.	0.35	468.	669.	816.	0.63
78.7	27.4	19.7	0.0	27.8	755.	0.35	460.	669.	812.	0.63
78.7	22.5	19.6	0.0	30.7	769.	0.32	425.	669.	792.	0.60
78.7	16.2	18.8	0.0	35.9	792.	0.26	361.	668.	760.	0.57
78.7	29.2	18.9	17.0	27.9	779.	0.40	544.	669.	862.	0.66
78.6	27.4	15.9	30.0	27.8	843.	0.42	587.	669.	890.	0.65
78.7	24.9	14.4	39.0	27.3	869.	0.45	635.	669.	923.	0.67
78.6	19.9	11.9	43.0	26.2	919.	0.43	622.	669.	914.	0.64
78.6	15.0	9.3	50.0	25.2	973.	0.41	615.	670.	909.	0.62
78.5	10.0	7.4	59.0	24.1	1019.	0.42	650.	670.	933.	0.62

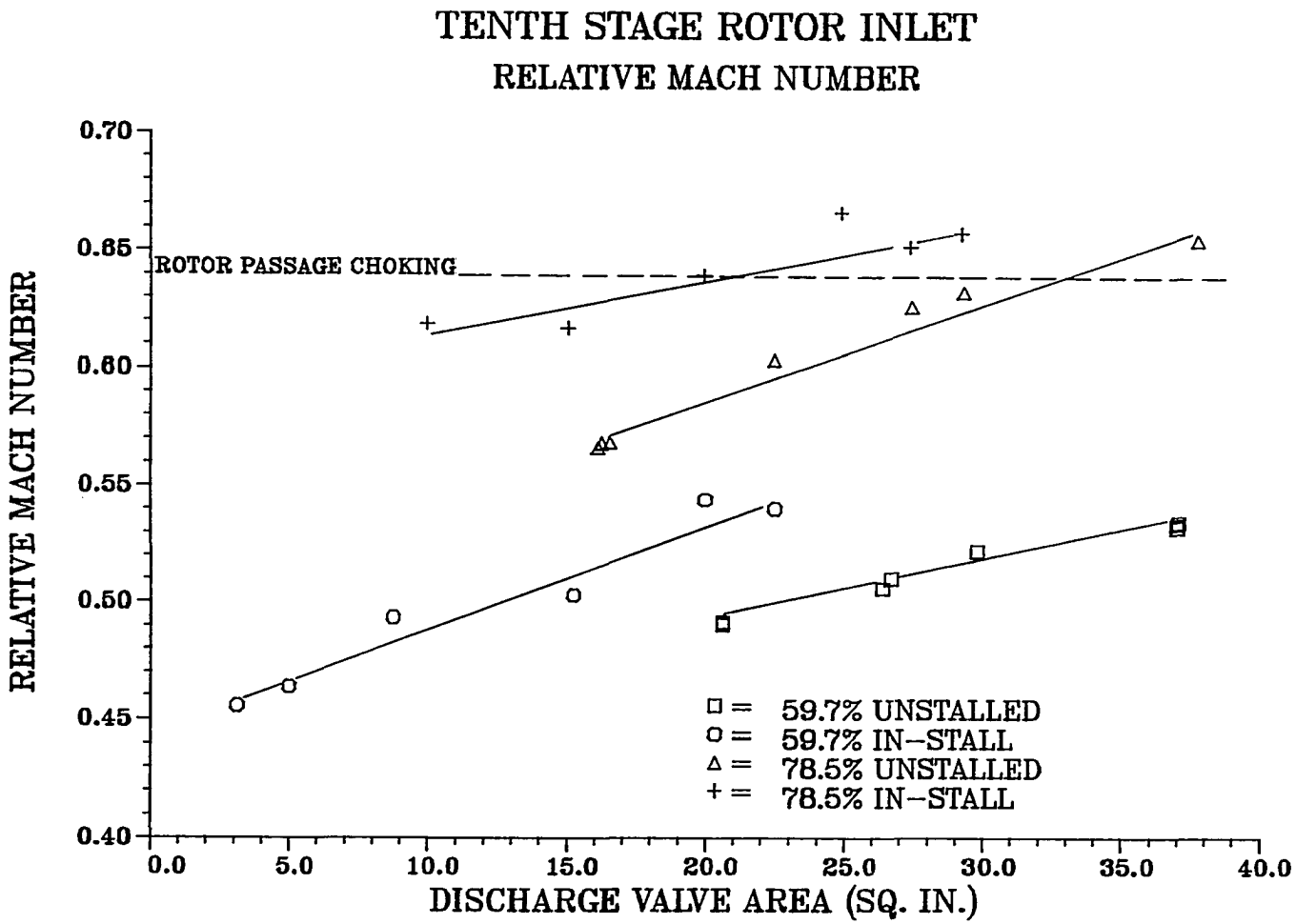

Figure 7.55 Test compressor exit throttle and speed effects on relative Mach numbers in the tenth stage rotor

The data in Figure 7.55 indicate that the highest relative Mach numbers occur for 78.5% design speed in-stall conditions.

Rotor ten choking from the unstalled flow depends on the entrance relative Mach number and the area reduction due to blade thickness. Based on the number of blades, their height and maximum thickness, the maximum thickness area to inlet area ratio is 1.145. With an area reduction of 1.145, relative Mach numbers of 0.64 and greater at the inlet to the tenth stage rotor will cause a sonic condition to exist somewhere within the tenth rotor. No consideration was made for the boundary layer thickness within the tenth stage rotor. A boundary layer would result in a smaller area ratio than 1.145 and therefore a lower Mach number than 0.64 at the inlet to cause choking at the minimum area. The data in Figure 7.55 suggest based on estimated relative Mach numbers values, that choking is present in the unstalled portion of the tenth stage rotor while the compressor is operating in rotating stall. These data also suggest that at 78.5% speed for unstalled conditions with the exit throttle area less than 37.6 in^2 (242.6 cm^2) that the relative Mach numbers at the entrance to rotor 10 are below 0.64 and choking does not occur. For

a exit throttle area of 37.6 in^2 (242.6 cm^2) or greater, while operating unstalled, choking may occur in the rotor. The tenth stage characteristic shown in Figure 7.56 indicates for the unstalled condition at an exit throttle area of 37.6 in^2 (242.6 cm^2) that a pressure drop does exist in the tenth stage, while for smaller exit throttle areas a pressure rise exists. It is believed that the drop in pressure across the stage, at 37.6 in^2 (242.6 cm^2) exit throttle area during unstalled operation is due to the extremely high velocities and therefore high losses in the rotor. This behavior during unstalled operation supports the determination that at 0.64 relative Mach number stage chocking occurs.

The data in Figure 7.55 also show that with the exit throttle closed to a level of 10 in^2 (64.5 cm^2), while the CRF test compressor was operating in rotating stall, the rotor inlet relative Mach number was 0.63. This Mach number is below the threshold value for chocking and indicates that the stage may not be choked for this throttle setting. Some additional error may exist for this throttle setting because the blockage was difficult to

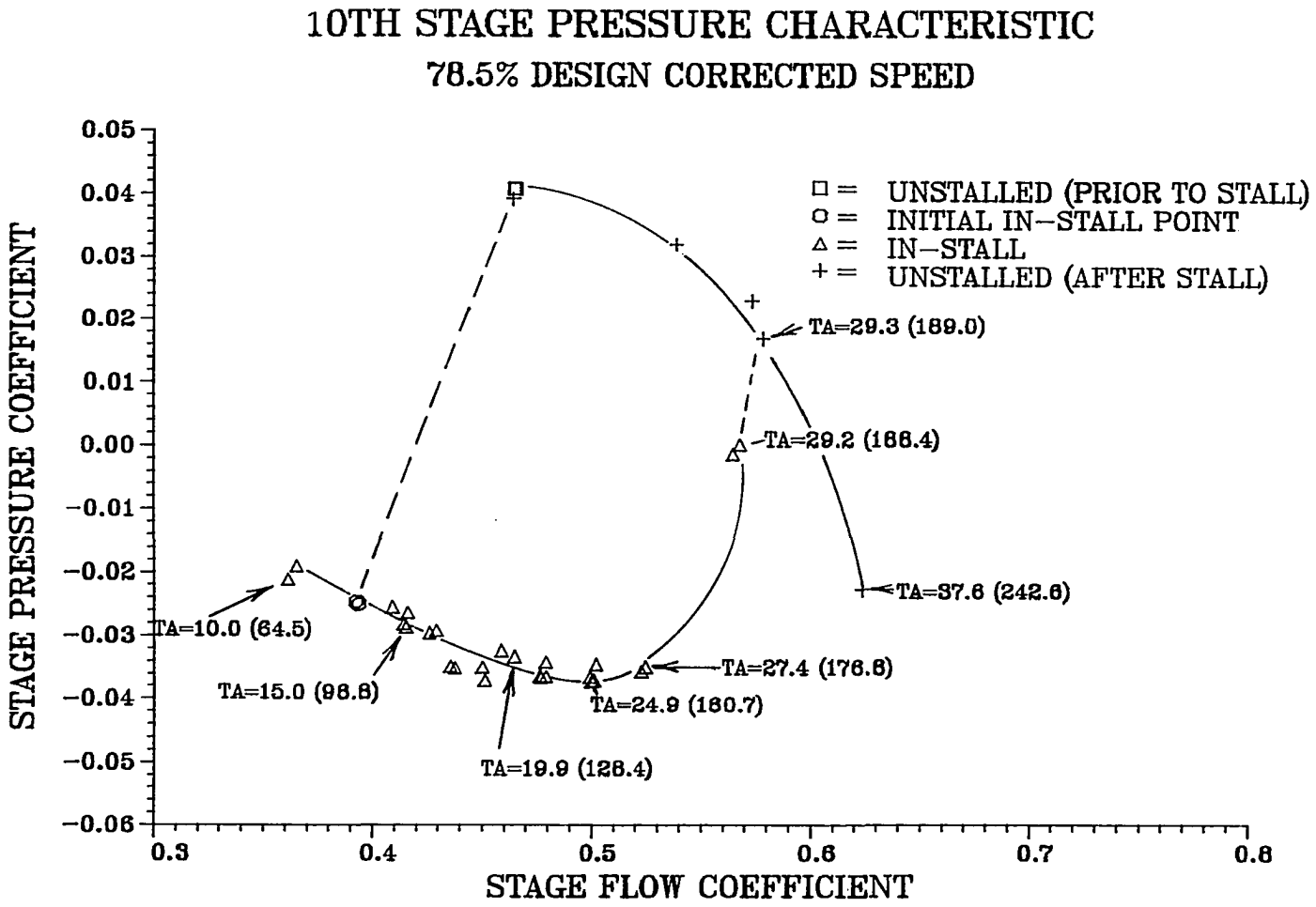

Figure 7.56 Test compressor tenth stage pressure characteristic (exit throttle area details)

determine as the boundaries between the stalled flow and unstalled flow were not well defined by pressure probe measurements (see Appendix H, Figure 19.6).

The same approximations of tenth stage rotor inlet relative mach numbers for 59.7% speed are also presented in Figure 7.55. These data show that at this speed, all relative Mach numbers are below 0.64 and therefore choking does not occur.

These results suggest that the CRF test compressor in-stall hysteresis extent is prolonged by partial choking of the rear stage after overall compressor stall has been initiated. The reason that operating conditions in the compressor could still be altered with the discharge valve, after choking occurs, is by communication to the front stages through the stalled portion of the flow. The rotating stall did not clear until the pressure generated by the front stages increased and the temperatures decreased thereby increasing downstream density and reducing relative Mach number levels in the tenth stage. Both factors (larger pressure rise and smaller or negative temperature change in upstream stages) increase the density of the fluid entering the tenth rotor, thereby making choking less likely.

At 78.5% speed, once the overall compressor has stalled, the front three stages produce high temperatures and allow high mass flows (operate at high flow coefficient levels) through the compressor. The high mass flows and temperatures result in high velocities which cause choking in tenth stage of the compressor based on the estimation procedures defined above. This condition is similar to the conditions that exists when starting a high design pressure ratio multistage compressor. In starting a high design pressure ratio multistage compressor from zero speed to design speed, the front stages and middle stages do not create enough pressure rise to reduce the density of the air to levels that the rear stages are designed for. This results in extremely high flows in the rear stages and thus choking there. This choking of the rear stages loads up the front stages and the compressor stalls during startup (see Ref. [49]). To eliminate this problem, multistage compressors are usually designed with variable geometry and bleeds in the front stages. The geometry of the front stages can be changed to increase their stall margin, making the front stages less likely to stall during startup. The bleeds can be used to remove mass flow from the compressor prior to the aft stages. This air flow

bleeding reduces velocity in those aft stages and avoid choking.

In the CRF test compressor, at 78.5% speed after overall compressor stalling had occurred (initiated by the seventh stage), the front stages were loaded to high pressure coefficient levels but did not stall. Velocities in the tenth stage were elevated to very high levels due to the blockage by the rotating stall cell. For the compressor to recover from stall the velocity levels in the tenth stage had to be reduced. To recover from stall at 78.5% speed, conditions had to be altered in a similar fashion to what is required for starting a high design-pressure-ratio multistage compressor. The density of the air entering the tenth stage had to be increased and the mass flow reduced to reduce relative flow velocities. When levels drop below choking levels and conditions unstalled the stage that initiated the rotating stall (for the CRF test compressor at 78.5% design speed it was the seventh stage) the compressor recovered. Without choking in the tenth stage, the compressor would recover, as in-stall hysteresis levels would be reduced. The presence of choked conditions in the tenth-stage, as is the case at

78.5% speed, impedes the recovery of the stall initiating stage and as a result stages involved in the overall compressor stall have lenghtened double valued pressure coefficient characteristics as shown in Figure 7.57. It is proposed that when operating at the lower of the two pressure coefficient values shown in Figure 7.57, if choking of the rear stage were removed, the stages involved in the stall would move to operate on the higher pressure level and compressor recovery would result. Because choking in the tenth stage rotor is not present at 59.7% speed as was shown in Figure 7.55, no double valued characteristics exists for any stage (see Appendix C, Figures 15.2 through 15.11).

In summary, based on the analysis presented above, it is proposed the in-stall hysteresis of the CRF 10-stage test compressor increase with increasing speed because of choking in the unblocked portion of the tenth stage. The hysteresis could be reduced at 78.5% speed if the density of the air entering the tenth stage rotor could be increased or if the flow rate through the tenth stage could be reduced by bleeding air in front of the tenth stage. Another possibility for reducing hysteresis would be to

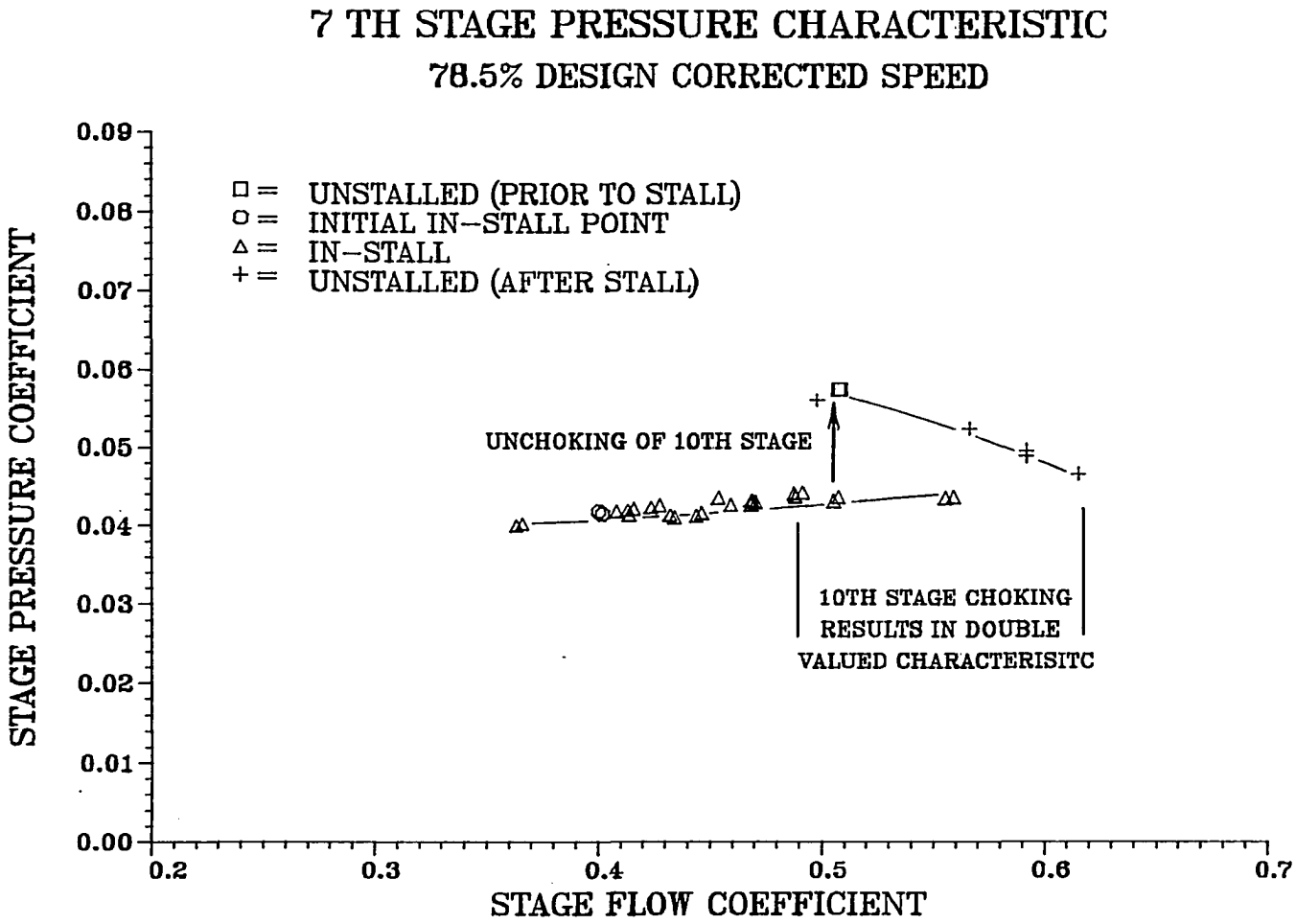

Figure 7.57 Test compressor 78.5% speed seventh stage double valved pressure characteristic

schedule the three vanes in the first three stages to a more closed position with resulting reduced flow through the compressor. It is also possible that if the first three stages were scheduled to be closer to stall when the overall compressor stalled, the first three stages would stall and the resulting blockage would reduce the flow levels and therefore velocities going to the rear stages. Velocity levels could also be reduced at the entrance to the tenth stage by increasing flow area in the rear of the compressor. From analysis of the results obtained from the time-resolved data it is clear that stage matching has a considerable effect on compressor in-stall performance and recoverability.

2. Dynamic stalling comparisons

Multistage compressor dynamic in-stall analytical models such as the one developed by Davis [44], are essential for exploration of the effects of stage matching on compressor in-stall performance. Therefore some consideration is given to the validation of the multistage model developed by Davis.

The control volumes for the analytical model were fixed to match, as near as possible, the flow volumes in the CRF test compressor. Matching of inlet and discharge volumes required a larger overall length for the modeled test compressor. This increase in length was needed to avoid numerical instabilities in the solution algorithm. The algorithm did not allow large changes in control volume areas from entrance to exit. The physical length of the compression section was maintained in the model and is identified between the two arrows on the analytical control volume configuration provided in Figure 7.58.

The experimental pressure and temperature characteristics obtained from the test compressor at 78.5% design corrected speed were input to the model for each stage. These characteristics were used to determine the shaft work input and pressure forces supplied to each control volume by the compressor rotor.

The transition into rotating stall at 78.5% design corrected speed was simulated by the model. The exit flow in the model was reduced until a dynamic instability resulted. Comparison of the Davis model exit total pressure and test compressor exit total pressure during transition into rotating stall is provided in Figure 7.59.

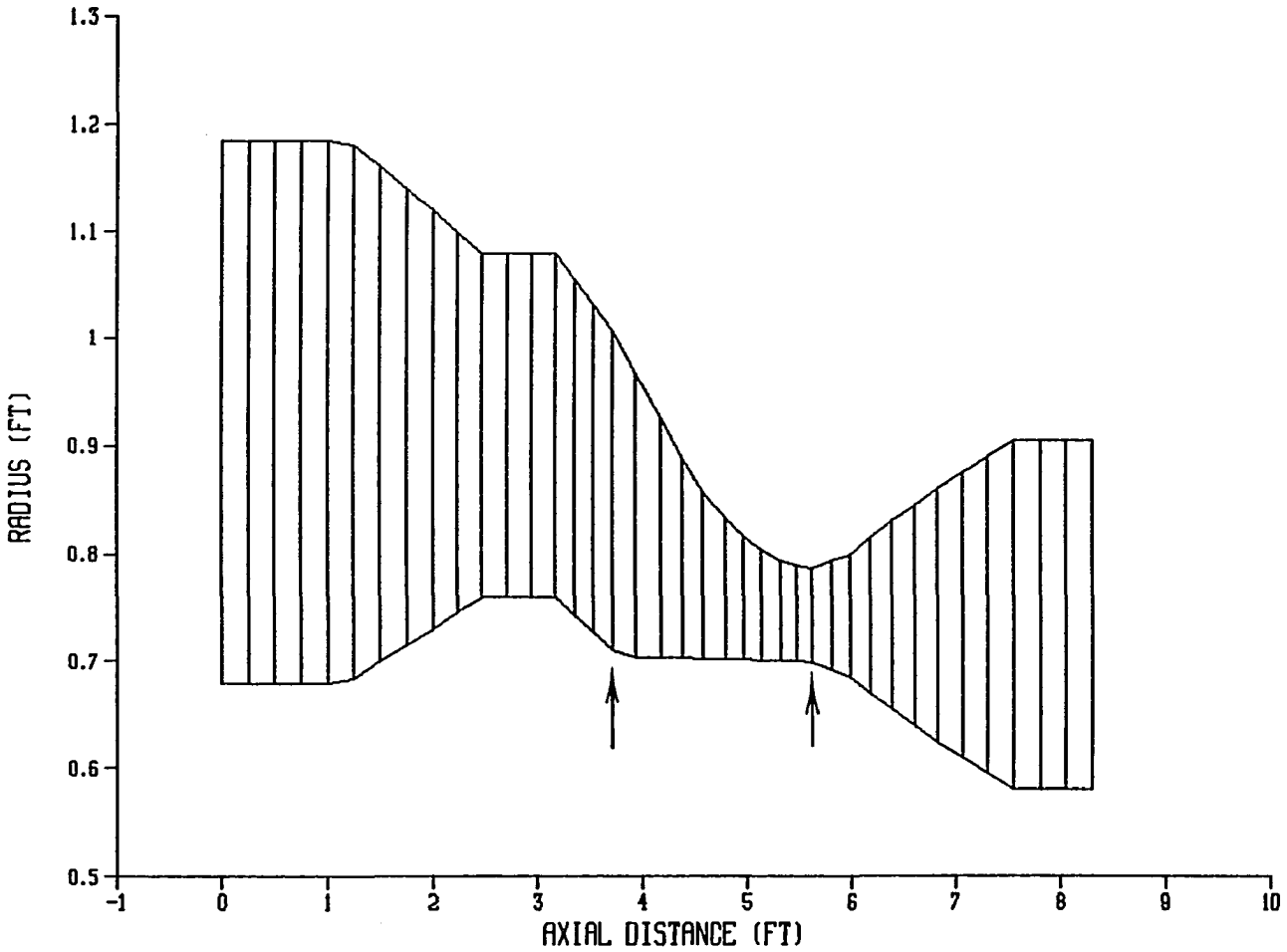

Figure 7.58 Multistage model control volume definition

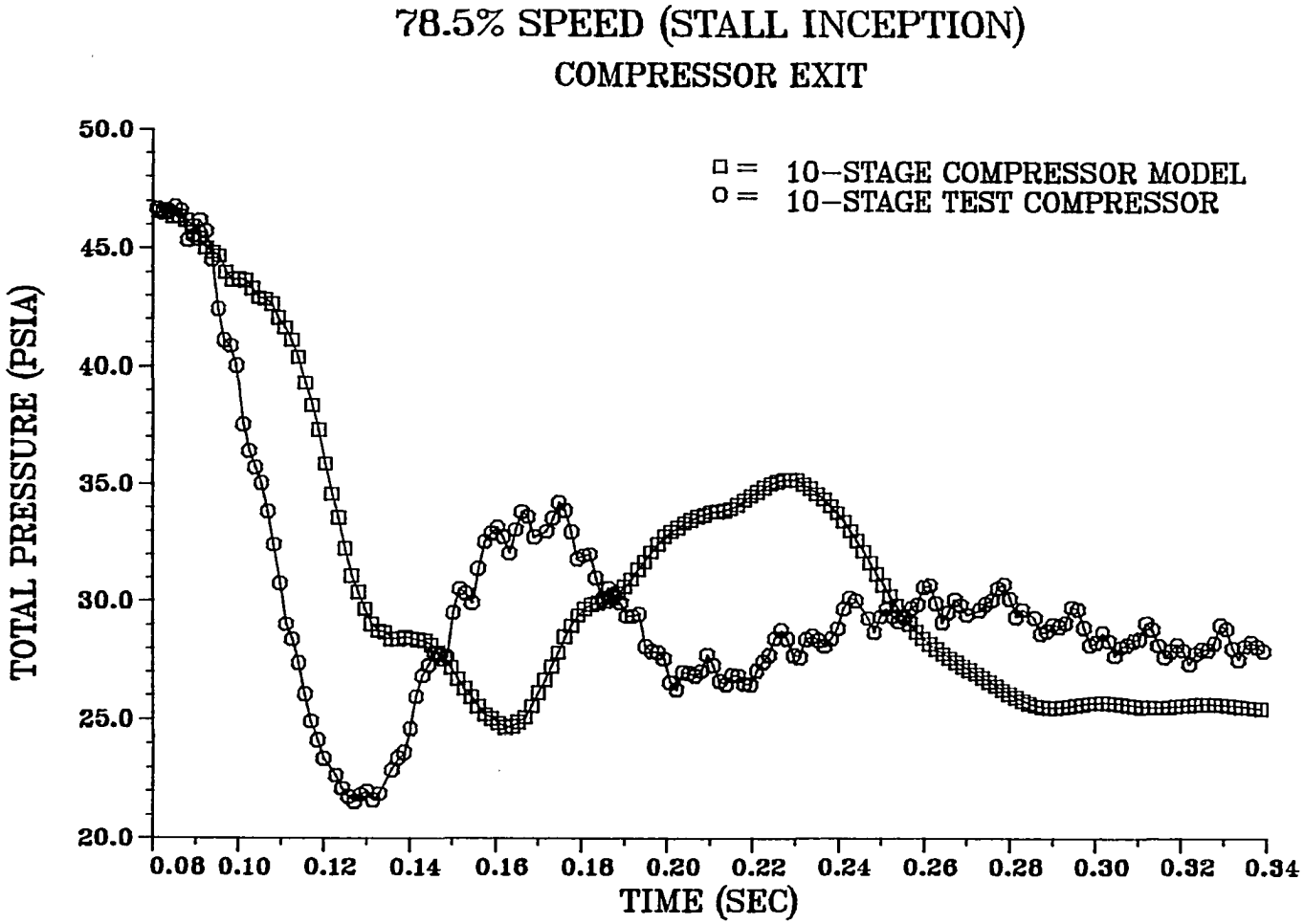

Figure 7.59 Exit total pressure during compressor stalling comparison

The results obtained with the close-coupled data acquisition system were numerically averaged over the exit measurement locations (defined in Appendix A, Figure 12.14) to determine a representative time-resolved exit pressure. This was necessary to allow for comparison with the results generated by the one-dimensional analytical model. Averaging of the test compressor pressure signals does not totally eliminate the circumferential effect caused by the rotating stall cell and therefore higher frequency pressure fluctuations are inherent in the experimental data. The analytical model does not simulate two-dimensional effects at all and does not therefore include these in the analytical time-resolved pressure values.

From Figure 7.59 it can be seen that the model accurately predicts the exit pressure level just before the dynamic stalling event. The comparison of the test and model results also show that after steady rotating stall has been established, 0.26 seconds from stall inception, the model predicts the exit pressure in-stall within 10 percent of the measured value. This may not appear to be very accurate considering the current status of steady-state unstalled compressor prediction capabilities. But for prediction of the performance of a multistage

compressor while in rotating stall, 10 percent accuracy is encouraging.

From the comparison of model and experimental data during transition into rotating stall shown in Figure 7.59 it is apparent that the model captures the overall trend of the dynamic transition. The model does not simulate the correct time lag of the event. The CRF 10-stage compressor test data indicate a sharper drop and then rise in pressure when the compressor stalls than the model predicts. The model results are greatly affected by the lagging of the stage pressure forces through first order lag functions (see Section VII.A) that are input. The model seems to require less lagging of forces to better simulate the event.

Interstage results from the model are also affected by the level of the lagging time constant. The data in Figure 7.60 show the total pressure at the entrance to the ninth stage during the transition into rotating stall at 78.5% design corrected speed. The comparison of model and test data suggests good agreement of the initial unstalled and in-stall operating pressures. The model also predicted the correct trend of the event with an initial rise in pressure and then a drop to the final in-stall level. This is the

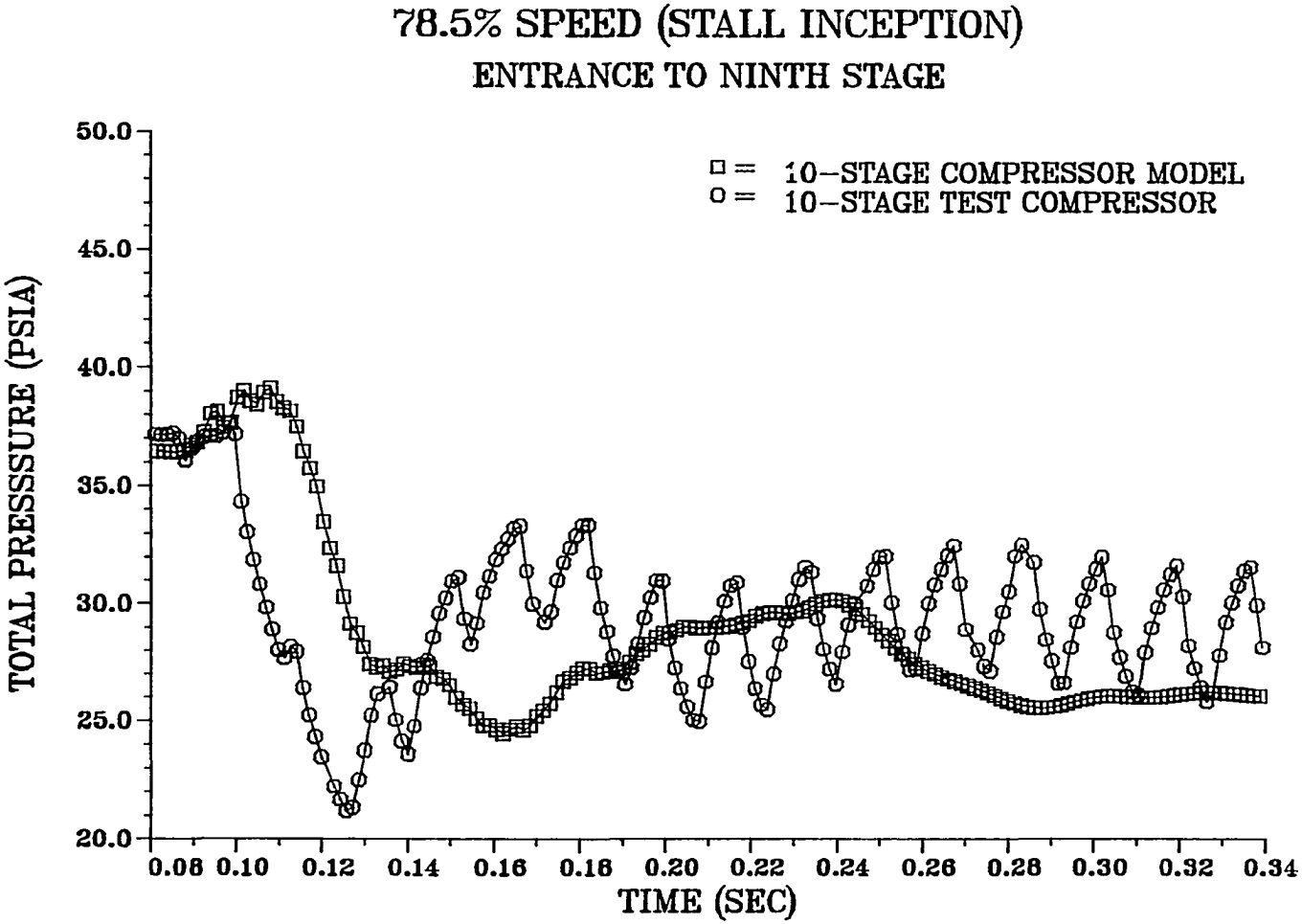

Figure 7.60 Entrance to ninth stage total pressure during compressor stalling comparison

first comparison of model and test compressor interstage pressures for a high-speed, multistage compressor in the open literature. The comparison shows that the model has potential as a tool for further analytical research.

Comparisons between model and test compressor results shown in Figures 7.61 and 7.62 for the seventh and fifth stages respectively, confirm the conclusions drawn for the ninth stage. The data in Figure 7.63 show that the model predicts the dynamic event for the third stage even more accurately than it did for stages five, seven and nine. The time lag discrepancies associated with modeling stages five, seven and nine did not occur for the third stage. This observation suggests that the input time constant used to lag the pressure forces, which was constant for all stages, more accurately represented the dynamics at the third stage. It is possible that smaller time lags are appropriate for the stage or stages that initiate the overall compressor stall, in this case at 78.5% design corrected speed, the seventh stage. The comparisons of model and test results suggest that the forces for each stage have different dynamic characteristics and therefore require individual consideration with a multistage model; the time constant for each stage is different.

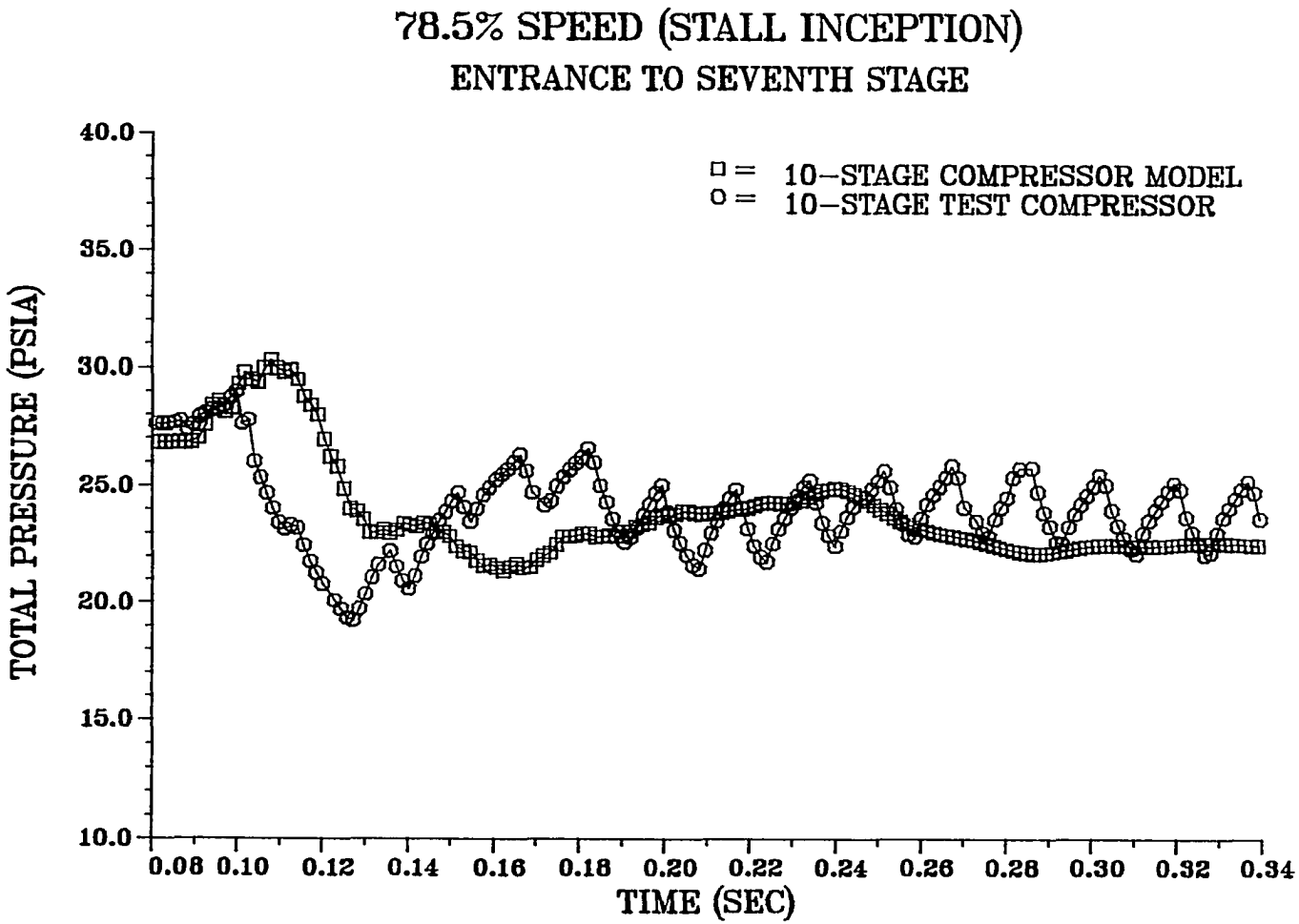

Figure 7.61 Entrance to seventh stage total during compressor stalling comparison

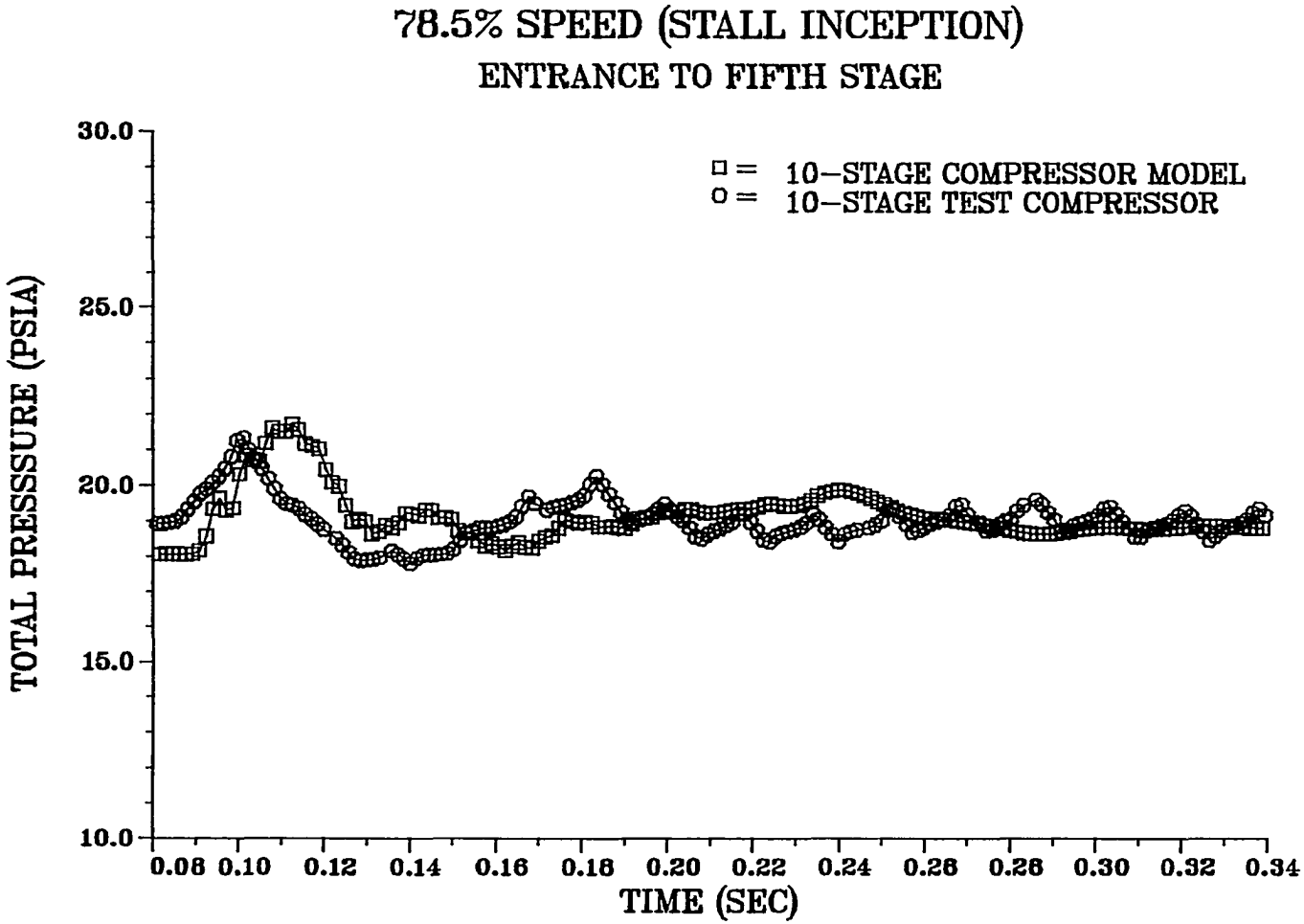

Figure 7.62 Entrance to fifth stage total pressure during compressor stalling comparison

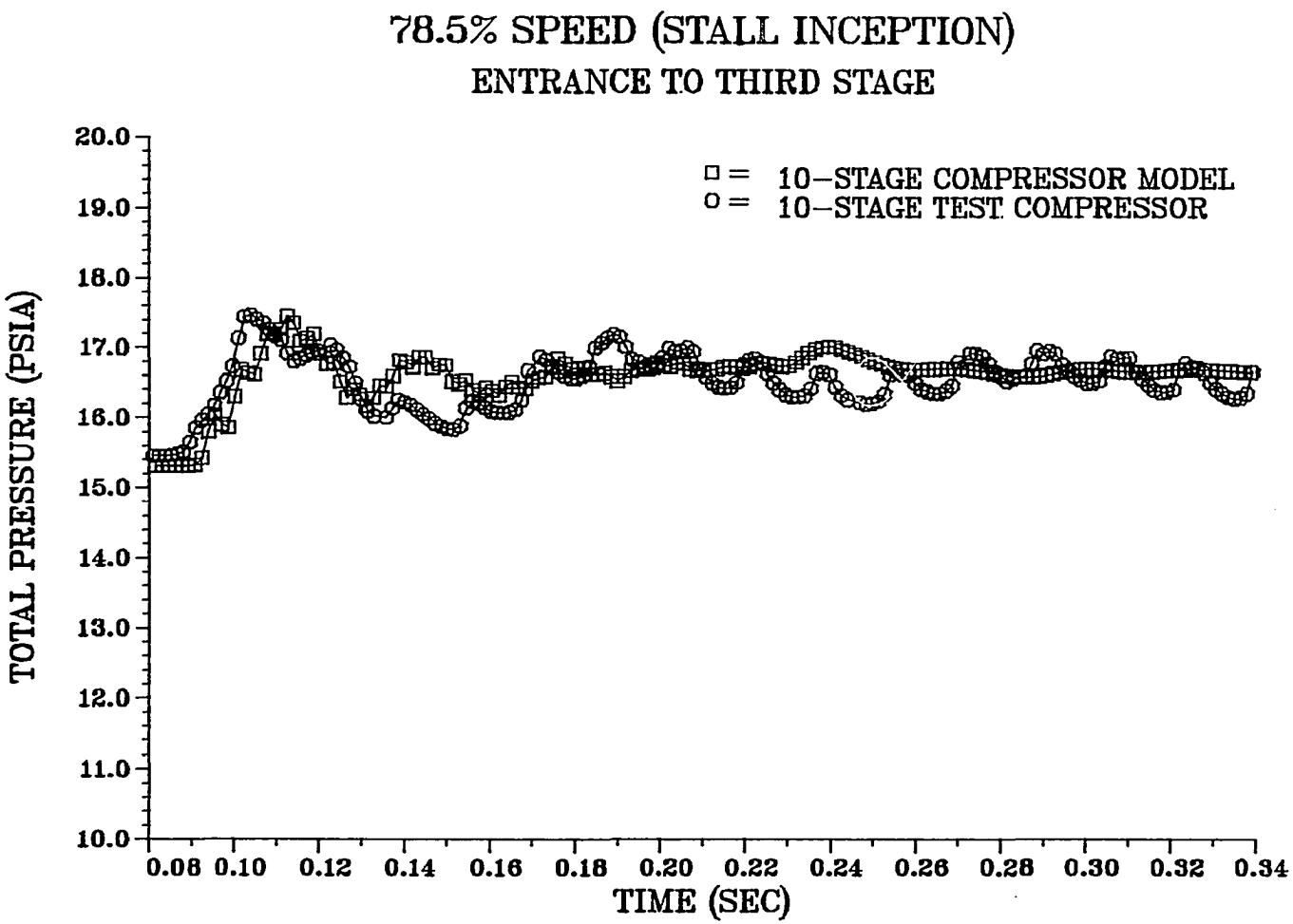

Figure 7.63 Entrance to third stage total pressure during compressor stalling comparison

The results presented here indicate that the Davis model can be used as an analysis tool for multistage compressor stalling and recoverability. The multistage model predicts in-stall compressor performance correctly. This was expected since the compressor in-stall characteristics were input into the model. It is of course desirable to predict in-stall performance prior to building and testing a compressor. Further improvements are recommended for the Davis multistage model to eliminate the need for stage characteristics by replacing this need with blade geometry inputs. The model is still very useful without this capability and should continue to be explored. Since stage characteristics have already been determined for the CRF test compressor, the model can be used with these characteristics to determine possible compressor in-stall recovery strategies. It can also be used to evaluate parameters such as bleeds, area changes and stage characteristics on recoverability of multistage compressors. Analysis of the CRF test compressor data suggests that these parameters are important for reducing in-stall hysteresis and thus increasing compressor recoverability.

It is also recommended that the model be improved to accept double valued stage characteristics. The results from the CRF test compressor test clearly indicate that double valued stage characteristics can exist in a multistage compressor operating in rotating stall.

In summary, the data obtained during the CRF 10-stage compressor tests provided for additional validation of the Davis multistage model for the prediction of compressor stalling behavior. Some improvements to the model have been recommended that will enhance the model's ability to predict multistage stalling events.

VIII. SUMMARY AND CONCLUSIONS

Modern, high-speed, multistage, axial-flow compressor evaluations are primarily based on four critical performance parameters, pressure rise, efficiency, stall margin, and recoverability from a stalling condition. The first three parameters have always been of major importance to compressor designers. The fourth parameter, recoverability, is of more recent concern, because the need for greater aircraft maneuverability imposes conditions on the engine compressor which can cause it to stall. After compressor stall occurs, rapid recovery from stall is imperative for sustained aircraft flight. Design guidelines to improve compressor recoverability are required.

The test program described in this dissertation was designed to yield information about high-speed multistage compressor recoverability from an in-stall condition. Details about the design features of the CRF test compressor and the test facility used in the test program were presented. Three methods of data acquisition, time-averaged, close-coupled and high-response, were used to obtain stalling and in-stall characteristics of the CRF

test compressor. Test procedures were designed to facilitate evaluation of the effects of speed and variable geometry on compressor recoverability.

A model developed by Davis [44], which attempts to predict multistage compressor dynamic response to stage stalling was described. This model is based on one-dimensional, compressible, unsteady aerodynamic theories. It utilizes a multiple control volume approach to determine the dynamics of a multistage compressor. Prior quantitative validation of the model was based primarily on in-stall data obtained from low-speed compressors.

The data obtained from the CRF test compressor provided information necessary to further validate the Davis model. In addition, the test compressor data suggest ways by which the Davis model can be improved.

The following conclusions about multistage compressor recoverability research are based on experience in testing the CRF 10-stage test compressor and analyzing the test data.

1. Extensive pretest data acquisition system preparation is required before obtaining time-averaged and time-resolved data from a multistage compressor going into and operating in quasi-steady rotating stall.

2. Obtaining time-resolved data with two separate and distinct data acquisition systems reinforces the validity of the data obtained from each. In addition, care must be taken when interpreting unsteady data. Data acquisition system frequency response limits the amount of information that can be collected. This was the case with the close-coupled data acquisition system used in the CRF test program. The limited frequency response of the close-coupled system prohibited interpretation of the details of the rotating stall cell. The close-coupled system did provide global information about compressor stalling that was useful.

3. Time-averaged unstalled and in-stall compressor pressure and temperature characteristics can be obtained from a high-speed, multistage compressor without facility or compressor failure if appropriate health monitoring of the compressor occurs.

The following conclusions about the CRF 10-stage test compressor are based on test data analysis.

1. Overall compressor in-stall pressure characteristics involved lower pressure levels than the unstalled characteristics. Pressure levels of the in-stall characteristics decreased with increasing shaft speed. The initial in-stall operating point of the overall compressor

occurred at lower flow coefficients with increase in compressor shaft speed.

2. Recovery of the CRF test compressor from in-stall operating points appeared to occur at the same pressure coefficient of approximately 0.44 regardless of shaft speed.

3. The time-averaged overall compressor in-stall performance data showed that the first three stages of the test compressor are not operating in full span rotating stall even after overall compressor stall occurs. This observation is supported by time-resolved, close-coupled data. It is possible, in fact, for the first three stages of the CRF test compressor to produce a greater pressure rise after overall compressor stalling occurs than before. Therefore, multistage compressor theories that assume that a full span stall cell extends axially throughout the compressor may not be generally valid.

4. When the overall compressor was in stall, the performance of the second and third stages of the CRF test compressor varied with shaft speed. The other stage characteristics did not vary significantly with speed. The performance changes with shaft speed in stages two and three resulted in a drop in the overall compressor pressure characteristic level with shaft speed.

5. Vane setting angle changes in the first three stages did affect the tenth stage pressure characteristic during overall compressor in-stall operation. Opening the vanes resulted in greater loss of total pressure in the tenth stage.

6. Variations of IGV, stator 1, and stator 2 setting angles did not effect the overall flow coefficient at the compressor initial in-stall point or at the near-recovery point. Setting angle variations did have a small influence on the overall in-stall characteristic pressure level. The overall in-stall characteristic is slightly lower with the vanes opened up by 7 degrees. This lowering of the characteristic is mainly due to the higher pressure loss of the tenth stage when the vanes were opened by 7 degrees.

7. Stage temperature characteristics did not vary significantly with shaft speed. Temperature characteristics for the first 5 stages involved a continuous rise of temperature with reduction of flow coefficient during overall compressor stall. The temperature data for stages six through ten exhibited an opposite trend, a drop in time-averaged temperature coefficient with reduction of flow coefficient.

8. Time-averaged overall compressor in-stall stage performance data indicate the possibility of large

amounts of reverse flow, in the stalled portion of the annulus, in stages 5 through 9. The stalled region of the compressor is primarily confined to stages 5 through 10.

9. Compressor shaft speed affected the overall stall recovery hysteresis of the CRF 10-stage test compressor. Higher shaft speeds resulted in higher levels of stall hysteresis. This is opposite to the trend previously presented for another high-speed multistage compressor [1]. Either trend is possible.

10. Stall cell blockage extent for a given exit throttle area did not vary significantly with shaft speed. Blockage extents decreased with increasing throttle area however. From time-resolved, high-response data, it was determined that stall cell blockage extents as low as 17 percent of the annulus cross section area existed in the CRF 10-stage test compressor while it operated in stall. This blockage extent is considerably less than previously reported blockage extents of about 30 percent [12],[17].

11. Stall cell rotation speed increased with increasing throttle area. Cell speed for a given blockage level did not vary significantly with shaft speed.

12. A decrease in the time-averaged pressure existed across the tenth stage for all in-stall operating points

and for large exit throttle area unstalled operating points at 78.5% speed. It was suggested that the decrease in time-averaged pressure was caused by choking of all or part of the tenth stage rotor row.

13. Time-resolved data indicated high relative Mach numbers at the entrance to the tenth stage rotor during overall compressor in-stall operation at 78.5% design corrected speed. Choking is likely in the unblocked portion of the tenth stage rotor row while the compressor is operating in rotating stall. Temperature rise across the first five stages contribute greatly to the choking by reducing the flow density at the tenth stage rotor entrance.

14. Overall compressor in-stall hysteresis at 78.5% design corrected speed is prolonged because of possible choking in the tenth stage. At lower speeds the hysteresis did not extend to stage flow coefficients where double values of stage pressure coefficient existed. For 78.5% speed this is not the case as double valued pressure coefficients exist for the stages in stall because of tenth stage choking.

15. Stage matching can have a significant effect on multistage compressor in-stall performance and recoverability. Mismatching of the stage performance characteristics of the CRF test compressor for 78.5% design

speed (first three stages operated far from stage stall and at very high flow coefficient levels, middle stages operated near stage stall at lower flow coefficient levels and the last stage operated far from stage stall at high flow coefficient levels) contributed to the high in-stall hysteresis levels at that speed.

16. The dynamic multistage compressor performance model developed by Davis has been further validated with interstage dynamic stalling pressures obtained from the CRF test compressor. The model predicts in-stall interstage pressure levels within 10 percent of the test data. The model also correctly predicted the trends of the dynamic event, although it fell short of predicting the time constants of the stalling event for all stages.

IX. RECOMMENDATIONS FOR FUTURE RESEARCH

Several new concepts about multistage compressor recoverability were identified. Further experimental and analytical research should be undertaken to more fully explore multistage compressor recoverability.

A follow on test of the CRF 10-stage test compressor is recommended. The following improvements to test procedures, test compressor, data acquisition system, and instrumentation are recommended.

1. High-response static and total pressure measurements should be made at the entrance and exit of the tenth stage to further validate choking at high speed in-stall conditions.

2. High-response temperature measurement techniques should be developed and used to determine the temperature difference between the blocked and unblocked regions of the annulus. The temperature measurement device should have a frequency response of at least 200 Hz.

3. The test compressor should be modified to allow for airflow bleeds at the entrance to the ninth and tenth stages. Bleeding air only in front of the tenth stage may result in choking of the ninth stage. Therefore bleeds would be required in front of both stages. Test procedures should be developed to fully exercise aft stage

bleed capability and to determine its effects on compressor recoverability.

4. Test procedures should also be developed to fully explore the effects of the IGV, stator 1, and stator 2 on in-stall hysteresis levels. It is recommended that stator 1 and 2 be scheduled to a more closed position during both unstalled and in-stall operation. Schemes should be developed to determine if scheduling of the vanes and bleeds can improve compressor recoverability.

5. Additional test procedures should be developed to determine the effect of in-stall speed drops on recoverability of the CRF test compressor. This better simulates conditions that may exist in a gas turbine engine when the compressor stalls.

6. It is recommended that stage characteristics of selected stages be graphically displayed during the follow on test. Near real time display of stage characteristics would result in a more efficient and timely test program. The effects of changes in vane setting angles, bleed amounts and shaft speed on stage performance could be observed directly. Test strategies could be modified during the test program based on this information.

7. Further study is required to determine why time-averaged in-stall stage characteristics can be changed

in the tenth stage of the CRF test compressor by varying vane positions of the front three stages.

The recommendations to follow apply to general research in multistage compressor stalling and in-stall operation.

1. Additional analytical modeling efforts should continue. The multistage compressor model developed by Davis [44], should be exercised further to determine if bleeds, area changes or shaft speed changes will reduce recovery hysteresis levels. Further research into determining individual time lags for each stage should be continued. This research would result in a more accurate simulation of stage dynamics during the stalling of a multistage compressor.

2. Improvements should be made to the Davis model to allow for simulation of a two-dimensional event. From the CRF 10-stage compressor test results it is clear that choking in the tenth stage is the result of the rotating stall traversing the annulus in the circumferential direction.

3. Mismatching of compressor stages for midrange speeds (70 to 80 percent of design corrected speed) of compressor operation should be avoided. This mismatching is likely to reduce the stall recoverability of the compressor.

X. REFERENCES

1. Hosny, W. H., C. H. Lenhardt, H. T. Liu, R. C. Lovell, and W. G. Steenken. "Energy Efficient Engine (ICLS/IOC) High Pressure Compressor Component Performance Report." NASA CR-174955, August 1985.

2. Cohen, H., G. F. C. Rogers, and H. I. H. Saravanamuttoo. Gas Turbine Theory. London: Longman Group Limited, 1974.

3. Greitzer, E. M. "Surge and Rotating Stall in Axial Flow Compressors. Part I: Theoretical Compression System Model." Transactions of the ASME, Journal of Engineering for Power 98 (April 1976): 190-198.

4. Greitzer, E. M. "Surge and Rotating Stall in Axial Flow Compressors. Part II: Experimental Results and Comparisons with Theory." Transactions of the ASME, Journal of Engineering for Power 98 (April 1976): 199-217.

5. Moore, F. K. "A Theory of Rotating Stall of Multistage Axial Compressors." NASA Contractor Report 3685, July 1983.

6. Moore, F. K. and E. M. Greitzer. "A Theory of Post-Stall Transients in Multistage Axial Compression Systems." NASA Contractor Report 3878, March 1985.

7. Koff, S. G., R. E. Davis, and E. M. Grietzer. "A Control Volume Model of Rotating Stall in Multistage Axial Compressors." Presented at the AIAA/SAE/ASME/ASEE 23 Joint Propulsion Conference, AIAA-87-2090, June 1987.

8. Davis, M. W. and W. F. O'Brien. "A Stage-By-Stage Post-Stall Compression System Modeling Technique." Presented at the AIAA/SAE/ASME/ASEE 23 Joint Propulsion Conference, AIAA-87-2088, June 1987.

9. Benrey, Ron. "Goodbye Stagnation: America's finest fighter engine outgrows a childhood ailment." Technology In Brief, Issue Two. United Technologies, Hartford Conn., 1979.

10. Moore, F. K. and E. M. Greitzer. "A Theory of Post-Stall Transients in Axial Compression Systems: Part I Development of Equations." ASME Paper No. 85-GT-171, March 1985.

11. Greitzer, E. M. and F. K. Moore. "A Theory of Post-Stall Transients in Axial Compression Systems: Part II Application." ASME Paper No. 85-GT-172, March 1985.

12. Small, C. J. and J. T. Lewis. "High Speed Compressor Rig as a Stall Recovery Research Tool." Presented at the AIAA/SAE/ASME/ASEE 21st Joint Propulsion Conference, AIAA-85-1428, June 1985.

13. Day, I. J., E. M. Greitzer, and N. A. Cumpsty. "Prediction of Compressor Performance in Rotating Stall." Transactions of the ASME, Journal of Engineering for Power 100 (January 1978): 1-14.

14. Rostafinski, W. "Analysis of Fully Stalled Compressor." NASA Technical Memorandum 87254, May 1986.

15. Koff, S. G. and E. M. Grietzer. "Axisymmetrically Stalled Flow Performance for Multistage Axial Compressors." Transactions of the ASME, Journal of Engineering for Power 108 (October 1986): 216-223.

16. Gamache, R. N. and E. M. Greitzer. "Reverse Flow in Multistage Axial Compressors." Presented at the AIAA/ASME/SAE/ASEE 22nd Joint Propulsion Conference, AIAA-86-1747, June 1986.

17. Hosny, W. M. and W. G. Steenken. "Aerodynamic Instability Performance of an Advanced High-Pressure-Ratio Compression Component." Presented at the AIAA/ASME/SAE/ASEE 22nd Joint Propulsion Conference, AIAA-86-1619, June 1986.

18. Huppert, Merle C., and William Benser. "Some Stall and Surge Phenomena in Axial-Flow Compressors." Journal of the Aeronautical Sciences 20, no. 12 (December 1953): 835-845.

19. Urasek, Donald C., Ronald J. Steinke, and Walter S. Cunnan. "Stalled and Stall-Free Performance of Axial-Flow Compressor Stage with Three Inlet-Guide-Vane and Stator-Blade Settings." NASA TN D-8457, May 1977.

20. Giannissis, G. L., A. B. Mckenzie and R. L. Elder. "Experimental Investigations of Rotating Stall in a Mismatched Three Stage Axial Flow Compressor." ASME Paper No. 88-GT-205, June 1988.

21. Iura, T., and W. D. Rannie. "Experimental Investigations of Propagating Stall in Axial-Flow Compressors." Transactions of the American Society of Mechanical Engineers 76, no. 3 (April 1954): 463-471.

22. Sears, W. R. "On Asymmetric Flow in an Axial-Flow Compressor Stage." Transactions of the ASME, Journal of Applied Mechanics, 75 (1953): 57-62.

23. Marble, F. E. "Propagation of Stall in a Compressor Blade Row." Journal of the Aeronautical Sciences 22, no. 8 (August 1955): 541-544.

24. Stenning, Alan H., Anthony R. Kriebel, and Stephen R. Montgomery. "Stall Propagation in Axial-Flow Compressors." NACA TN-3580, June 1956.

25. Emmons, H. W., C. E. Pearson, and H. P. Grant. "Compressor Surge and Stall Propagation." Transactions of the ASME 77 (May 1955): 455-469.

26. Sexton, M. R. and W. F. O'Brien Jr. "A Model for Dynamic Loss Response in Axial-Flow Compressors." ASME Paper No. 81-GT-154, 1981.

27. Takata, H. and S. Nagano. "Nonlinear Analysis of Rotating Stall." Transactions of the ASME, Journal of Engineering for Power 94 (October 1972): 279-293.

28. Dunham, J. Non-axisymmetric Flows in axial Compressors. London: Institution of Mechanical Engineers, Mechanical Engineering Science Monograph no. 3, 1965.

29. Mazzawy, R. S. "Multiple Segment Parallel Compressor Model for Circumferential Flow Distortion." Transactions of the ASME, Journal of Engineering for Power 99, (April 1977): 288-296.

30. Day, I.J. "Detailed Flow Measurement During Deep Stall in Axial Flow Compressors." In AGARD Conference Proceedings 177, Unsteady Phenomena in Turbomachinery, 1976.

31. Day, I. J. and N. A. Cumpsty. "The Measurement and Interpretation of Flow Within Rotating Stall Cells in Axial Compressors." Journal of Mechanical Engineering Science 20, no. 2 (1978): 101-114.

32. Na'covska', Katrina. "Temperature Rise in the Multistage Axial Flow Compressor During Rotating Stall and Surge." ASME Paper No. 88-GT-323.

33. Ludwig, G. R., J. P. Nenni, and R. H. Aerndt. "Investigation of Rotating Stall in Axial Flow Compressors and the Development of a Prototype Rotating Stall Control System." AFAPL-TR-73-45, May 1973.

34. Ludwig, Gary R. and Joseph P. Nenni. "Basic Studies of Rotating Stall in Axial Flow Compressors." AFAPL-TR-79-2083, September 1979.

35. Epstein, A. H. "Smart Engine Components: A Micro in Every Blade?" Aerospace America, 24 (January 1986): 60-64.

36. Copenhaver, William W. "Compressor Research Facility F100 High Pressure Compressor Inlet Total Pressure and Swirl Profile Simulation." AFWAL-TR-84-2030, September 1984.

37. Nyland, T. W., England, David R., Anderson, Robert C. "On the Dynamics of Short Pressure Probes: Some Design Factors Affecting Frequency Response." NASA TN d-6151, February 1971.

38. Bergh, H. and H. Tijdeman. "Theoretical and Experimental Results for the Dynamic Response of Pressure Measuring Systems." Report NLR-TR-F.238, National Aero-and Astronautical Research Institute, Amsterdam, January 1985.

39. Coleman, L. "Experimental Determination of Frequency Response of 0.020 Inch Inner Diameter Tubes and Validation of a Theoretical Model." AFWAL-TR-88-2025, April 1987.

40. Bell and Howell, Technical Manual, "Magnetic Tape Recording Technical Fundamentals." Bell and Howell, Pasadena, Califorina, 1982.

41. Patterson, G. T. "Techniques for Determinating Engine Stall Recovery Characteristics." AGARD paper 28, 1982.

42. Abernethy, R. B. and J. W. Thompson Jr. "Handbook Uncertainty in Gas Turbine Measurements." AEDC-TR-73-5, February 1973.

43. Bendat, J. S. and A. G. Piersol. RANDOM DATA: Analysis and Measurement Procedures. New York: John Wiley and Sons, Inc., Copyright 1971.

44. Davis, Milton W. "A Stage-By-Stage Post-Stall Compression System Modeling Technique: Methodology, Validation, and Application." Ph.D. diss., Virginia Polytechnic Institute and State University, 1986.

45. MacCormack, R.W. "The effect of Viscosity in Hypervelocity Impact Cratering." AIAA Paper No. 69-354, May 1969.

46. Gamache, R.N. "Axial Compressor Reversed Flow Perfromance." Ph.D. diss., Massachusetts Institute of Technology, 1985.

47. Browell, R.W., L.D. Reynolds, and W.P. Core. "COCODEC: Combined Compressor Design and Evaluation Code." Union Carbide Corporation, Nuclear Division, CTC-INF-1039, May 1972.

48. Johnsen, Irving A. and Robert O. Bullock, ed. Aerodynamic Design of Axial-Flow Compressors. Vol. 11, Compressor Stall and Blade Vibration, by Robert W. Graham and Eleanor Costilow Guentert. Washington: National Aeronautics and Space Administration, 1965.

49. Johnsen, Irving A. and Robert O. Bullock, ed. Aerodynamic Design of Axial-Flow Compressors. Vol. 13, Compressor Operation with One or More Blade Rows Stalled, by William A. Benser. Washington: National Aeronautics and Space Administration, 1965.

XI. ACKNOWLEDGMENTS

The author would like to express his appreciation to Professor Theodore H. Okiishi, Dr. Fritz Ostdiek and Dr. Walter F. O'Brien for their continual advice, guidance and encouragement throughout the course of this research effort. The author is also grateful to the members of his Doctor of Philosophy degree graduate program of study committee for their input and support during this research program. The test effort described in this dissertation could not possibly be accomplished without extensive planning and assistance of managers, engineers and technicians. Therefore, the author would also like to express his appreciation to all those members of the Compressor Research Facility (CRF) test team who contributed to the successful completion of the test program. The following test team members deserve special thanks for their efforts during the test, Charles Elrod (CRF Director), Norman Poti (Test Director), Lt. Jack Downey (Test Engineer), and Christopher J. Worland (Data Acquisition Engineer). Furthermore, the author would also like to acknowledge the efforts of Dr. Douglas Rabe for his technical input into the design and layout of the test

compressor instrumentation and for his advice and insight during testing. In addition the author expresses appreciation to Pratt & Whitney Aircraft for the design and construction of the test compressor. The author also extends his thanks to members of the CRF test support staff from Battelle Columbus Laboratories who were instrumental in the development of data acquisition and analysis techniques used in the test program. The author is also grateful to Janice McCloskey of Systems Research Laboratories, and Pam Slightam and Penny Pelhan of Selecttech corporation for their assistance in assimilating and presenting the large amount of test data obtained. The author acknowledges the efforts of Lt. Keith Boyer who prepared and exercised the multistage compressor model used for comparisons with test data. The author is also grateful to his supervisor Mr. Ron Berger who provided much needed patience and understanding during the final months of this effort. Finally the author wishes to acknowledge Air Force Aero Propulsion and Power Laboratory for supporting this advanced training effort.

XII. APPENDIX A: DETAILED INSTRUMENTATION LOCATIONS

Detailed locations of CRF test compressor instrumentation are povided in Figures 12.1 through 12.14. The measurements called out on the figures were used for all three types of data acquisition during the tests, time-averaged, close-coupled and high-response.

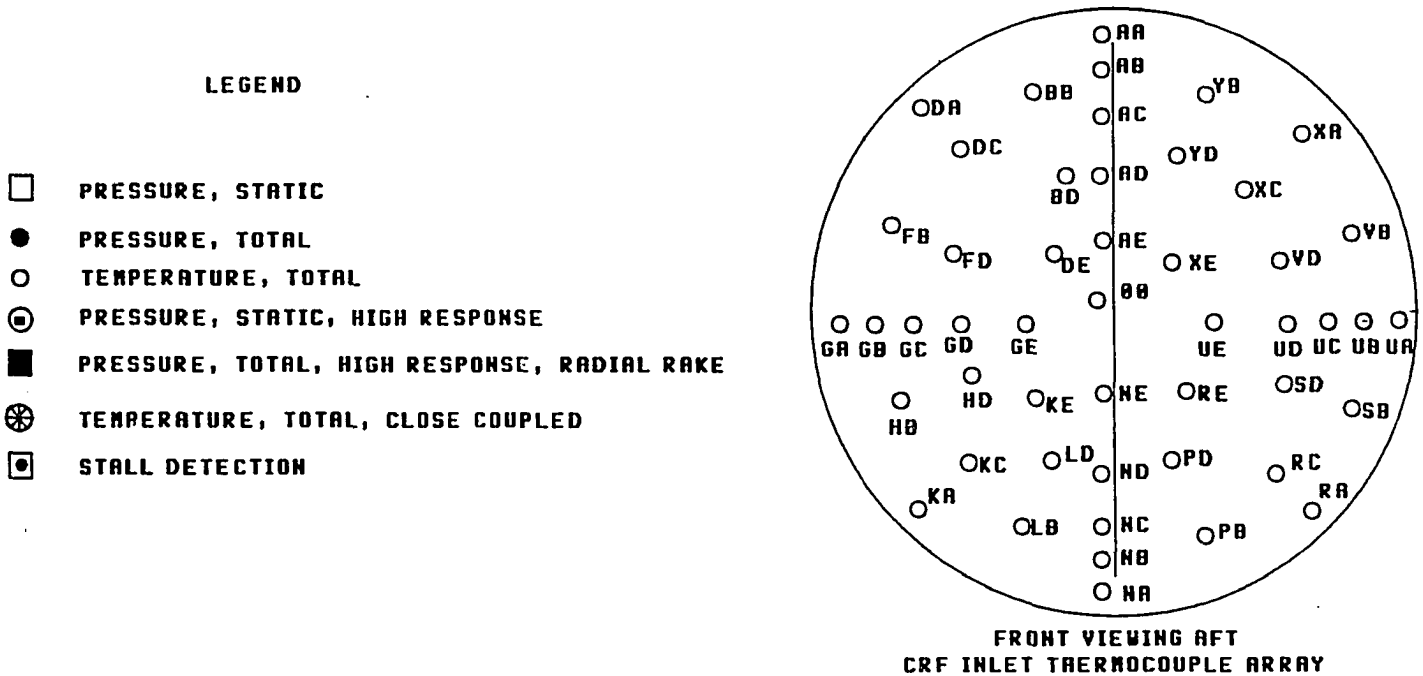

Figure 12.1 Test compressor detailed instrumentation locations (inlet flow conditioning screen)

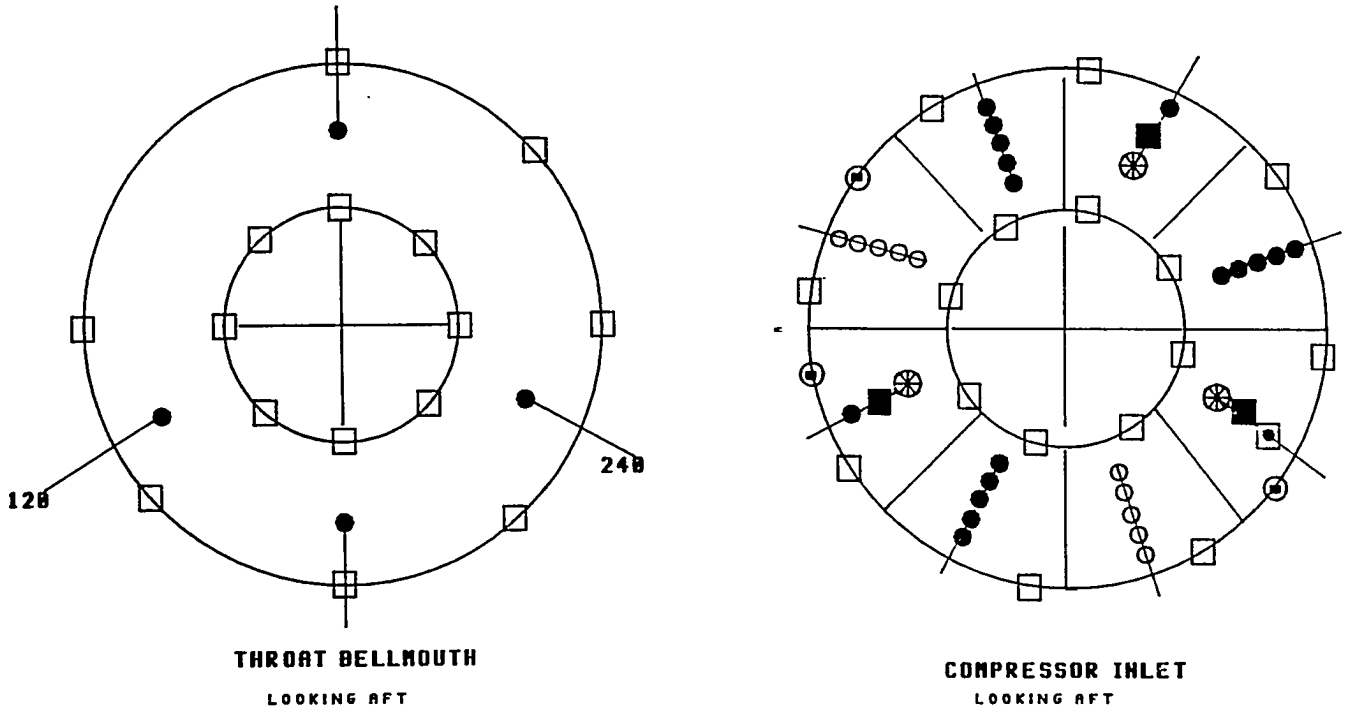

Figure 12.2 Test compressor detailed instrumentation locations (bellmouth throat and compressor inlet)

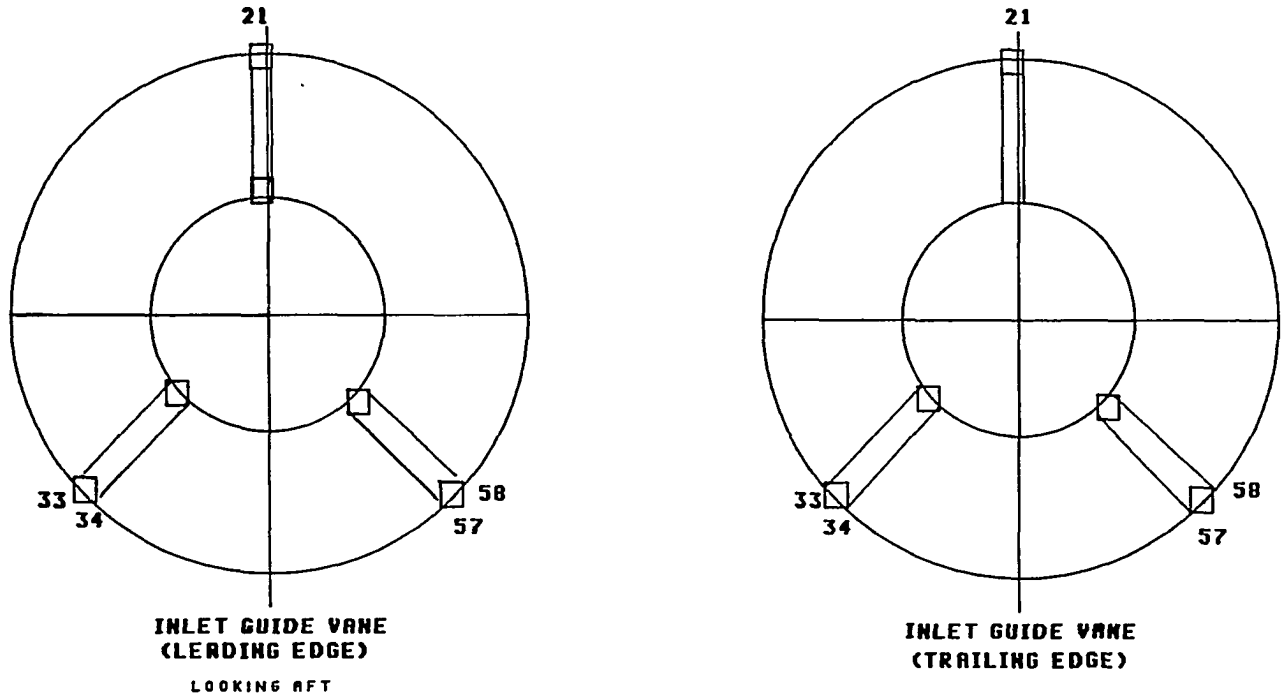

Figure 12.3 Test compressor detailed instrumentation locations (inlet to stage 1)

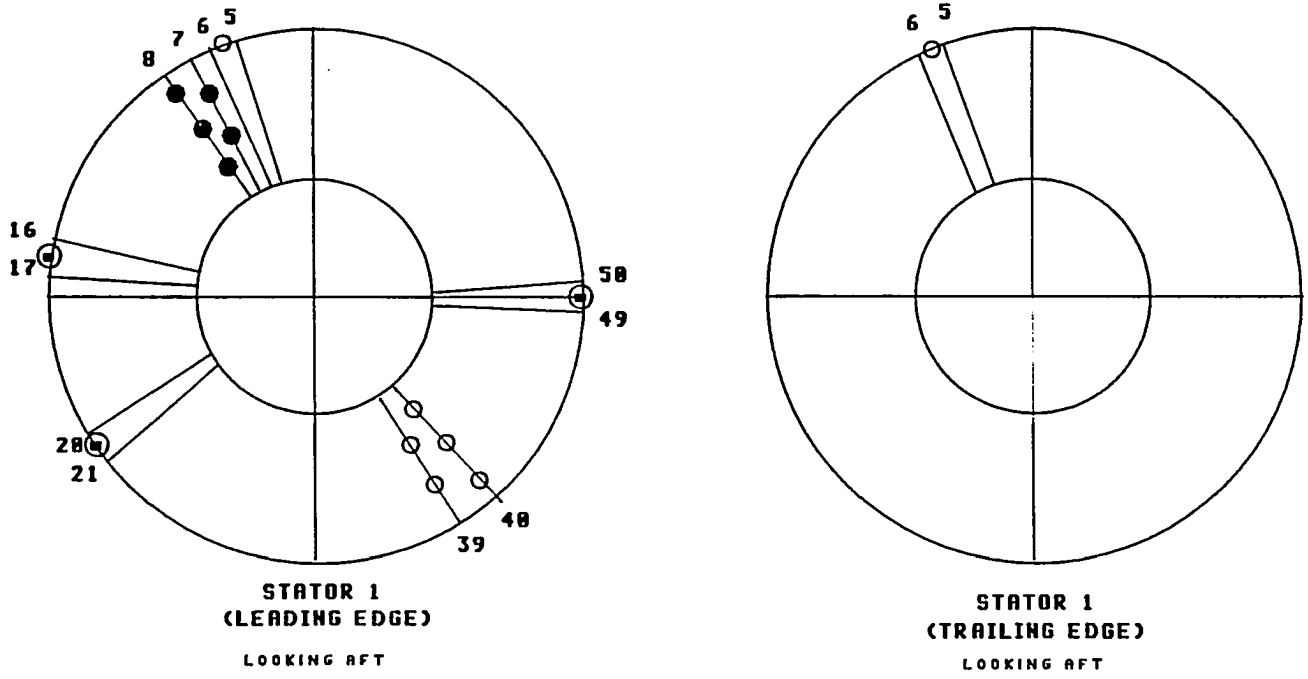

Figure 12.4 Test compressor detailed instrumentation locations (inlet to stage 2)

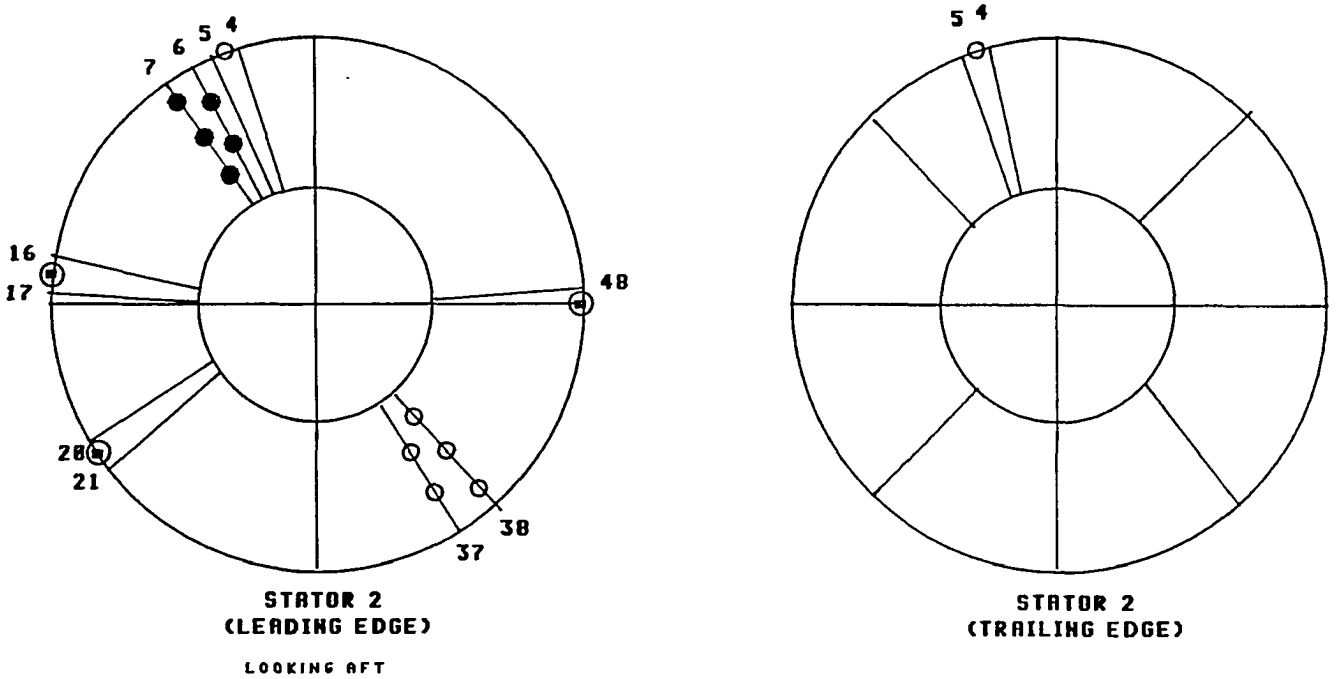

Figure 12.5 Test compressor detailed instrumentation locations (inlet to stage 3)

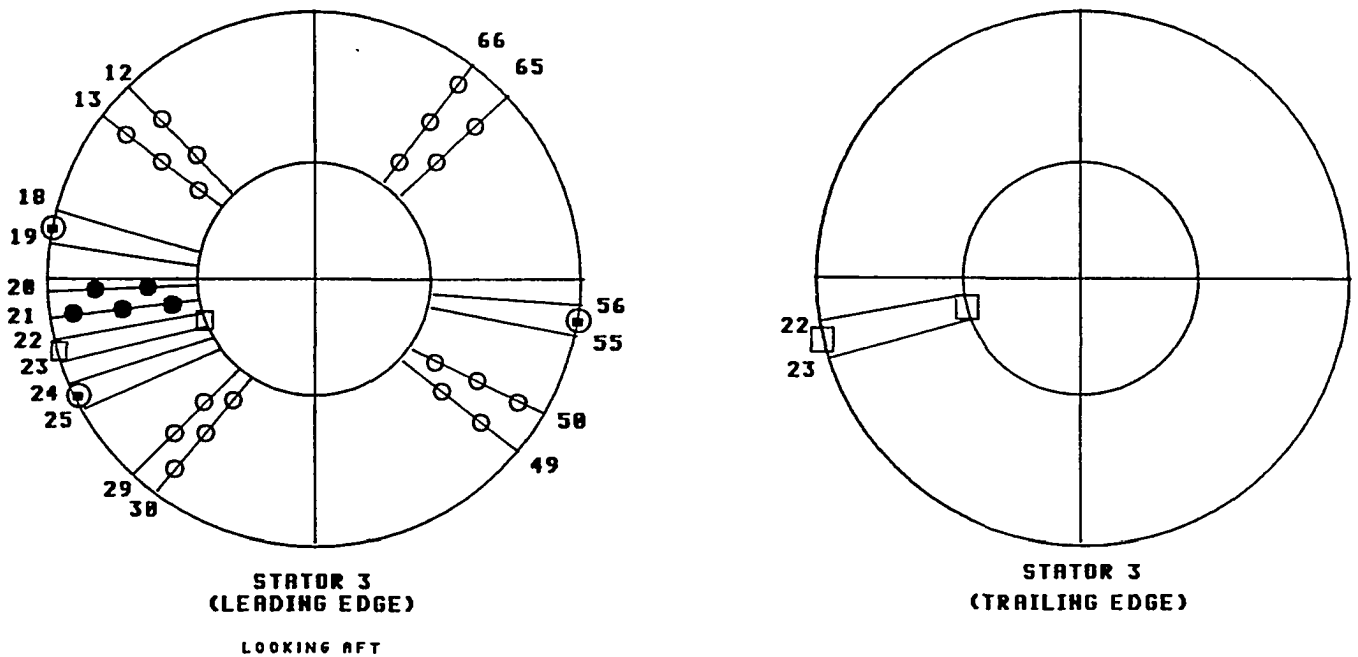

Figure 12.6 Test compressor detailed instrumentation locations (inlet to stage 4)

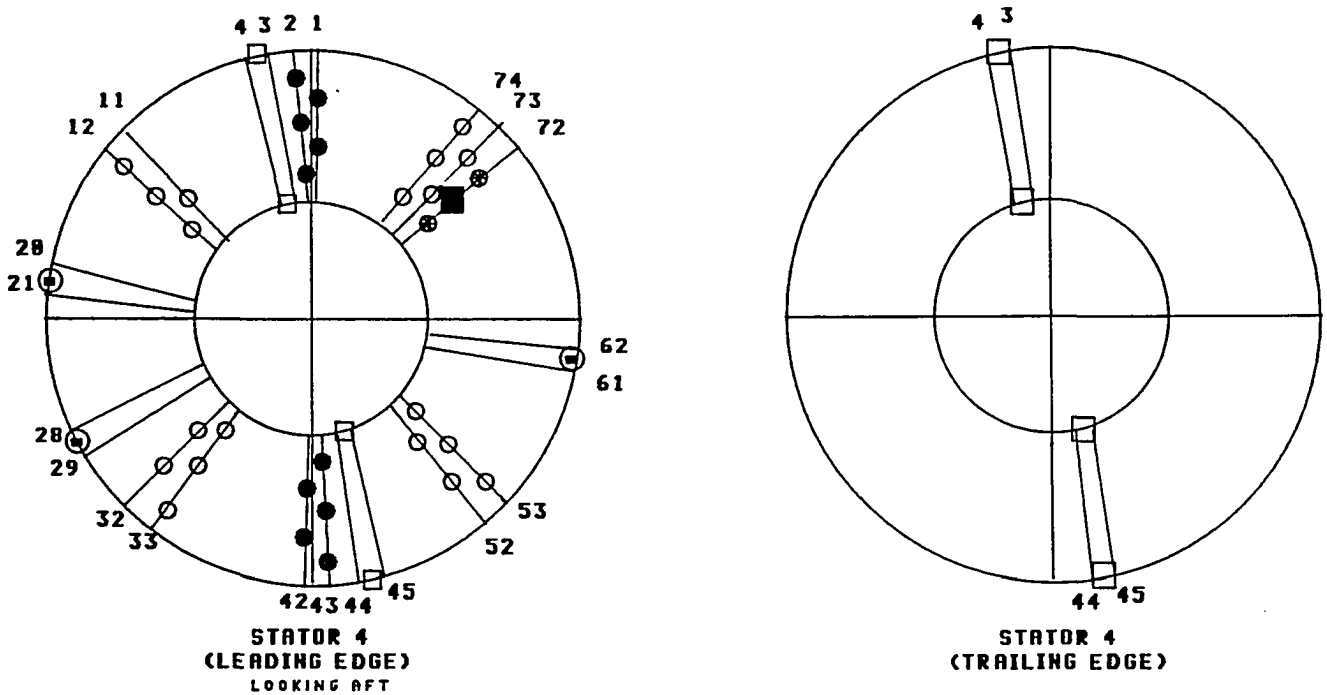

Figure 12.7 Test compressor detailed instrumentation locations (inlet to stage 5)

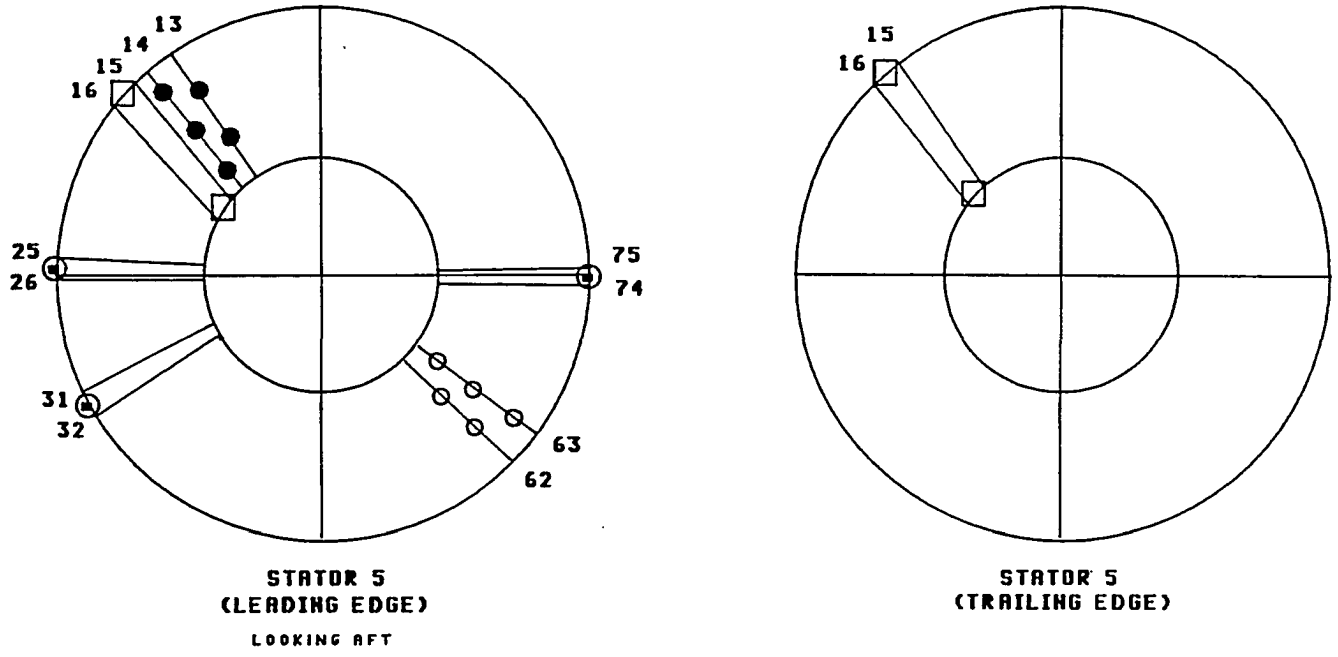

Figure 12.8 Test compressor detailed instrumentation locations (inlet to stage 6)

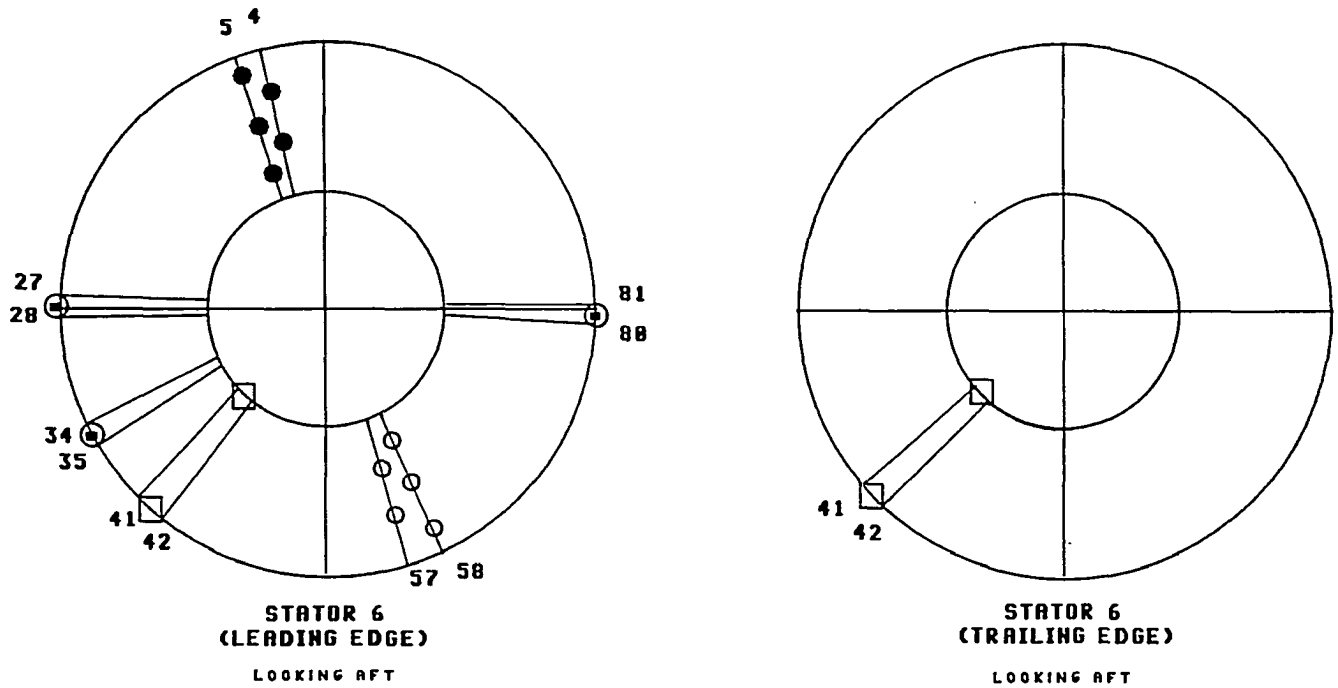

Figure 12.9 Test compressor detailed instrumentation locations (inlet to stage 7)

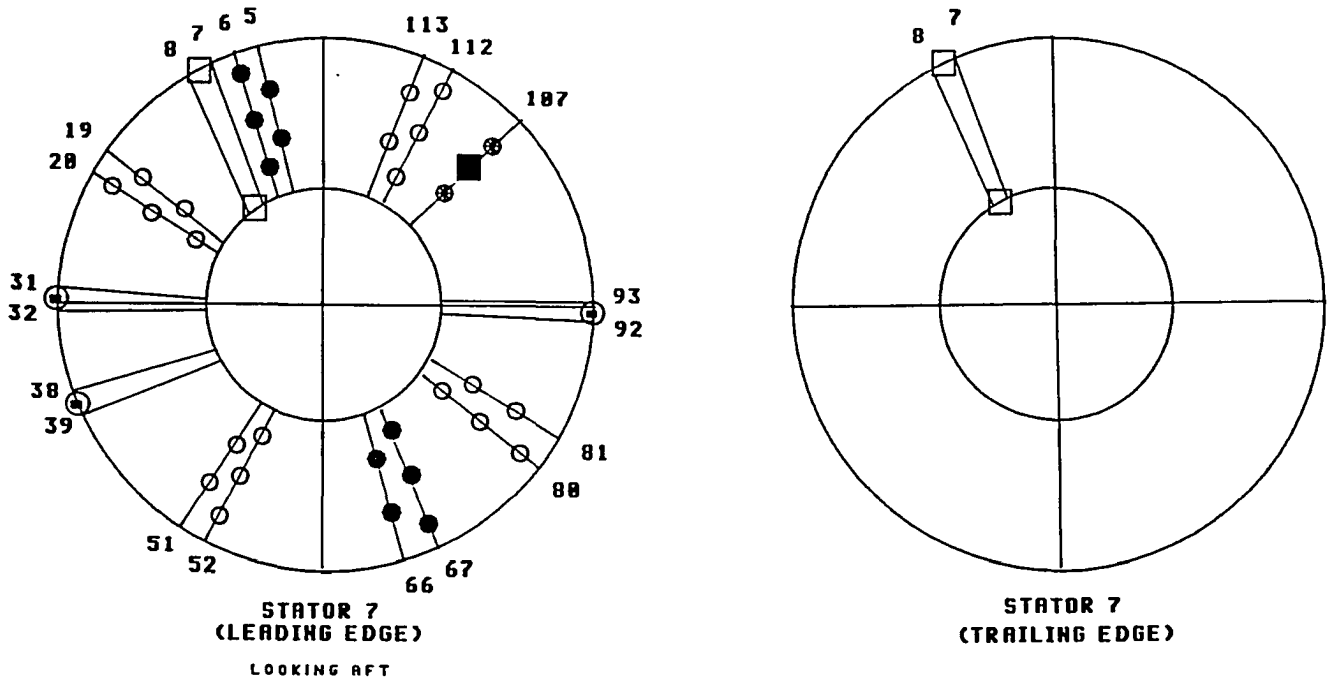

Figure 12.10 Test compressor detailed instrumentation locations (inlet to stage 8)

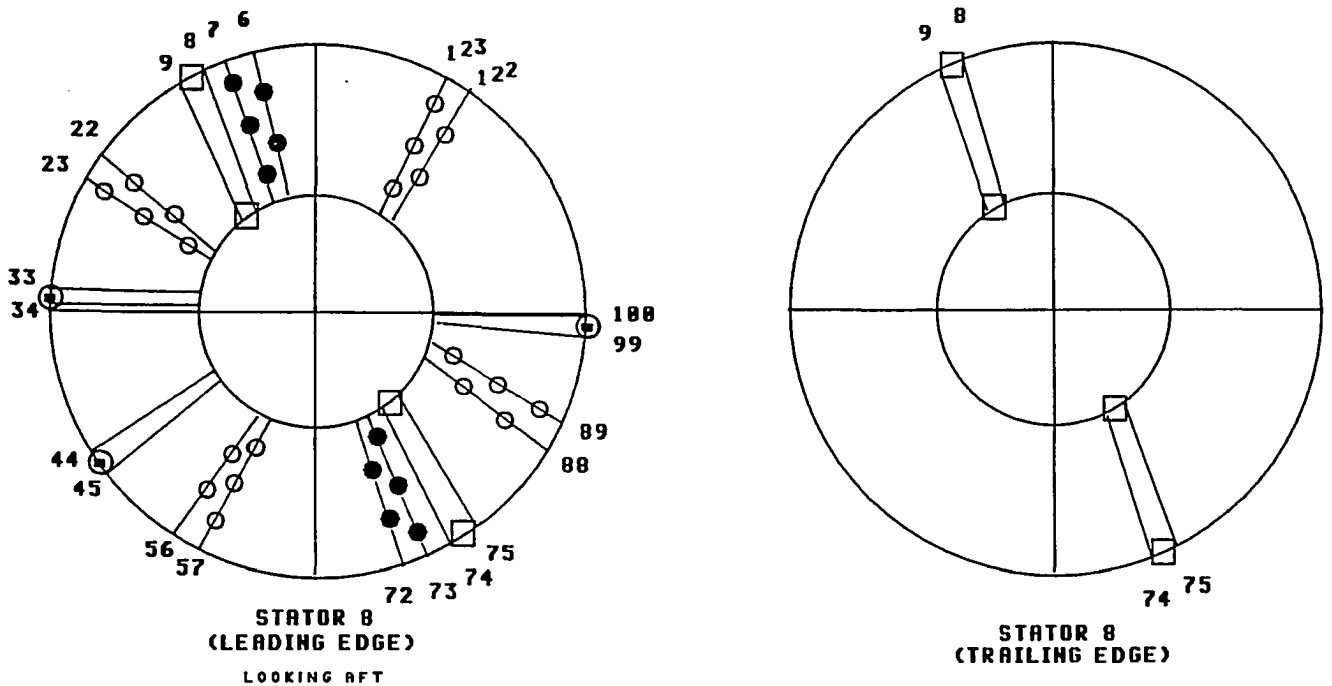

Figure 12.11 Test compressor detailed instrumentation locations (inlet to stage 9)

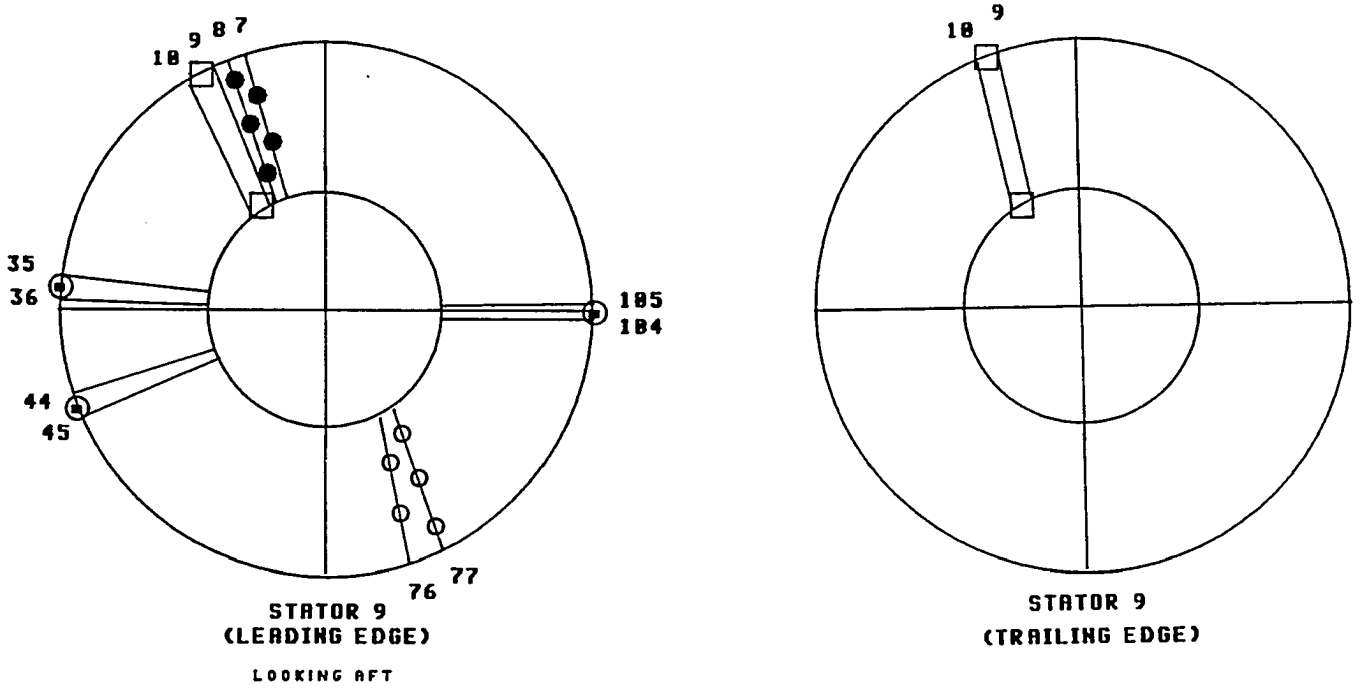

Figure 12.12 Test compressor detailed instrumentation locations (inlet to stage 10)

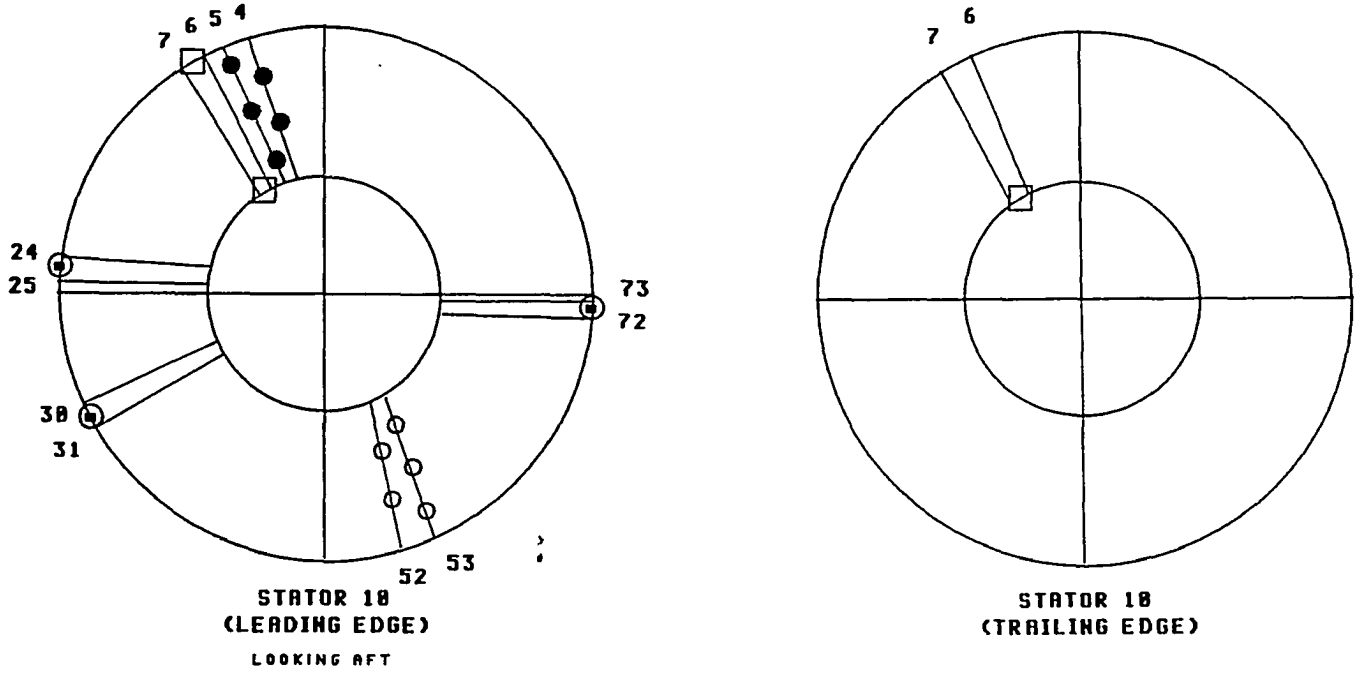

Figure 12.13 Test compressor detailed instrumentation locations (exit to stage 10)

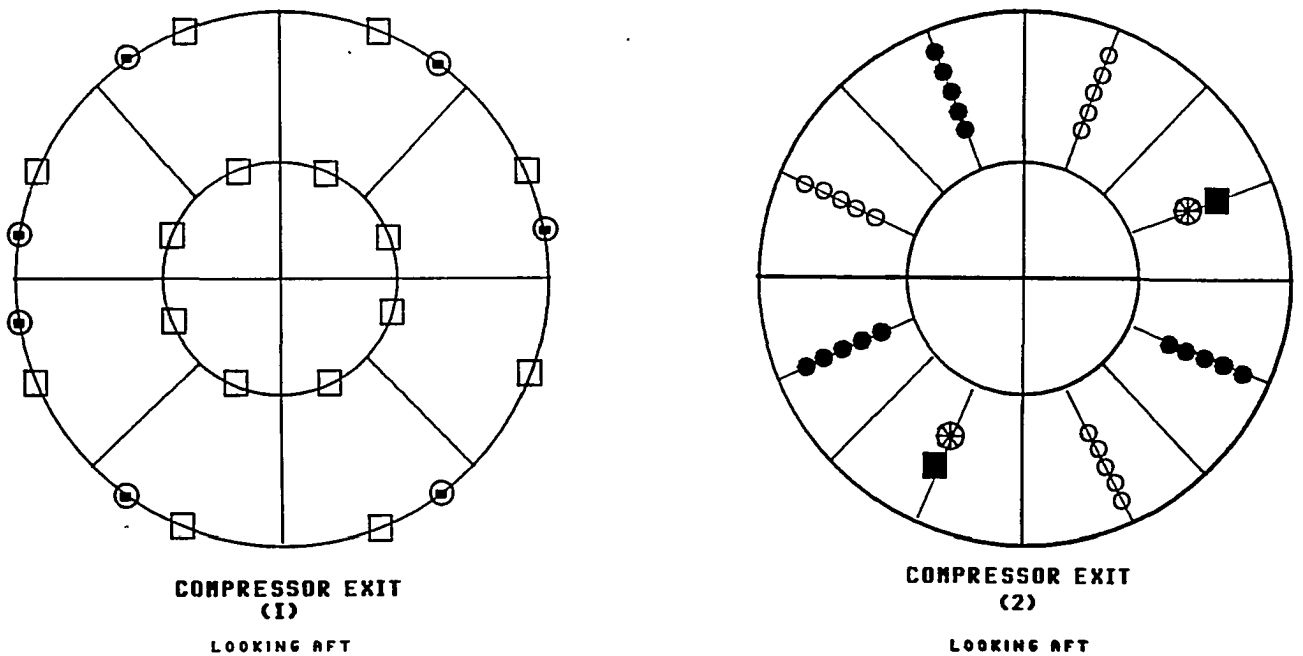

Figure 12.14 Test compressor detailed instrumentation locations (discharge)

XIII. APPENDIX B: DETAILED CHARACTERISTICS

49.8% DESIGN SPEED

The data shown in Figure 13.1 represent the detailed overall compressor temperature and pressure characteristics for the nominal variable vane configuration for the test compressor at 49.8% design corrected speed. Data are presented for four different operating conditions, the first two being, unstalled (prior to stall) operating on the overall compressor unstalled characteristic, and at the overall compressor initial in-stall condition. The data presented at the initial in-stall condition were obtained by slowly closing the exit throttle while the compressor was operating unstalled and stopping when stall occurred. The compressor was allowed to stabilize for 3 minutes and then the data were obtained. The third operating condition is for the compressor in-stall for different exit throttle area settings. The last condition is a repeat of the first after the compressor recovered from stall. The data in Figures 13.2 through 13.11 are the individual stage characteristics for the CRF test compressor. These characteristics are plotted in stage pressure and temperature coefficient and stage flow coefficient coordinates for the overall compressor condition described above.

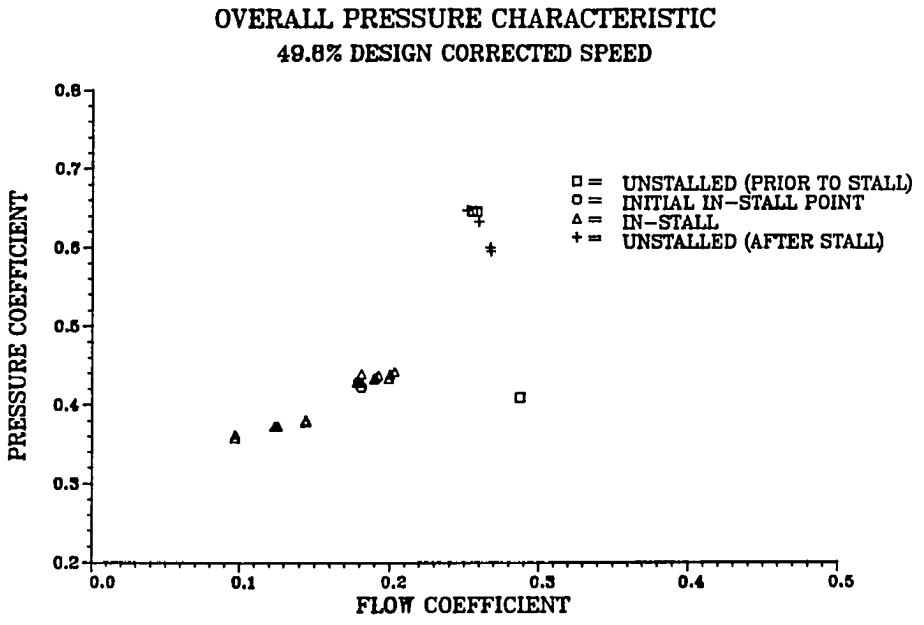

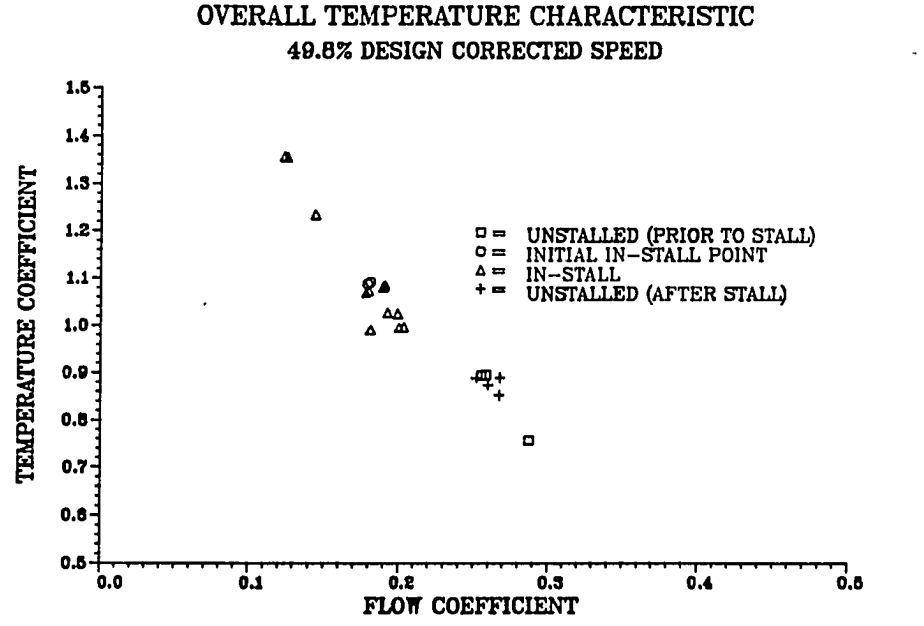

Figure 13.1 Test compressor overall characteristics 49.8% design corrected speed

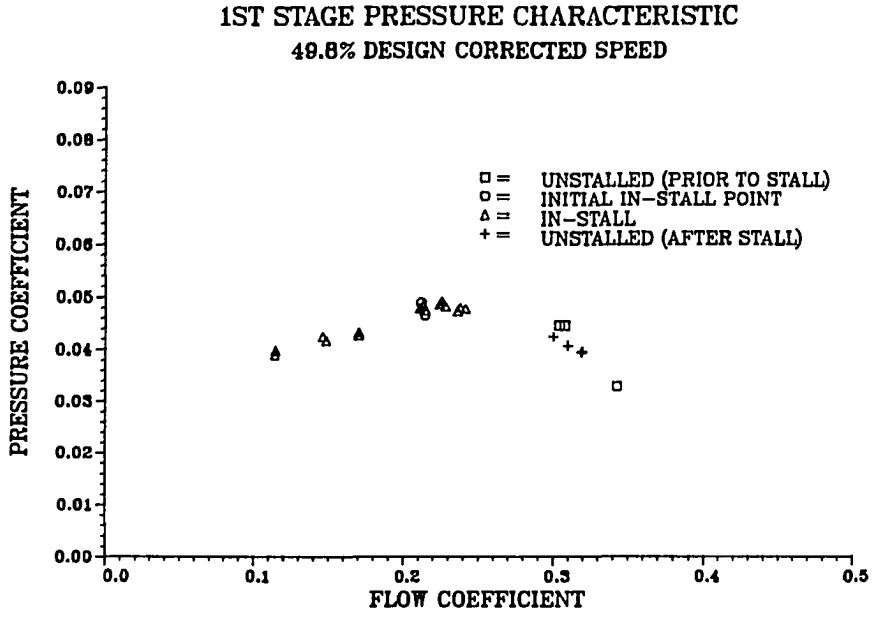

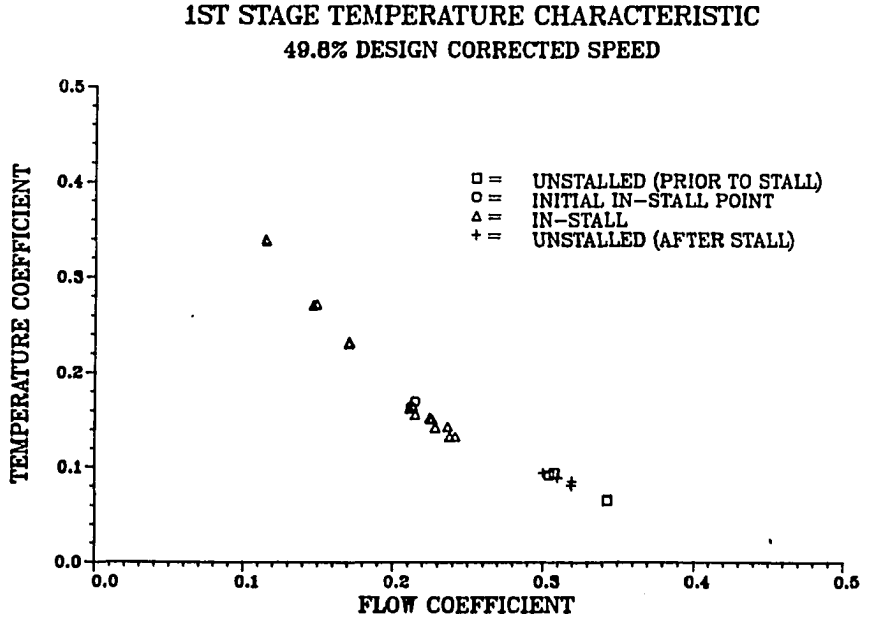

Figure 13.2 Test compressor first stage characteristics 49.8% design corrected speed

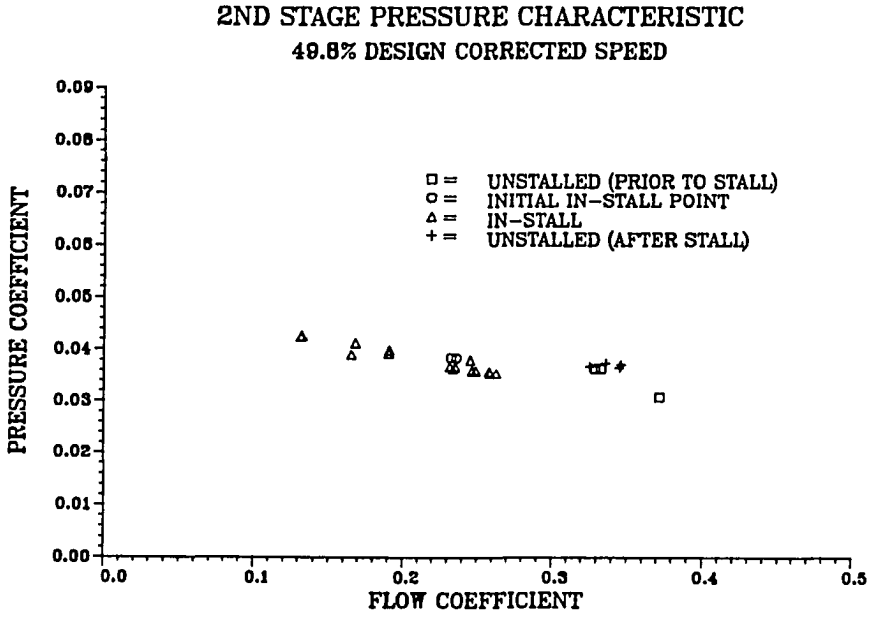

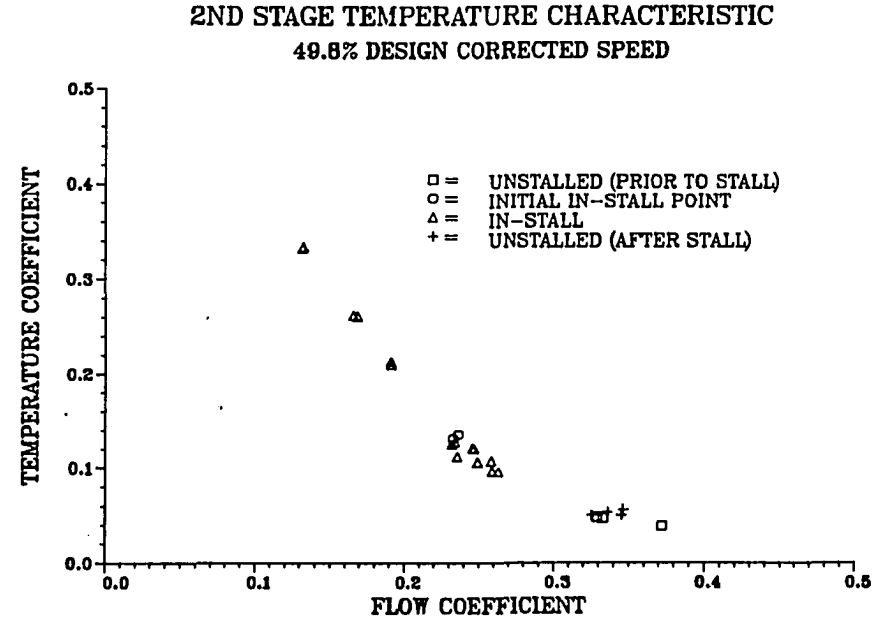

Figure 13.3 Test compressor second stage characteristics 49.8% design corrected speed

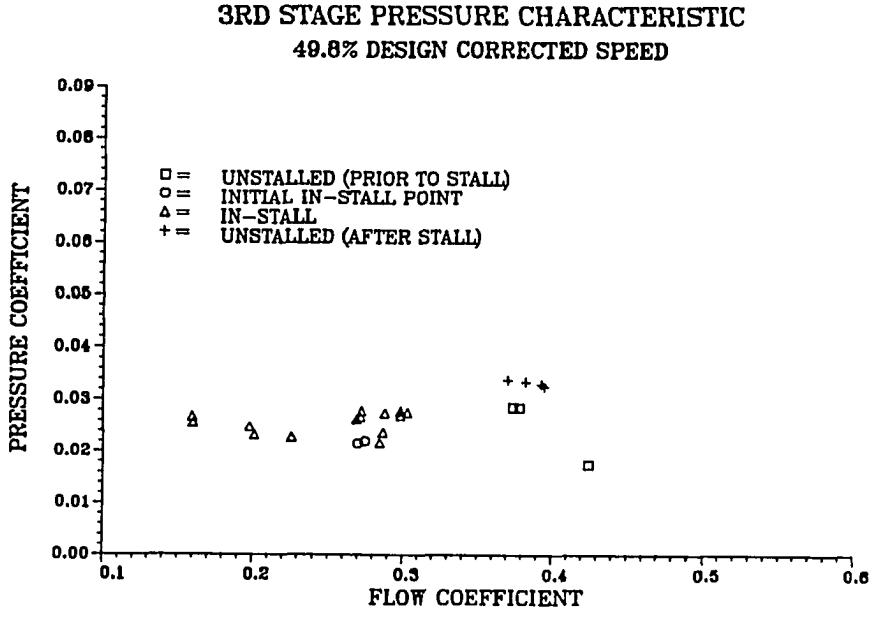

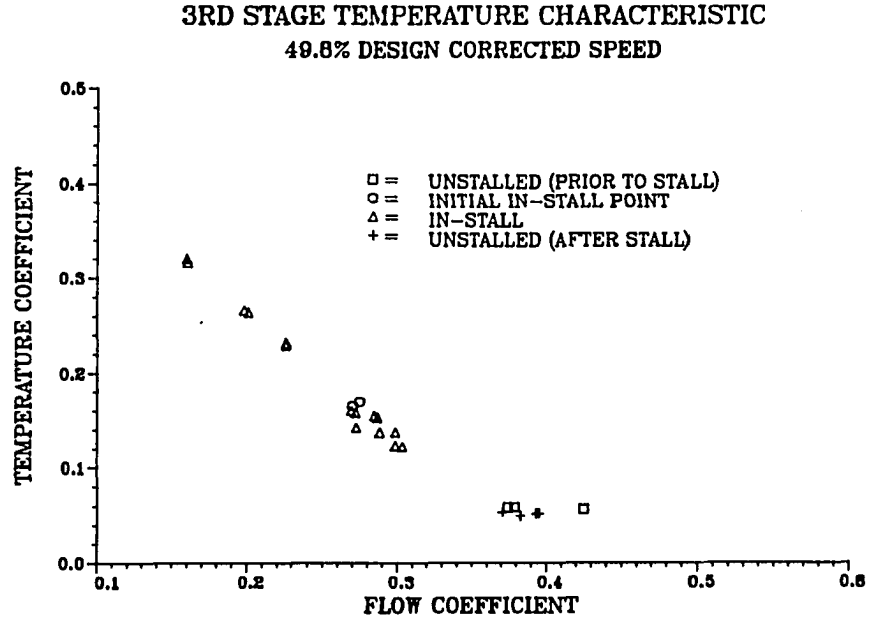

Figure 13.4 Test compressor third stage charcteristics 49.8% design corrected speed

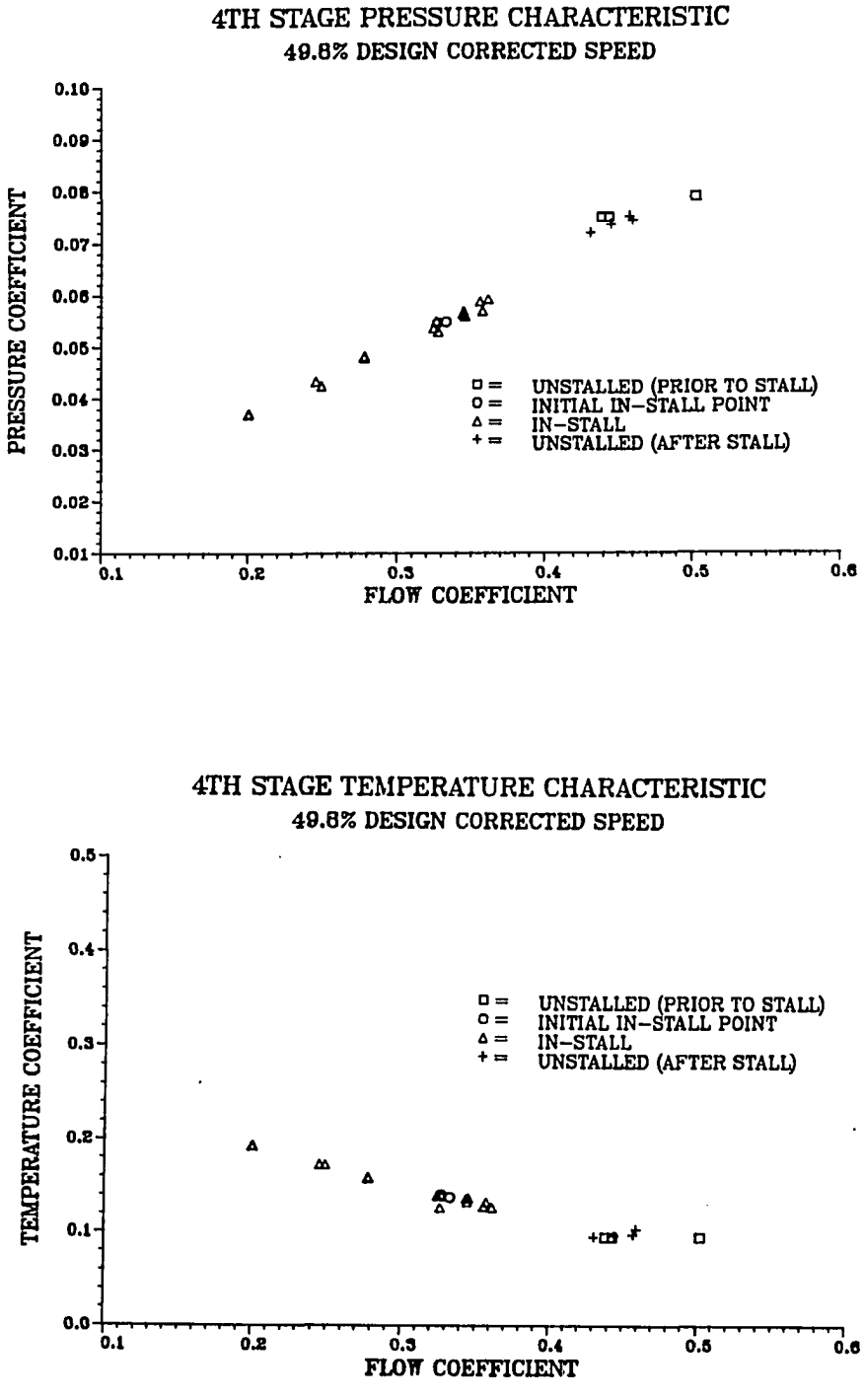

Figure 13.5 Test compressor fourth stage characteristics 49.8% design corrected speed

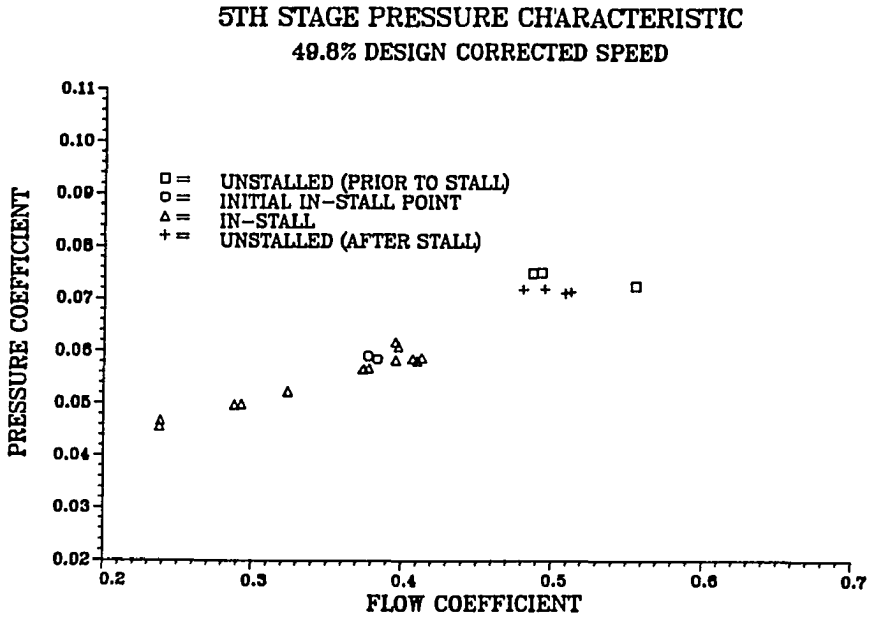

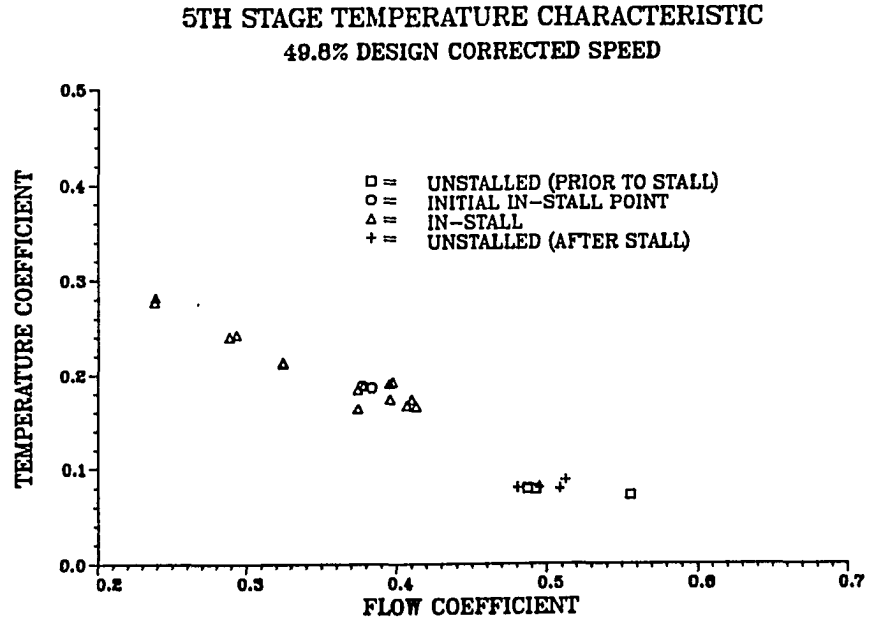

Figure 13.6 Test compressor fifth stage characteristics 49.8% design corrected speed

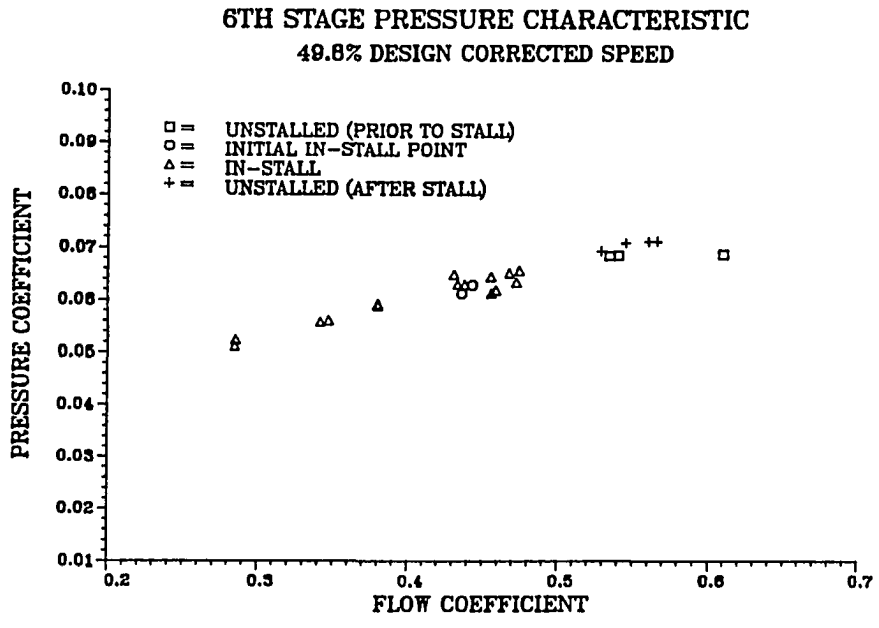

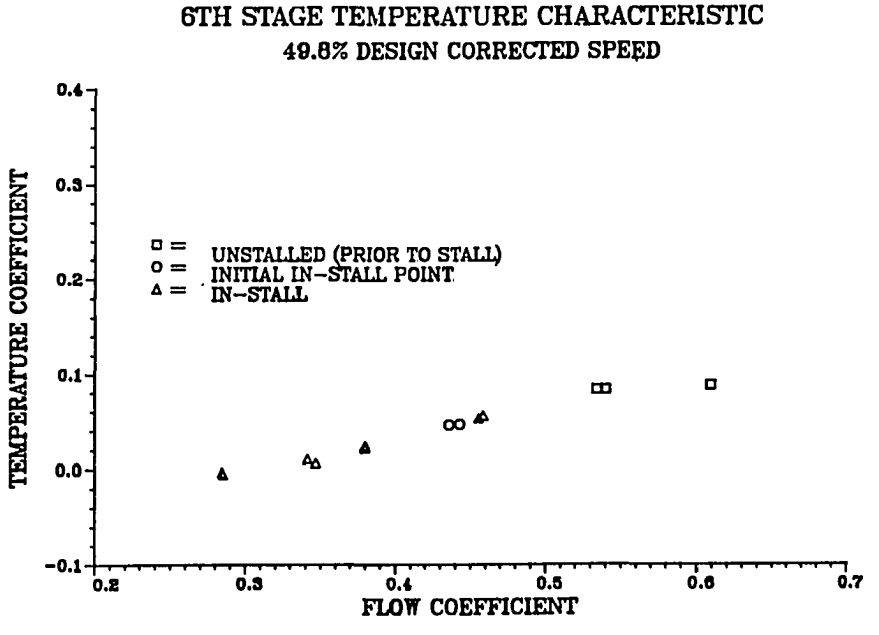

Figure 13.7 Test compressor sixth stage characteristics 49.8% design corrected speed

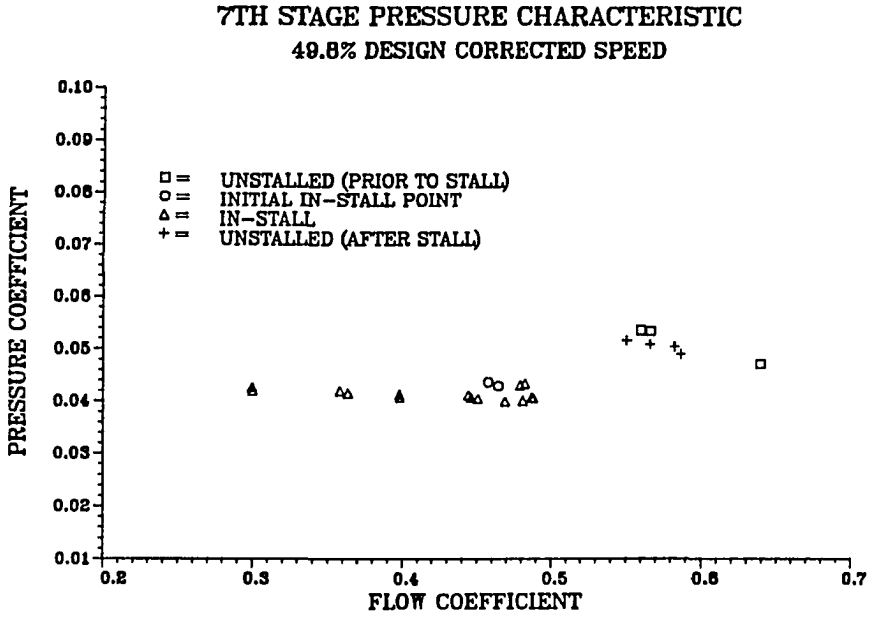

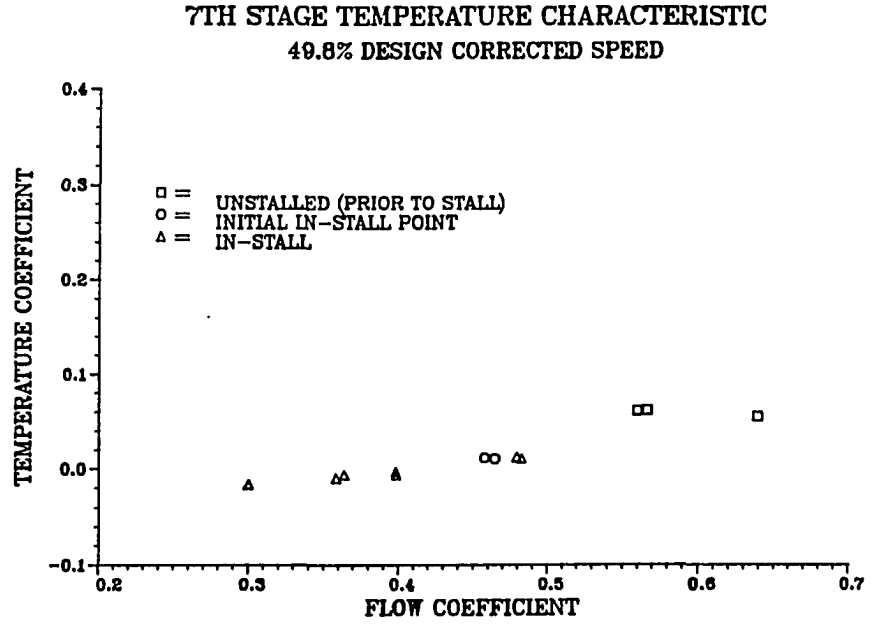

Figure 13.8 Test compressor seventh stage characteristics 49.8% design corrected speed

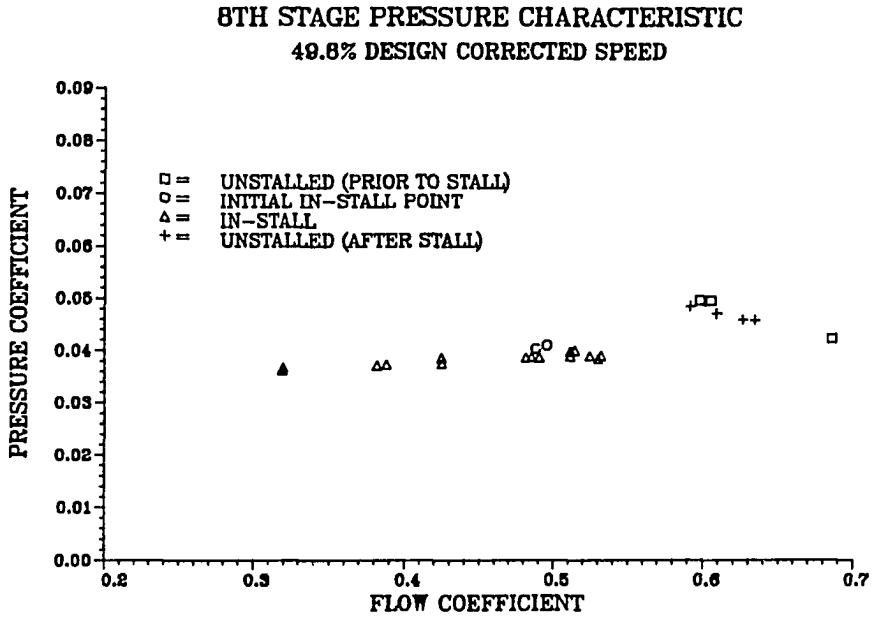

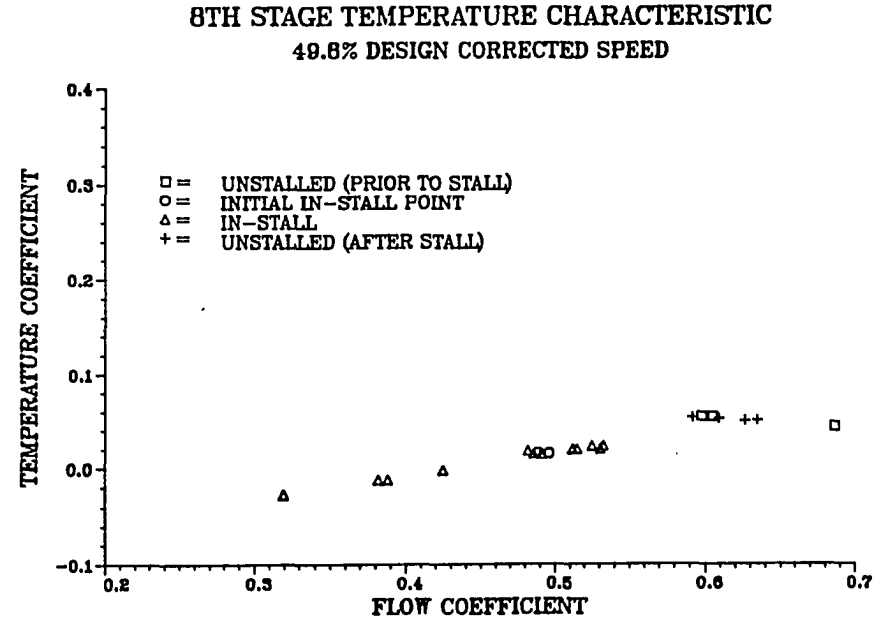

Figure 13.9 Test compressor eighth stage characteristics 49.8% design corrected speed

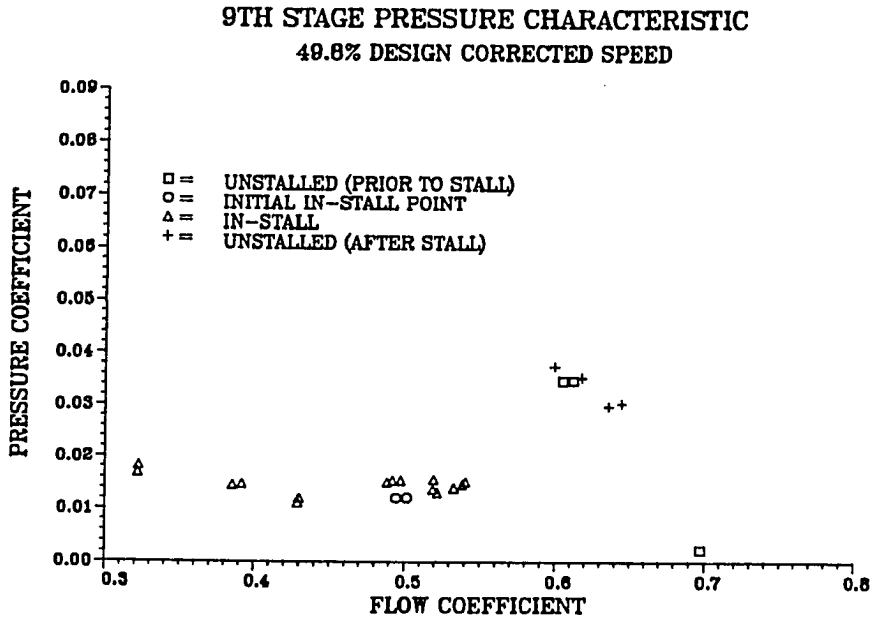

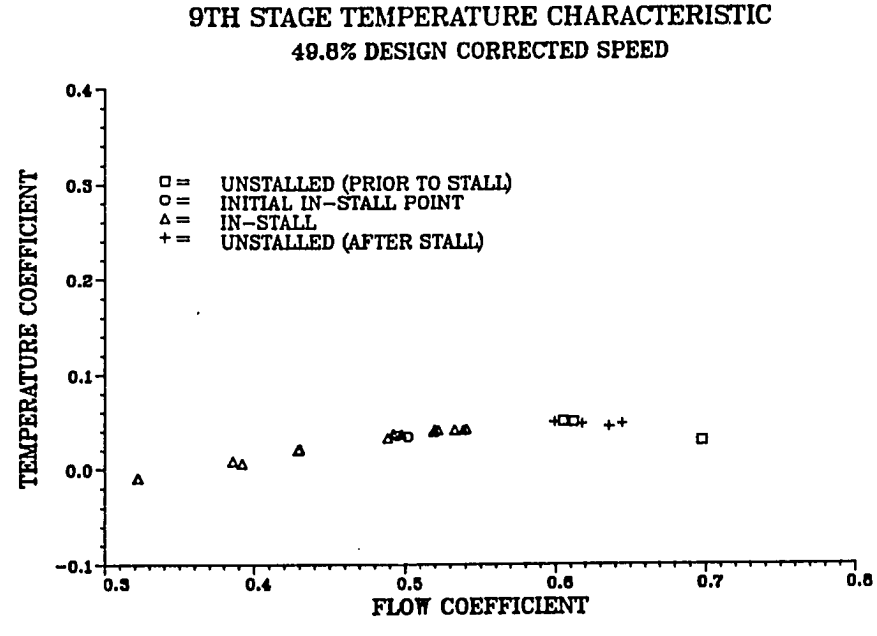

Figure 13.10 Test compressor ninth stage characteristics 49.8% design corrected speed

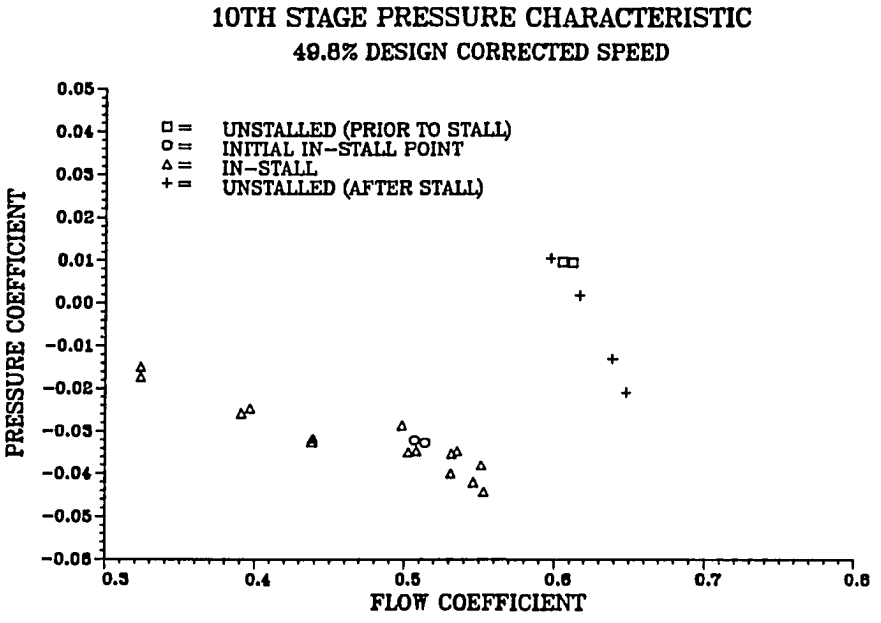

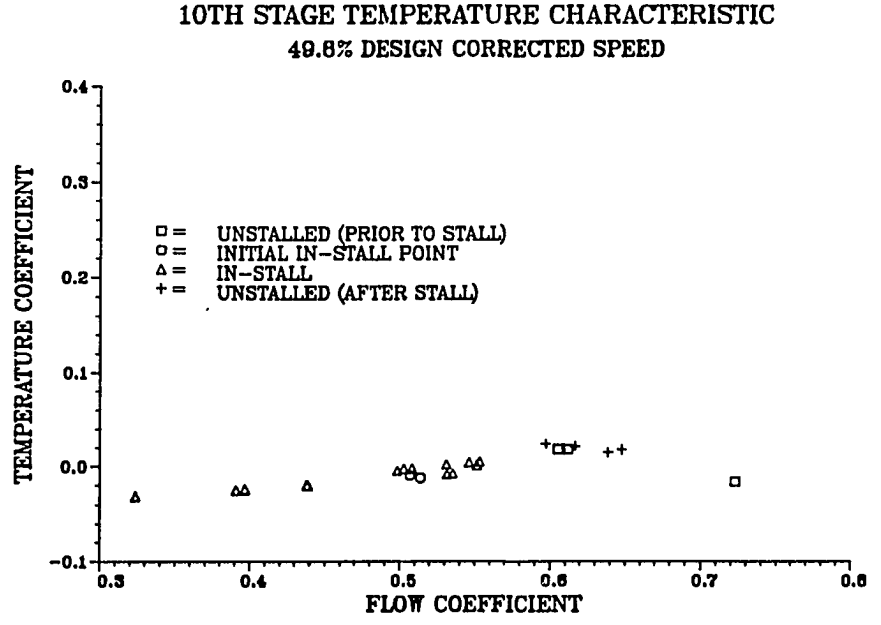

Figure 13.11 Test compressor tenth stage characteristics 49.8% design corrected speed

XIV. APPENDIX C: DETAILED CHARACTERISTICS

59.7% DESIGN SPEED

The data shown in Figure 14.1 represent the detailed overall compressor temperature and pressure characteristics for the nominal variable vane configuration for the test compressor at 59.7% design corrected speed. Data are presented for four different operating conditions, the first two being, unstalled (prior to stall) operating on the overall compressor unstalled characteristic, and at the overall compressor initial in-stall condition. The data presented at the initial in-stall condition were obtained by slowly closing the exit throttle while the compressor was operating unstalled and stopping when stall occurred. The compressor was allowed to stabilize for 3 minutes and then the data were obtained. The third operating condition is for the compressor in-stall for different exit throttle area settings. The last condition is a repeat of the first after the compressor recovered from stall. The data in Figures 14.2 through 14.11 are the individual stage characteristics for the CRF test compressor. These characteristics are plotted in stage pressure and temperature coefficient and stage flow coefficient coordinates for the overall compressor condition described above.

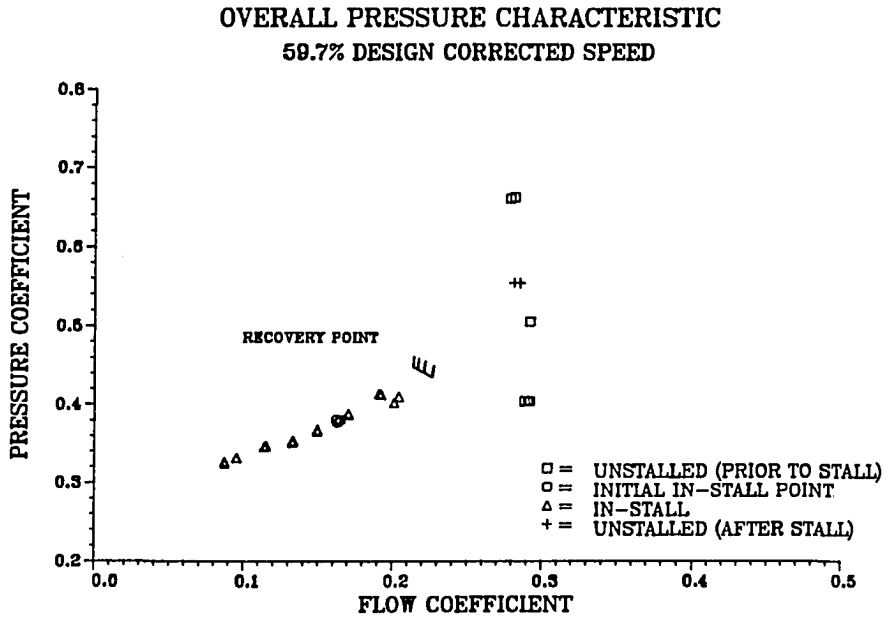

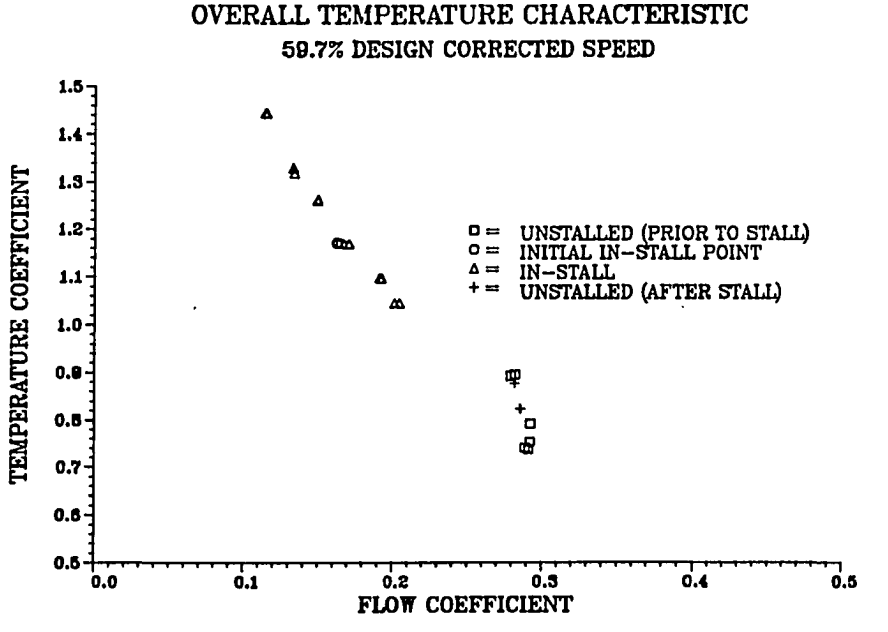

Figure 14.1 Test compressor overall characteristics 59.7% design corrected speed

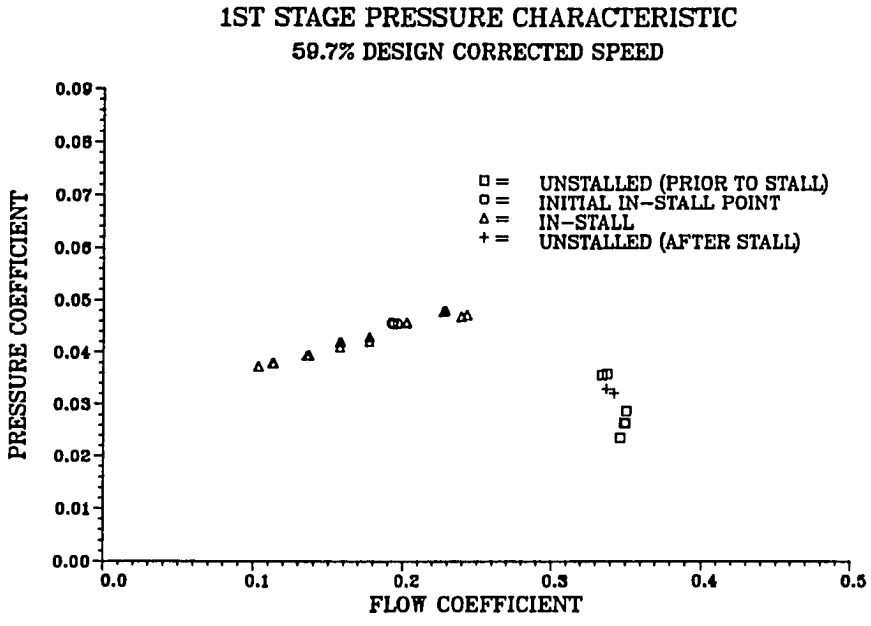

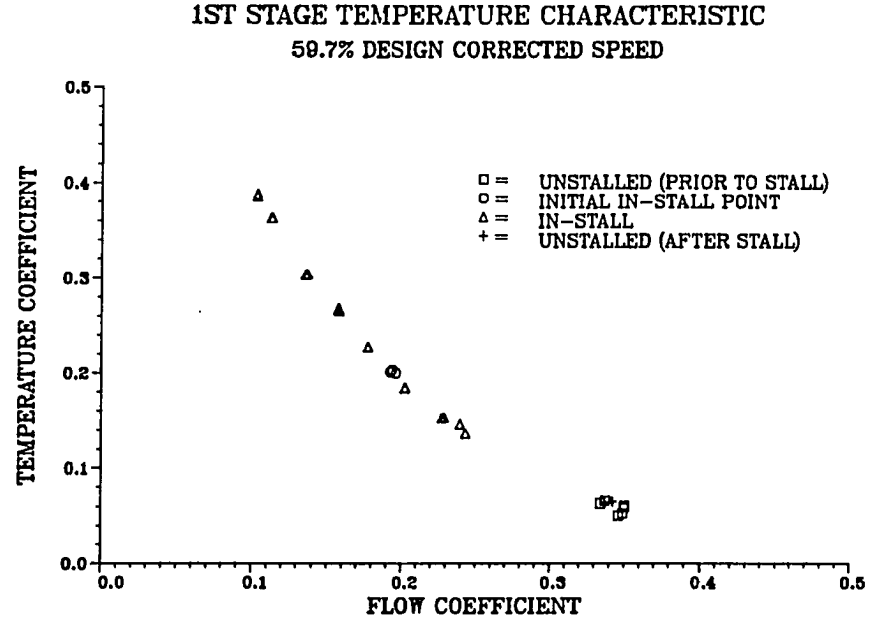

Figure 14.2 Test compressor first stage characteristics 59.7% design corrected speed

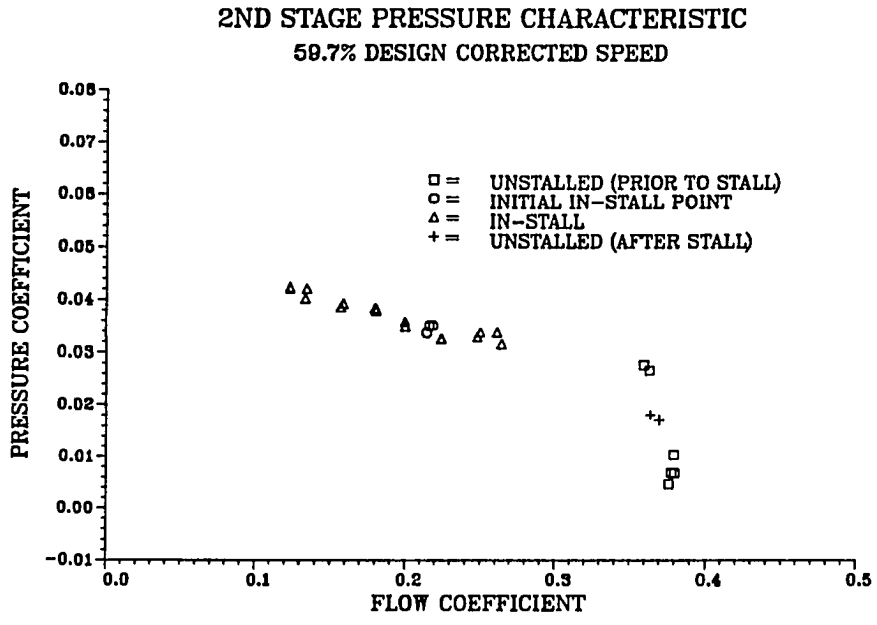

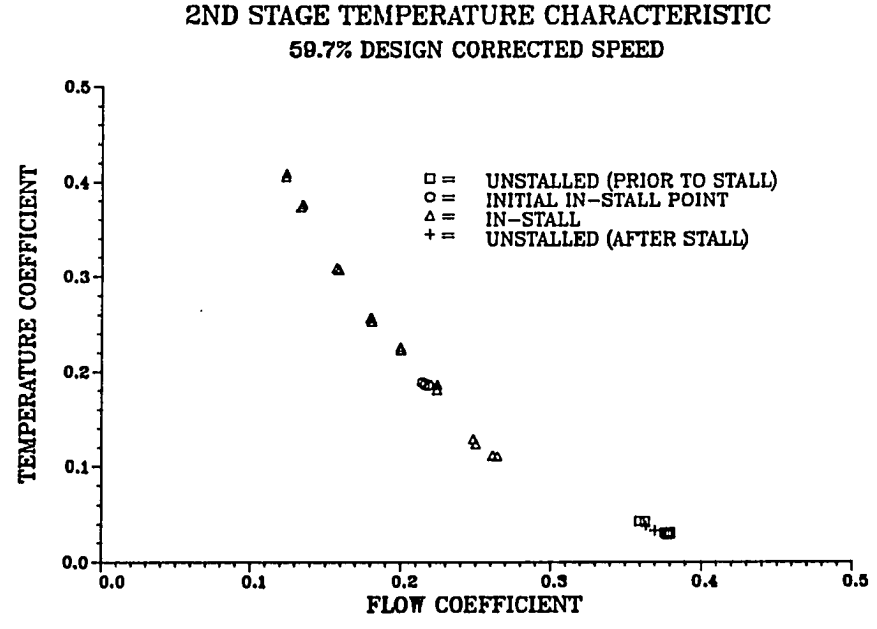

Figure 14.3 Test compressor second stage characteristics 59.7% design corrected speed

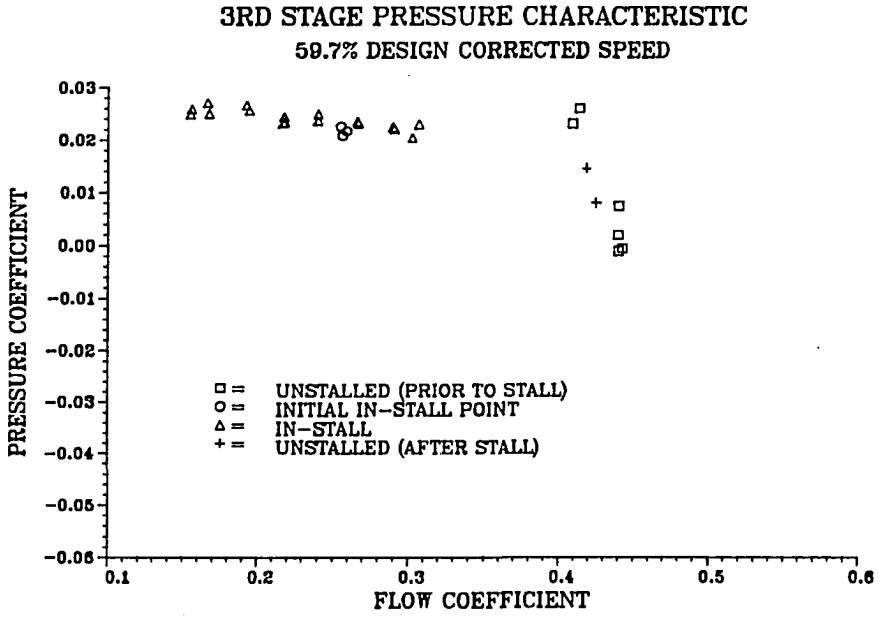

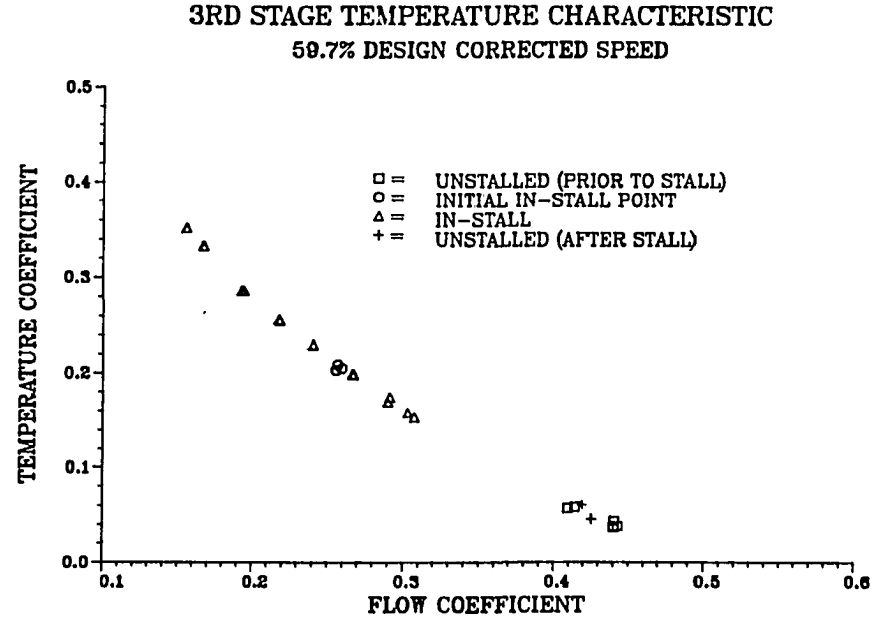

Figure 14.4 Test compressor third stage characteristics 59.7% design corrected speed

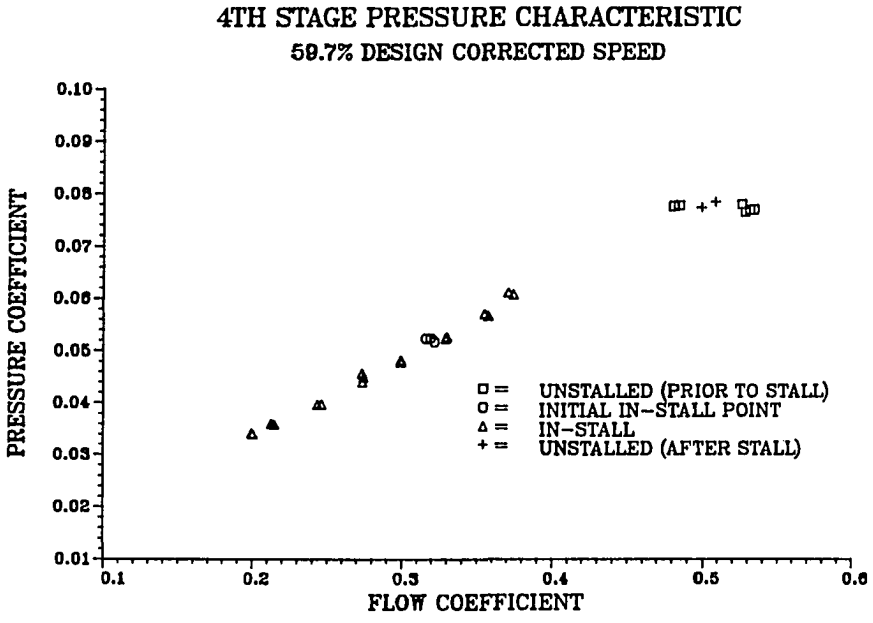

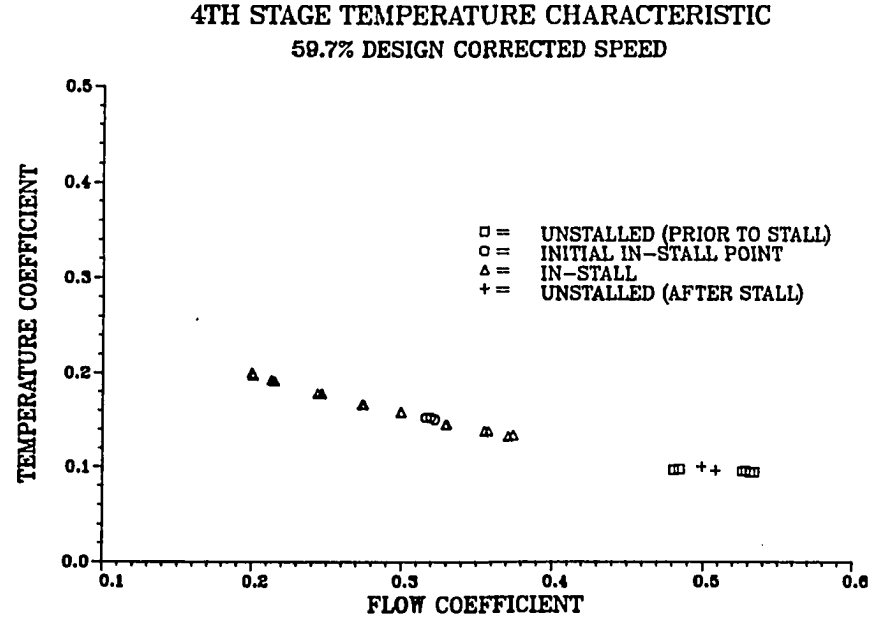

Figure 14.5 Test compressor fourth stage characteristics 59.7% design corrected speed

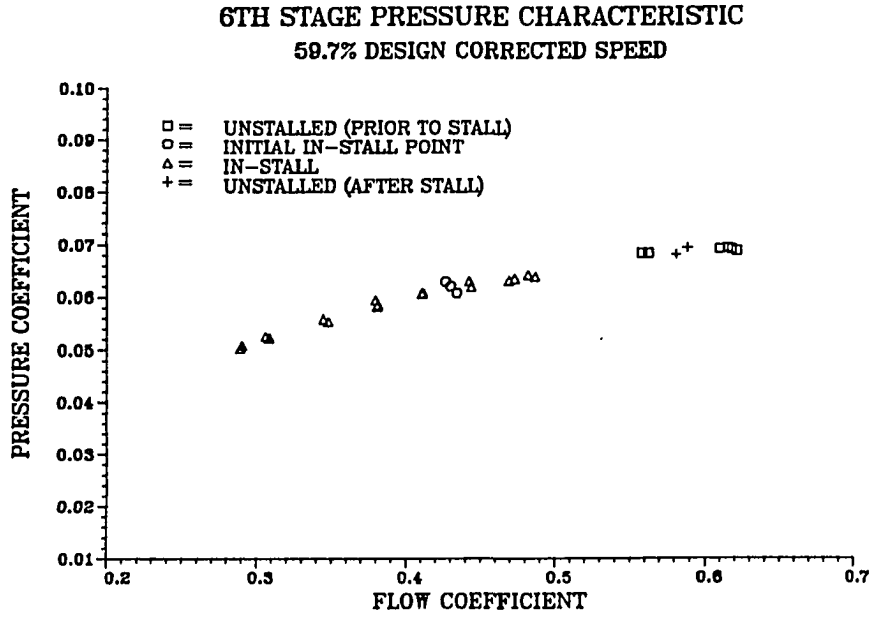

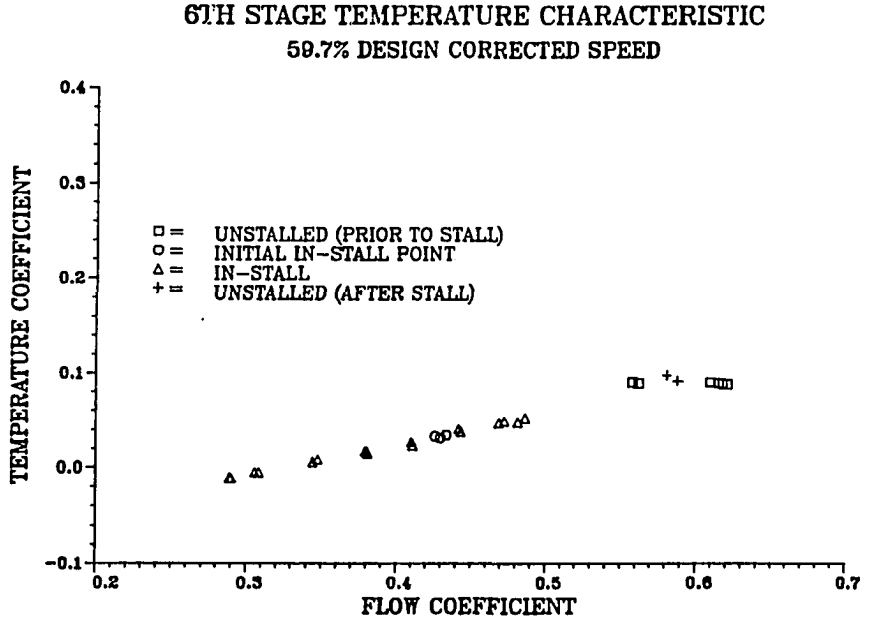

Figure 14.6 Test compressor fifth stage characteristics 59.7% design corrected speed

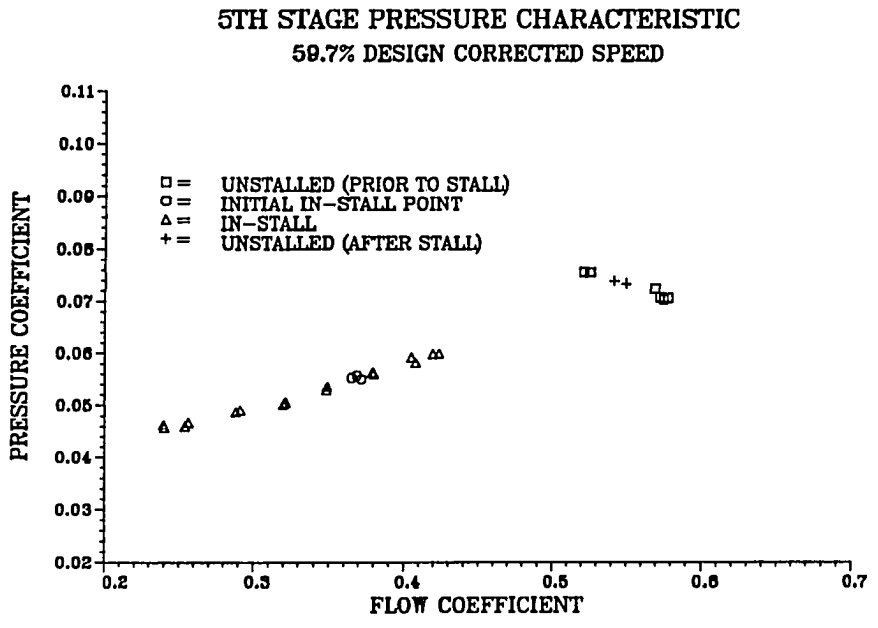

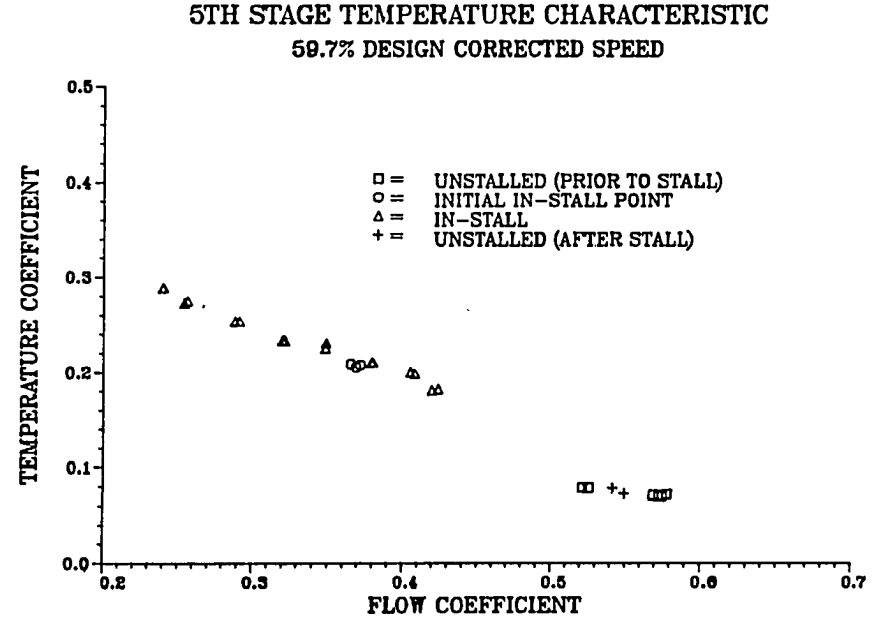

Figure 14.7 Test compressor sixth stage characteristics 59.7% design corrected speed

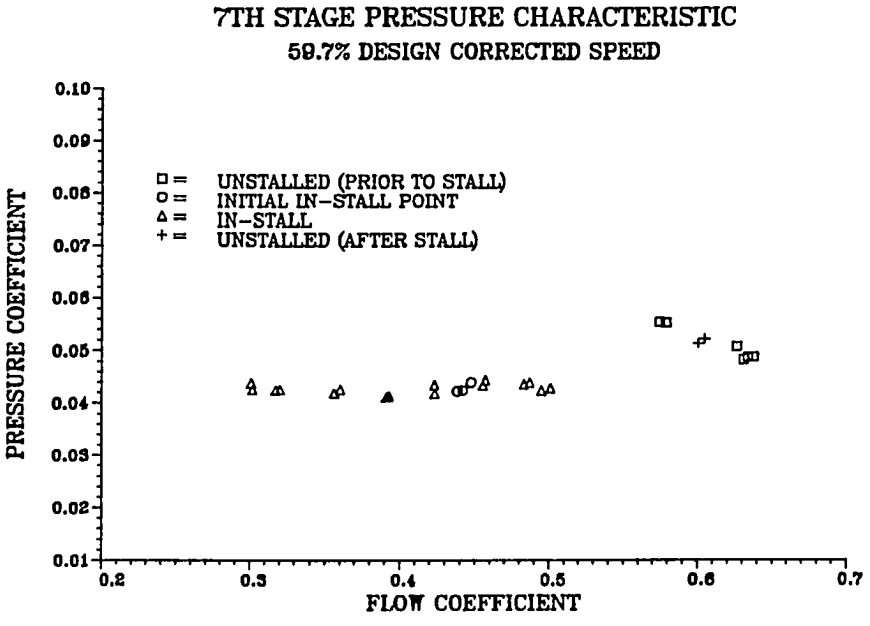

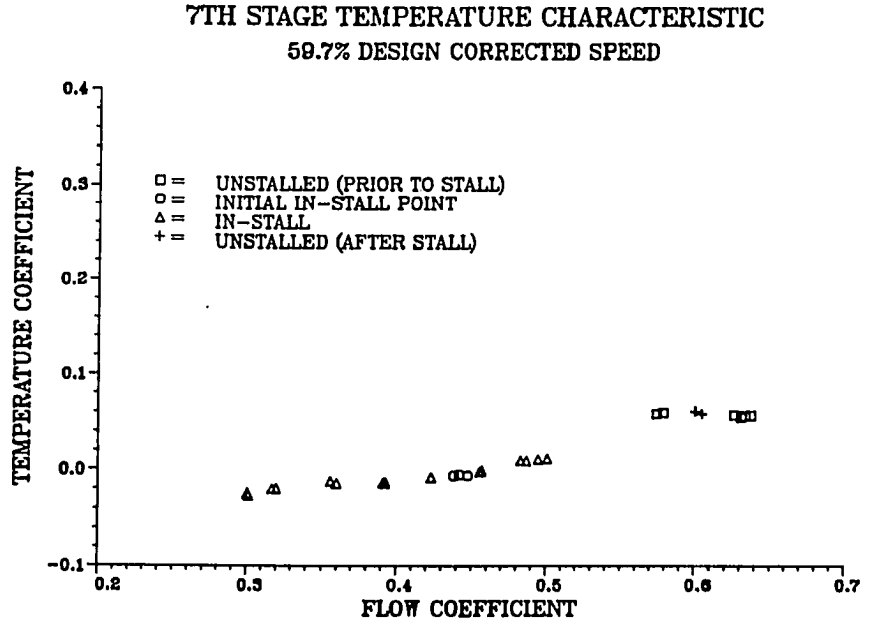

Figure 14.8 Test compressor seventh stage characteristics 59.7% design corrected speed

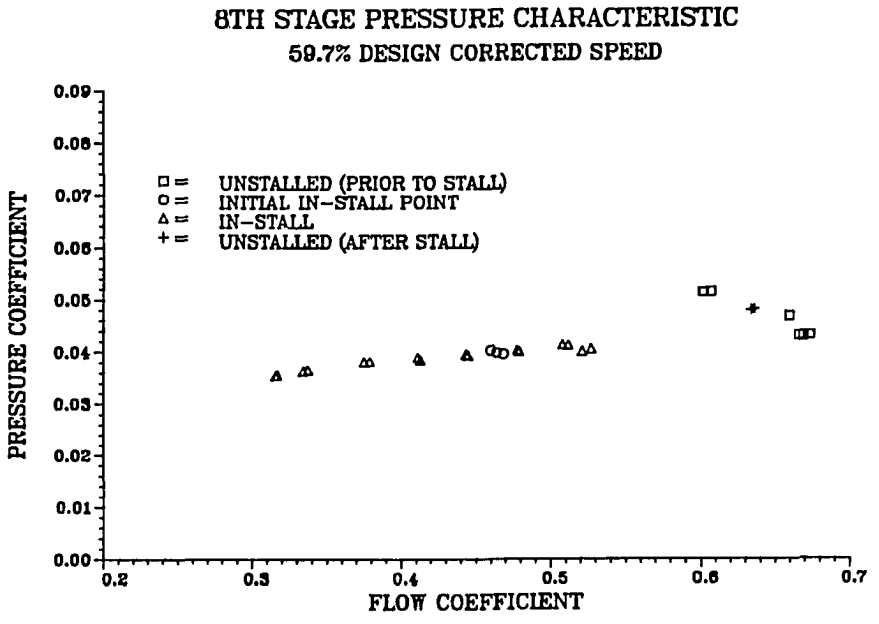

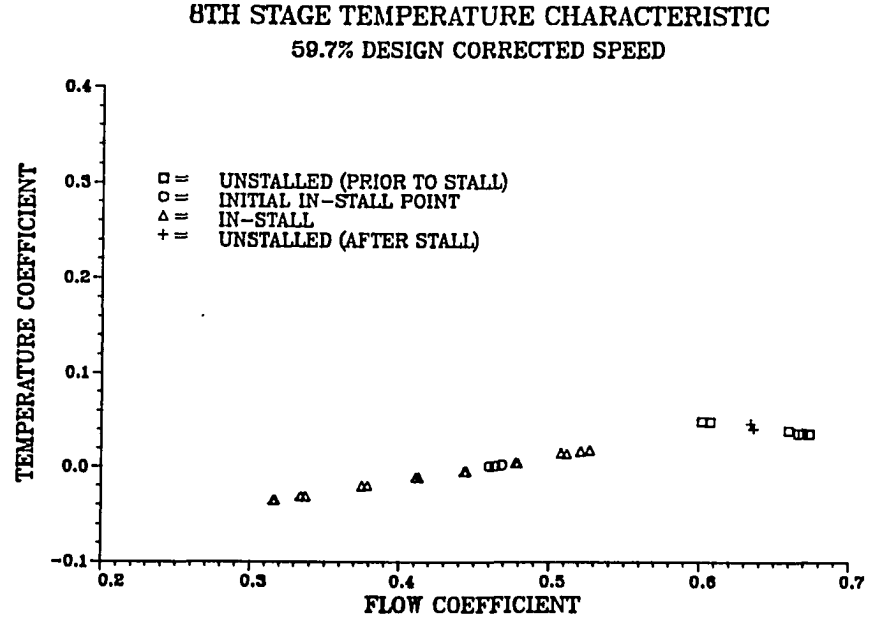

Figure 14.9 Test compressor eighth stage characteristics 59.7% design corrected speed

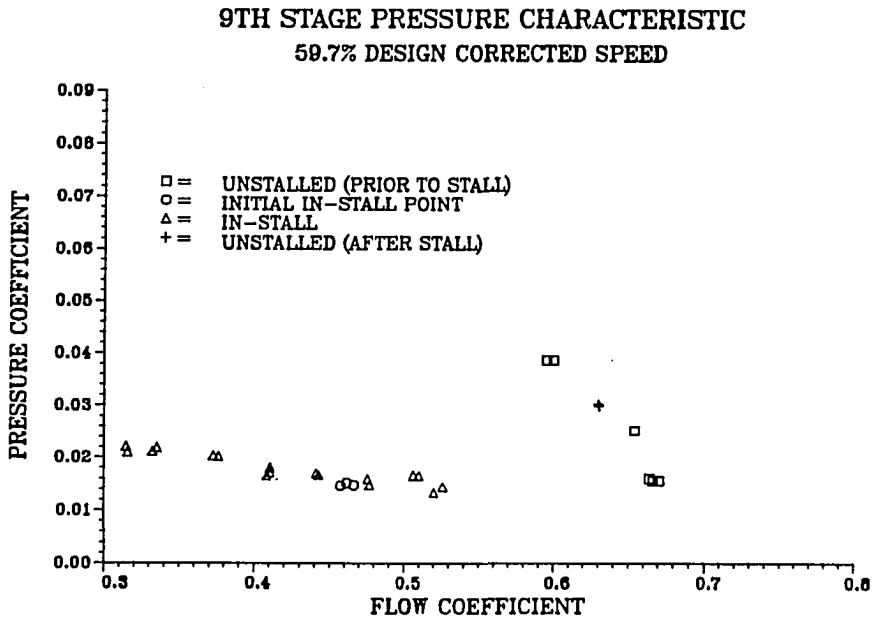

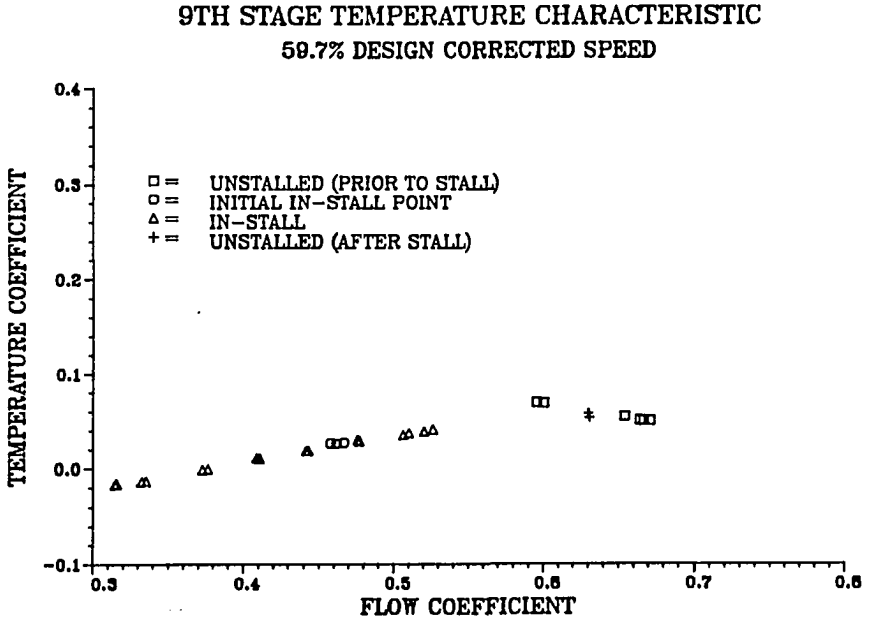

Figure 14.10 Test compressor ninth stage characteristics 59.7% design corrected speed

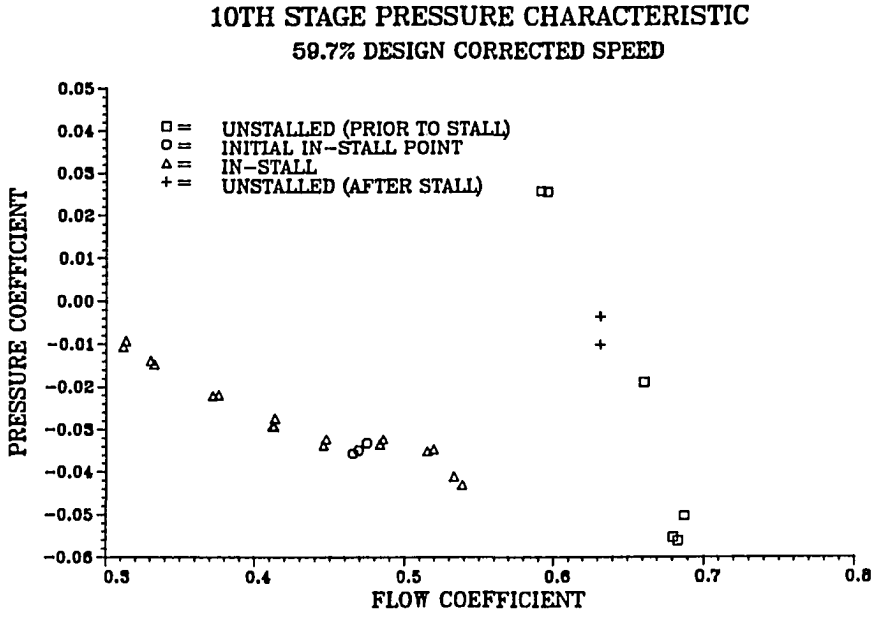

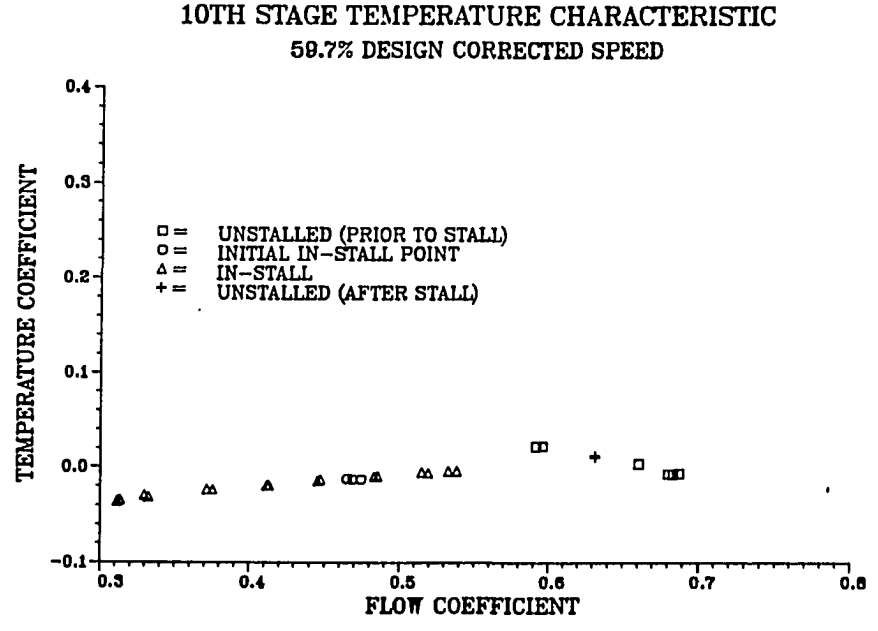

Figure 14.11 Test compressor tenth stage characteristics 59.7% design corrected speed

XV. APPENDIX D: DETAILED CHARACTERISTICS

67.7% DESIGN SPEED

The data shown in Figure 15.1 represent the detailed overall compressor temperature and pressure characteristics for the nominal variable vane configuration for the test compressor at 67.8% design corrected speed. Data are presented for four different operating conditions, the first two being, unstalled (prior to stall) operating on the overall compressor unstalled characteristic, and at the overall compressor initial in-stall condition. The data presented at the initial in-stall condition were obtained by slowly closing the exit throttle while the compressor was operating unstalled and stopping when stall occurred. The compressor was allowed to stabilize for 3 minutes and then the data were obtained. The third operating condition is for the compressor in-stall for different exit throttle area settings. The last condition is a repeat of the first after the compressor recovered from stall. The data in Figures 15.2 through 15.11 are the individual stage characteristics for the CRF test compressor. These characteristics are plotted in stage pressure and temperature coefficient and stage flow coefficient coordinates for the overall compressor condition described above.

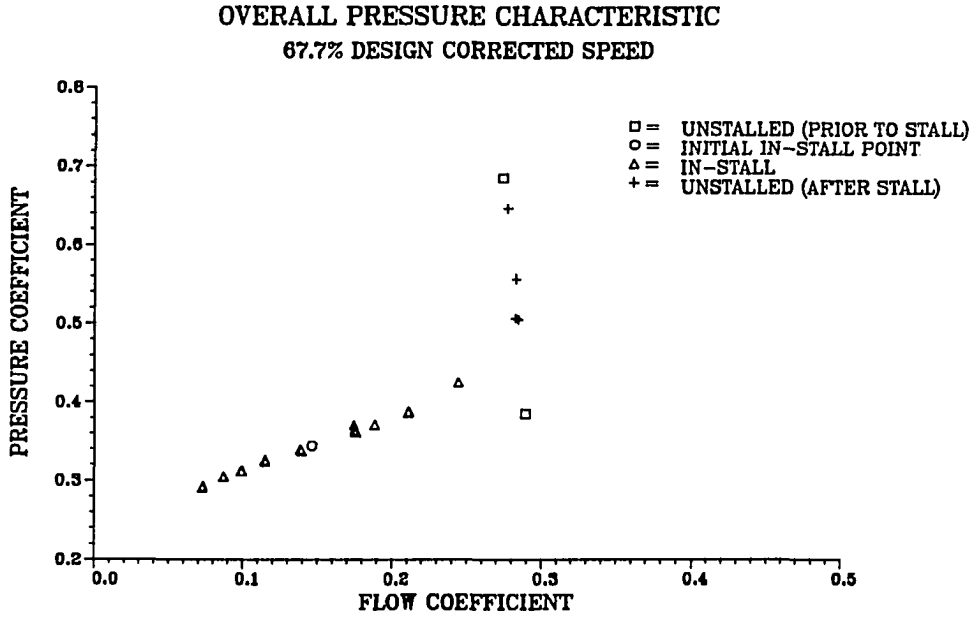

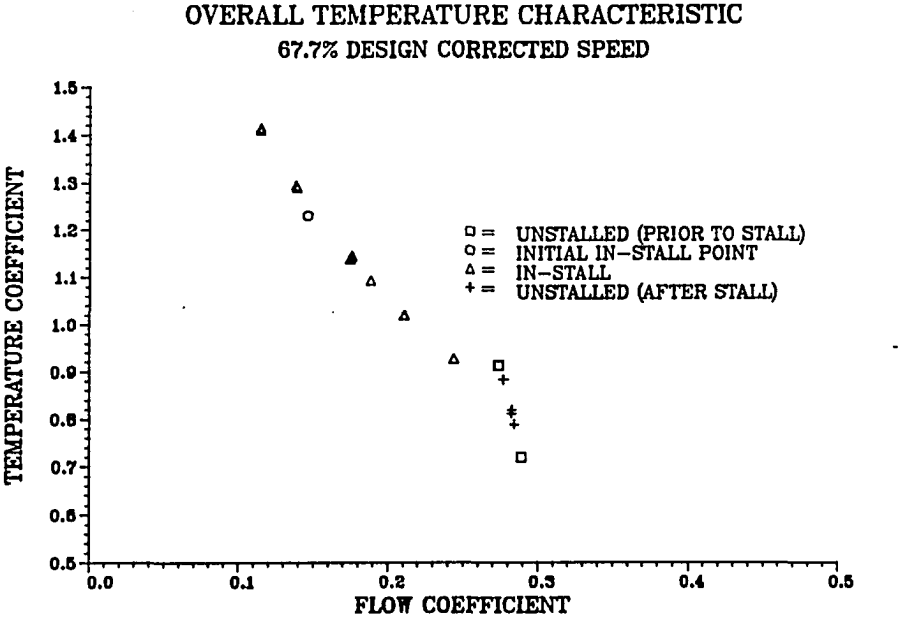

Figure 15.1 Test compressor overall characteristics 67.7% design corrected speed

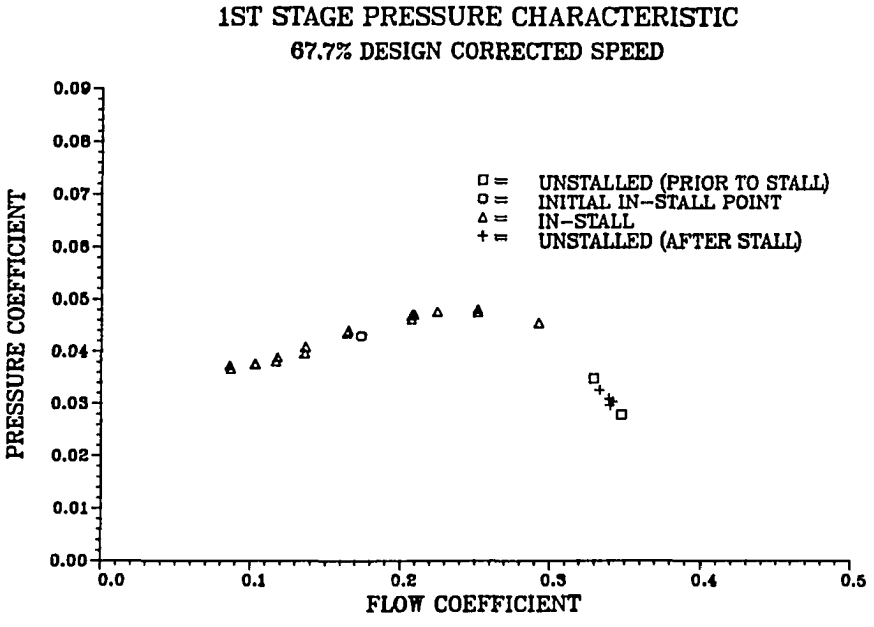

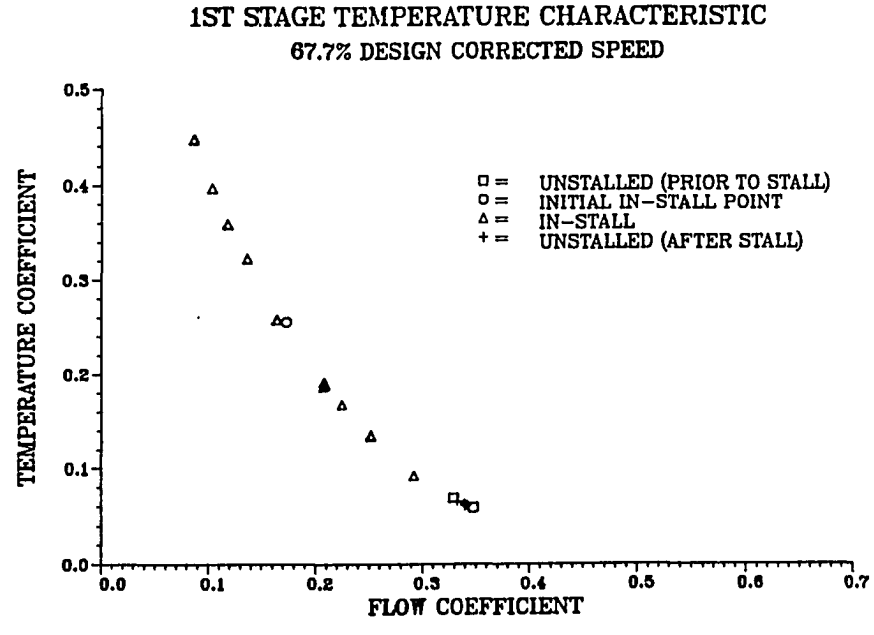

Figure 15.2 Test compressor first stage characteristics 67.7% design corrected speed

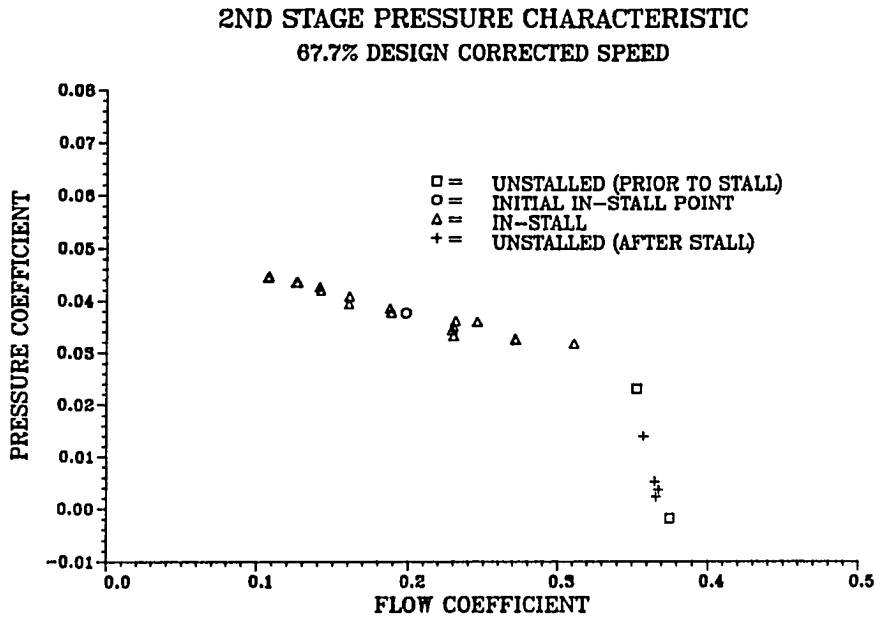

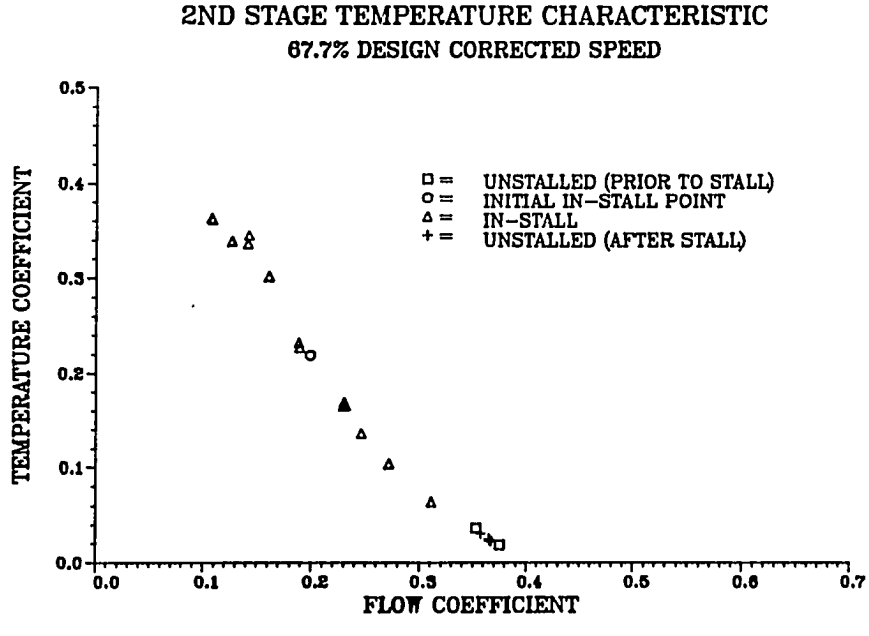

Figure 15.3 Test compressor second stage characteristics 67.7% design corrected speed

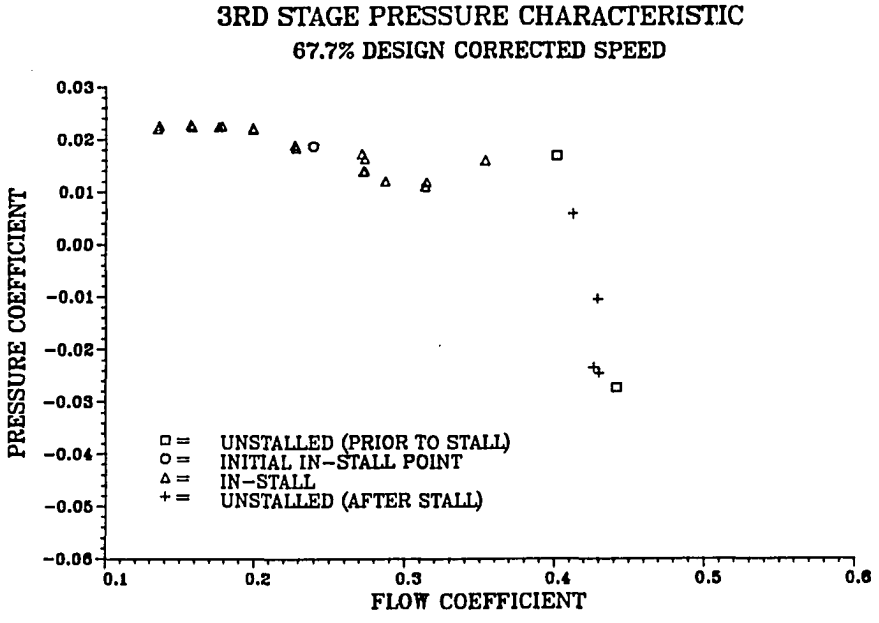

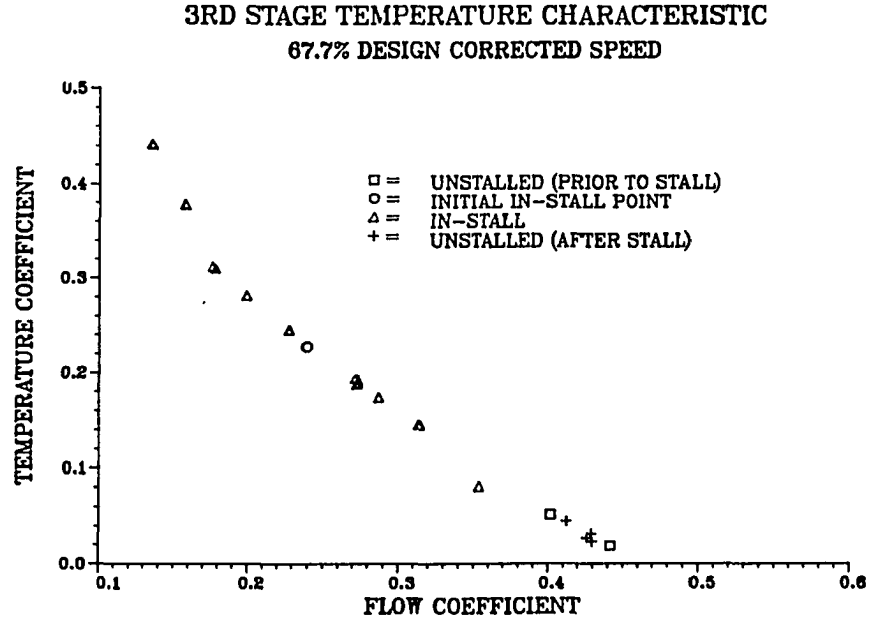

Figure 15.4 Test compressor third stage characteristics 67.7% design corrected speed

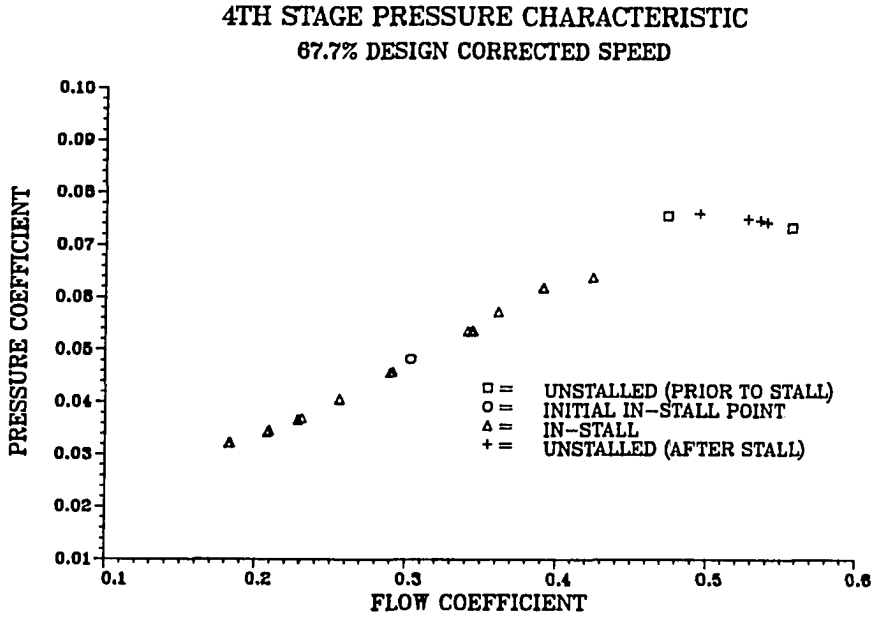

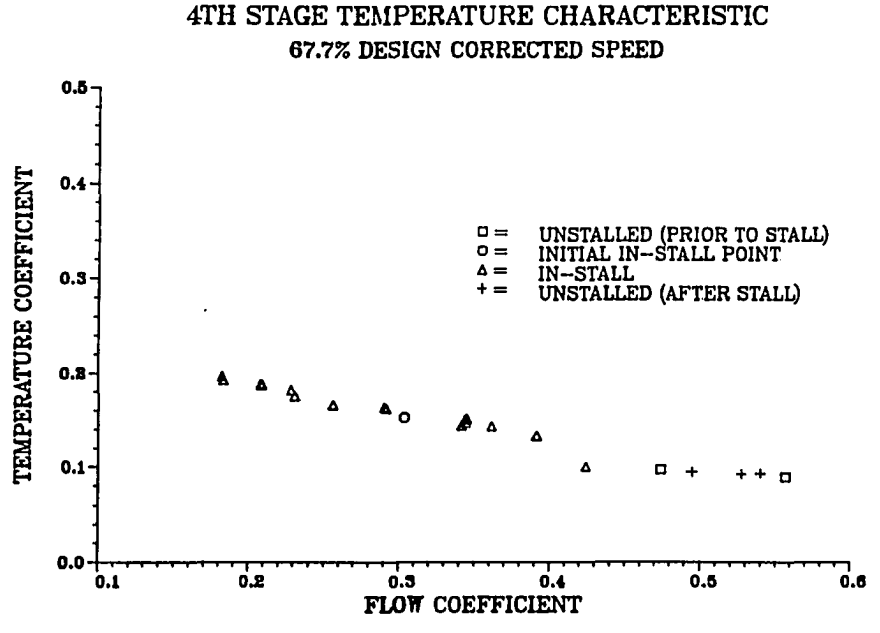

Figure 15.5 Test compressor fourth stage characteristics 67.7% design corrected speed

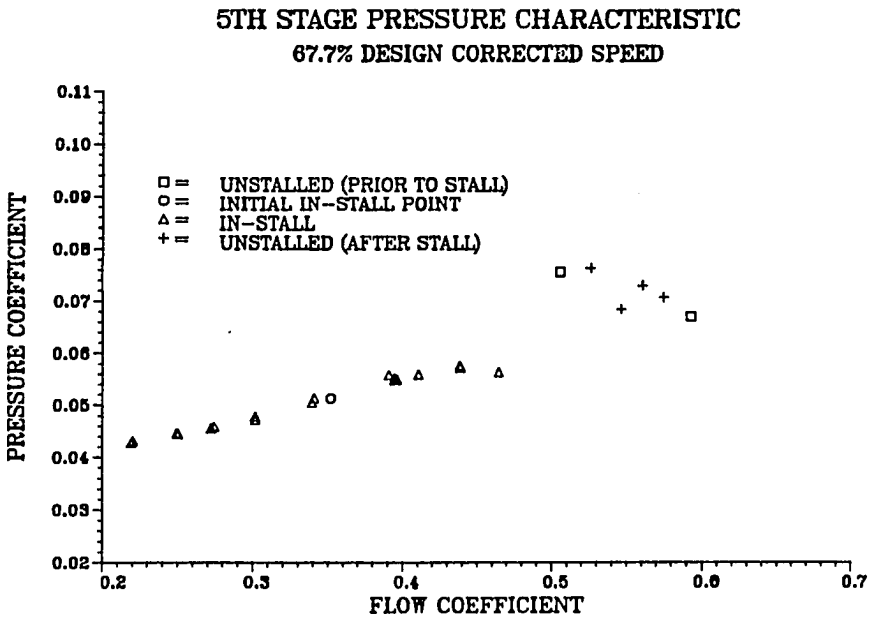

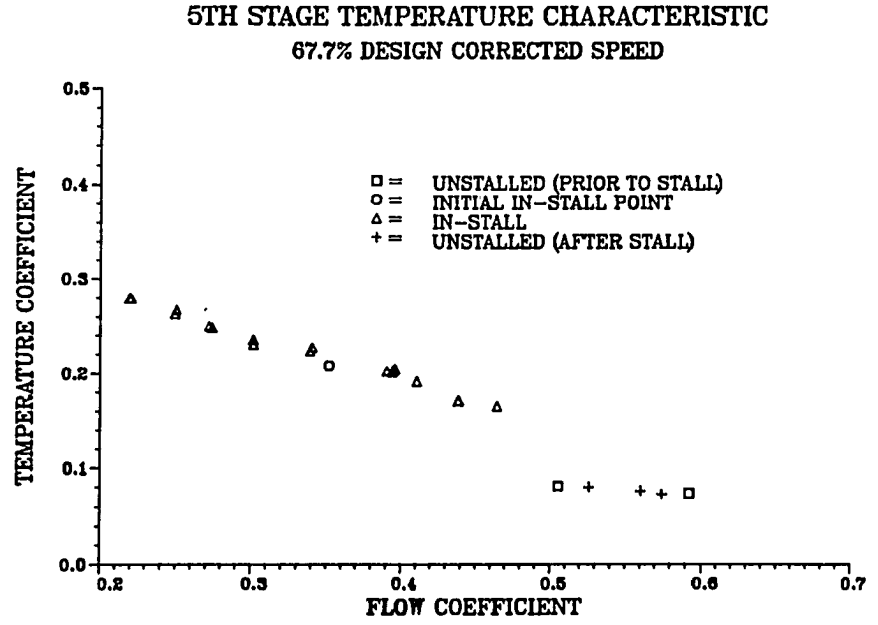

Figure 15.6 Test compressor fifth stage characteristics 67.7% design corrected speed

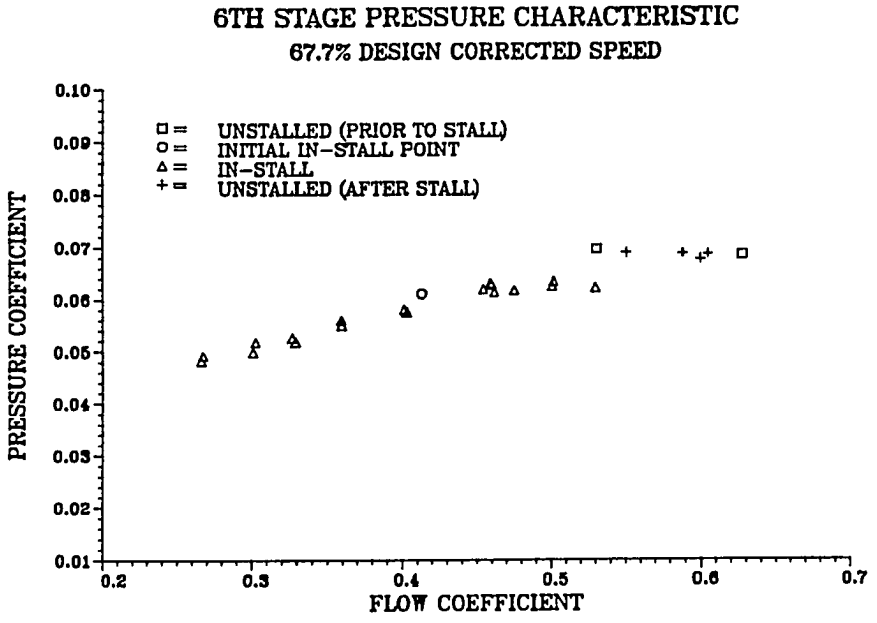

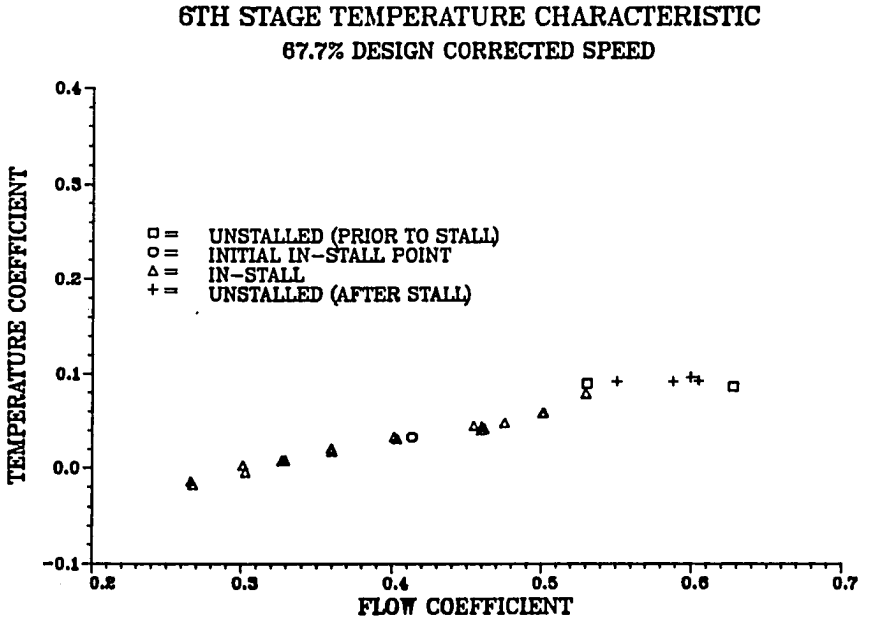

Figure 15.7 Test compressor sixth stage characteristics 67.7% design corrected speed

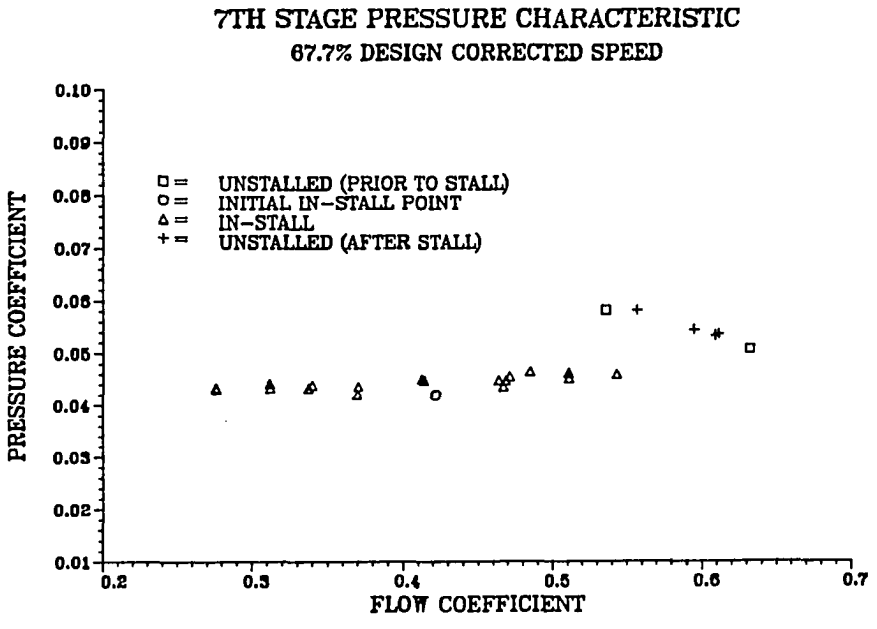

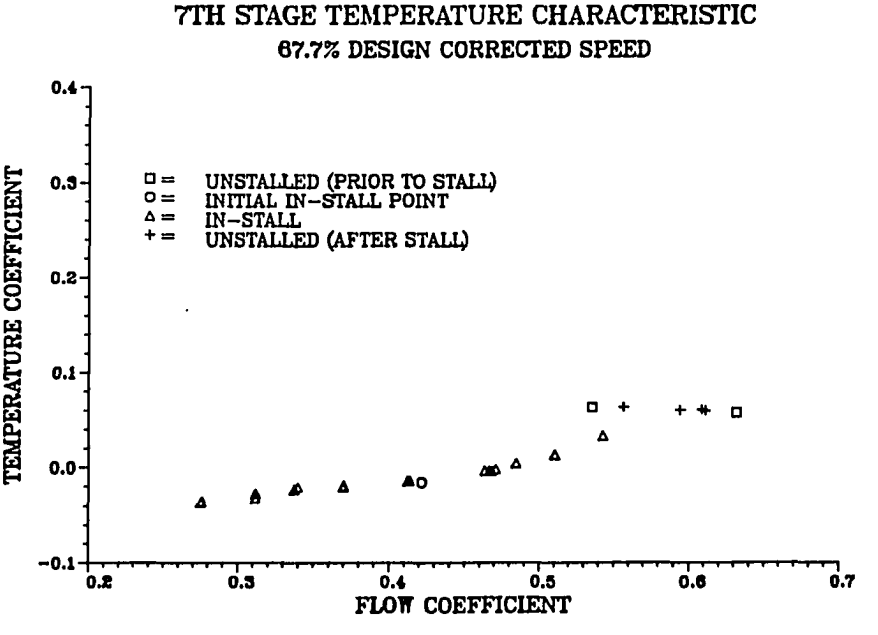

Figure 15.8 Test compressor seventh stage characteristics 67.7% design corrected speed

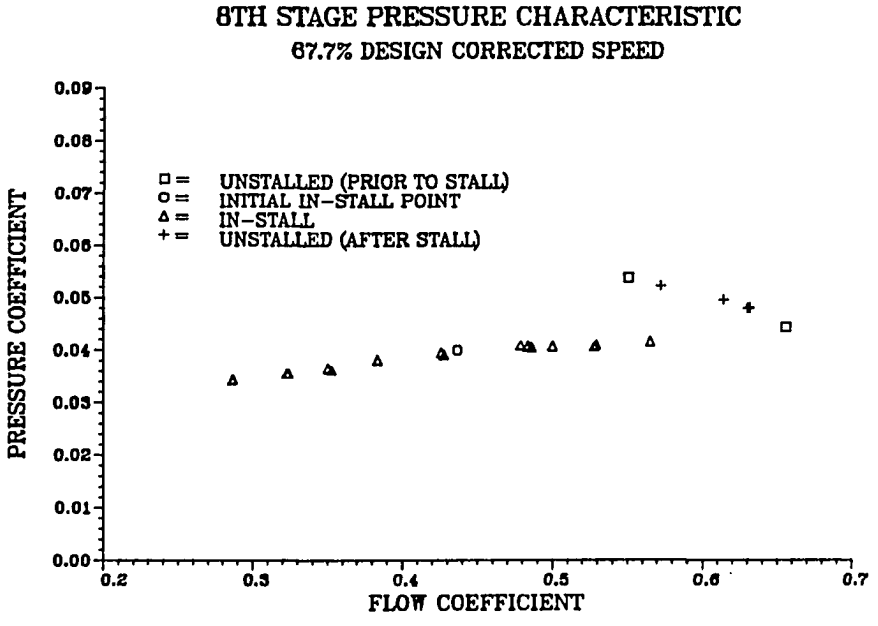

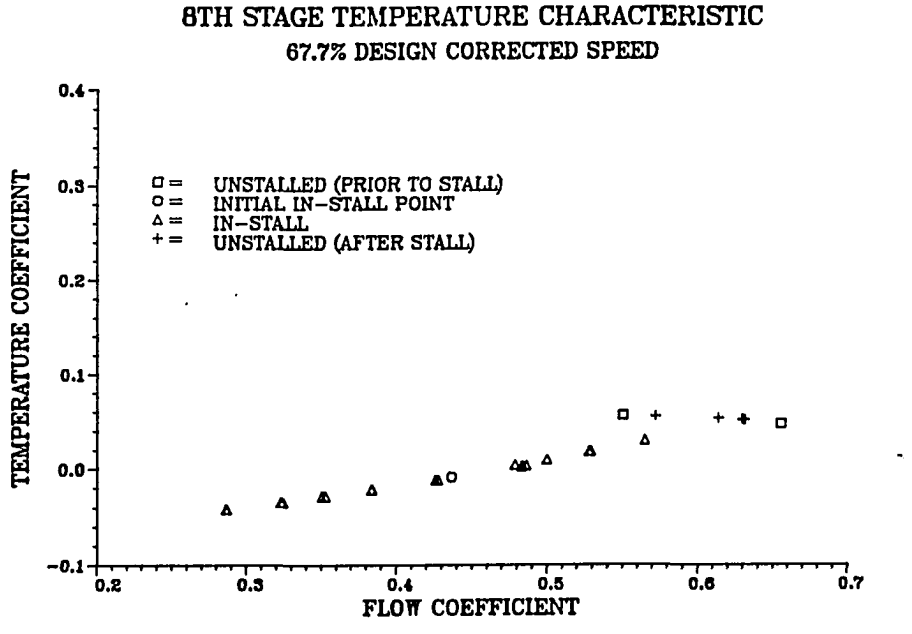

Figure 15.9 Test compressor eighth stage characteristics 67.7% design corrected speed

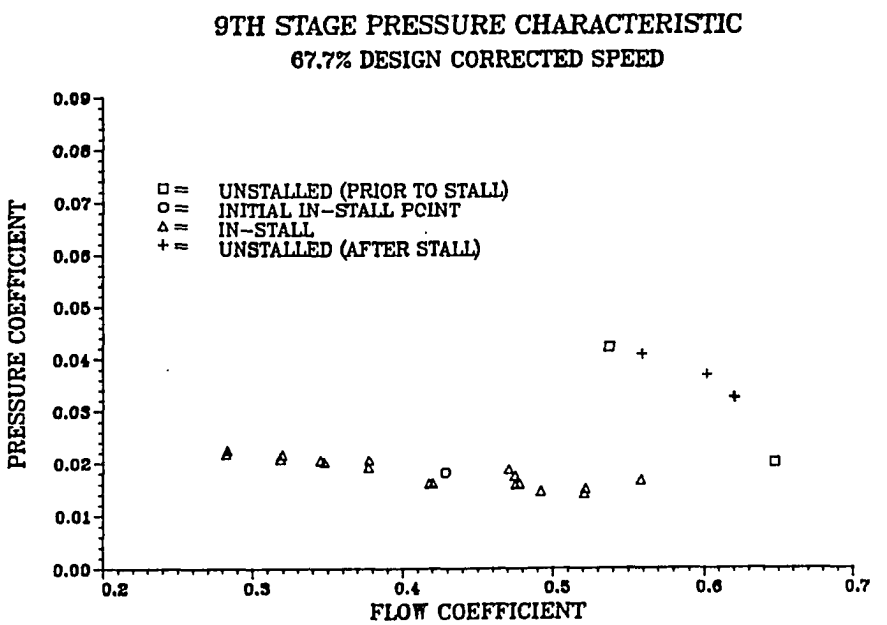

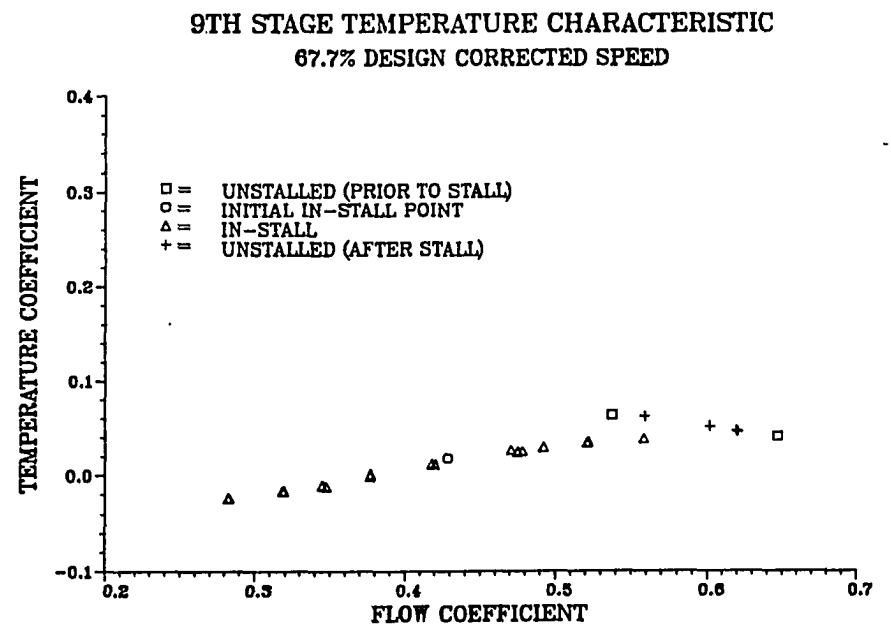

Figure 15.10 Test compressor ninth stage characteristics 67.7% design corrected speed

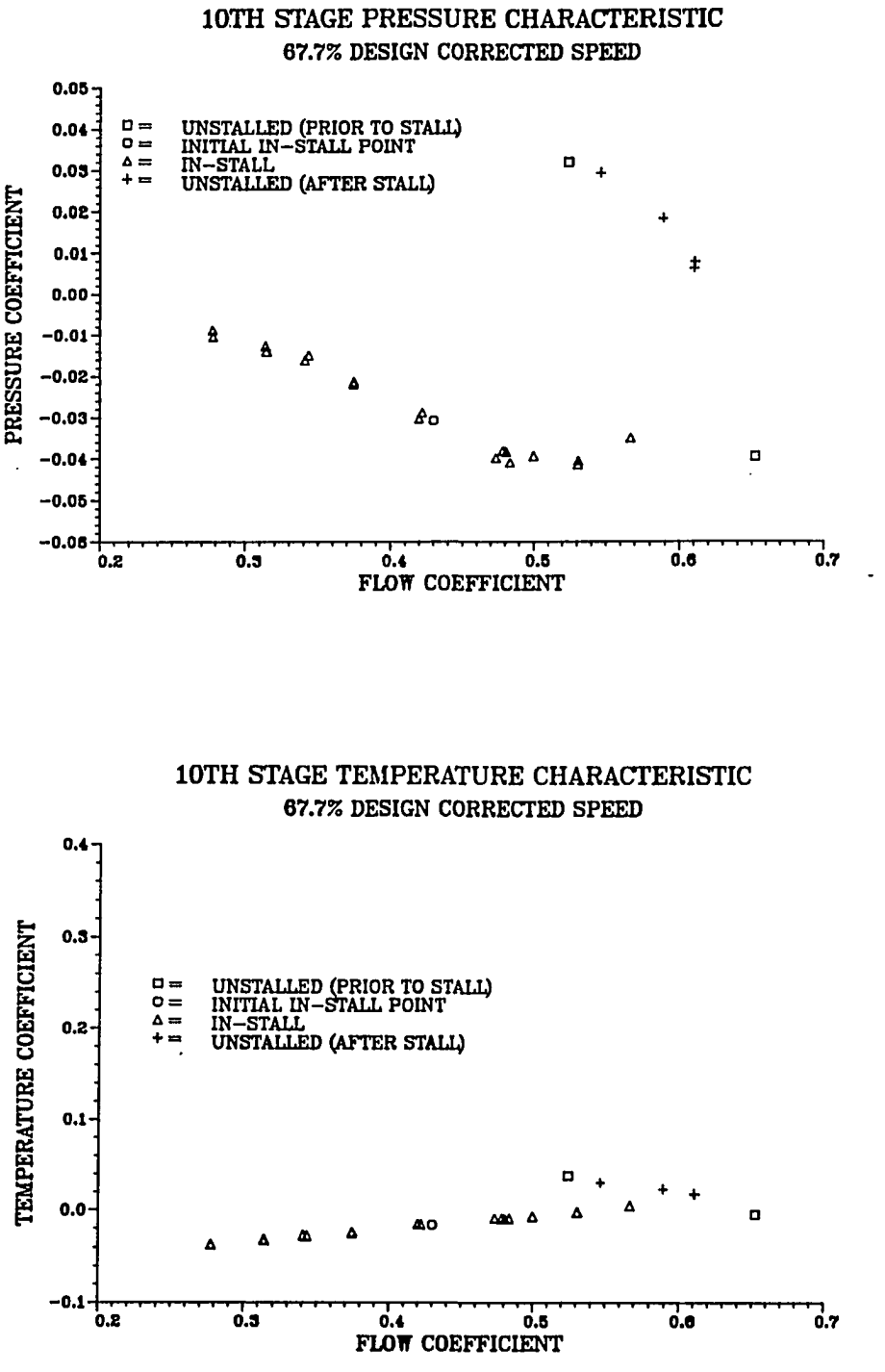

Figure 15.11 Test compressor tenth stage characteristics 67.7% design corrected speed

XVI. APPENDIX E: DETAILED CHARACTERISTICS

74.5% DESIGN SPEED

The data shown in Figure 16.1 represent the detailed overall compressor temperature and pressure characteristics for the nominal variable vane configuration for the test compressor at 74.5% design corrected speed. Data are presented for four different operating conditions, the first two being, unstalled (prior to stall) operating on the overall compressor unstalled characteristic, and at the overall compressor initial in-stall condition. The data presented at the initial in-stall condition were obtained by slowly closing the exit throttle while the compressor was operating unstalled and stopping when stall occurred. The compressor was allowed to stabilize for 3 minutes and then the data were obtained. The third operating condition is for the compressor in-stall for different exit throttle area settings. The last condition is a repeat of the first after the compressor recovered from stall. The data in Figures 16.2 through 16.11 are the individual stage characteristics for the CRF test compressor. These characteristics are plotted in stage pressure and temperature coefficient and stage flow coefficient coordinates for the overall compressor condition described above.

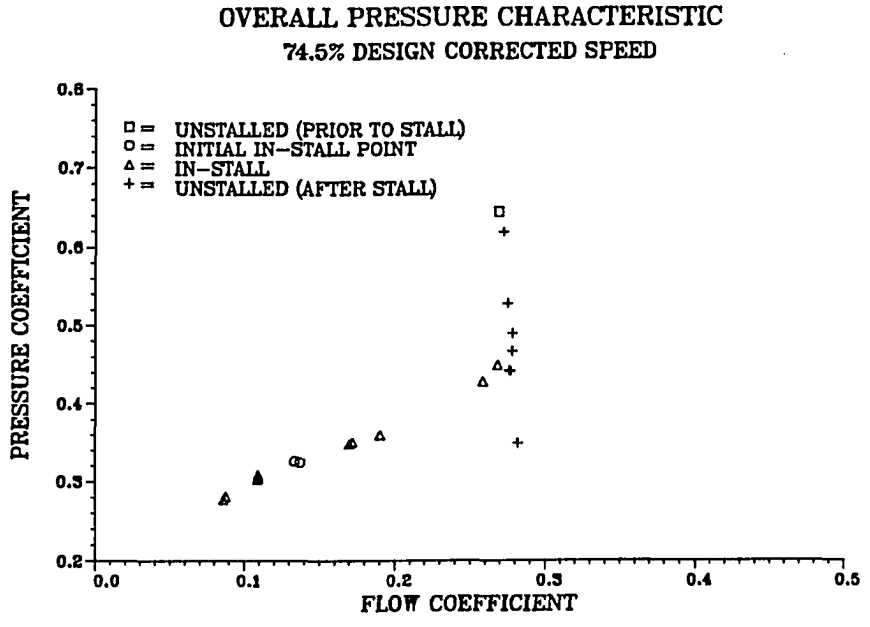

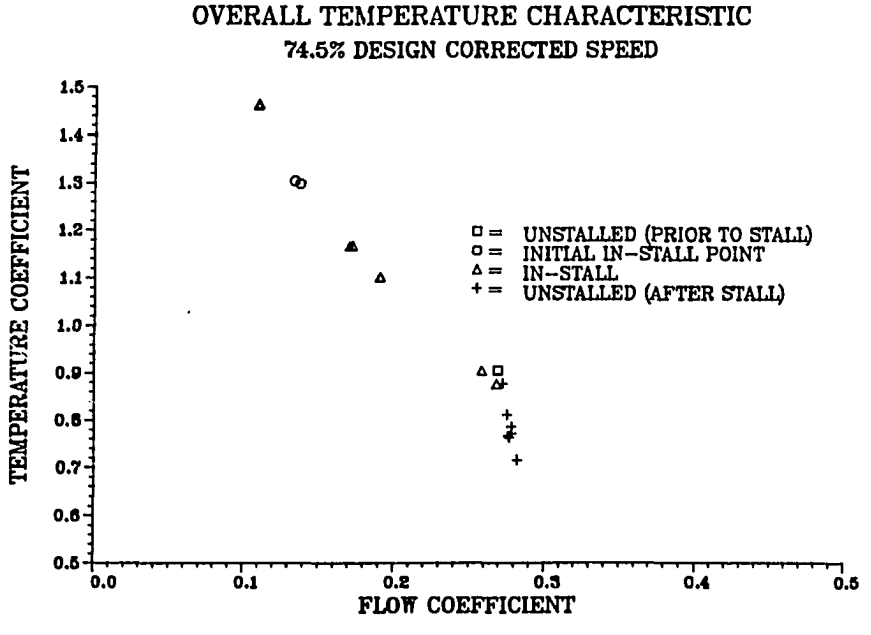

Figure 16.1 Test compressor overall characteristics 74.5% design corrected speed

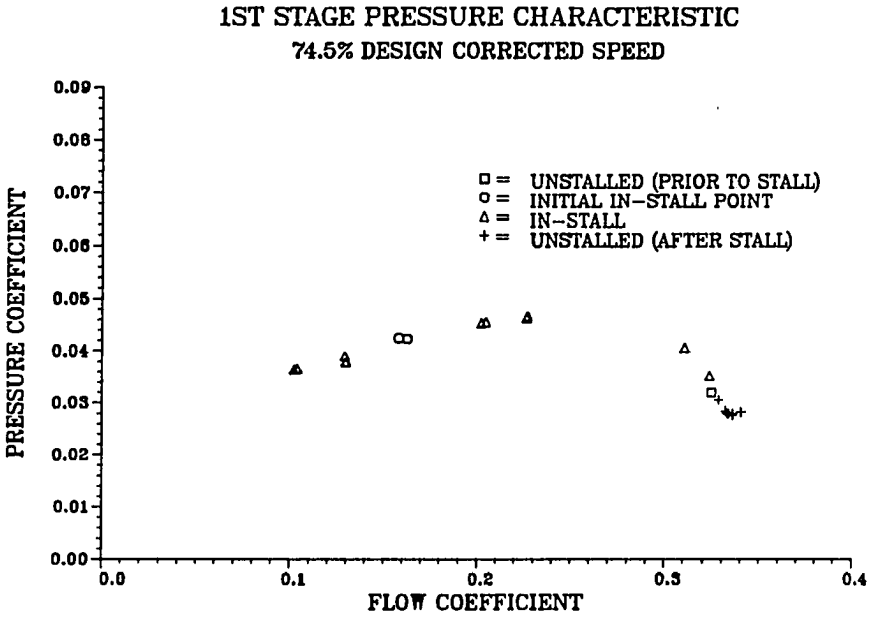

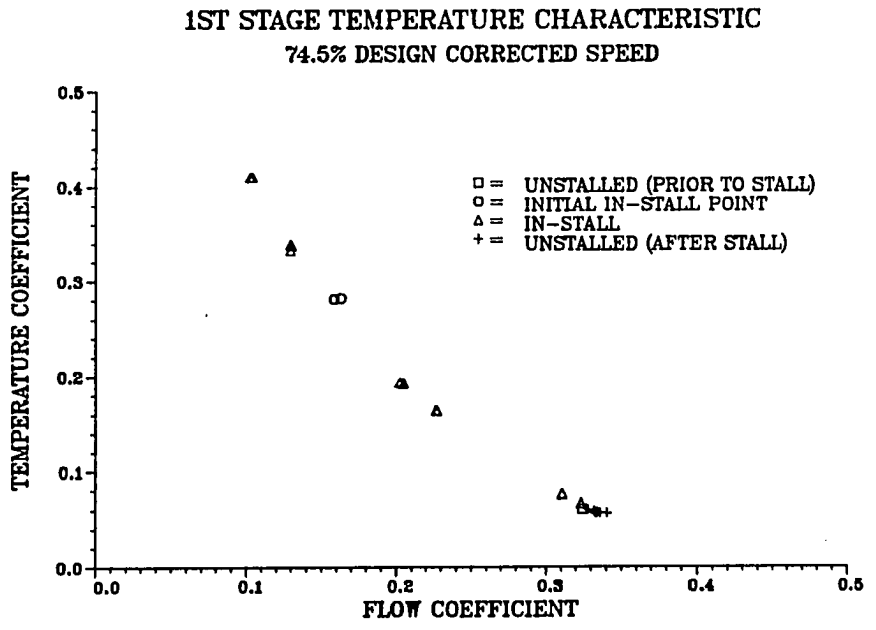

Figure 16.2 Test compressor first stage characteristics 74.5% design corrected speed

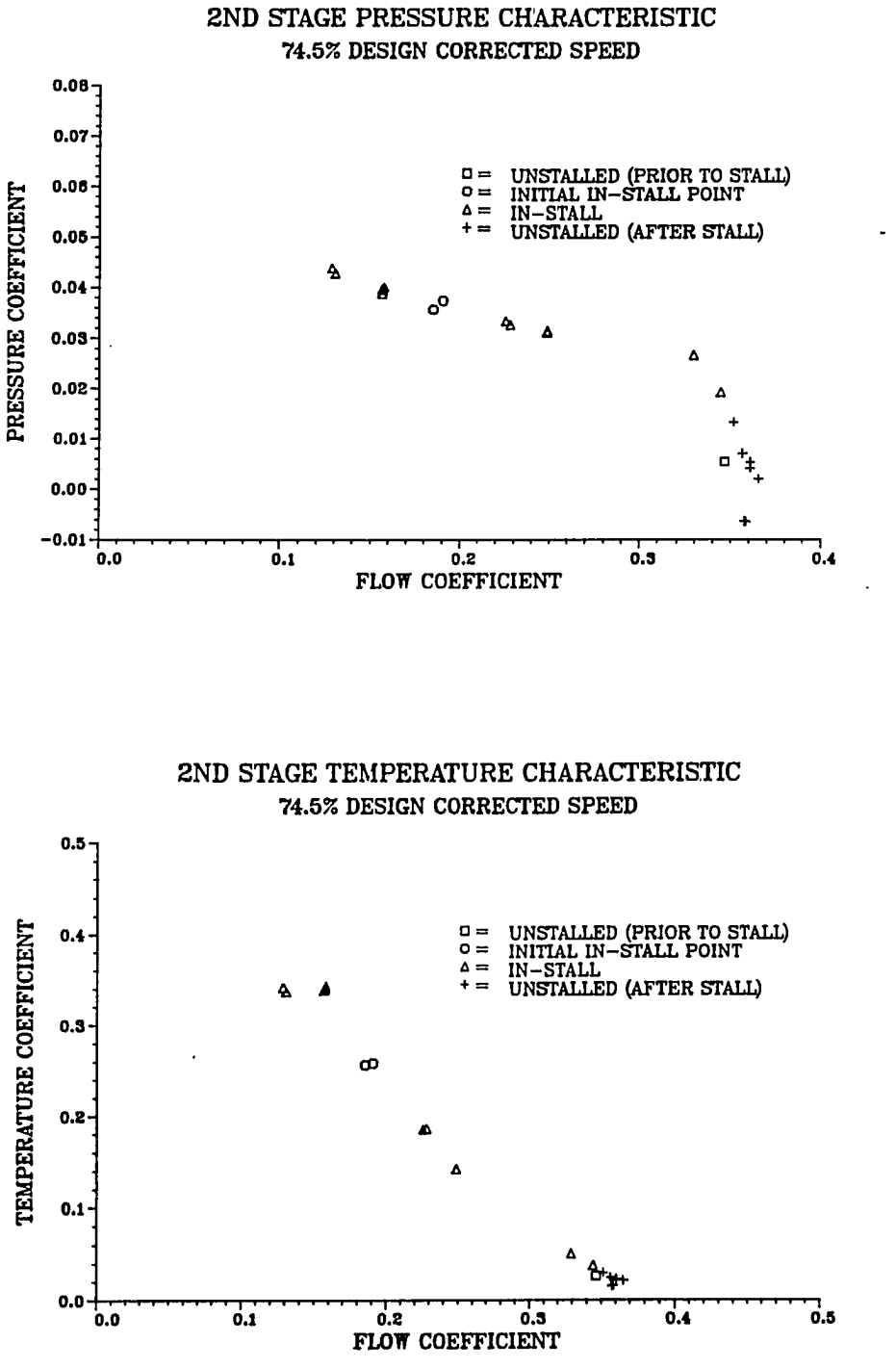

Figure 16.3 Test compressor second stage characteristics 74.5% design corrected speed

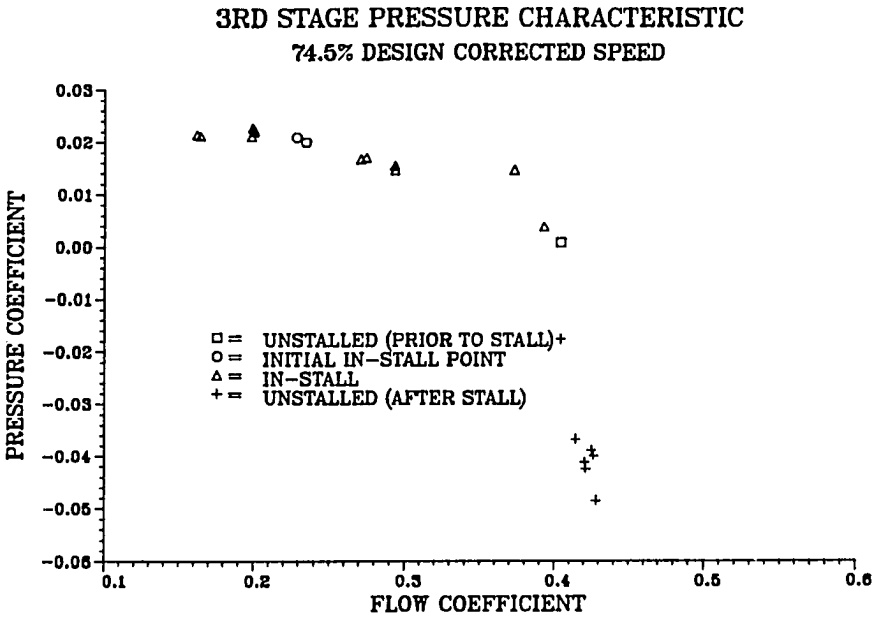

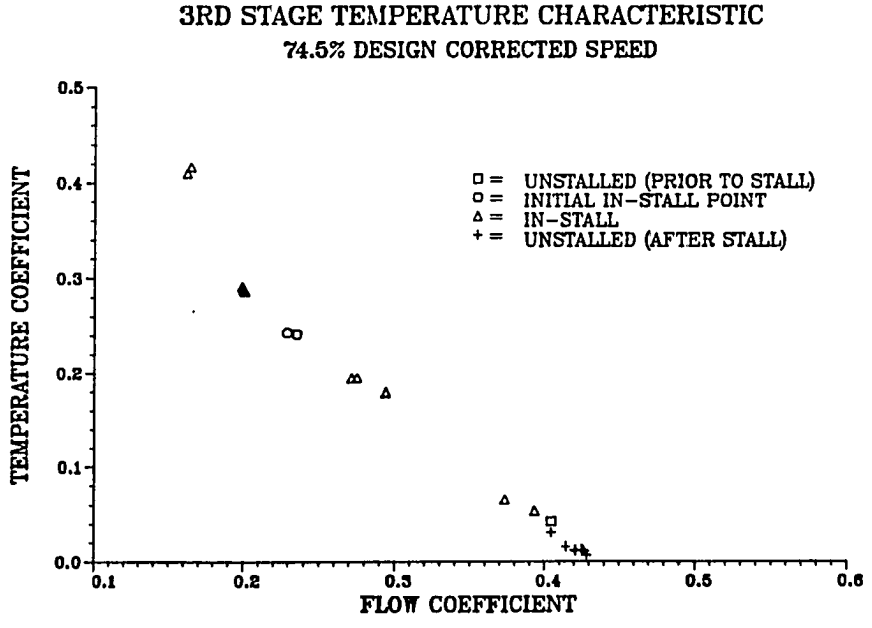

Figure 16.4 Test compressor third stage characteristics 74.5% design corrected speed

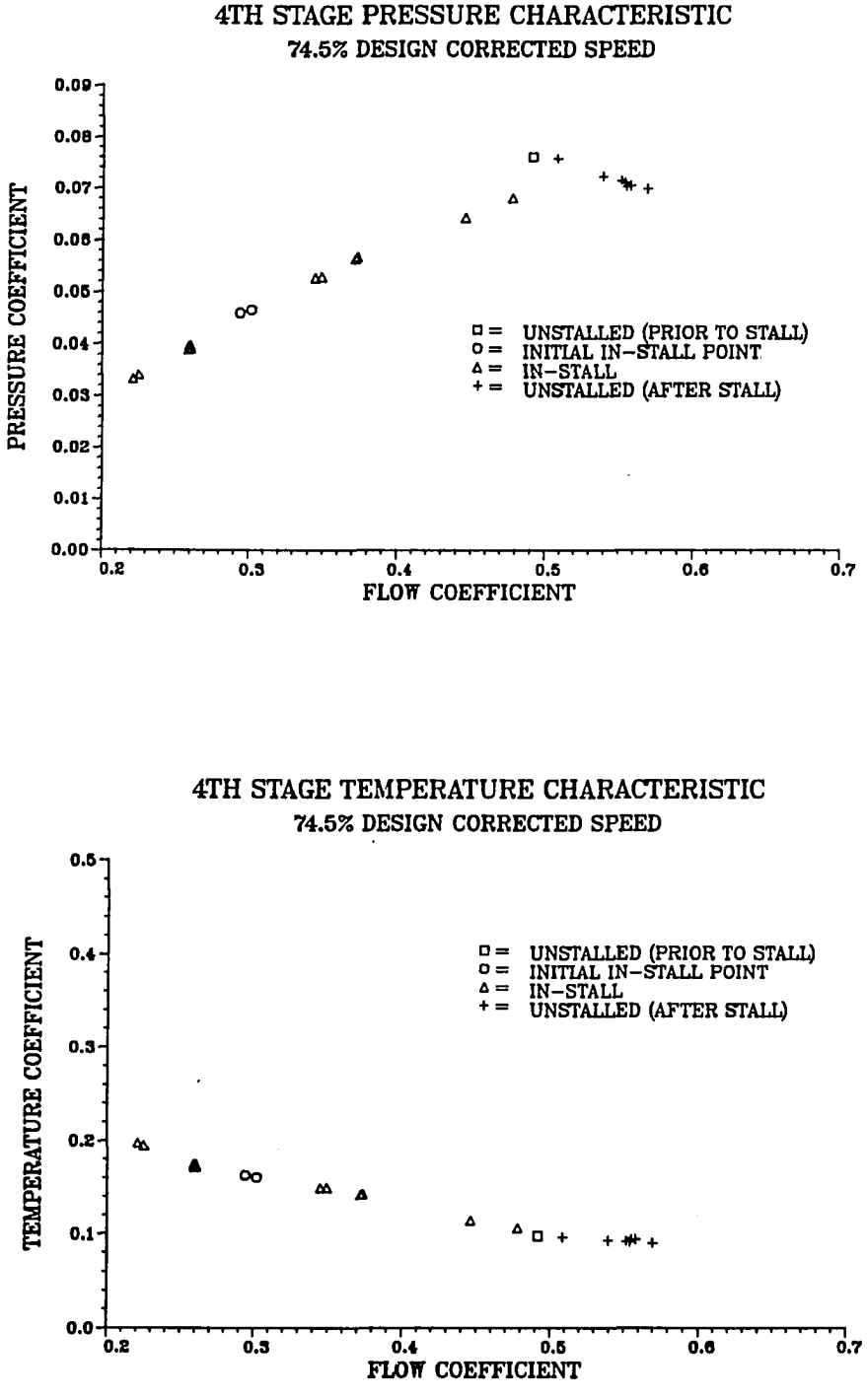

Figure 16.5 Test compressor fourth stage characteristics 74.5% design corrected speed

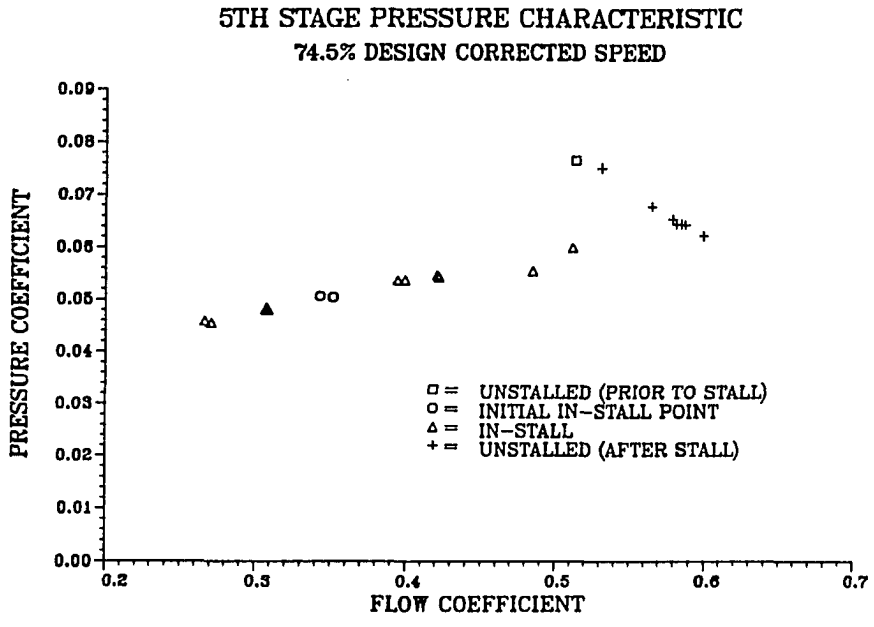

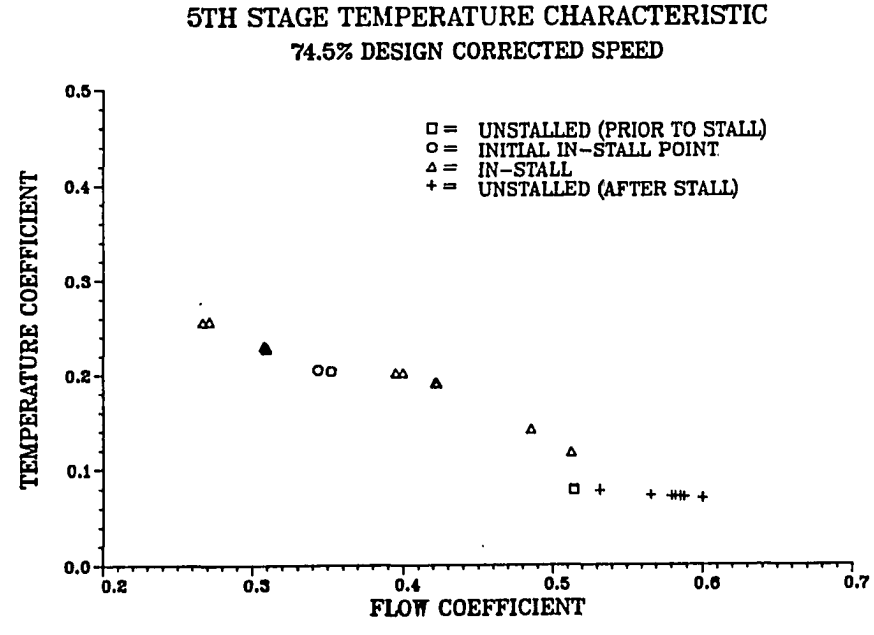

Figure 16.6 Test compressor fifth stage characteristics 74.5% design corrected speed

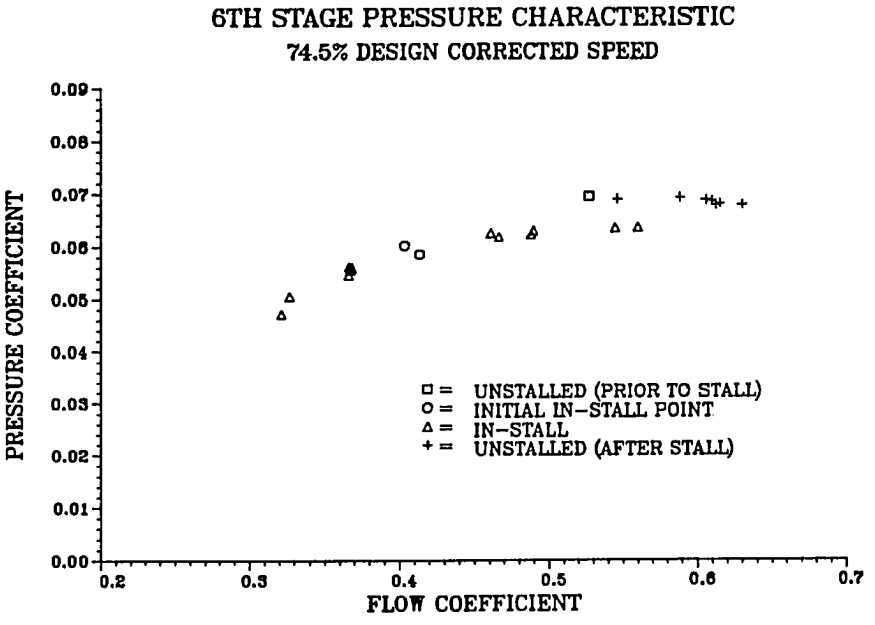

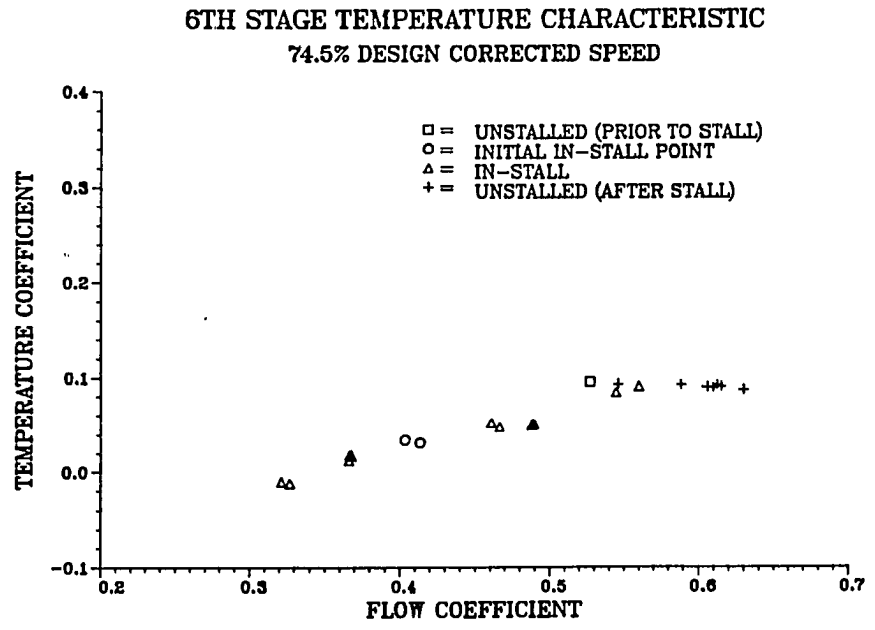

Figure 16.7 Test compressor sixth stage characteristics 74.5% design corrected speed

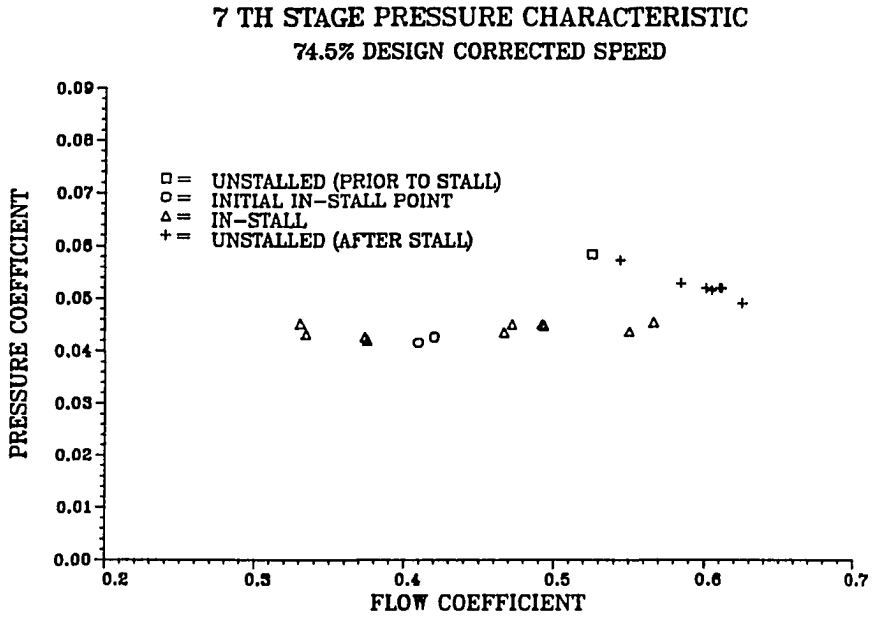

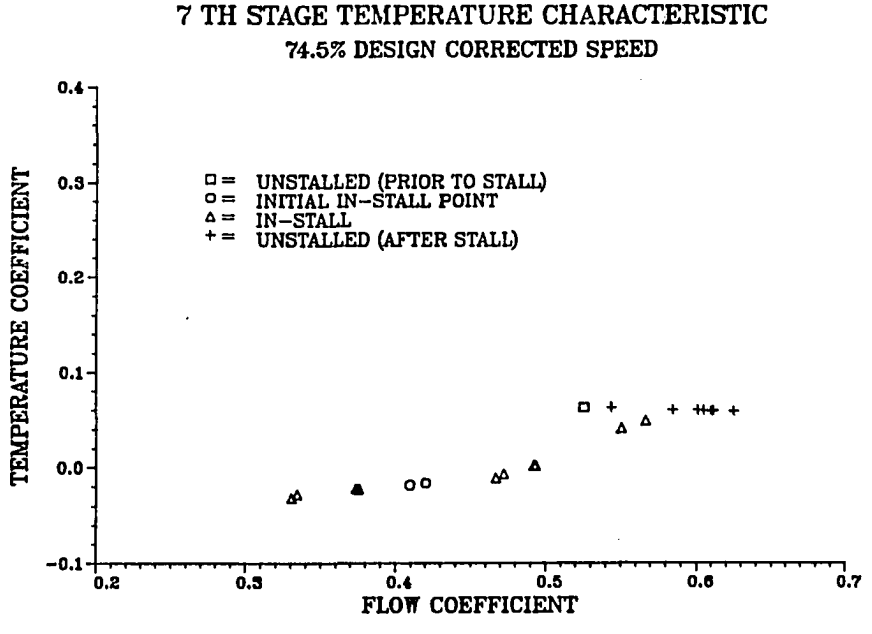

Figure 16.8 Test compressor seventh stage characteristics 74.5% design corrected speed

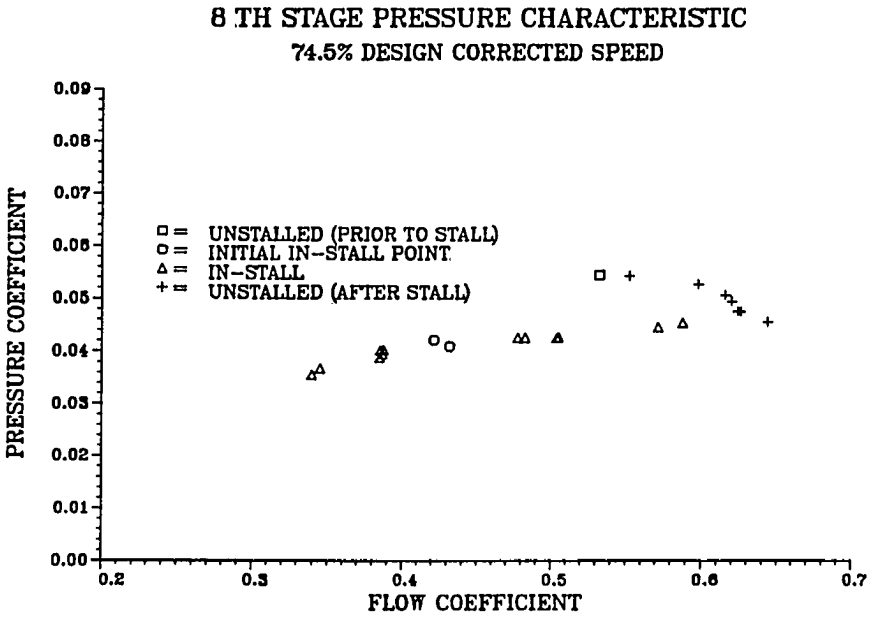

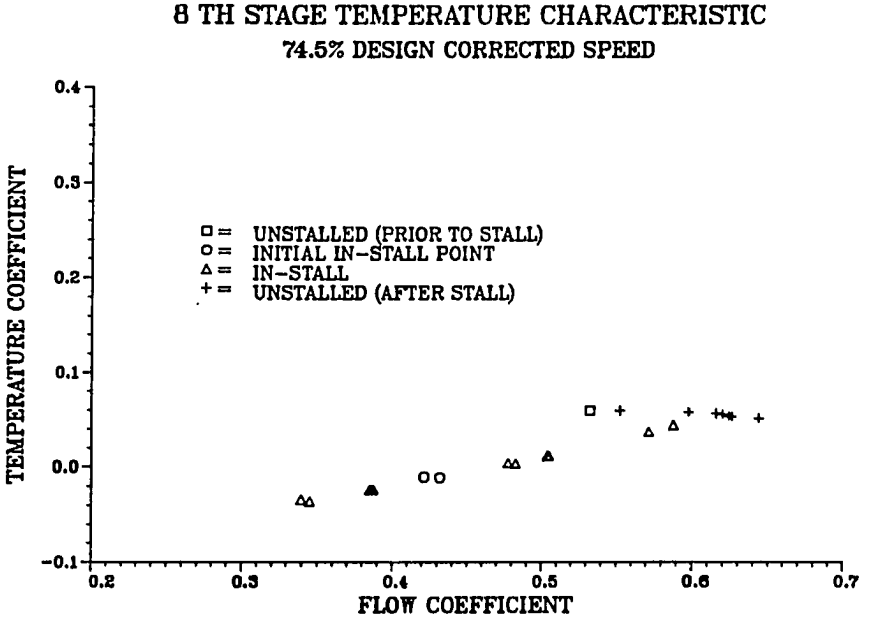

Figure 16.9 Test compressor eighth stage characteristics 74.5% design corrected speed

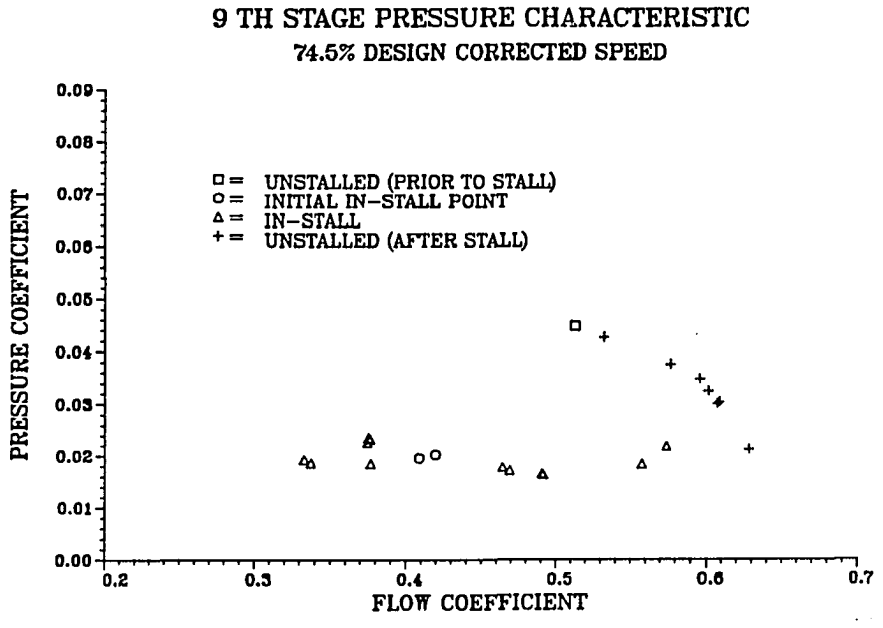

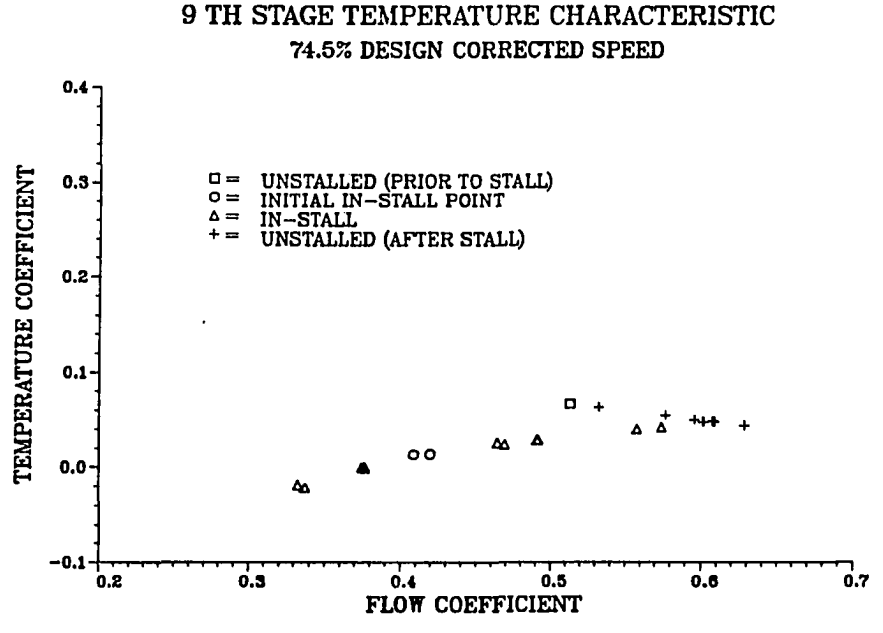

Figure 16.10 Test compressor ninth stage characteristics 74.5% design corrected speed

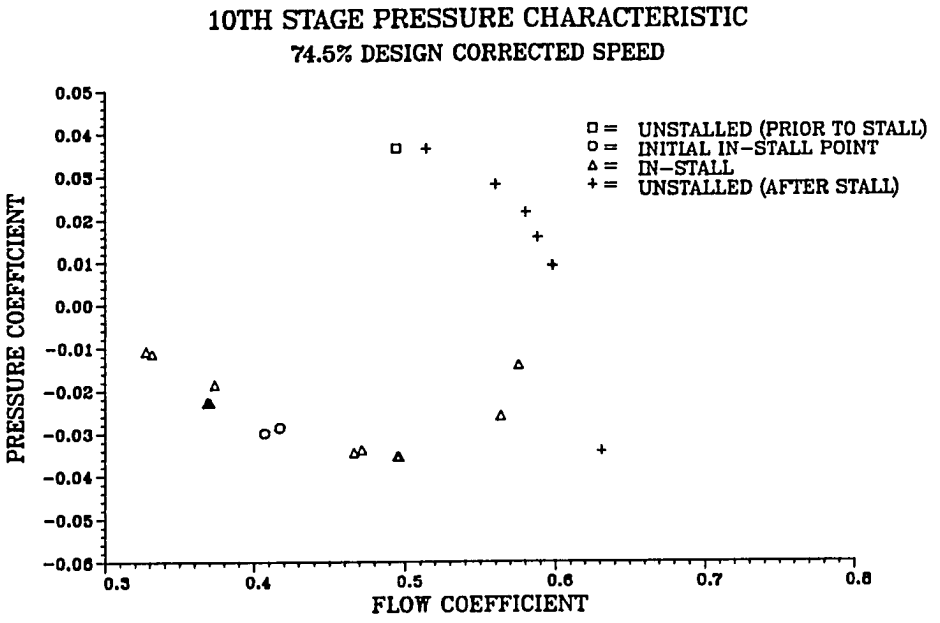

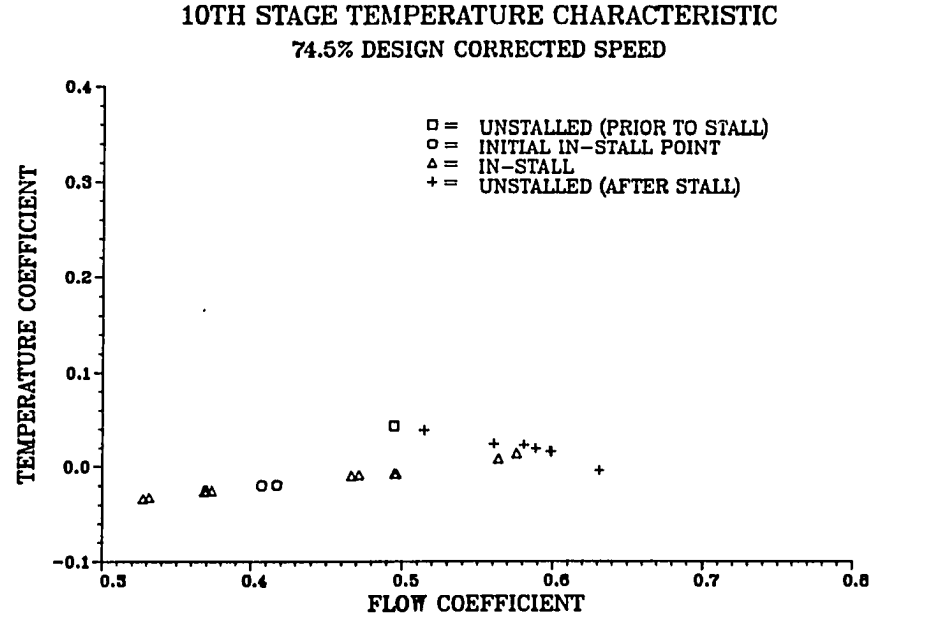

Figure 16.11 Test compressor tenth stage characteristics 74.5% design corrected speed

XVII. APPENDIX F: DETAILED CHARACTERISTICS

78.5% DESIGN SPEED

The data shown in Figure 17.1 represent the detailed overall compressor temperature and pressure characteristics for the nominal variable vane configuration for the test compressor at 49.8% design corrected speed. Data are presented for four different operating conditions, the first two being, unstalled (prior to stall) operating on the overall compressor unstalled characteristic, and at the overall compressor initial in-stall condition. The data presented at the initial in-stall condition were obtained by slowly closing the exit throttle while the compressor was operating unstalled and stopping when stall occurred. The compressor was allowed to stabilize for 3 minutes and then the data were obtained. The third operating condition is for the compressor in-stall for different exit throttle area settings. The last condition is a repeat of the first after the compressor recovered from stall. The data in Figures 17.2 through 17.11 are the individual stage characteristics for the CRF test compressor. These characteristics are plotted in stage pressure and temperature coefficient and stage flow coefficient coordinates for the overall compressor condition described above.

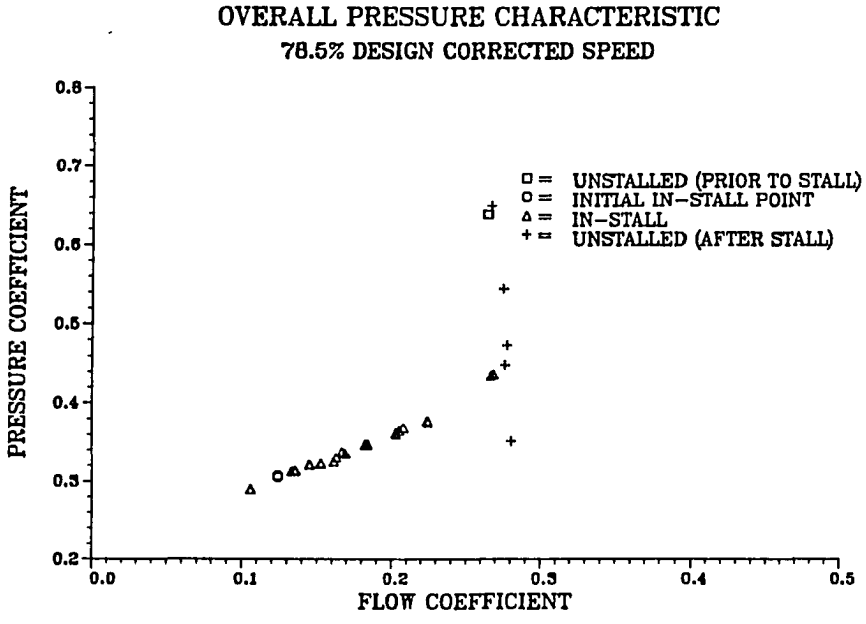

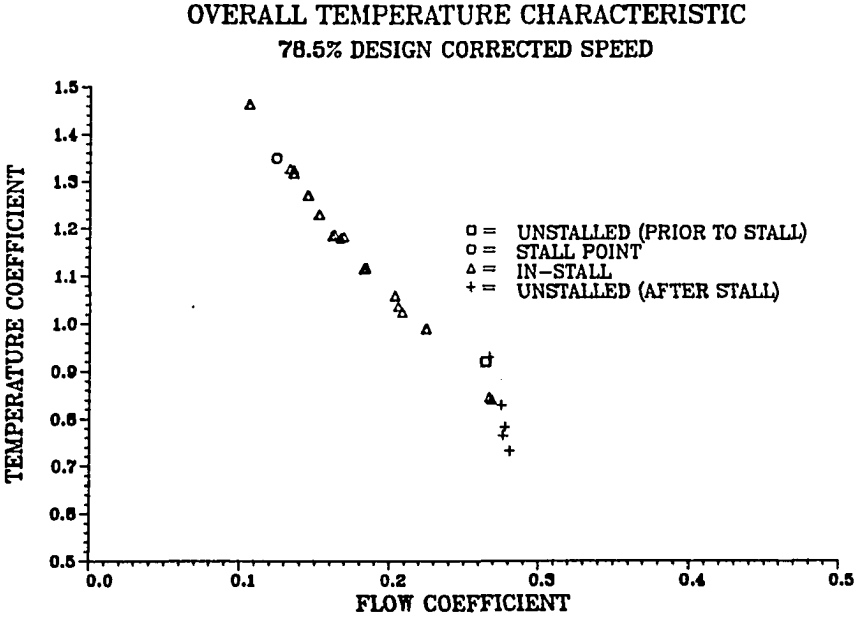

Figure 17.1 Test compressor overall characteristics 78.5% design corrected speed

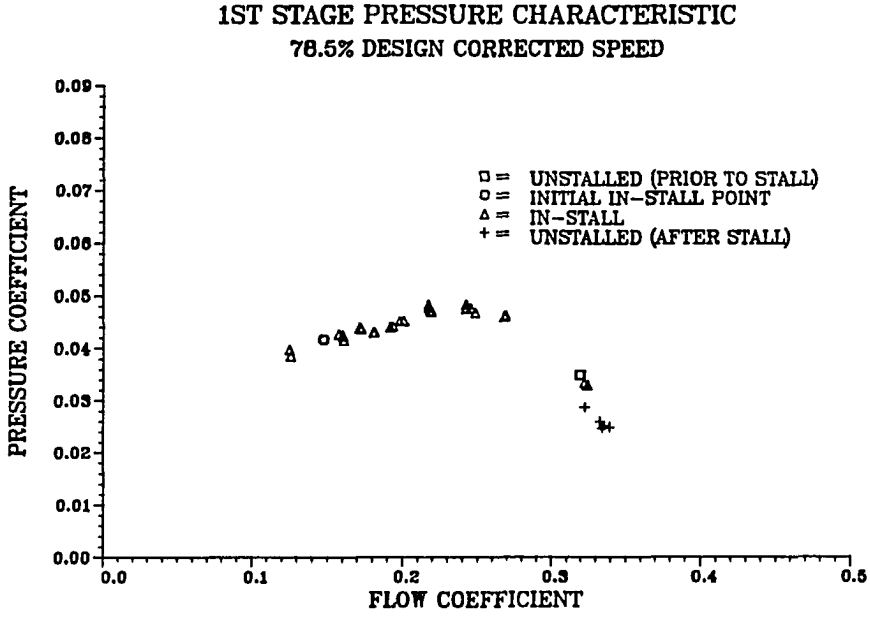

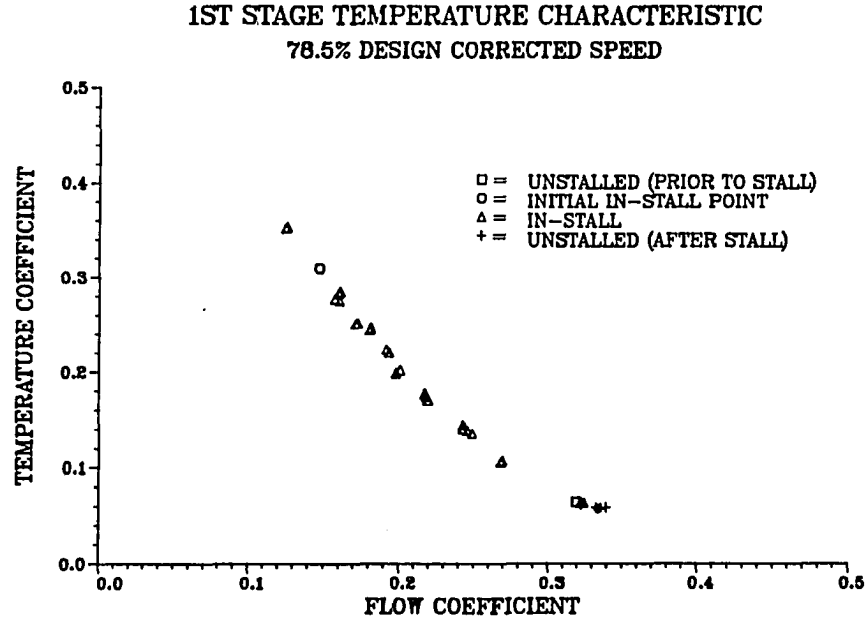

Figure 17.2 Test compressor first stage characteristics 78.5% design corrected speed

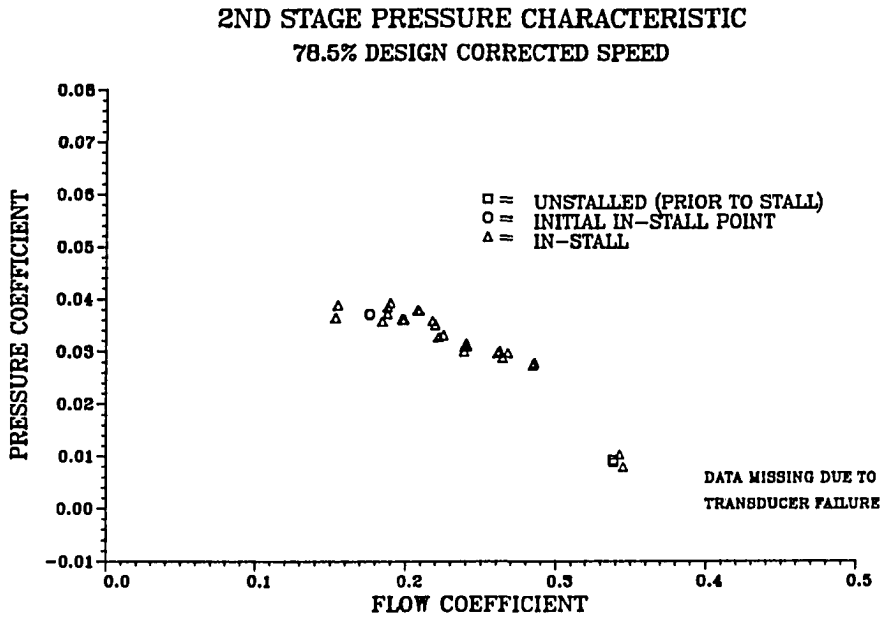

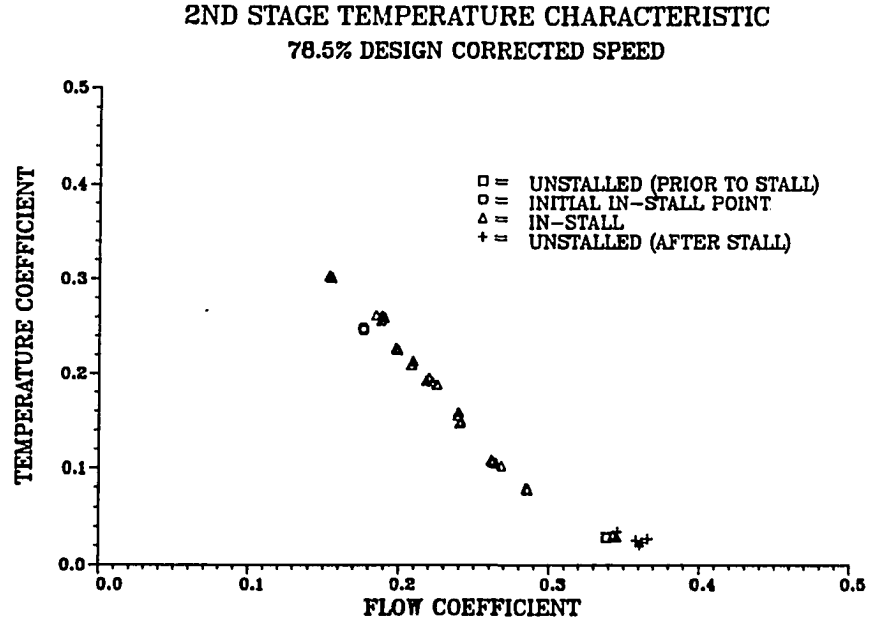

Figure 17.3 Test compressor second stage characteristics 78.5% design corrected speed

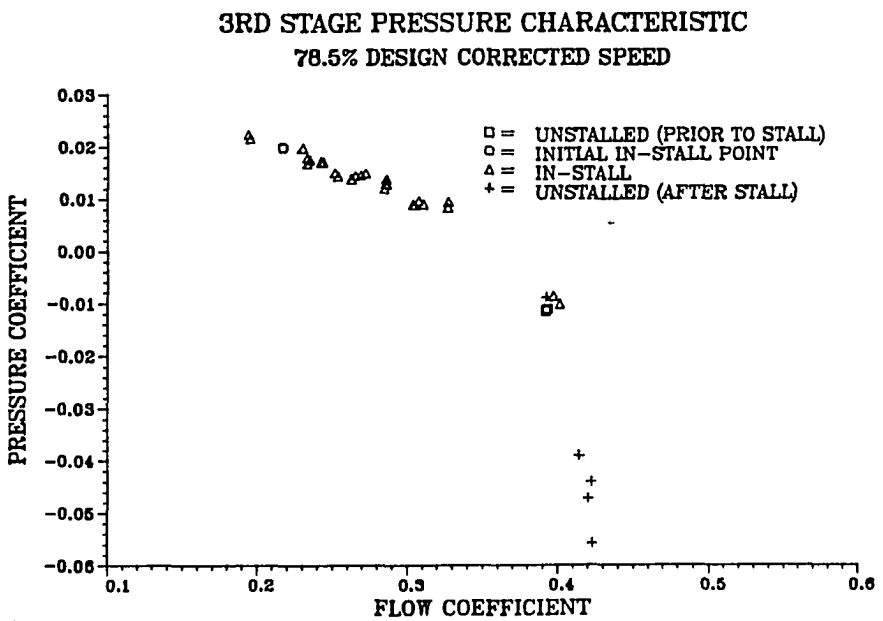

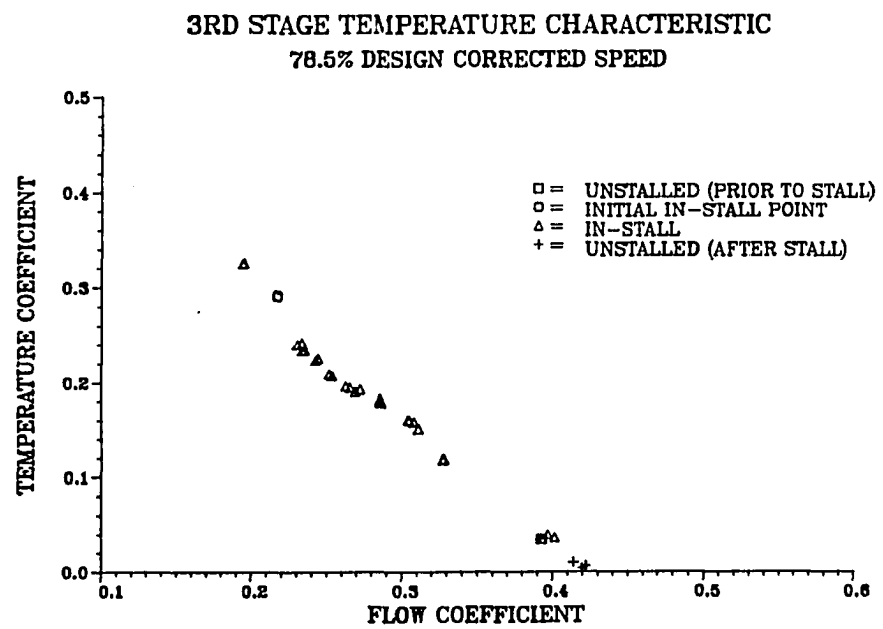

Figure 17.4 Test compressor third stage characteristics 78.5% design corrected speed

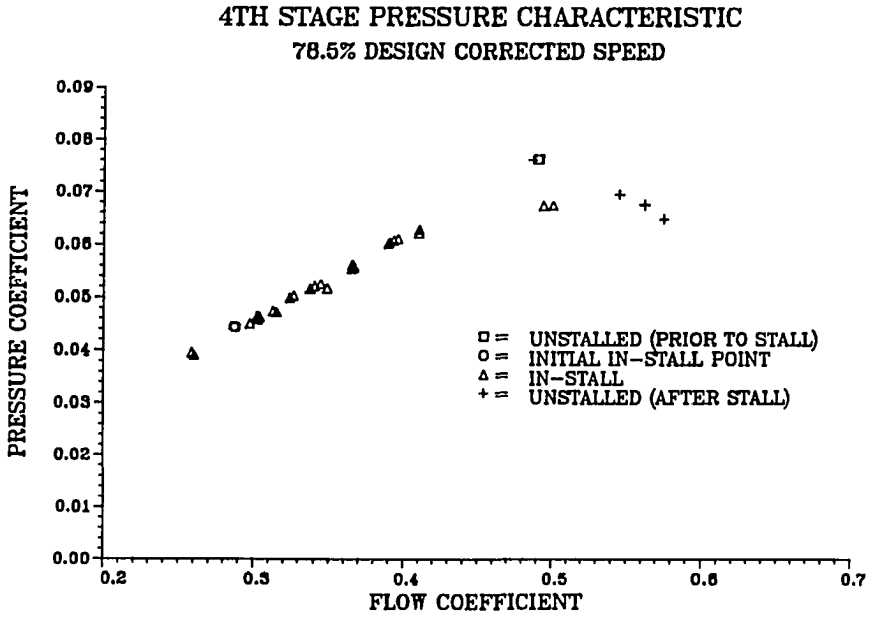

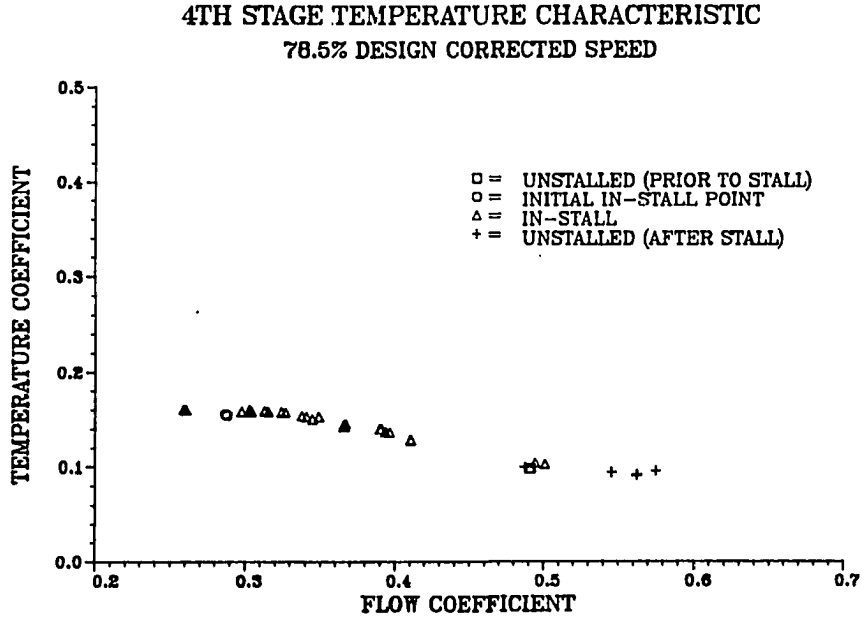

Figure 17.5 Test compressor fourth stage characteristics 78.5% design corrected speed

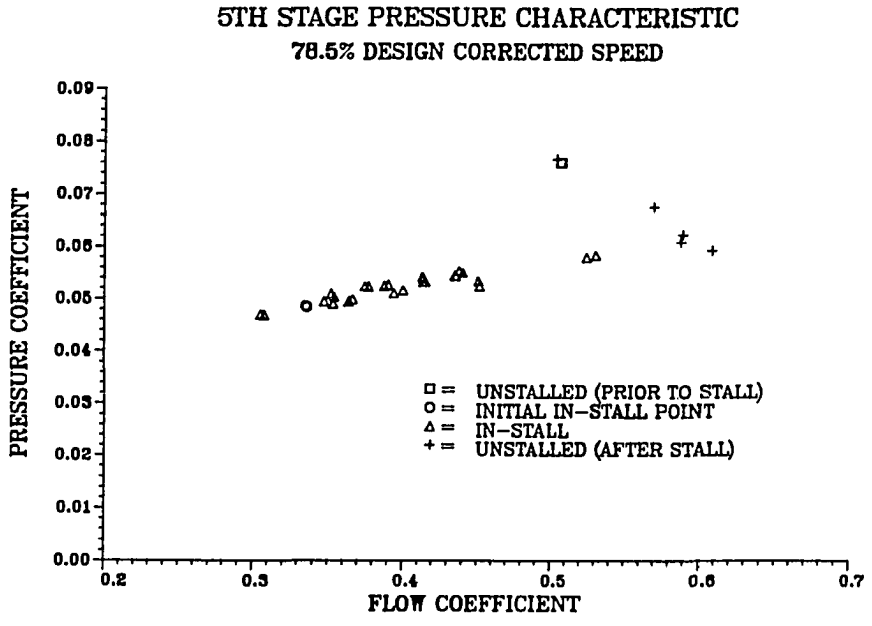

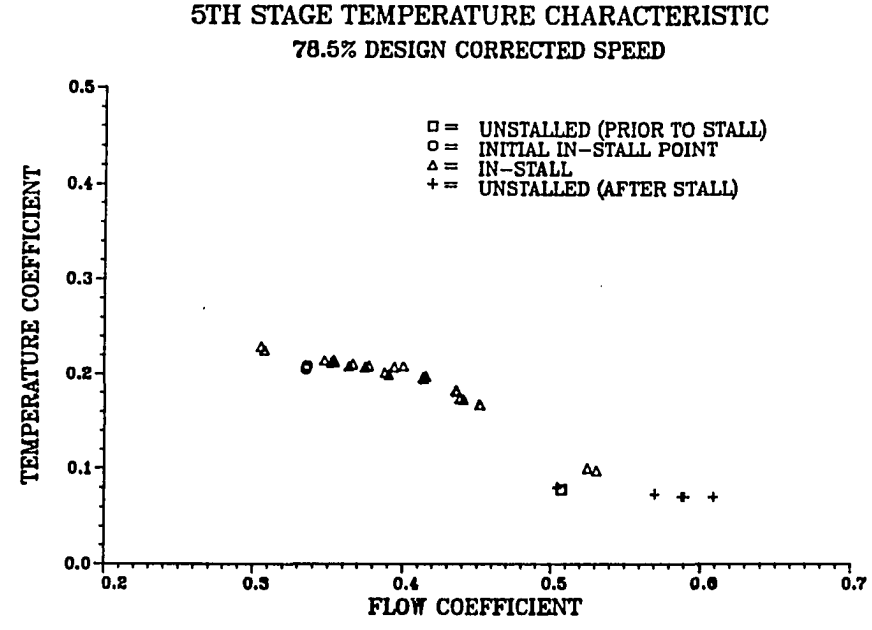

Figure 17.6 Test compressor fifth stage characteristics 78.5% design corrected speed

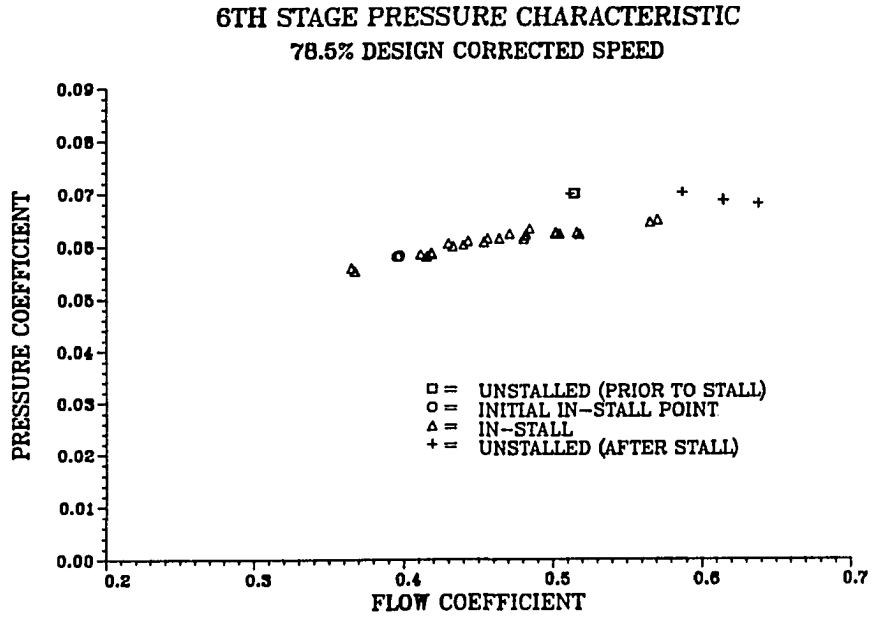

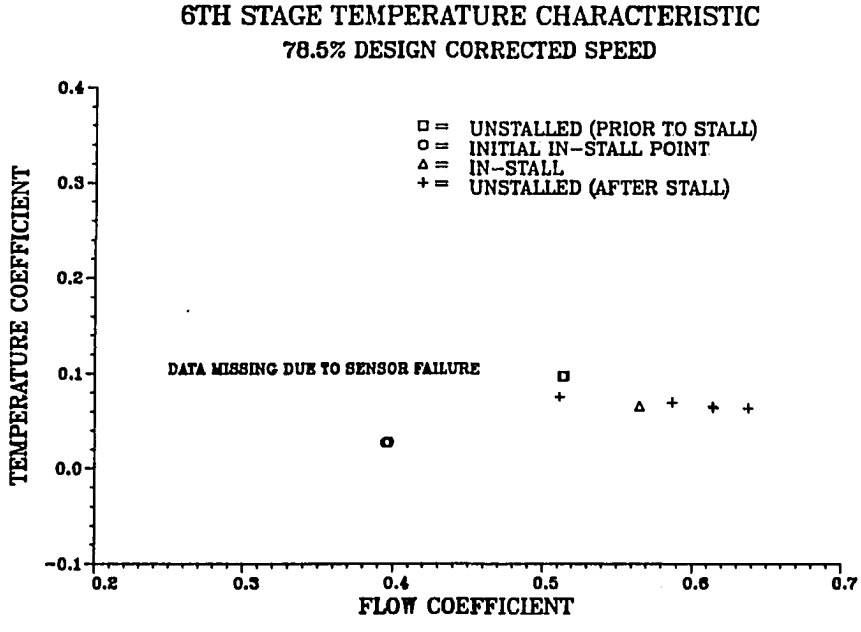

Figure 17.7 Test compressor sixth stage characteristics 78.5% design corrected speed

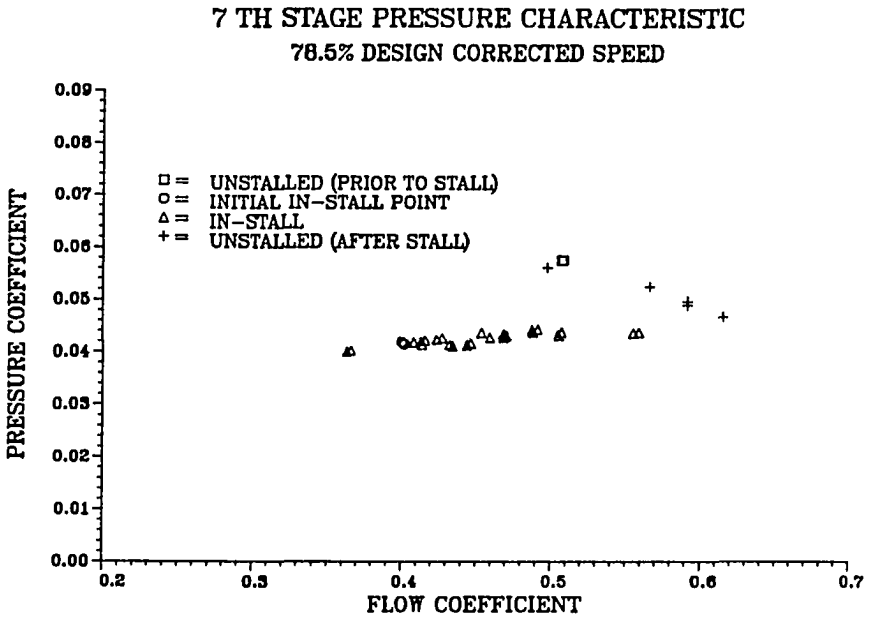

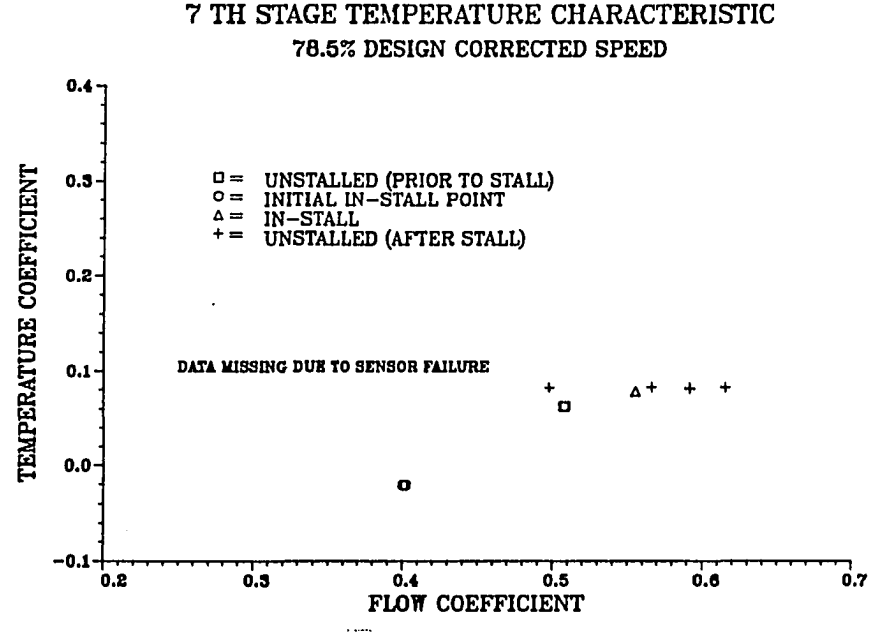

Figure 17.8 Test compressor seventh stage characteristics 78.5% design corrected speed

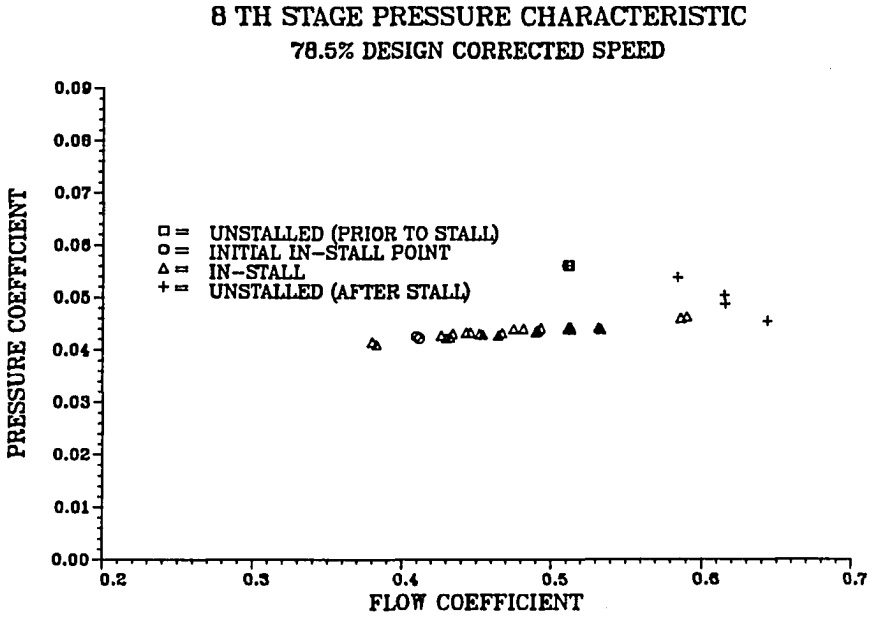

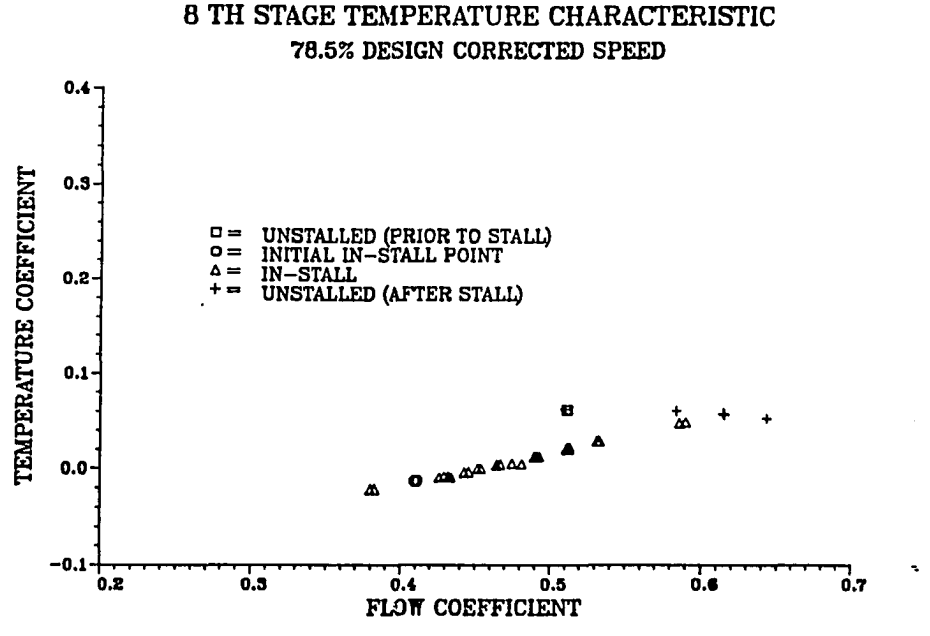

Figure 17.9 Test compressor eighth stage characteristics 78.5% design corrected speed

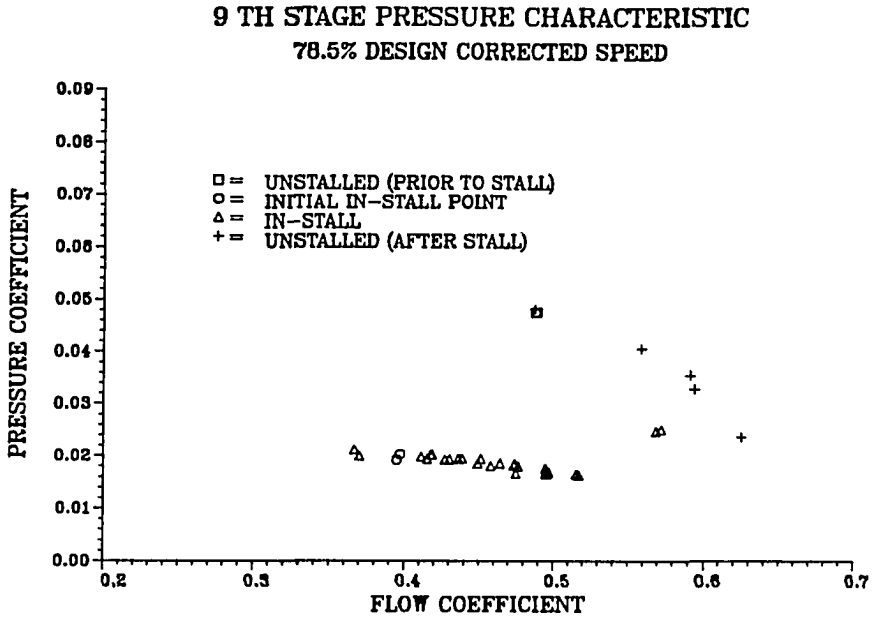

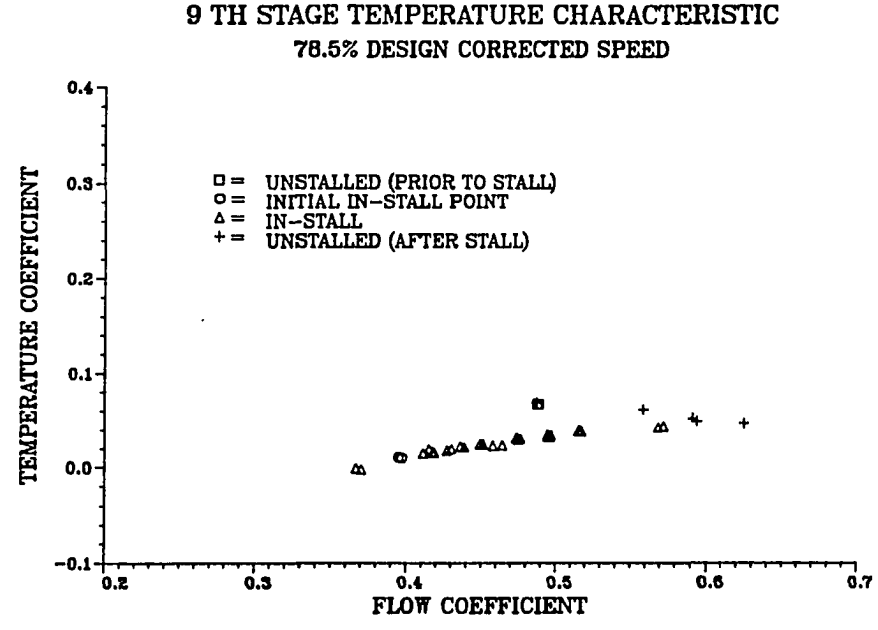

Figure 17.10 Test compressor ninth stage characteristics 78.5% design corrected speed

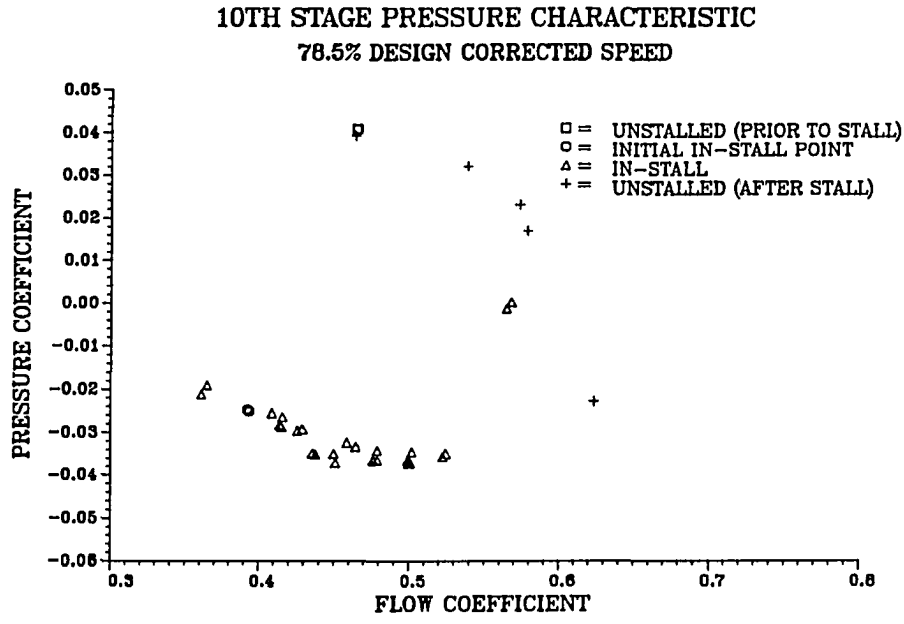

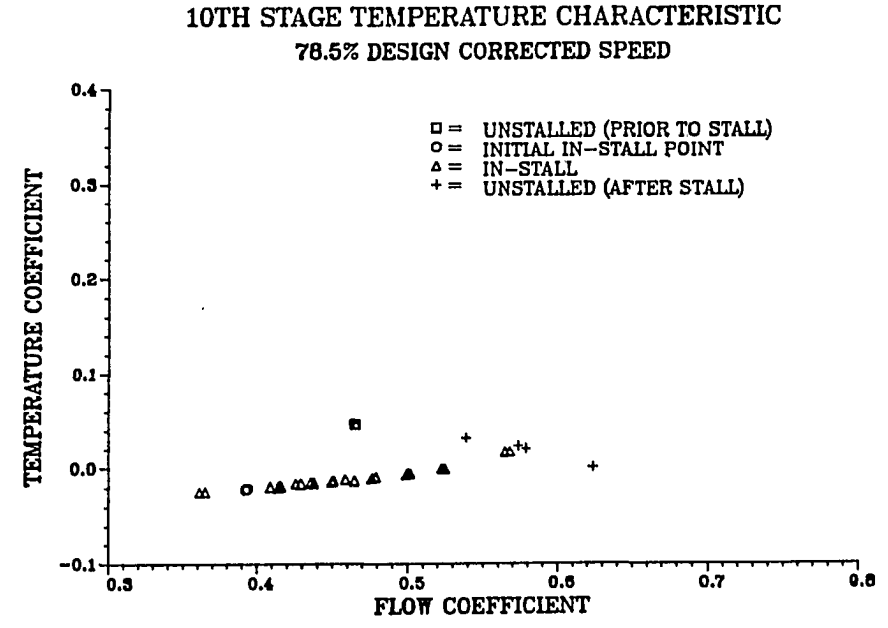

Figure 17.11 Test compressor tenth stage characteristics 78.5% design corrected speed

XVIII. APPENDIX G: DETAILED CHARACTERISTICS

74.5% DESIGN SPEED +7VV

The data shown in Figure 18.1 represent the detailed overall compressor temperature and pressure characteristics for the +7 variable vane configuration for the test compressor at 74.5% design corrected speed. Data are presented for four different operating conditions, the first two being, unstalled (prior to stall) operating on the overall compressor unstalled characteristic, and at the overall compressor initial in-stall condition. The data presented at the initial in-stall condition were obtained by slowly closing the exit throttle while the compressor was operating unstalled and stopping when stall occurred. The compressor was allowed to stabilize for 3 minutes and then the data were obtained. The third operating condition is for the compressor in-stall for different exit throttle area settings. The last condition is a repeat of the first after the compressor recovered from stall. The data in Figures 18.2 through 18.11 are the individual stage characteristics for the CRF test compressor. These characteristics are plotted in stage pressure and temperature coefficient and stage flow coefficient coordinates for the overall compressor condition described above.

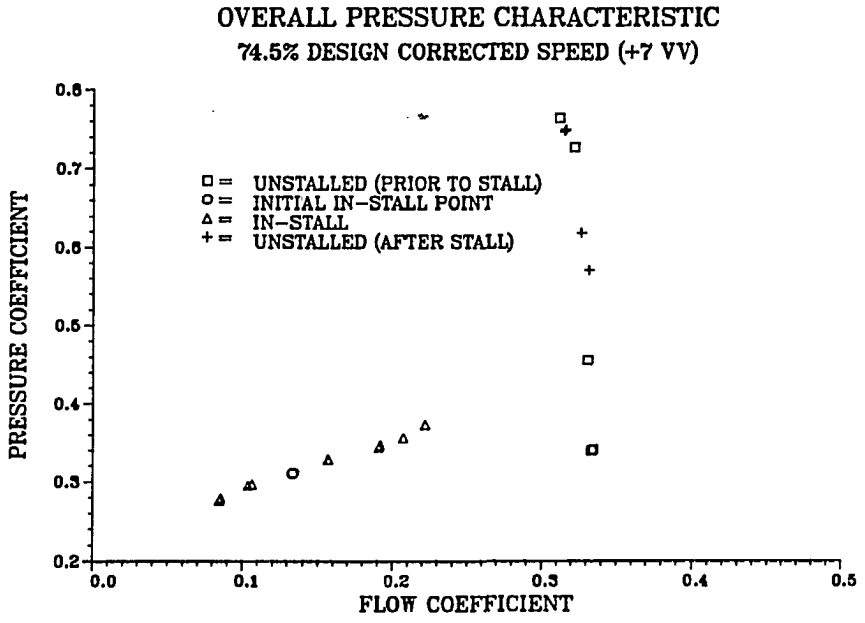

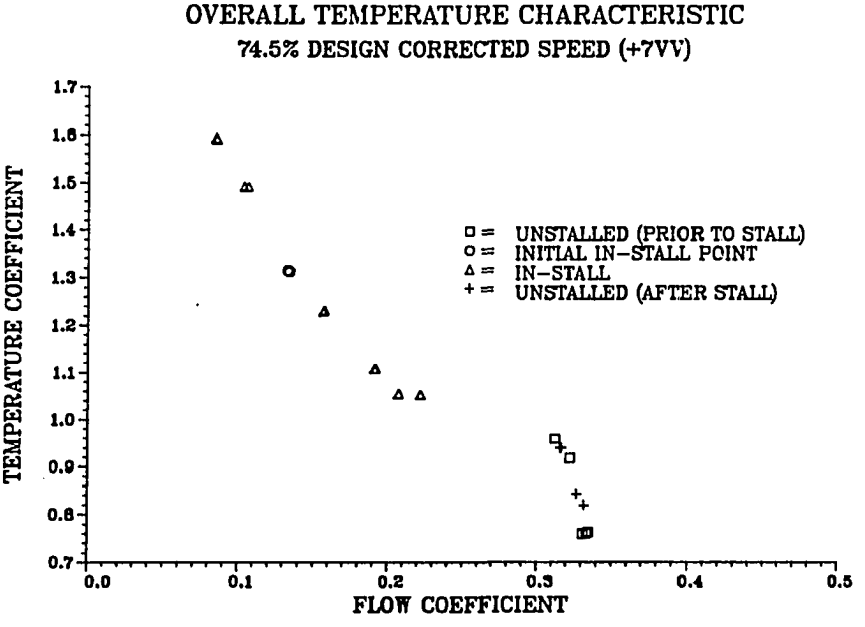

Figure 18.1 Test compressor overall characteristics 74.5% design corrected speed (+7 VV)

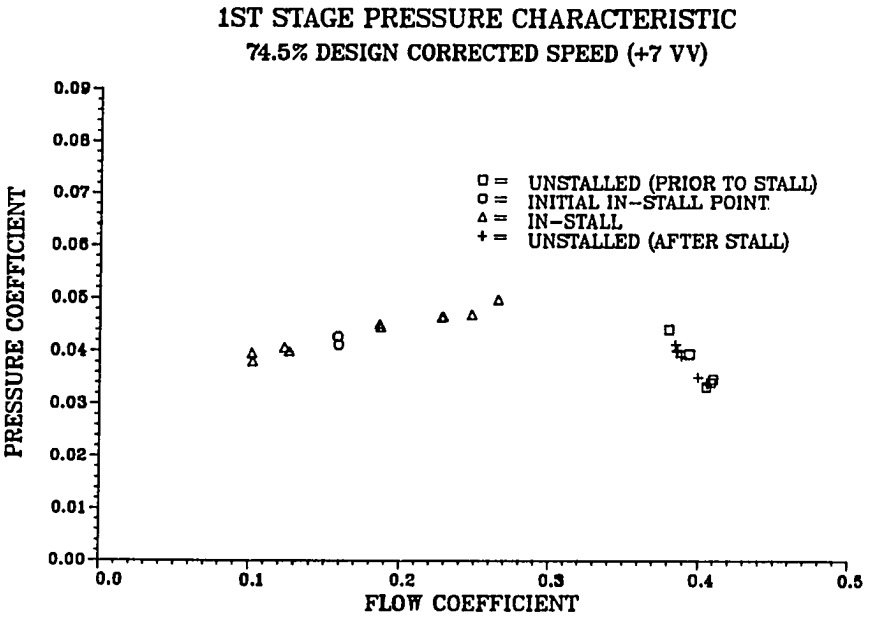

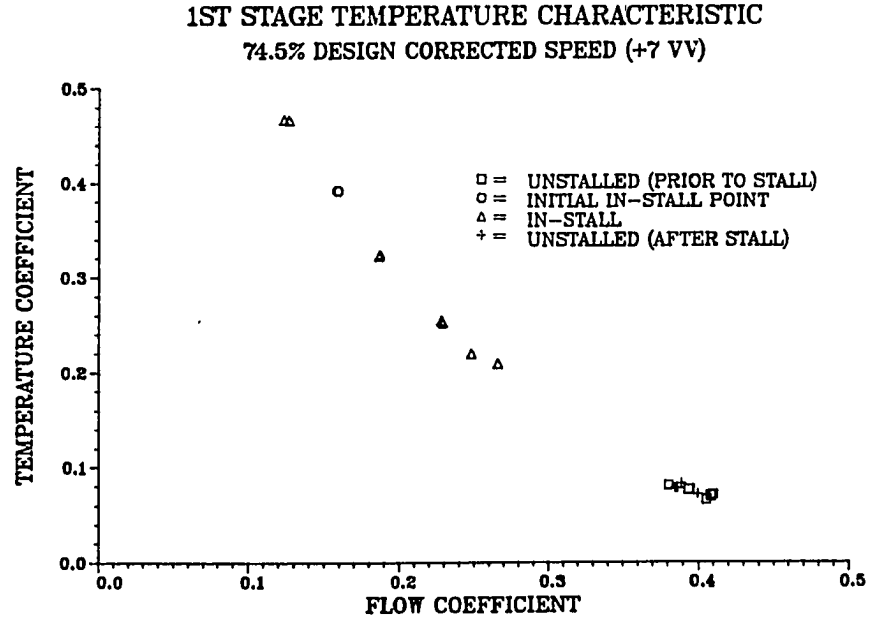

Figure 18.2 Test compressor first stage characteristics 74.5% design corrected speed (+7 VV)

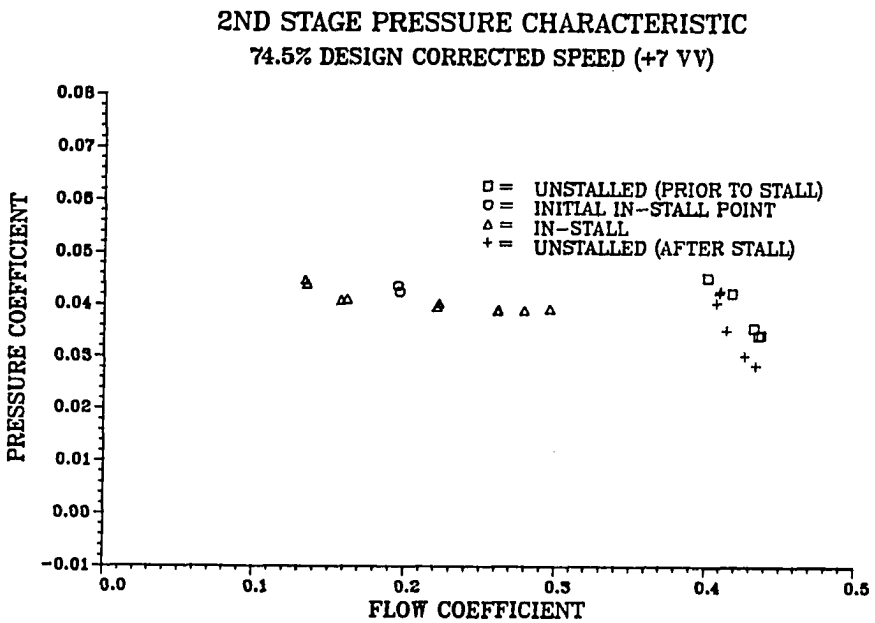

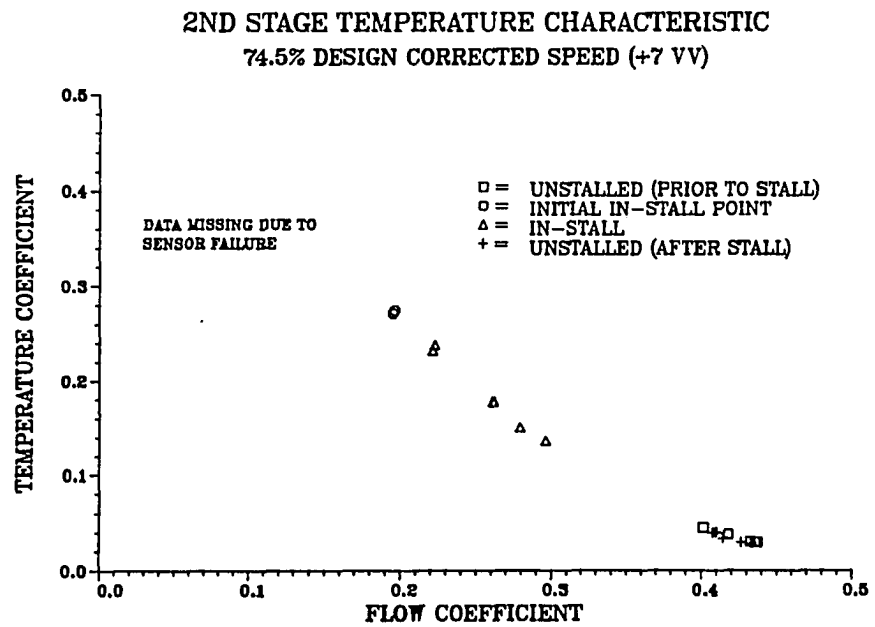

Figure 18.3 Test compressor second stage characteristics 74.5% design corrected speed (+7 VV)

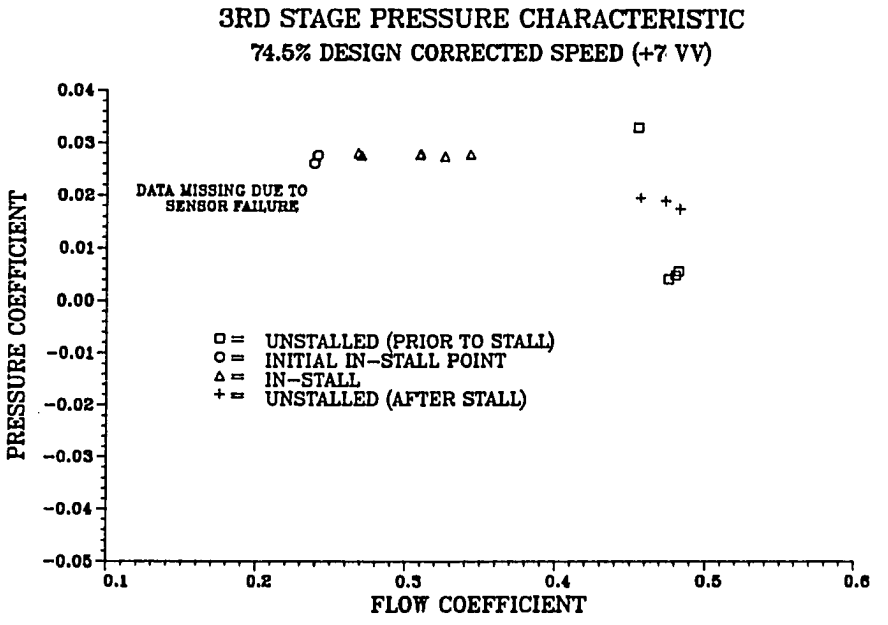

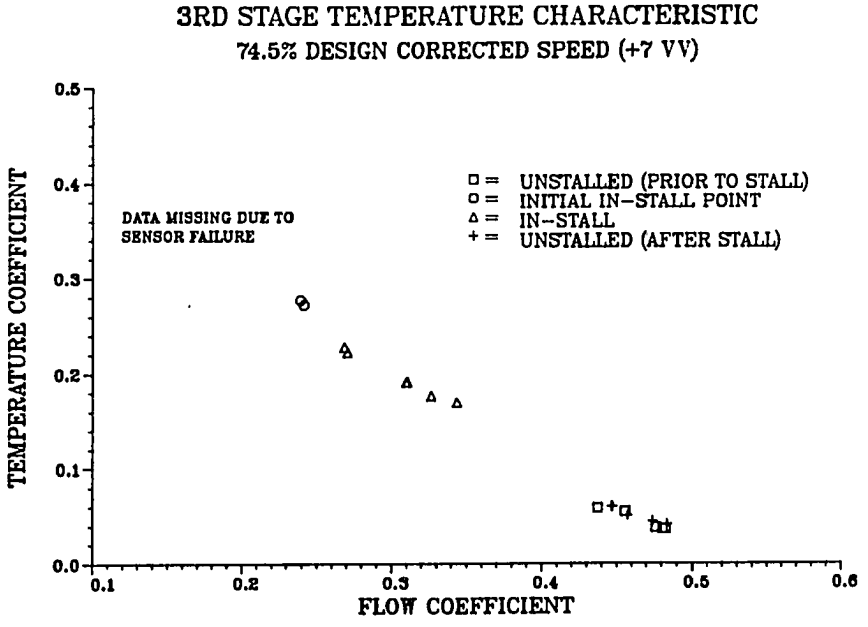

Figure 18.4 Test compressor third stage characteristics 74.5% design corrected speed (+7 VV)

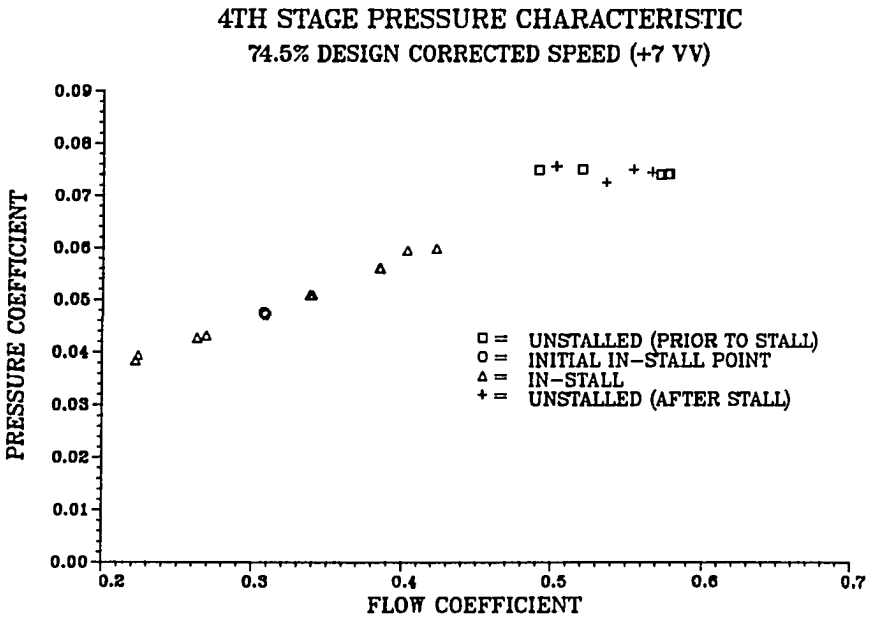

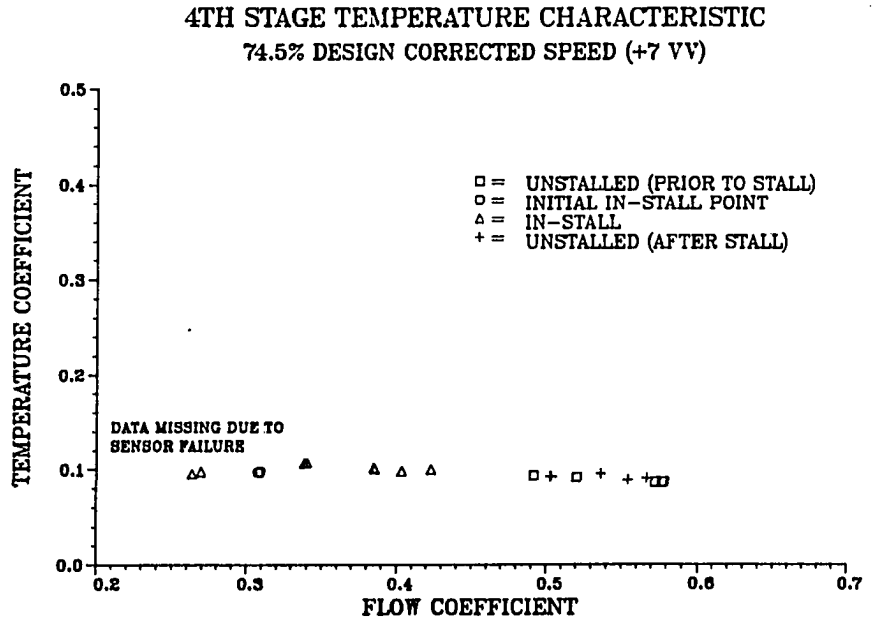

Figure 18.5 Test compressor fourth stage characteristics 74.5% design corrected speed (+7 VV)

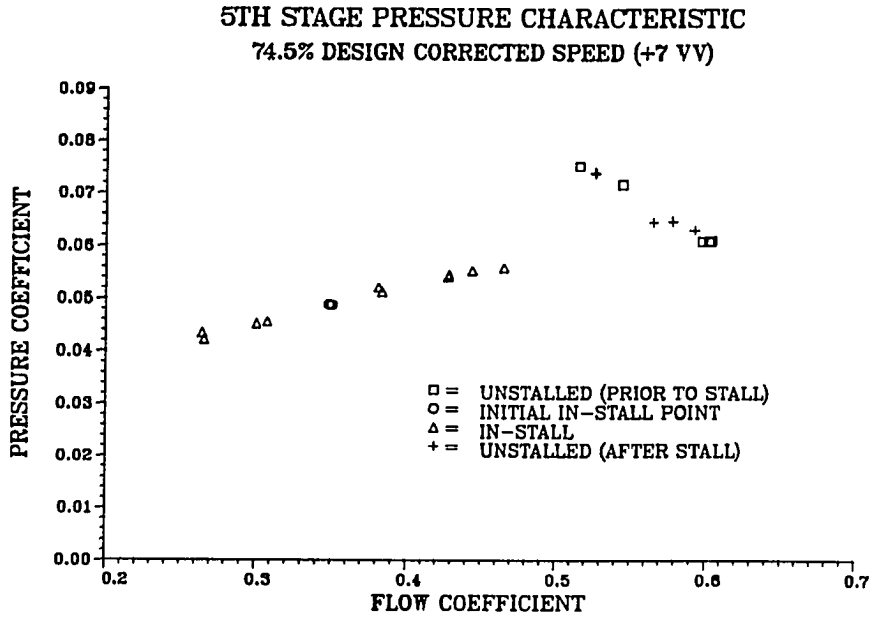

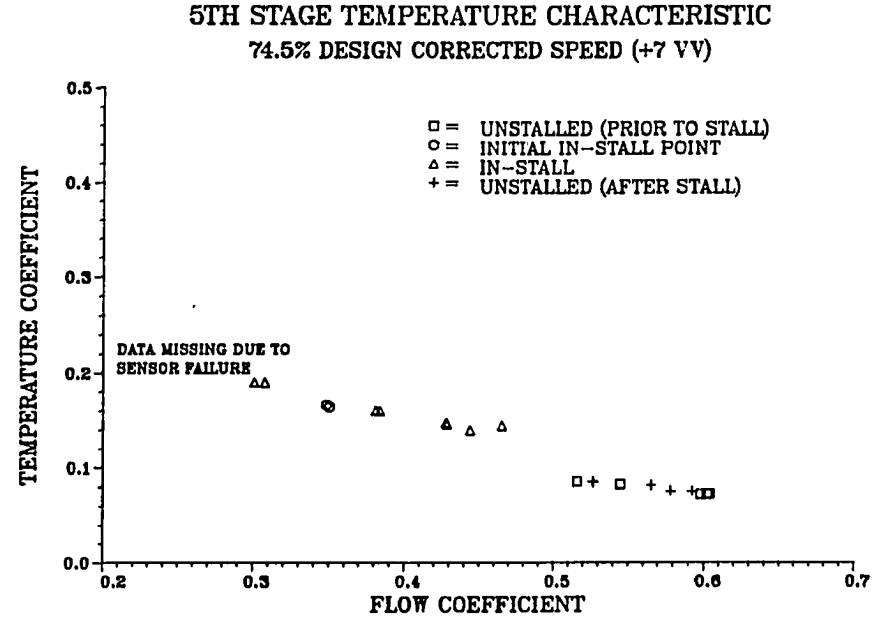

Figure 18.6 Test compressor fifth stage characteristics 74.5% design corrected speed (+7 VV)

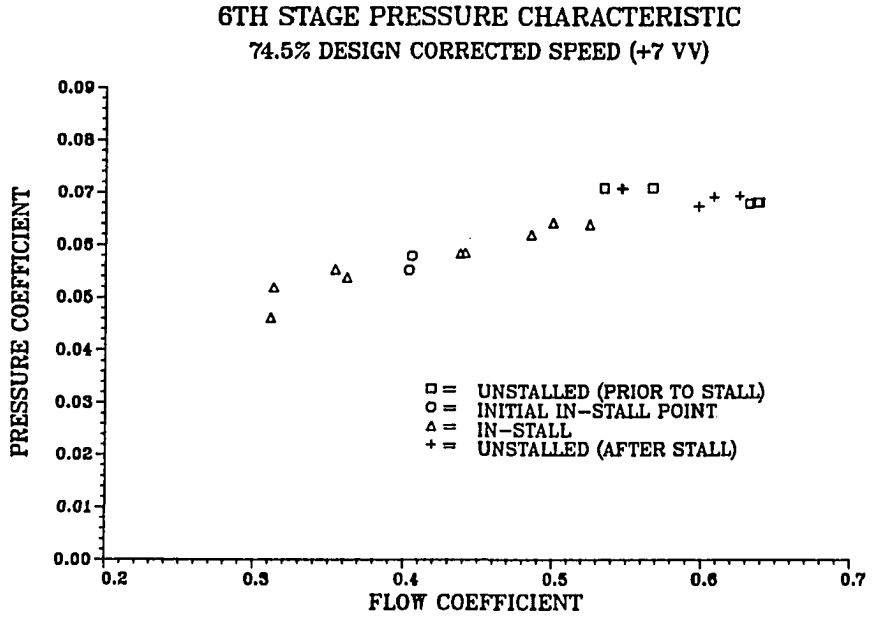

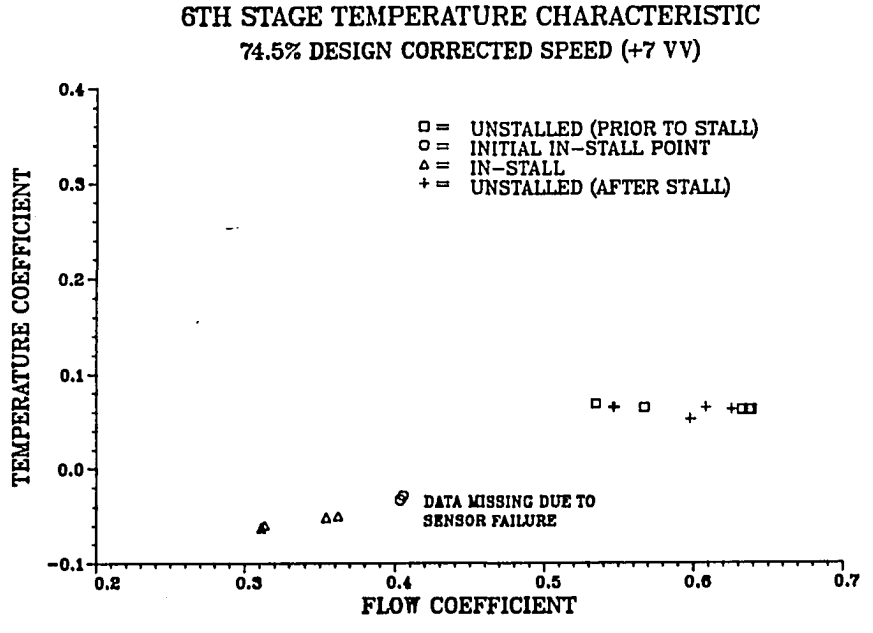

Figure 18.7 Test compressor sixth stage characteristics 74.5% design corrected speed (+7 VV)

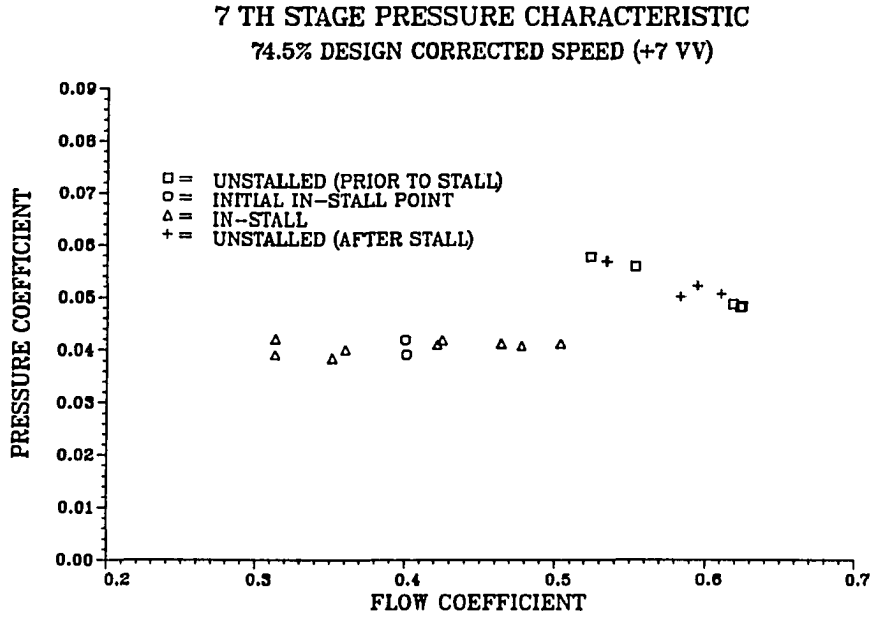

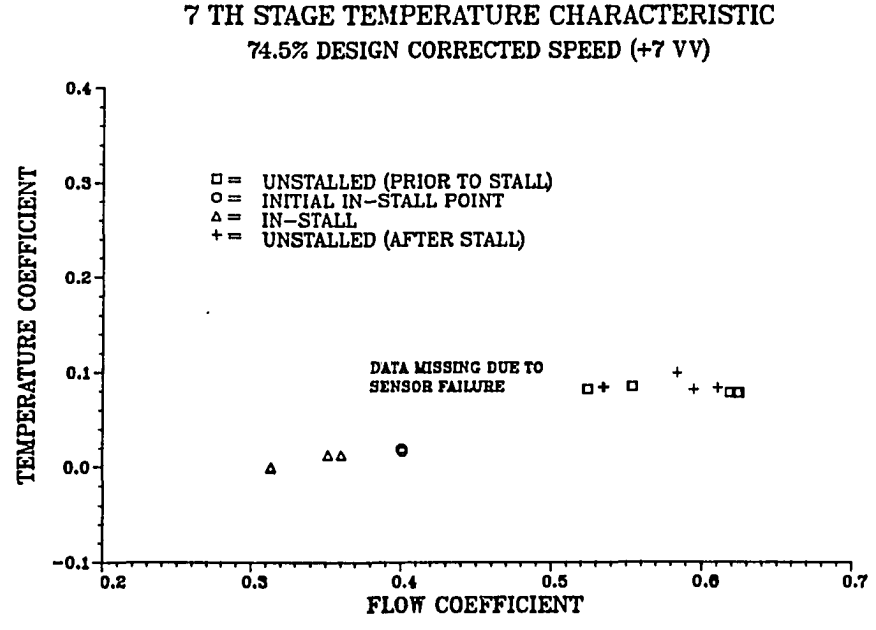

Figure 18.8 Test compressor seventh stage characteristics 74.5% design corrected speed (+7 VV)

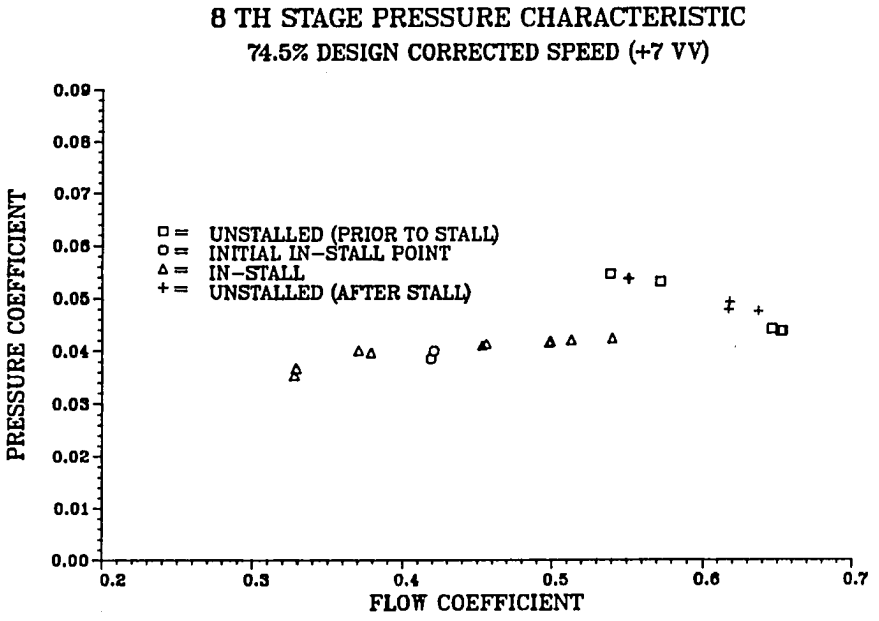

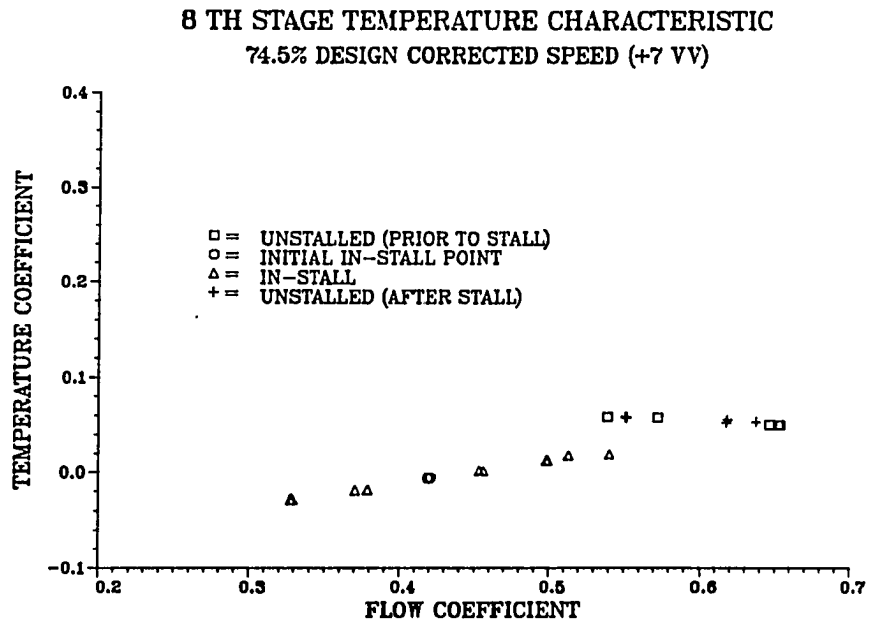

Figure 18.9 Test compressor eighth stage characteristics 74.5% design corrected speed (+7 VV)

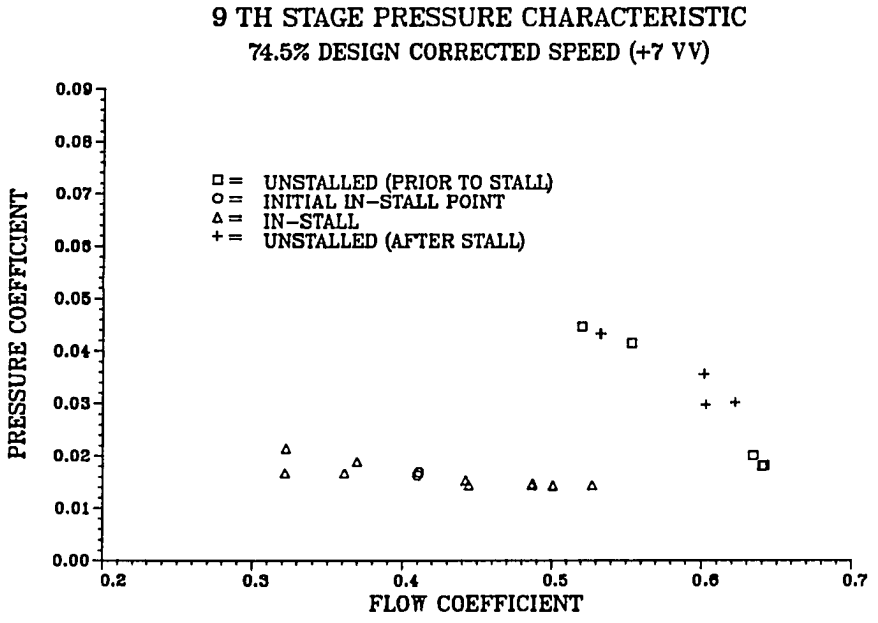

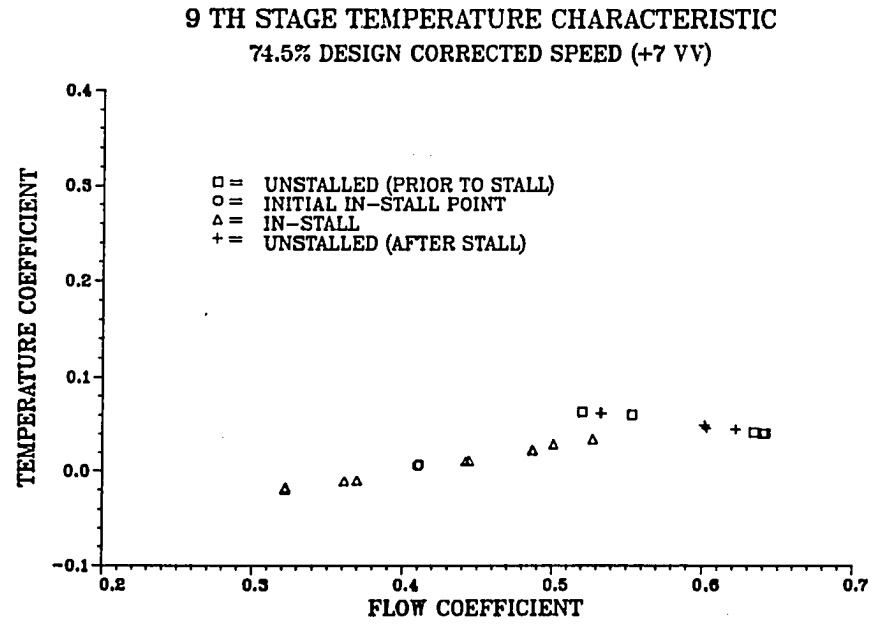

Figure 18.10 Test compressor ninth stage characteristics 74.5% design corrected speed (+7 VV)

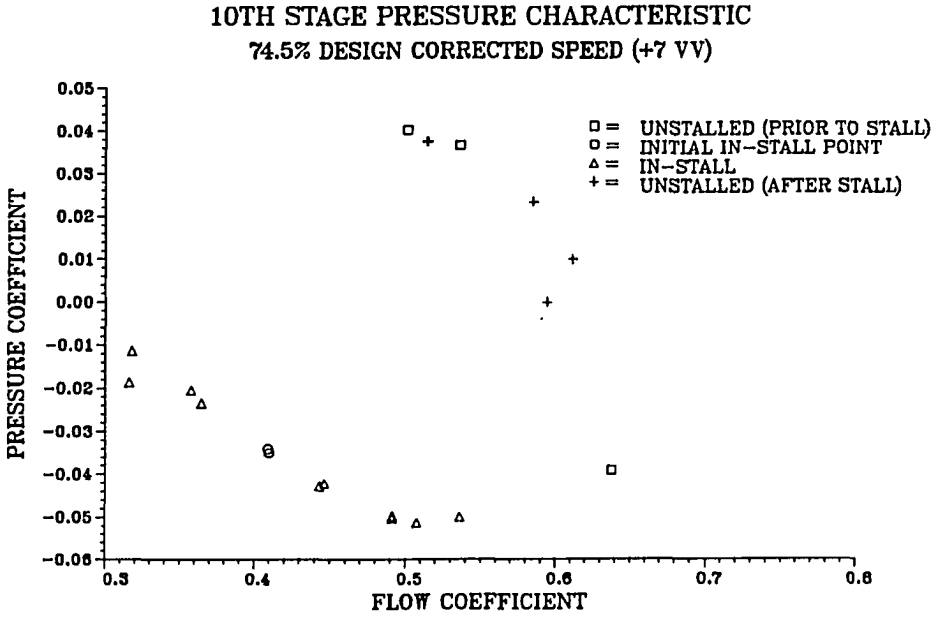

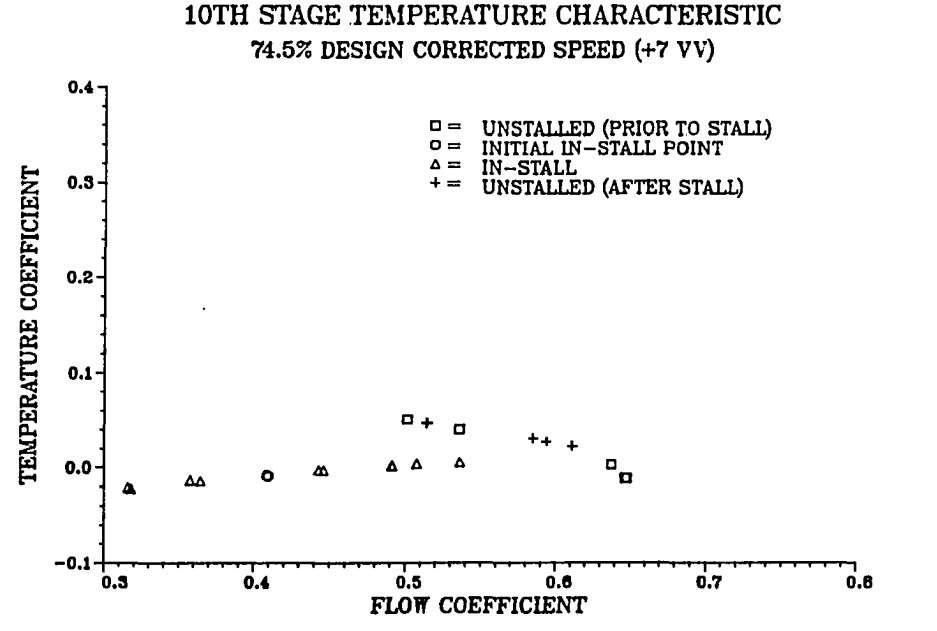

Figure 18.11 Test compressor tenth stage characteristics 74.5% design corrected speed (+7 VV)

XIX. APPENDIX H: HIGH-RESPONSE FORWARD AND AFT FACING PROBE SIGNALS

The pressure signals obtained from the exit forward and aft pressure probe detailed in section IV for the operating conditions defined in Figure 7.48 at 59.7% design speed are presented in Figures 19.1 through 19.5. The data detail the annulus blockage extent for five different in-stall operating conditions at 59.7% design speed. The same type data for in-stall operation at conditions defined in Figure 7.44 at 78.5% design speed are detailed in Figures 19.6 through 19.10. Again the circumferential extent of stall cell blockage provided.

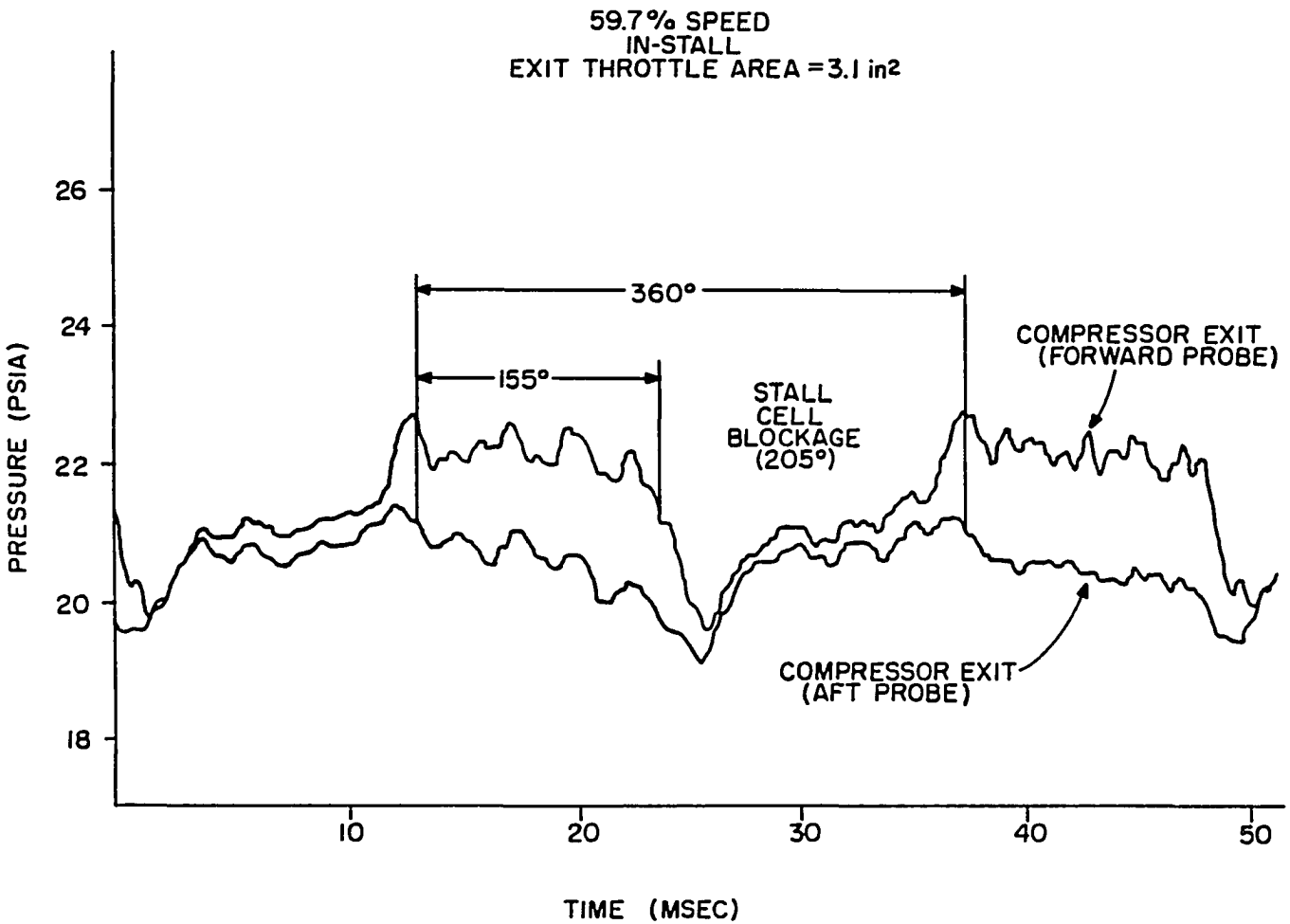

Figure 19.1 High-response compressor exit forward and aft facing pressure probe signals with stall cell blockage extent detailed, 59.7% design corrected speed, exit throttle area 3.1 sq. in. (20.0 sq. cm)

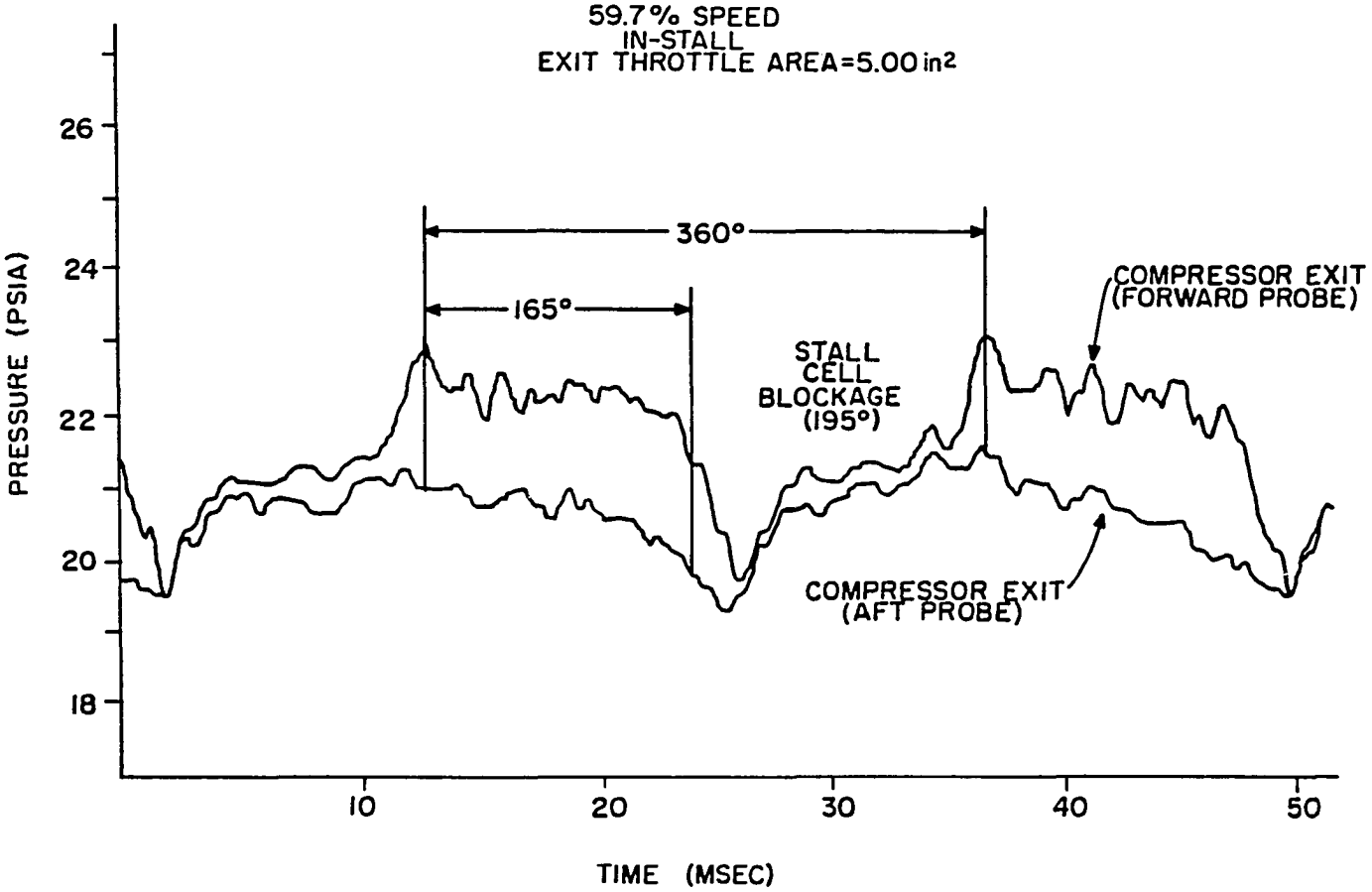

Figure 19.2 High-response compressor exit forward and aft facing pressure probe signals with stall cell blockage extent detailed, 59.7% design corrected speed, exit throttle area 5.0 sq.in. (32.2 sq. cm)

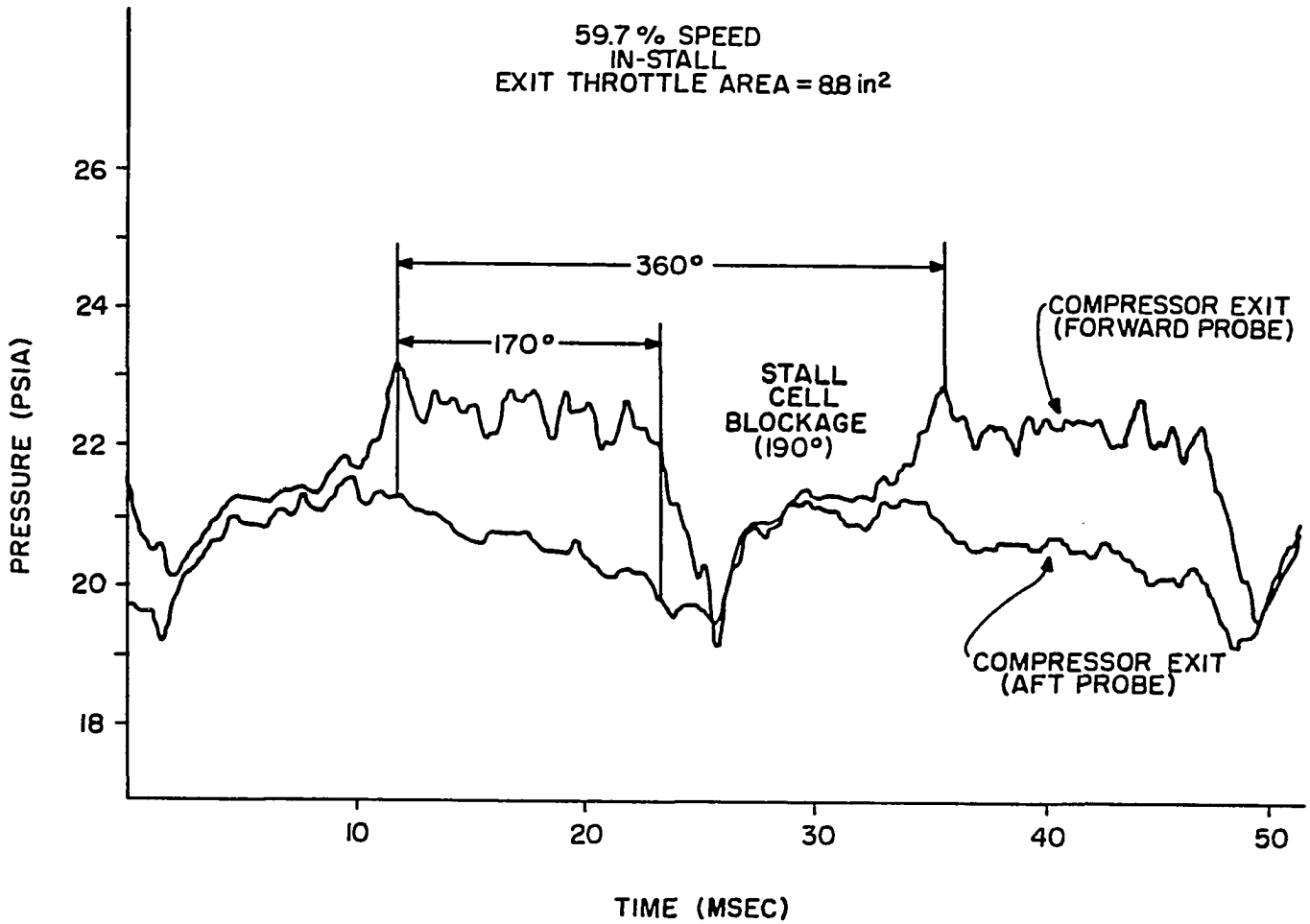

Figure 19.3 High-response compressor exit forward and aft facing pressure probe signals with stall cell blockage extent detailed, 59.7% design corrected speed, exit throttle area 8.8 sq. in. (56.8 sq. cm)

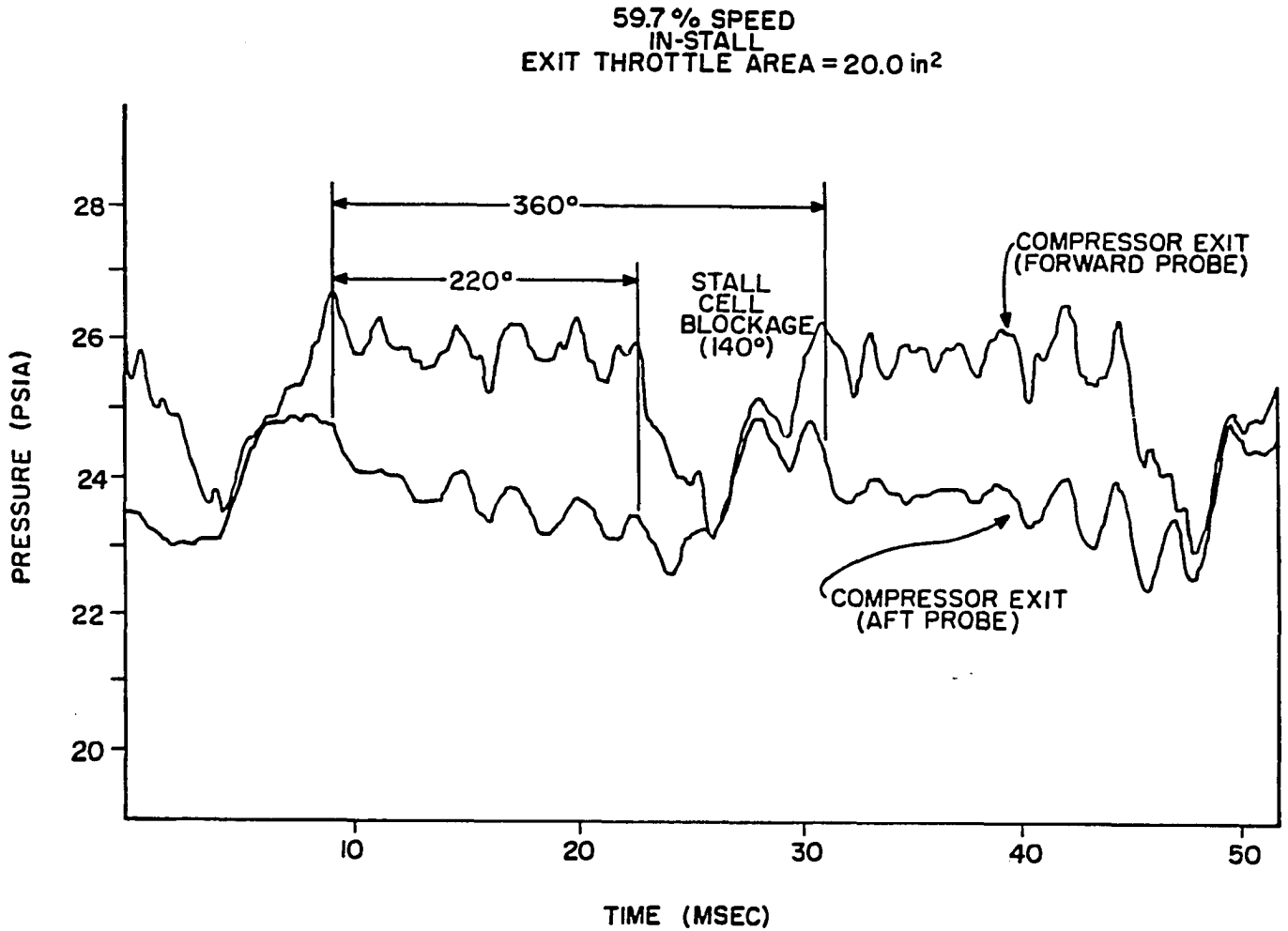

Figure 19.4 High-response compressor exit forward and aft facing pressure probe signals with stall cell blockage extent detailed, 59.7% design corrected speed, exit throttle area 20.0 sq. in. (129.0 sq. cm)

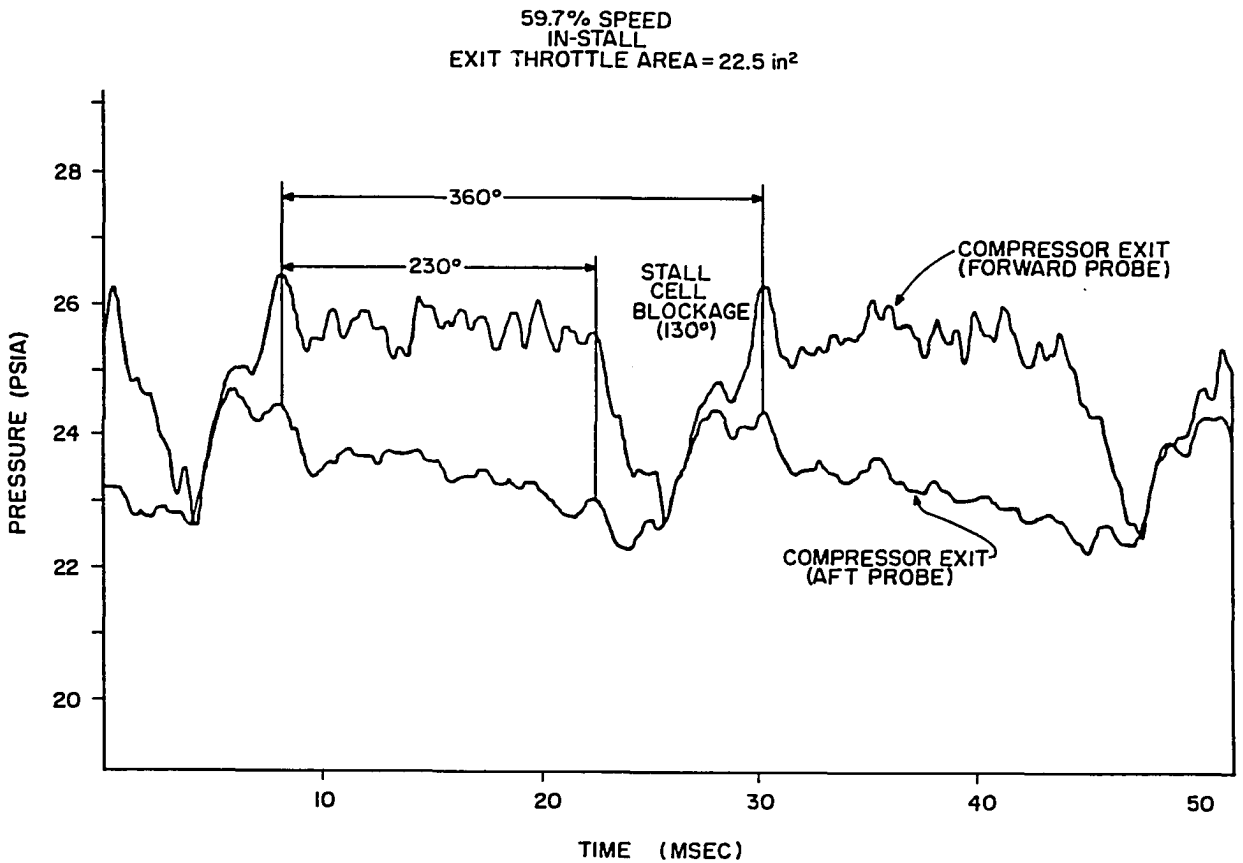

Figure 19.5 High-response compressor exit forward and aft facing pressure probe signals with stall cell blockage extent detailed, 59.7% design corrected speed, exit throttle area 22.5 sq. in. (145.2 sq cm)

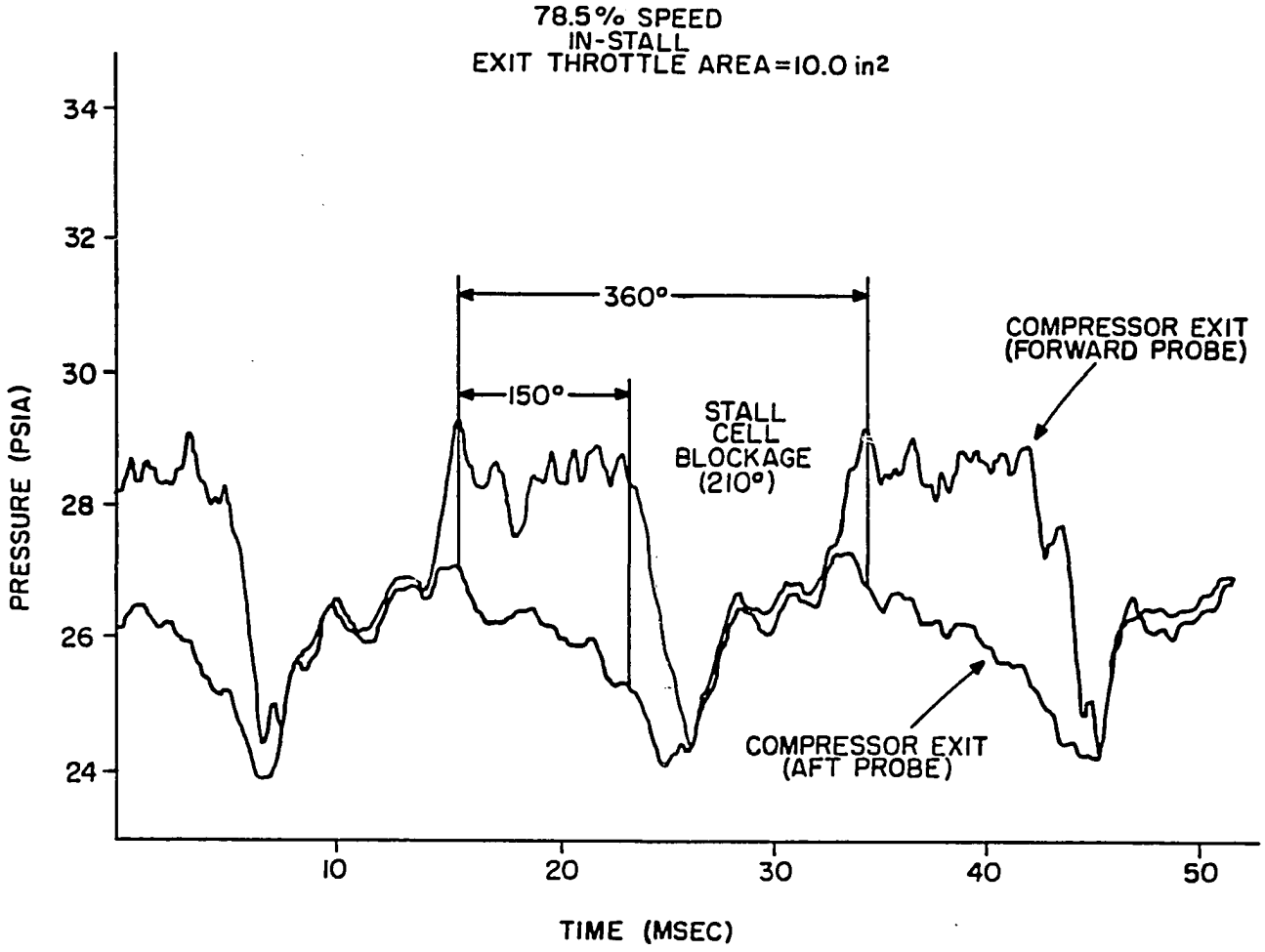

Figure 19.6 High-response compressor exit forward and aft facing pressure probe signals with stall cell blockage extent detailed, 78.5% design corrected speed, exit throttle area 10.0 sq. in. (64.5 sq. cm)

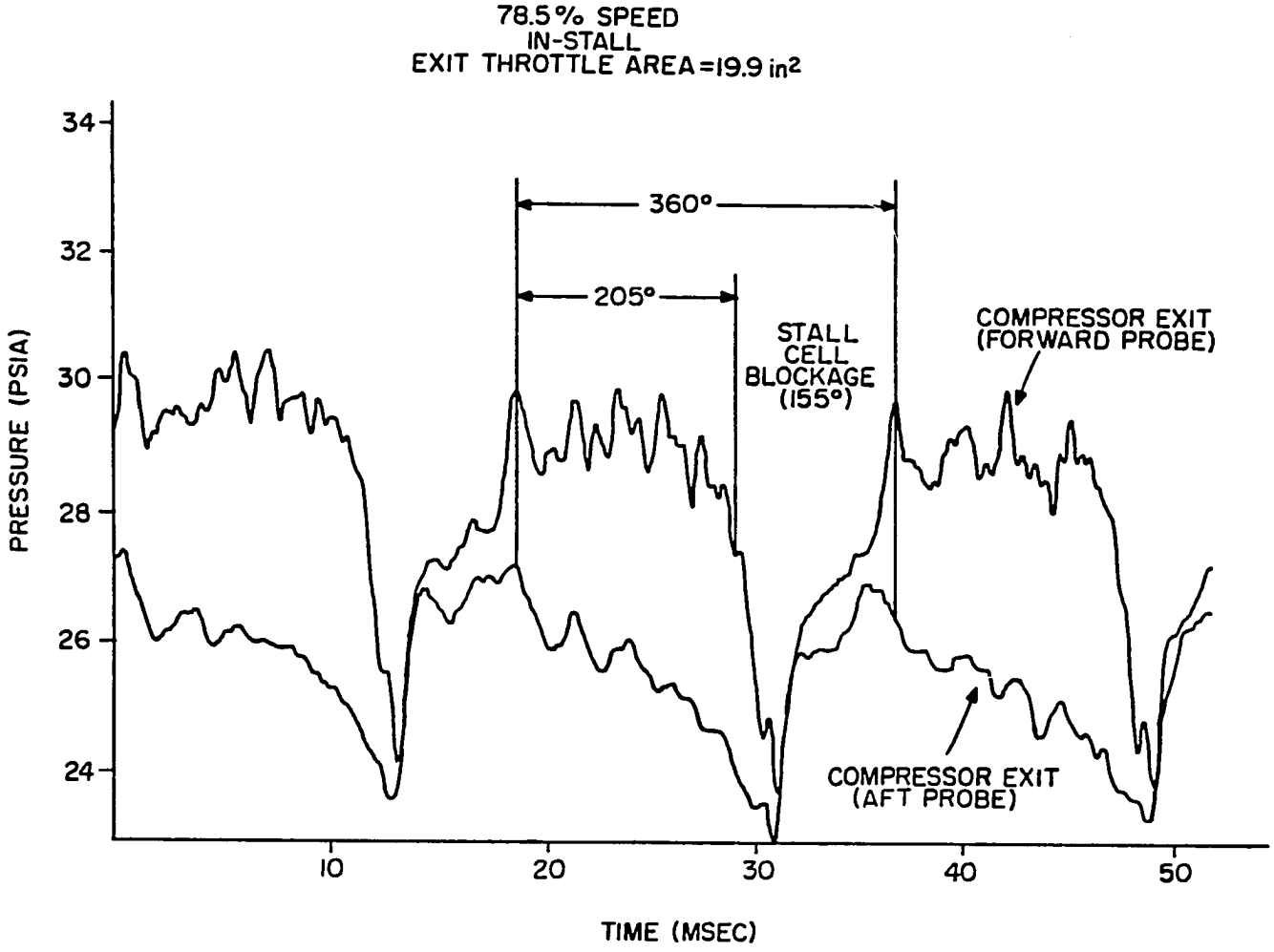

Figure 19.7 High-response compressor exit forward and aft facing pressure probe signals with stall cell blockage extent detailed, 78.5% design corrected speed, exit throttle area 19.9 sq. in. (128.4 sq. cm)

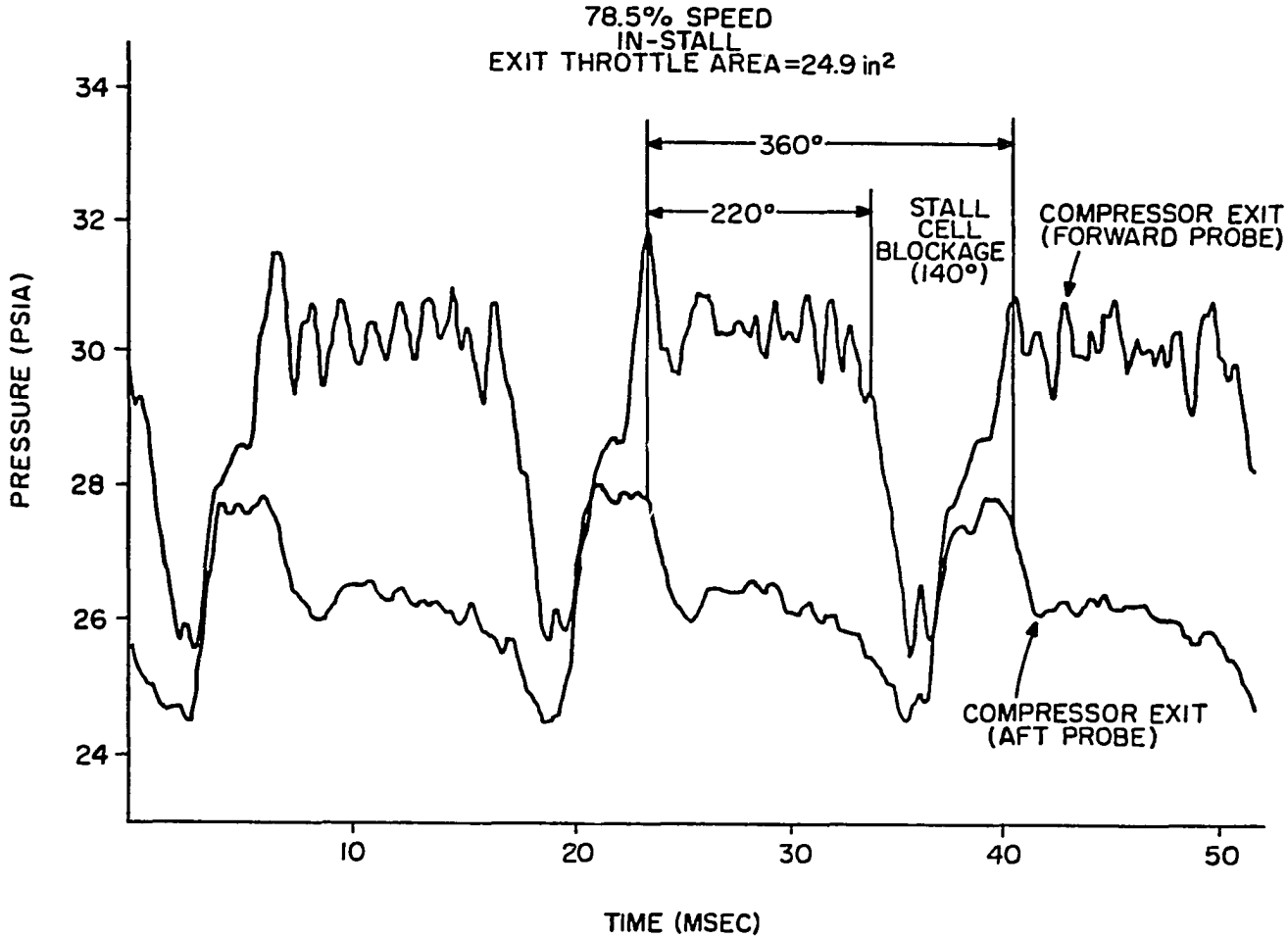

Figure 19.8 High-response compressor exit forward and aft facing pressure probe signals with stall cell blockage extent detailed, 78.5% design corrected speed, exit throttle area 24.9 sq. in. (160.6 sq. cm)

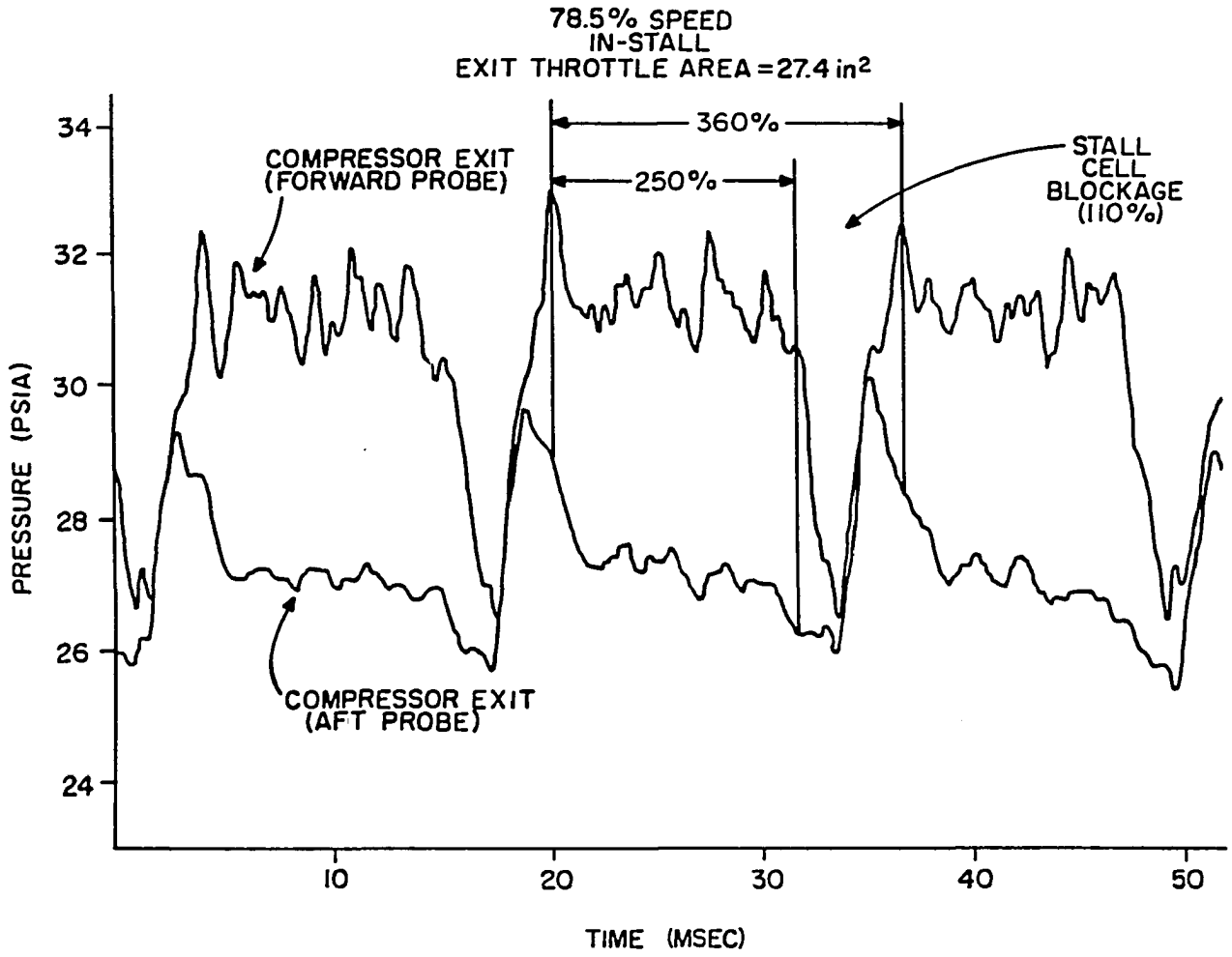

Figure 19.9 High-response compressor exit forward and aft facing pressure probe signals with stall cell blockage extent detailed, 78.5% design corrected speed, exit throttle area 27.4 sq. in. (176.8 sq. cm)

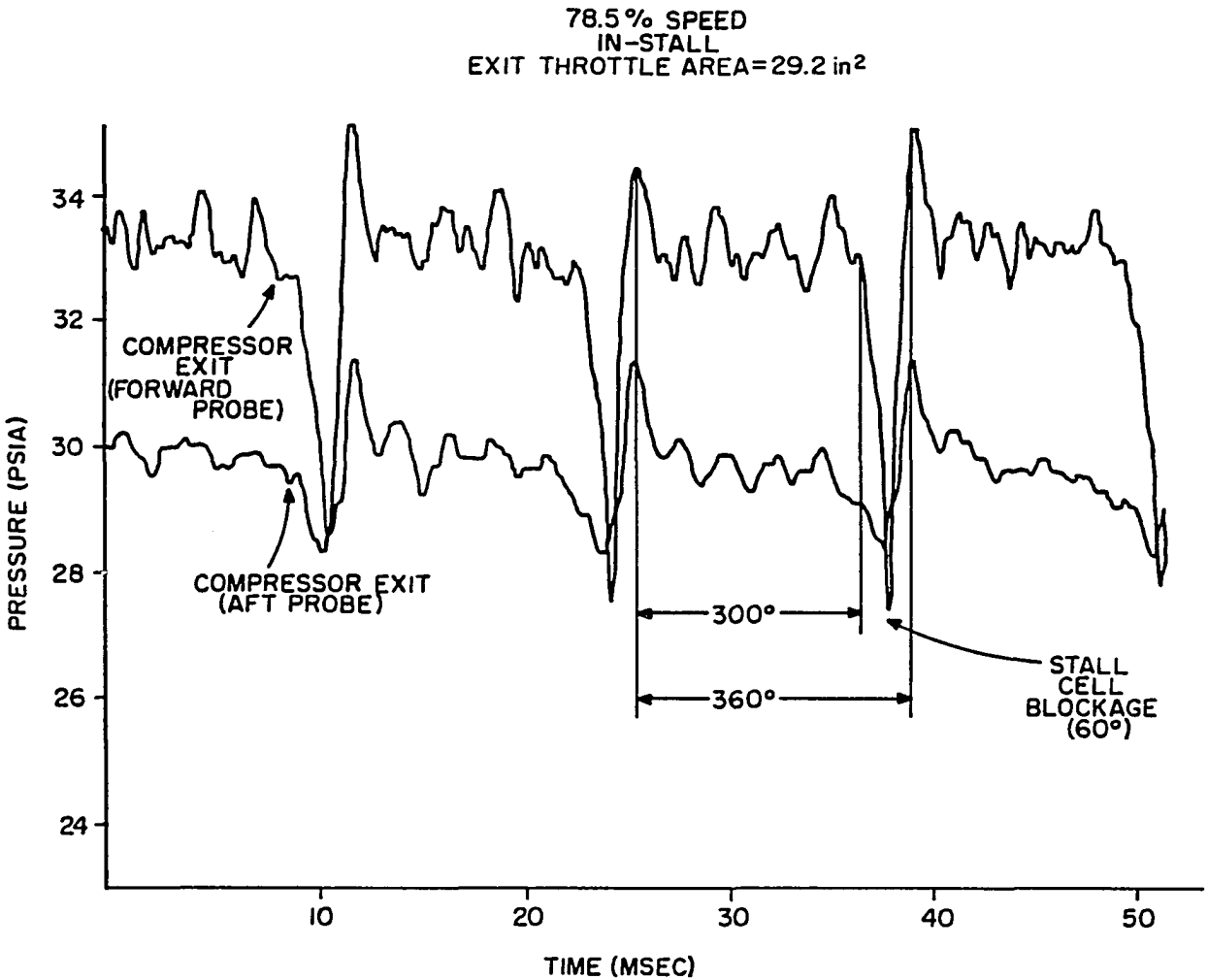

Figure 19.10 High-response compressor exit forward and aft facing pressure probe signals with stall cell blockage extent detailed, 78.5% design corrected speed, exit throttle area 29.2 sq. in. (188.4 sq. cm)